Pharmaceutical Water Systems and the 6D Rule

A Computational Fluid Dynamics Analysis

B. G. Corcoran (MSc. C.Eng.)

PhD. 2003

Pharmaceutical Water Systems and the 6D Rule

A Computational Fluid Dynamics Analysis

By

Brian G. Corcoran (C.Eng. MSc. M.I.Mech.E. M.I.E.I.)

Thesis presented at Dublin City University in fulfillment of the requirements for the Degree of Doctor of Philosophy

Under the Supervision of

Prof. M.S.J. Hashmi

School of Mechanical and Manufacturing Engineering
Dublin City University
Ireland

July 2003

Preface

Declaration

I hereby certify that the material, which I now submit for assessment on the programme of study leading to the award of Degree of Doctor of Science is entirely my own work and has not been taken from the work of others save and to the extent that such work has been cited and acknowledged within the text of my work.

Signed : Brian Corcoran.

ID No: 97971073

Date: 18th September 2003

Acknowledgements

I would like to acknowledge the following people for their support, encouragement and advice during this research:

- My wife Dee. Who is and always will be my soul mate. She encouraged me when I was down, challenged me when I wanted to give up and above all supported and loved me throughout. I will be forever grateful for the time you afforded me to chase my dream. Thanks you from the bottom of my heart!!

- My kids Emma and Ben. You both bring so much joy into my life and watching you both grow over the duration of this work has been inspiring to me. At times I felt so guilty for running off to study and the times I failed to play with you but this experience for me will have far reaching benefits for you both into the future. I am so proud of you both and hope you always find life exciting and challenging.

- My parents Vera and Sean. You both wish you were better educated but you are so experienced in the university of life. You have taught me how to love, to care about what I do and to have balance in my life. Mum every day I thank God for giving us this extra time together. Dad most of what I have learned and practice in life I have learned for you both. Thanks for doing such a good job on us all and the support you give us every day.

- My brothers Alan and Derek who also offered constant support and encouragement when I was feeling low. As Dad says 'Its done and finished'.

- My supervisor Prof. Hashmi for his encouragement, support and advice during this project. I have enjoyed travelling with you, your stories and your life experiences.

- Paul Young and Harry Esmonde. Paul you should be a multi-millionaire with your IT skills. Thanks for all the times you sorted out my computer problems. Harry the consummate academic. You set me straight early on in the project and I never looked back. I have more faith in myself at this point you will be glad to know. Thanks to you both!!

- My final year students who inspire and challenge me constantly and in particular those who assisted me during the flow visualisation studies.

- The Technical staff of the Mechanical Engineering Department at Dublin City University with whom I have a particular affiliation. Thanks for endless support and advice over the duration of this work it was much appreciated.

- The CFD Engineers at Fluent Europe and the staff of the Pharmaceutical Companies visited during this project for their assistance and advice during this work.

Abstract

Title: Pharmaceutical Water Systems and the 6D-Rule
A Computational Fluid Dynamics Analysis

By

Brian G. Corcoran (C.Eng. MSc.)

The problem of piping system dead-legs are frequently encountered in high purity water systems throughout the pharmaceutical and semi-conductor industries. The installation of a pipe tee in sterile process pipework often creates a stagnant dead-leg zone which can result in the formation of bio-film and compromise the entire system. Considerable basic research is required to address the lack of understanding of this problem and to assist during design, manufacture, installation and operation of these critical systems. This study involves the application of CFD (computational fluid dynamics) techniques to the study of turbulent flow in Pharmaceutical pipe tee-junctions.

Numerical models have been developed to initially study divided turbulent flow in a range of standard Pharmaceutical tee-junctions and then to study dead-leg flow. Numerical predictions were compared with previously presented experimental results based on Laser Doppler Velocimetry. Turbulent models such as the $k-\varepsilon$ and Reynolds Stress model (RSM) were used to analyse the flow. Dye injection studies highlighted the lack of penetration of the dead-leg and complex branch flow patterns for both sharp and round entry tees. Hydrogen bubble techniques gave clear evidence of the presence of a slow rotating vortex at entry to each branch and the presence of stagnation zones throughout the dead-legs.

The effect of mainstream velocity and loop to branch ratios on dead-leg flow patterns was analysed. Stagnation zones were identified within each branch and the presence of a slow rotating cell within the dead-leg resulted in a lack of exchange of mainstream fluid from the distribution to the branch. The 6D-rule was found to be industrially irrelevant. 1 to 2D configurations should be used to avoid stagnation. No configuration resulted in high wall shear stress within the branch and a reduction in branch to loop diameter increased branch stagnation. There was no evidence of exchange of fluid between the loop and branch and all configurations had some quiescent (dormant/inactive) water.

Table of Contents

List of Figures

List of Tables

No tables used in this section

NOMENCLATURE

CFU	Coli Forming Unit
WFI	Water For Injection
GPH	Gallons per Hour
USP	United States Pharmacopeia
DI	Deionised Water
CFD	Computational Fluid Dynamics
LDA	Laser Doppler Anemometry
PIV	Particle Image Velocimetry
Vpart	Particle Velocity
Vfluid	Fluid Velocity
RO	Reverse Osmosis
CDI	Continuous Deionisation
LVP	Large Volume Parenterals
CFR	Code of Federal Regulations
GMP	Good Manufacturing Practice
cGMP	Current Good Manufacturing Practice
FDA	Food and Drug Administration
PI	Pressure Indicator
FCV	Flow Control Valve
CIP	Cleaning in Place
SIP	Steam in Place
k	Turbulent Kinetic Energy
ε	Turbulent Dissipation Rate
μ_t	Turbulent Viscosity
P	Pressure
Re	Reynolds Number
I	Turbulent Intensity
l	Turbulent Length Scale
L	Characteristic Length
$\theta_{\min}$	Smallest face/cell angle
$\theta_{\max}$	Largest face/cell angle
θ_e	Angle for equiangular face/cell
Cf	Skin Friction Coefficient
y	Distance in the y-plane
x/d	Normalised Distance in the x-direction
y/d	Normalised Distance in the y-direction
$\frac{1}{7}$ Power Law	$\frac{U}{U_{\max}} = \left(\frac{R-r}{R}\right)^{\frac{1}{7}}$
$\frac{U}{U_{\max}}$	Normalised Velocity
$\overline{\rho u_i' u_j'}$	Reynolds Stress
δ_{ij}	Kronecker Delta

ρ	Fluid Density
$\mu\left(\frac{\partial u_i}{\partial x_j}+\frac{\partial u_j}{\partial x_i}\right)$	Rate of Deformation of a fluid element
$\frac{\partial}{\partial t}(\rho k)$	Rate of change of k
$\frac{\partial}{\partial x_i}(\rho u_i k)$	Rate of transport of k by convection
$\frac{\partial}{\partial x_i}\left(\frac{\mu_t}{\sigma_k}\frac{\partial k}{\partial x_i}\right)$	Rate of transport of k by diffusion
$G_k + G_b$	Production terms
P_{ij}	Rate of production of Reynolds Stress
ϕ_{ij}	Transport of Reynolds Stress by Pressure/Strain interaction
ε_{ij}	Rate of Dissipation of Reynolds Stress
J_{ijk}	Turbulent Diffusion
k	Von Kormans Constant = 0.42
E	Empirical Constant = 9.81
Up	Mean Fluid Velocity at point P
kp	Turbulent Kinetic Energy at point P
yp	Distance from point P to the wall
μ	Dynamic Viscosity
τ_w	Wall Shear Stress
y_v	Viscous sublayer thickness
y^+	Normalised distance to wall
v	Kinematic Viscosity

CHAPTER 1. INTRODUCTION AND LITERATURE SURVEY

1.1 PHARMACEUTICAL WATER.

Water is the blood of the pharmaceutical industry. Every manufacturing facility requires it and its quality is critical to virtually all pharmaceutical production processes. Each water system is dynamic and unique. Understanding a water purification system (figure 1.1) requires knowledge of many disciplines including chemistry, physics and microbiology and also fluid dynamics, materials and instrumentation. Maintaining control over purified water systems can be a daunting task and one that typically involves a multi-disciplined approach [Anon, 1994. Cross, 1997].

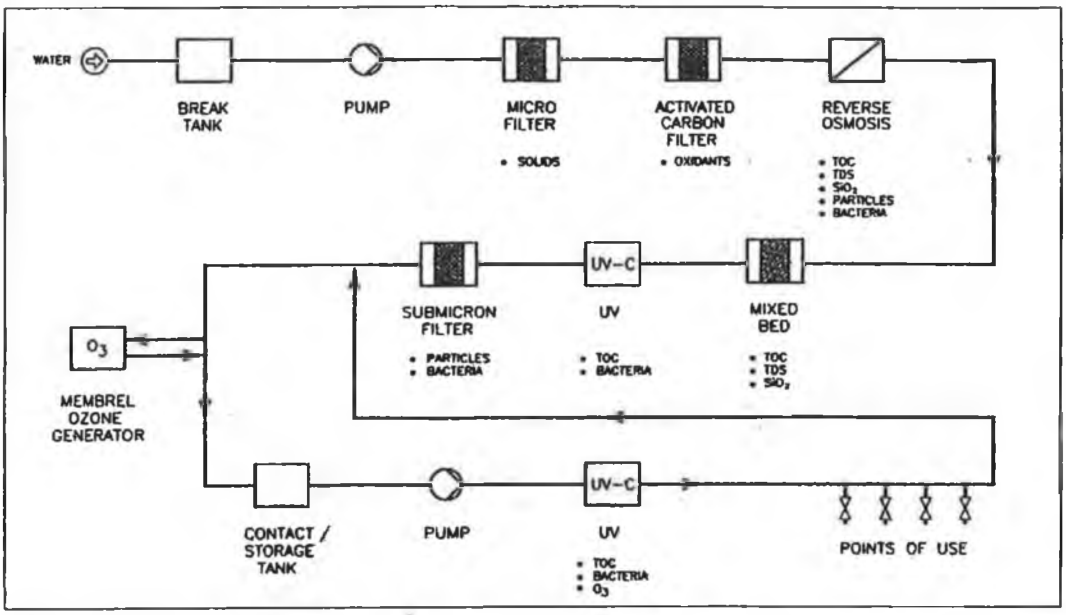

Figure 1.1: A typical pharmaceutical water purification system

The design, construction, commissioning and validation of pharmaceutical water systems offer significant challenges for manufacturers, equipment suppliers and system operators. The cost of bringing these systems on line has been continuously rising in recent years, in some cases due to conservative system design approaches. One reason for this over design has been inconsistent interpretation of regulatory requirements. This has resulted in unnecessary facility capital and operating expenses, inefficient systems and in some cases complete over design of the entire system [Nickerson, 1990. Keer, 1995].

Although this thesis will concentrate on pipe dead-legs and their impact on high purity water systems, a short introduction to the technology of water purification and system distribution will set the background for detailed analysis of dead-legs, their configuration and the detrimental effect they can have on purified water systems.

1.2 HOW PURE IS OUR WATER?

Waters encountered in nature are hardly pristine in purity. Having had contact with their surroundings, they have leached and dissolved minerals and salts from the earth and rocks they have encountered. Falling as rain they have scrubbed various gases from the atmosphere. As runoffs and streams they have picked up and carried a wide variety of additional impurities. Natural water serves to nurture organisms, bacteria and viruses. These waters require purification into high purity waters before use in any pharmaceutical or semi-conductor processes [Gagnon, et al. 1994. Anon, 1994. Cross, 1997.Nykanen, et al. 1990]. The quality of water used in any pharmaceutical process should be sufficient to obtain the required quality specified by the regulatory bodies for the final drug product.

This specification is usually outlined in what the industry calls the Drug Master Plan. Pharmaceutical water uses can be categorised as:

- A dosage form ingredient
- For manufacture of Bulk Active Pharmaceutical Ingredient (API) or Bulk Pharmaceutical Chemical (BPC)
- Equipment washing, flushing, cleaning or rinsing

Water intended for use as a dosage form ingredient **must be USP monograph water** and must be produced consistently to this specification. Specifications for water used as an ingredient (exclusive of sterile bulks) in the manufacture of API's and BPC's must be determined by the manufacturer based on the potential for contamination of the final drug product [Mc William, 1995]. Non-compendial pharmaceutical water (including drinking water) may only be used for washing, cleaning and rinsing once strict microbial alert and action levels have been established. US Pharmacopoeia (USP) recommended action limits, which are used to alert manufacturers to impending purification problems, are outlined in table 1.1.

Pharmaceutical Water	***USP Action Limit***
Water for Injection	10cfu/100ml
Purified Water	100cfu/ml
Drinking Water	500cfu/ml

Table 1.1: US Pharmacopoeia Action Limits for Pharmaceutical Water

Guidance on establishing specification for monographed USP water is provided in the United States Pharmacopeia (USP). This specification was initially recognised in the Drugs and Medicines Act of 1848 which made reference to the USP for standards of strength and purity. In 1906 the Food and Drugs Act designated the USP as the source of standards of strength, purity, and quality of medicinal products. Since then the USP has continued and extended its recognition as the official compendium. The USP includes monographs for Purified Water (PW), Water for Injection (WFI) and a range of other waters used in the production, processing and formulation of pharmaceutical products. [Carmody, et al. 1989. Burns, et al. 1998].

1.3 cGMP COMPLIANCE ISSUES.

Current Good Manufacturing Practice (cGMP) recognises that all systems in a pharmaceutical facility require some form of commissioning, validation and qualification [Weitnauer, 1996]. Inconsistent interpretation of cGMP requirements as applied to high purity water systems can result in over-conservative design and lead to contamination problems. In any water system there are certain fundamental conditions that can always be expected to cause problems of a microbial nature [Cross, 1997]. These include system and pipe-work designs which result in stagnant conditions, areas of low flow rate and poor quality supply water. Some basic measures that have been shown to alleviate such problems are:

- Continuous turbulent flow
- Smooth clean internal surface finish
- Frequent flushing, draining and sanitizing
- Flooded, continuously re-circulating distribution pipe-work

1.4 PRETREATMENT PROCESSES

The preparation of water of the qualities required for applications in the pharmaceutical and semi conductor industries is generally divided into three stages: pretreatment (figure 1.2), principal purification and polishing or point-of-use treatment. The principal purification process is generally one of a combination of ion exchange, reverse osmosis or distillation [Huchler, 2002. Cartwright, 1999].

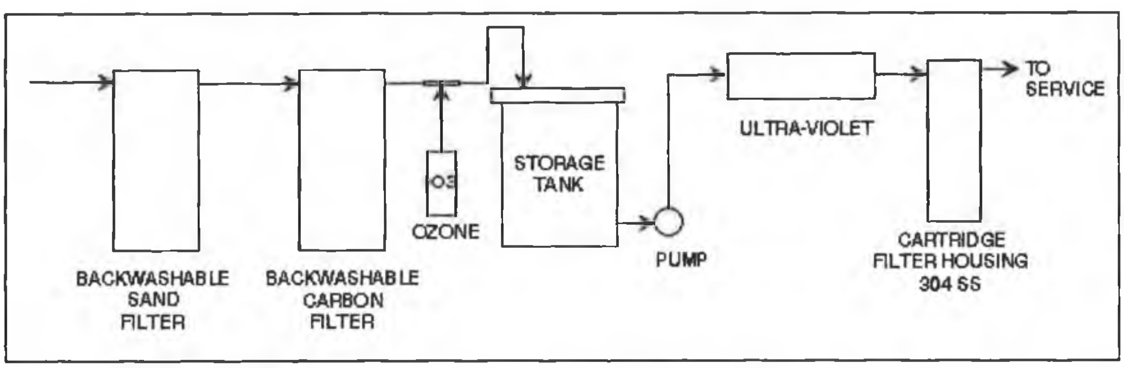

Figure 1.2. Water Purification Pretreatment Processes.

To render the principal purification process practical in economic terms, pretreatment of the source water is always required. Pretreatment generally deals with higher levels and quantities of impurities than principal purification/polishing processes and it is used to protect and extend the service life of final treatment units. There is no single right or magic answer to the process design of pretreatment system. Rather the pretreatment system process design is a series of choices and options, each with advantages and disadvantages. Pharmaceutical pretreatment processes may include some or all of the following processes:

1.4.1 *Chlorination*: Water is chlorinated to control microbial growth. Chlorine is added to a water supply until a residual concentration of 0.5 to 2 ppm is achieved [Muraca et al. 1990]. Chlorine is usually added to water directly as a gas from storage cylinders. However the use of liquid hypochlorite solutions avoids the hazards associated with gas cylinders. Carmody and Marthak (1989) in dealing with an IBM high purity water system utilised sodium hypochlorite as a source of chlorine. Chlorine combines readily with nitrogen in cellular proteins and renders itself toxic to microbiological organisms. Following chlorination water is generally treated to remove suspended solids.

1.4.2. Deep Bed Filtration: Sand bed filters are used to remove total suspended solids. These filters must be capable of accommodating large volumes of suspended material, prevent the passage of suspended matter and hold the retained solids so loosely as to be amenable to easy cleaning by backwashing (figure 1.3). Deep bed filters serve as havens where organisms can proliferate. Chlorination prior to entry to these filters serves to keep them sanitised. Silica sand is the most commonly used medium for constructing deep bed filters [Ogedengde, 1984].

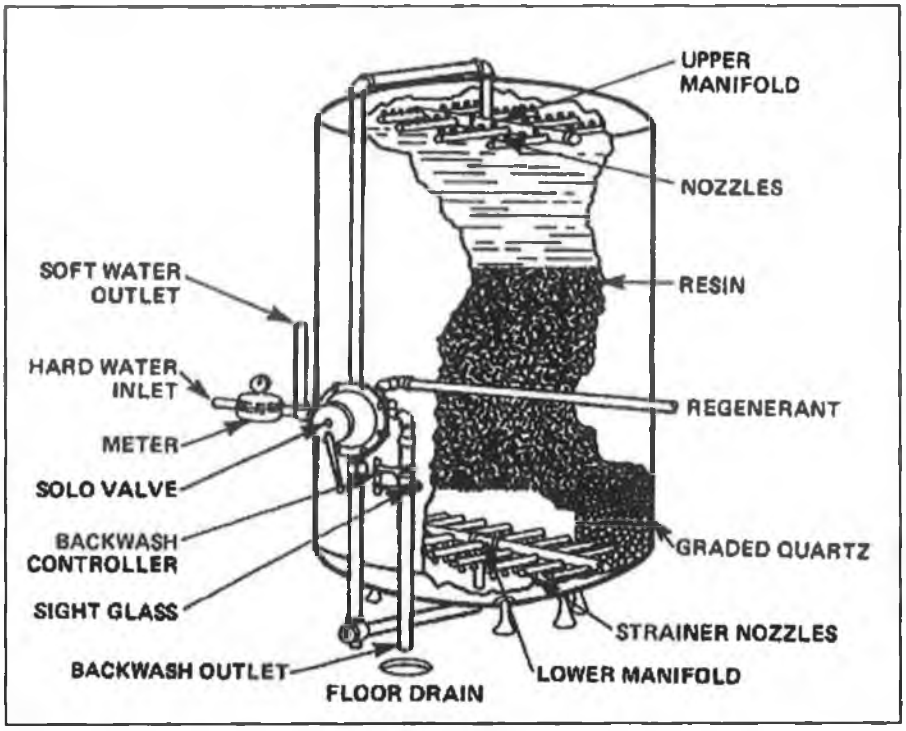

Figure 1.3: Deep Bed Filtration Pre-treatment Equipment

Adin and Hatukai (1991) offer models for optimisation of deep bed filters which serve as a substitute for the commonly performed empirical pilot plant studies.

1.4.3. Removal of Hardness and Metals: Essentially, water hardness is due to the presence of calcium and magnesium ions. Water softening (ion exchange which removes divalent and trivalent ions and replaces them with sodium) is a very common process used in the pretreatment of pharmaceutical water. This technique of Ion Exchange is well understood and easy to operate, it is applicable to all flow rates and to all levels of hardness. It involves the handling of only salt and produces a non-hazardous waste stream [Drimal, 1990. Harries, 1991]. However the water softening operation provides an opportunity for the invasion of the water system by micro-organisms due to the use of Brine for regeneration [Weitnauer, 1996]. Brine itself is not a sanitiser and the brine make-up tank serves as a haven for organism proliferation. The addition of calcium or sodium hyprochlorite was found by Weitnauer to greatly reduce the growth rate of such organisms.

1.5 FINAL TREATMENT AND POLISHING

Various unit operations and systems exist for the manufacture of both compendial USP purified water and water for injection. A brief description of these systems is now presented with the emphasis on the critical operating parameters. These systems included Ion Exchange, Continuous Deionisation, Reverse Osmosis and Distillation [Nykanen, et al. 1990].

1.5.1. Ion Exchange: The purpose of ion exchange equipment (figure 1.4) in purified water systems is to satisfy the conductivity requirements of USP 23. Deionisation (DI) systems are often used alone or in conjunction with reverse osmosis to produce pharmaceutical grade purified water. As water passes through the ion exchange bed, the exchange of ions in the water stream for hydrogen and hydroxide ions held by the resin occurs readily, usually driven by a concentration gradient. These systems are available in various configurations which include two-bed DI and mixed-bed DI units [McGarvey, 1990]. A two bed ion exchange system includes both cation and anion resin tanks. Mixed bed systems are typically used as secondary or polishing systems [Harries, 1991].

Figure 1.4: Ion Exchange Equipment.

These systems consist of a single tank with a mixture of anion and cation removal resins. Table 1.2 outlines the advantages and disadvantages of deionisation systems.

ADVANTAGES	DISADVANTAGES
Simple in Design and Operation	High operating cost
Flexible during high demand	Requires chemical handling on-site
Excellent upset recovery	High floor space
Low capital cost	DI vessels are breeding grounds for microbes

Table 1.2: Advantages and disadvantages of Ion-Exchange water purification systems

1.5.2. Continuous Deionisation: This method of water purification uses ion exchange membranes, ion exchange resins and electricity to purify and deionise water by continuously separating ions form a pretreated feed water stream. Feed water enters diluting and concentrating compartments in parallel where the anion and cation exchange resins capture the dissolved ions [Ganzi, et al. 1990]. This is a continuous process not requiring chemicals for regeneration of the ion exchange resins [Huchler, 2002].

The use of a direct current (DC) serves to motivate ions to move from the compartments containing resin into adjoining sections. Table 1.3 outlines the advantages and disadvantages of Continuous Deionisation systems.

ADVANTAGES	DISADVANTAGES
Simple in Design and Operation	Limited number of suppliers
Elimination of chemical handling	May require further bacterial reduction
Elimination of off-site regeneration	Requires RO pretreatment
Provides some bacterial control	Requires periodic sanitisation

Table 1.3: Advantages and disadvantages of Continuous Deionisation water purification systems

1.6 WATER FOR INJECTION

Purification options for the production of Water for Injection are limited by the USP monographs and they include only two production methods: Reverse Osmosis and/or Distillation [Mukhopadhyay, 1997]. Water for Injection would normally be use for the manufacture of parenteral, some ophthalmic and inhalation products. Although U.S. Pharmacopoeia allow the use of either method for WFI production, only Distillation may be used under current European regulations. USP water for injection monograph states that WFI should be produced from Drinking Water in accordance with conductivity and TOC substance limits and with no more than 0.25 Endotoxin units per ml. A microbial action limit of 10cfu per 100ml applies [Mukhopadhyay, 1997].

1.6.1. Reverse Osmosis: A typical Reverse Osmosis water purification system is presented in figure 1.5. This is a pressure driven process utilising a semi-permeable membrane capable of removing dissolved organic and inorganic contaminants from water. The membrane is permeable to some substances such as water while preventing the passage of most acids, bases, bacteria and endotoxins [Guan and Ding, 1999].

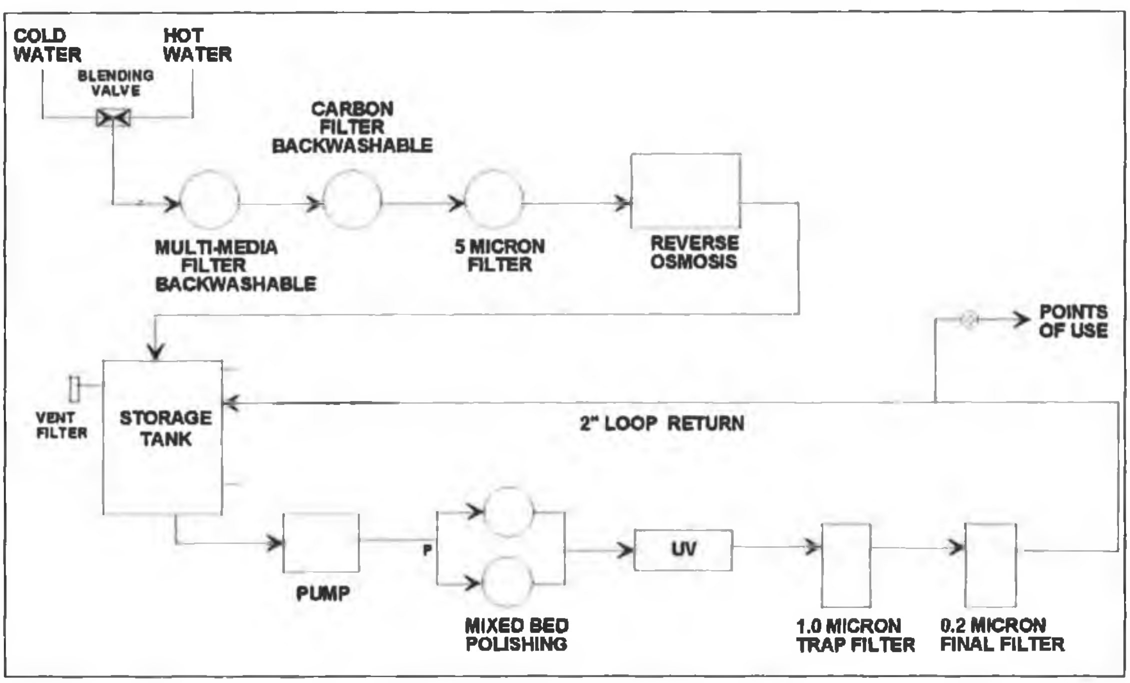

Figure 1.5: Final treatment Reverse Osmosis system

Single stage systems are only capable of reducing contaminants by 90 to 95% which does not meet the requirements for purified water treatment. Two pass Reverse Osmosis units are generally capable of producing water which meets the requirements of USP 23 for both TOC and conductivity [Weitnauer, et al. 1996 (b)]. Table 1.4 outlines the advantages and disadvantages of Reverse Osmosis systems [Joyce et al, 2001. Guan, 1999].

ADVANTAGES	DISADVANTAGES
More effective microbial control than ion exchange systems	Water consumption high
Elimination of chemical handling	Energy demands high
Simple integrity tests	Requires periodic sanitisation

Table 1.4: Advantages and disadvantages of Reverse Osmosis water purification systems

1.6.2. Distillation: The Pharmaceutical Still, chemically and microbiologically purifies water by phase change and entrainment separation. Water is evaporated into steam leaving behind dissolved solids, non-volatile substances and high molecular weight impurities. However endotoxins are carried with the water vapour and a separator is required to remove them before the purified vapour is condensed into Water for Injection [Kuhlman, 1981. Anon, 1995]. A variety of different still designs are available including single effect, multi effect and vapour compression . Table 1.5 outlines typical capacities and temperatures of water produced by each process.

	Single Effect Still	Multi Effect Still	Vapour Compression Distillation
Capacity (GPH)	1-100	25-3000	100-6000
WFI Temperature (C°)	35-100	35-100	Ambient

Table 1.5: Comparison of stills used in the production of Water for Injection

1.7 PHARMACEUTICAL WATER STORAGE AND DISTRIBUTION

Once the process water has been purified to the required standard it must be stored and distributed to various points of use within a plant (figure 1.6). The purpose of a storage system is to smooth out peak flow requirements in order to optimise the sizing and efficient operation of the water system components. The storage system must maintain and protect the feed water quality to ensure correct specification at each point of use.

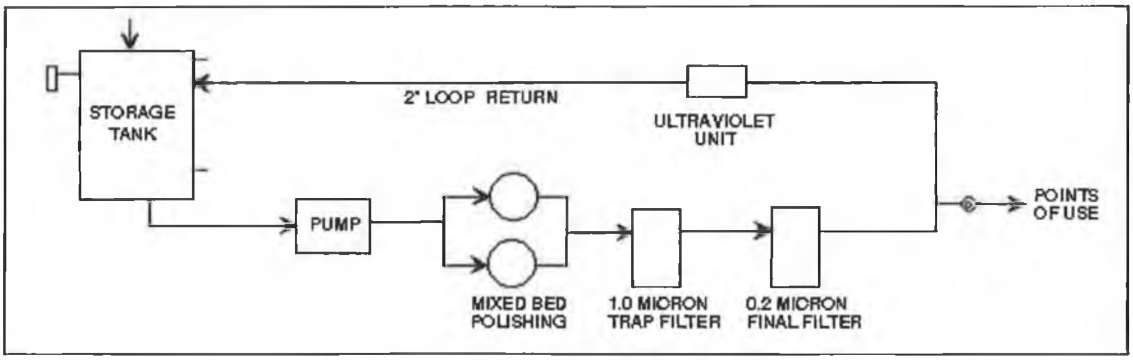

Figure 1.6: Purified Water Storage and Distribution

The advantage of a storage tank system over a tankless system is that it allows a smaller less costly pretreatment system which can operate closer to the ideal requirements of continuous dynamic flow. One disadvantage of the storage tank is it introduces a region of slow moving water that can promote bacterial growth [Youngberg, 1985]. Correct design of both the water storage and distribution system is critical to the success of any purified water system. Optimal design must accomplish three critical objectives:

- Maintain water quality within acceptable limits
- Deliver water to points of use at required flow rate
- Minimise capital and operating costs

As technology has improved in recent years many design features such as blanketing of storage vessels with nitrogen, constant circulation in the distribution loop, use of sanitary connections, the use of highly polished pharmaceutical grade tubing, orbital welding and the use of diaphragm valves have all contributed to increased control of water quality following final treatment. However such design features have led to ever increasing costs. A more reasonable approach would be to utilise design features based on sound engineering principles that provide the greatest reduction in contamination risk [Pitts, 1997].

1.8 DISTRIBUTION DESIGN CONCEPTS

Two basic concepts, referred to as batch and dynamic/continuous systems, have evolved for the distribution of pharmaceutical water [Mc William, 1995]. The batch concept utilises at least two storage tanks. While one is being filled, the other is in service providing water to various points of use. Only after testing to ensure compliance with

USP specifications is a tank put into service. The major advantage of this system is that the water is tested before use.

Figure 1.7: Dynamic/Continuous tank recirculation with hot distribution

The dynamic/continuous concept off-sets peak system demands utilising a single storage vessel which simultaneously receives final pretreated water and distributes it continuously to points of use. This type of system is usually operated as a hot distribution loop. Figure 1.7 above presents a photo of a typical dynamic/continuous tank re-circulating system. The major advantages of this system are less complex pipework, lower life cycle costs and more efficient operation.

Each of the above configurations vary in the degree of microbial control provided. Better microbial control is usually achieved by minimising the amount of time water is exposed to conditions favouring growth. Such conditions include circulation through the distribution loop at high temperature (above 65°C) and at turbulent conditions which is expected to provide better microbial control than stagnant systems. However areas of concern for hot loop systems include protection of workers from scalding, cavitation in the circulating pump, degradation of the tank vent filter and the formation of rouge. These systems are not without their problems. High purity water at high temperature is an aggressive solvent and is highly corrosive [Coleman and Evens, 1991]. Rouge, a colloidal form of rust can form on the inside of pipework leaching iron, chromium and nickel into the distribution network leading to product contamination. These agents are also highly carcinogenic. Hot systems also have the disadvantage of cooling the water to ambient temperature before use. Thus many systems operate an ambient storage and ambient distribution network as shown in figure 1.8 below.

Figure 1.8: Ambient temperature storage and distribution system

Microbial control is not as good with these systems as in hot storage configurations, however this may be improved provided sanitisation is conducted on a frequent basis. Cooling of the distribution loop may be required to prevent temperature increases due to heat build up from the pump and for cooling following sanitisation. Most pharmaceutical water users have found that storing and distributing water at ambient temperatures is both safe and cost effective [Self, et al. 1993. Tomari, 1997].

1.9 MICROBIAL CONTROL DESIGN CONSIDERATIONS

In any given water storage and distribution system there are certain fundamental conditions that can always be expected to aggravate a microbial problem [Sanders and Fume 1986. Nykanen et al, 1990 (a)]. Likewise, there are several basic measures that will tend to counteract such problems. Conditions likely to aggravate the problem include:

- Stagnant conditions and areas of low flowrate
- Temperatures that promote microbial growth
- Poor quality supply water
- Badly designed water treatment systems

Some measures used by the pharmaceutical and semi-conductor industry to alleviate such problems include:

- Materials of construction
- Continuous turbulent flow

- Smooth clean surfaces that minimise nutrient accumulation
- Frequent draining, flushing and sanitising
- Ensuring there are no leaks in the system
- Maintaining system positive pressure

1.9.1 MATERIALS OF CONSTRUCTION

High purity water is highly corrosive because it has been freed of Ions in the pretreatment processes. Deionised water has a neutral pH only at 25°C and as the water temperature rises the waters pH value drops below 7.0. Deionisation or even softening of water exposes the storage and distribution loop to a relentless corrosive attack [Lerman, 1988]. Because high purity water is chemically aggressive the choice of materials for distribution is highly important. In order to achieve high quality water at the point of use, the materials used in the storage and distribution systems must be carefully selected [Culter and Nykanen, 1988]. In the pharmaceutical industry stainless steels have been the material of choice. Semiconductor industries also use ABS, PVC and PVDF. Table 1.6 offers a comparison of materials of construction for storage and distribution systems [Yamanaka, et al. 1997; Balazs, 1996].

In general those found in regular use in the pharmaceutical and semi-conductor industry include 316L stainless steel tube and ABS plastic. 316L stainless is used due to the fact that it can be steam sterilized, requires little support and can be easily welded using an orbital welding technique which ensures an excellent internal surface finish. ABS is also in wide spread use due to the fact that it can be joined using solvent adhesives and its low cost. A major disadvantage is the number of support points required when used in high temperature applications. Because stainless steel pipes are rigid and its rigidity is unaffected by high temperature (80C) the number of support points required for long runs can be kept to a minimum. Thus the overall installation cost for stainless steel networks are much lower than for plastic pipe distribution networks [Pitts, 1997. Holden, et al. 1995].

	PVDF	**ABS**	**PVC**	**316L Tube**	**304L Tube**	**316L Pipe**	**304L Pipe**
Installed Cost	M	M	L	M	M	M	M
Steam Sanitisable	N	N	N	Y	Y	Y	Y
Susceptible to Rouging	N	N	N	Y	Y	Y	Y
Corrosion Resistance	H	H	H	H	M	H	M
Extractables	L	M	H	L	L	L	L
Thermal Expansion	H	H	H	L	L	L	L
Support Required	H	H	M	L	L	L	L
Joining Methods							
• **Triclamp**	Y	N	N	Y	Y	Y	Y
• **Solvent**	N	Y	Y	N	N	N	N
• **Fusion**	Y	N	N	N	N	N	N
• **Welding**	N	N	N	Y	Y	Y	Y

(H = High. M = Medium. L = Low. Y = Yes. N = No.)

Table 1.6: Comparison of Materials of Construction for High Purity Water Storage and Distribution Systems

1.9.2 TURBULENT FLOW IN PIPE DISTRIBUTION SYSTEMS AND PIPE TEES

Engineers have been involved in obtaining solutions to pipe flow problems where turbulence plays a major role for many years. Although advances have been made in relation to many turbulent flow problems, exact solutions have only been found for some simple cases. One of the most researched areas, due to its simplicity and more importantly its wide spread use, has been that of fully developed turbulent flow of single phase fluids in cylindrical pipes. These pipe systems form the backbone of all high purity water distribution systems and in conjunction with bends, tees, valves and a range of instrumentation aim to supply water at points of use at a given flowrate and to a specified quality [Mathews, 1994. Mc Williams, 1995].

A natural progression from the investigation of turbulent flow in cylindrical pipes would seem to be the analysis of flow in pipe tee junctions [Kottler, 1990]. At each point of use within a distribution network a tee junction is required to divert water from the re-circulating distributions ring main to a vessel requiring water through a high specification isolating valve (figure 1.9).

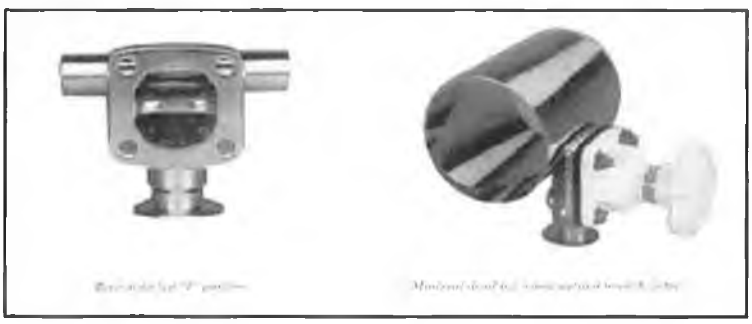

Figure 1.9: High Purity Water System Isolating Valves

Although many researchers have investigated these fittings there is still a considerable lack of understanding in relation to flow patterns and turbulent flow within them [Pop and Sallet, 1983. Hager, 1984. Bates, et al. 1995. Sierra –Espinosa, 1997]. Research related to pipe tee junctions can be traced back as far as Leonardo da Vinci and one would expect that these junctions would be well understood at least to the same level as fully developed pipe flow, but they are not. One area of agreement across current research is that the flow is highly complex. Another is that little published research exists in relation to turbulent flow in pharmaceutical pipe tee junctions and in particular to dead-leg flow configurations. Much of the current knowledge in relation to tee-junctions has evolved from extensive studies related to U-bends and 90° bends [Monson, et al. 1990].

Most researchers to date have been interested in investigating divided flow through pipe [Chen and Patel, 1988. Sierra-Espinosa, et al. 2000(a and b)]. Under these conditions the fluid entering the tee junction is usually divided in some ratio between the straight through leg of the tee and the branch, which is usually at 90 degrees to the flow. Considerable research has taken place over the past decade in this area much of which concentrated on analysing flow patterns within the tee under various operating conditions. Recently with the advent of CFD techniques researchers have turned their attention to the application of various turbulent models and the validation of these models when applied to divided flow in tee junctions [Sierra–Espinosa, et al. 1997]. Laser Doppler Anemometry (LDA) and Particle Image Velocimetry (PIV) techniques have been used to great effect in the validation of results and the modification of models to ensure accurate prediction of flow problems related to tee junctions. However following extensive literature reviews the author has found little interest by researchers into considering what occurs when fluid is prevented from entering the tee due to the activation of an isolating valve placed in the branch line at the points of use. To date dead-legs have been seen as a biological problem with the assumption that once the 6D rule is adhered to, turbulence in the branch will take care of the rest.

1.9.3 SURFACE SMOOTHNESS AND ITS EFFECT ON CONTAMINATION

No surface has been found to be exempt from biofouling. Surface structure has been found to influence the rate of fouling only over the initial first few hours of exposure. In general, smooth surfaces were found to foul at a slower rate than rough surfaces. [Ridgeway, et al. 1985. Arnold, 2000. Block, et al. 1994. Tide, et al. 1999 Percival, et al. 1998].

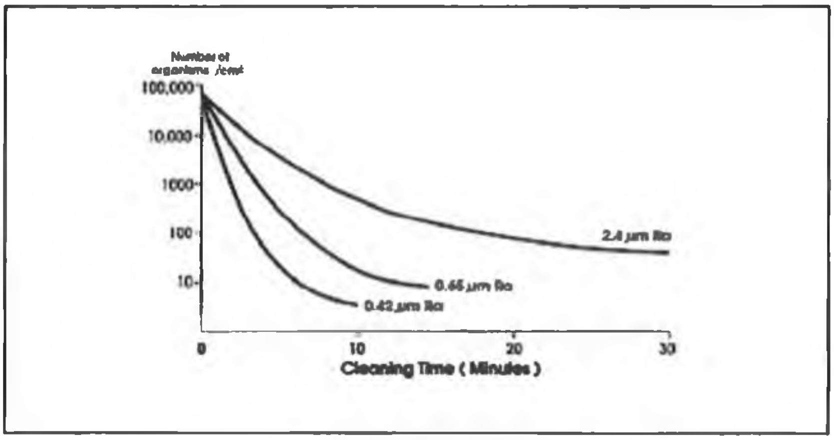

Figure 1.10: Effect of Surface Finish on Cleaning Time [Ridgeway, et al. 1985]

However the effect of surface smoothness has not found consistent experimental expression. Cooper (1987) states that surface smoothness does not affect biofilm formation and goes on to state; 'One cannot help but contemplate the efforts spent in recent validation programmes with the encouragement of 'experts' to assure that inside surfaces are smooth and polished'. Mittleman (1985) stated that 'although surface characteristics do influence biofilm structure, bacterial attachment does not appear to be significantly influenced by construction materials. Smoother surfaces delay the initial build-up of attached bacteria but do not appear to reduce the total number attached.' However for every group that say surface finish has little if any effect another group say it has a major effect [Arnold and Bailey, 2000].

Surface finish in the distribution loop is very important as crevices may prevent impurities being removed and rough surfaces are considered more encouraging to Bio-film formation. Care must be taken to ensure that mechanical finishing (polishing) does not trap impurities. Electro-polishing is considered to be best method of finishing for high purity water systems. Above all, the piping must preserve the purity of the water being conveyed by it [Vanhaeke et al. 1990]. No surface is exempt from bio-film formation and current information is confusing in relation to the effect of surface finish on bio-film formation. One suggestion is that it takes twice as long to clean 1.0 μm Ra stainless steel as it does 0.5 μm Ra. Some commentators suggest that less bio-film formation on distribution loops if mirror finished stainless steel (Ra less than 0.2 μm) is used but with little backup (figure 1.11).

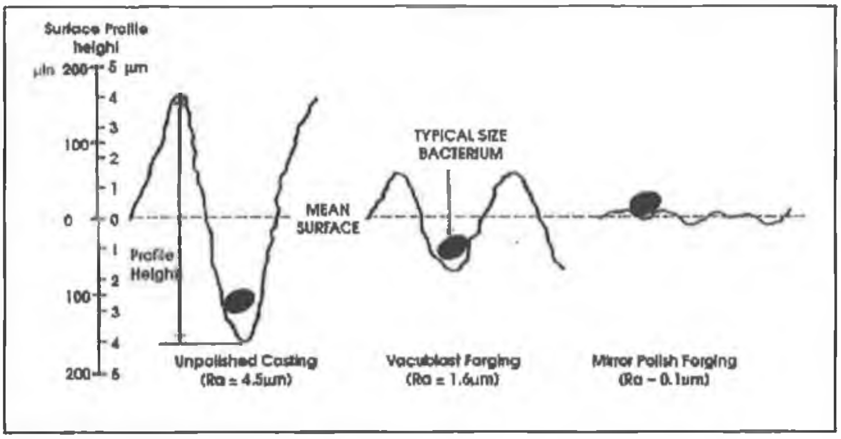

Figure 1.11: Comparison of Surface Finish with Size of Microbial Cell

It is the authors opinion that surface smoothness should have some influence as biofilm is a surface phenomenon. The rougher the surface the more biofilm has generally been found.

1.10 BIO-FILM: THE FIRST ACHILLES HEEL OF PURE WATER SYSTEMS

Biofilm is a layer of living and dead organisms. Their metabolic products and various organic and inorganic substances come to characterise virtually all surfaces in contact with water. This biofilm and its by-products can form rapidly and are the product of many different factors. Marshall (1992) cities evidence the Pseudomonas begins to form biofilm on the wall of pipe networks within one hour. This biofilm is 75% irreversible within 6 hours and is 90% so after 22 hours.

Biofilms are of interest in the present context because they intermittently shed bits and pieces of their structure into the contacting waters. As self-replicating entities, the shed organisms compromise the microbial integrity of the WFI and Purified Water systems [Okouchi, 1994]. When surfaces of water systems come in contact with water they immediately become coated by a layer of trace organics present in all systems. Small particle transport in aqueous systems involves mechanisms such as temperature dependant molecular diffusion, gravity effects such as sedimentation, chemotaxis (the movement of organisms in response to a nutrient gradient), along with flow effects due to laminar or turbulent flow. [Characklis, 1981. Camper, et al. 1994. Hunt, 1982]. Biofilm is one achilles heel of every distribution network and while current literature suggests it is impossible to eliminate, it must be kept to a minimum to ensure the integrity of the high purity water system [Husted and Rutkowski, 1991].

Transport of particles to surfaces and walls within pipe networks is a complicated process. There is considerable ongoing research in this field and some common ground has been found in relation to how particles are transported from the main stream flow to the pipe wall [McCoy and Costerton, 1982. El Din, et al. 2003]. Small particles (0.01 – 0.1 μm), similar to those found in high purity water systems, were found to be transported by turbulent eddies. It is suggested that these particles are 'propelled' into the laminar sub-layer by their own momentum and that the turbulent eddies supply the impetus. Frictional drag slow the particle as it approaches the wall and the drag force becomes proportional to the velocity of the particle less the velocity of the fluid ($V_{part} - V_{fluid}$). Neither viscous boundary layer effect nor eddy diffusion were found to be significant in transport of small particles to the wall than with larger particles (0.5 – 10 μm).

Cleaver and Yates (1973 and 1975) suggested the concept of 'Turbulent Bursts' as a means of explaining how particles penetrate the laminar sub-layer and deposit on the pipe wall. They believe that these turbulent fluctuations occur within the laminar sublayer driven there by turbulence within the main pipe flow. The residence time for particles at the wall was found to decrease with increasing shear stress.

1.10.1 EFFECT OF WATER VELOCITY ON BIO-FILM FORMATION

The effect of fluid velocity on biofilm and its formation on the inside wall of cylindrical pipes is still somewhat uncertain. Both the structure and induction time for formation have been found to be influenced by fluid velocity [McCoy and Costerton 1982. Corcoran 1996]. At high flowrates a denser more tenacious biofilm was formed. As a result these surfaces often appear to be free from foulants since they are not slimy to the touch. McCoy et al (1981) utilised low and high velocities to analyse biofilm formation. The low velocity induction phase, as measured by the frictional resistance of water flow, was found to be 20 hours and that of the high velocity to be 65 hours. In each case the occurrence of a firmly adherent filamentous bacteria in the biofilm was found. At high flowrates this became a permanent part of the biofilm only after the surface had acquired large amounts of extracellular material. Regardless of the water velocity it was found that the layers adjacent to the pipe wall favoured organism attachment. This region forms the laminar sub-layer of the flow and is a region of low shear stress a factor known to enhance biofilm formation.

Pittner and Berler (1988) investigated the shear force present in a semiconductor pure water distribution system and concluded that in none of their investigations were the shear forces strong enough to remove bacteria from the pipe wall . Patterson, et al. 1991 on examination of an IBM high purity water system found a marked difference between the results of a microbial assay sampled at a pipe wall and those drawn from the centre of the pipe. This constituted at least indirect evidence of the existence of biofilm and on removal of a pipe section for detailed analysis confirmation of this resulted. It is noteworthy that numerous Gram-positive isolates were found during this investigation which confounds the widely held belief that a lack of nutrients and a high Reynolds number will keep the walls clean. These organisms, unlike Gram negative, require significant sources of nutrients. It is a widely held belief that organism growth is diminished in flowing (recirculating) waters which is confirmed by the face that stagnant waters do yield higher numbers [Husted and Rutkowski, 1991]. Therefore to prevent or at least discourage bio-film formation areas of stagnation should be avoided where possible and turbulent flow encouraged to ensure high shear stress along pipe walls.

Researchers have found that increased flowrates have resulted in denser tenacious biofilm on the walls of pipes and that the structure and the induction time for deposit formation are influenced by changes in velocity. Bacteria where found to favour deposition on the inner surface of bends were decreased velocities and lack of turbulence are prevalent. This is one reason why the regulatory bodies insist on continuous recirculation of water in the distribution loop. Huster (1991) found little advantage in recirculation velocities above 0.9m/sec. The decrease in growth is attributed to the fact that the biofilm becomes highly hydrated and at high velocities is compressed making it difficult to dislodge and confining bacteria to limited areas of the distribution loop.

1.10.2 BIOFILM REMOVAL FROM DISTRIBUTION SYSTEMS

Given the ubiquity and persistence of biofilm, there is considerable interest in how to remove it. To date there is no unanimity regarding how this can be done, nor indeed that it can actually be achieved. Sanitization techniques are seen to operate primarily against planktonic organisms, those that break loose from the biofilm. This method may reduce populations in the outer-layer of the film but in the deeper layers many organisms remain protected and therefore remain free to assert themselves over time [Holden, et al. 1995. Martyak, et al. 1993].

Mittleman (1985) advises that, contrary to popular belief, hydrogen peroxide is effective against free floating organisms but is far less effective against those enclosed in the biofilm. McCoy (1987) lists in Table 1.7 below the relative effectiveness of various physical methods in removing biofilm from surfaces. Flushing, one of the most common and simplest methods, has limited effectiveness. However, the rapid rates employed are viewed as compressing the existing biofilm and by this densification of the film minimise the release of planktonic organisims. Backwashing is used on loosely adhered biofilm on filters and deep beads. Sand blasting was found to be difficult to control and may be too abrasive for some pipe wall materials. One of the most effective methods employed in the industry was found to be brushing. This method offers the best results and although by many it is seen as too expensive and time consuming it is often employed for treatment of dead-leg branch cleaning.

TECHNIQUE	COMMENTS
Flushing	Simplest/ Limited effectiveness
Backwashing	Effective on loosely adhered films
Air Bumping	Limited use
Abrasive and Non abrasive balls	Effectively used throughout industry
Sand Scouring	Difficult to control abrasive effects
Brushing	Expensive but very effective

Table 1.7: Physical Methods Used to Clean Biofilm Deposits from Surfaces

Pittner (1988) noted that 85 –90% of particles present in distribution loops are bacteria or fragments of bacteria. There is little agreement within the industry as to the source of these bacteria following pretreatment processes such as RO and CDI. Pittner suggests that they are in the system prior to assembly and that they are prolific reproducers. It is now known that Biofilm are layers of living and dead organisms [Marshall, 1992]. Their metabolic products and various organic and inorganic substances are all trapped within a polymeric matrix. They are found to develop rapidly. For example Pseudominas are found in water systems within one hour. If untreated they are found to be 75% irreversible within 6 hours and 90% irreversible within 24hours [Cloete, et al. 2003. Hallam, et al. 2001].

Virtually all bacteria isolated from purified water are gram negative rods which in biological terms means they are Pathogens. Pittner noted that the adhesive force of these bacteria (or Biofilm) exceeds the shear force placed on them by the fluid within the laminar sub-layer by a factor of 100. He also pointed out that the widely held opinion that high loop velocity results in clean pipe walls is a fallacy. Increasing or decreasing the flow velocity did little more than cause fluctuation of the thickness of the laminar sub-layer. However some researchers believe that Biofilm is minimised when operating between 1 – 1.2 m/sec [McWilliam, 1995].

Some confusion also persists in industry in relation to whether the continuously re-circulating water in the distribution loop should be hot or cold [Nobel, 1994]. Ambient temperature water systems are breeding grounds for bacteria and some experts suggest chilling the loop water to below 8°C decreases growth. Prior to 1976 Good Manufacturing Practice suggested that high temperature re-circulation be used particularly for Water for Injection processes. These systems operate a loop temperature of 80°C. A commonly held belief is that once this high temperature was removed that its protective influences vanished. Another problem is one of operating cost. Water in these loops must be cooled before use. This is usually achieved using refrigerated heat exchangers.

1.11 DEAD LEGS: THE SECOND ACHELLIES HEEL OF WATER SYSTEMS

Any unused portion of pipe connected to another pipe through which water is flowing may contain relatively quiescent or stagnant water. This non-flowing water is of major concern in pharmaceutical water systems because of the higher planktonic organism counts found in such water systems. These unused sections of pipe are formally known as ***system dead legs (figure 1.12).***

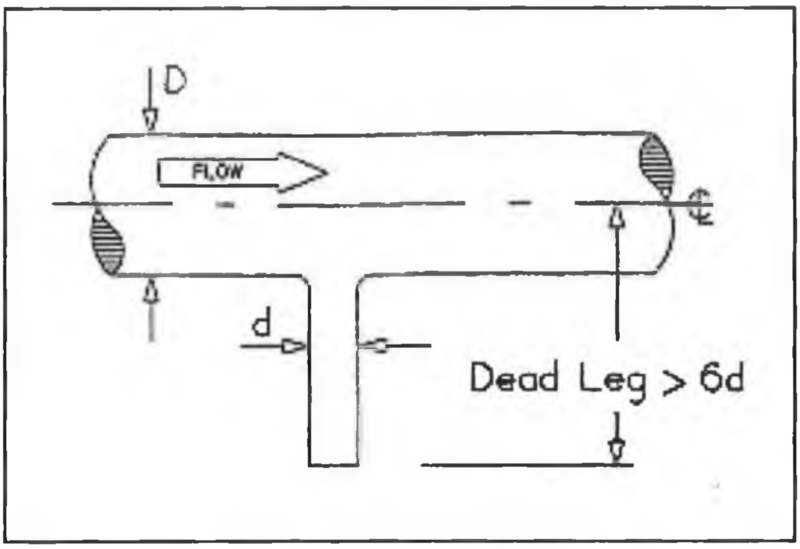

Figure 1.12: Classic Dead Leg Configuration

This term has been extended to any section of non-flowing water during a stagnation period, even if the stagnation period is not continuous. This situation is further complicated when thermometer wells, filter housings and various other fittings and instruments are placed into the water distribution loop which is carrying highly purified water (Figure 1.13). The presence of such fittings may create channels whose dimensions may result in dormant or inactive quantities of water which compromise the quality of the purified water once it enters the distribution loop. ***When applied to purified water systems, GMP (Good Manufacturing Practice) suggests that dead legs should be minimised or eliminated where possible.*** In fact it is a common design practice to limit dead legs to 6 pipe diameters or less. This stems from the '6D' rule contained in the 'Good Manufacturing Practice Guide for Large Volume Parenterals (LVP) Section 212.49' of the Code of Federal Regulations CFR 212, 1976. This guide requires that,

> *'Pipelines for the transmission of water for manufacture or final rinse and other liquid components shall; not have an unused portion greater than six diameters of the unused portion of pipe measured from the axis of the pipe in use'.* (See Figure 1.12 above)

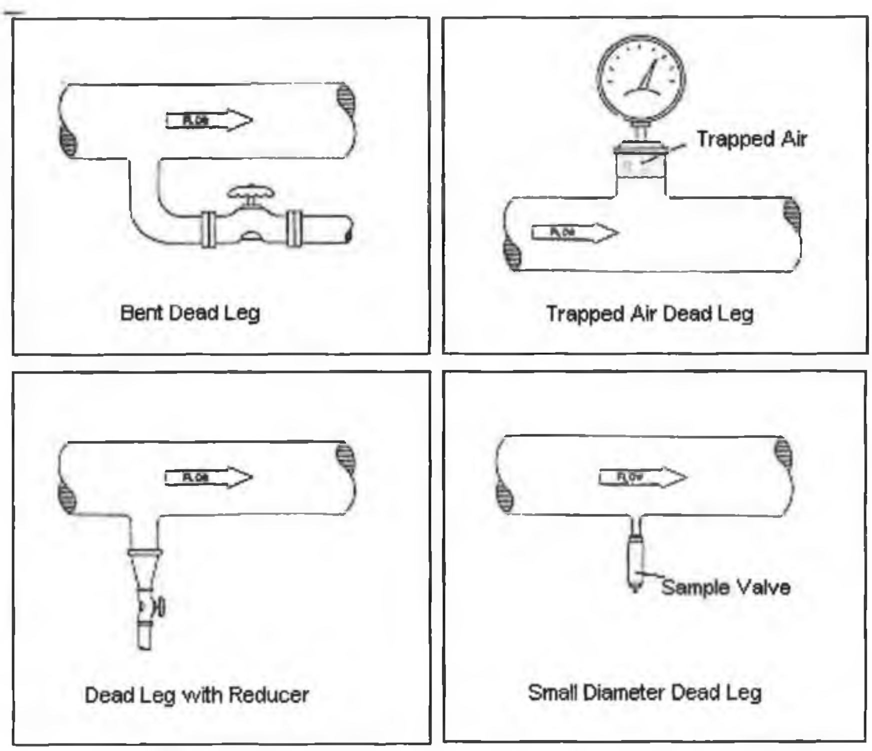

Figure 1.13: Various Dead Leg Configurations

1.11.1 Industry Confusion: Dead legs are an often misunderstood problem. As stated previously Good Manufacturing Practice suggests that dead legs should be minimised or eliminated where possible. The FDA operate and encourage the use of the 6D rule. Recently, however, considerable confusion has arises during the application of this rule.

- Recently design engineers have suggested using ratios of 4 to 1 or even 3 to 1 rather than the 6D rule as outlined and operated by the FDA (Food and Drug Administration).

- Additional confusion relates to the point from which the 6D rule is measured. Proponents of the 4D or 3D rules suggest that the length of the dead leg be measured form outer wall of the pipe. The original 6D rule measurers the distance form the centerline of the pipe to the end of the dead leg.

- Expensive Zero dead leg valves (similar to those presented in figure 1.9) have been designed and are frequently used in high purity water systems to address the issue of possible contamination. However the benefits of inclusion of such valves are not fully understood by system designers nor by FDA inspectors. A recent quote from an industry guideline documents indicates this:

  'If zero dead leg valves were replaced with less expensive valves with larger dead legs, one might consider increasing

the minimum circulation velocity to help compensate'

This quote suggests that by increasing the velocity across the top of the dead leg then some 'flushing' benefit will be gained within the dead leg. To date the author has seen no data to back up such a suggestion.

- Recent quotes from industrial experts suggest that to avoid confusion in the future that the length of a dead leg be considered from the outer wall of the pipe. Overnight this quote added further to an already misunderstood problem. By measuring from the wall of the pipe the original '6D' rule (measured form the centerline of the pipe) had become the '6D less one radius' rule, making the dead leg shorter.

Too address the above confusion a sentence was added to the FDA 'Baseline' guide on Pharmaceutical Water Systems stating that 'Good Engineering Practice requires that dead legs be minimised and that there are many good instruments and valves available to do so.' What they failed to include was that such instruments and valves are considerable more expensive and that they should only be included based on *sound engineering analysis* following *detailed investigation of the factors influencing flushing of dead legs.*

Industrial designers of water purification distribution loops, in order to comply with the regulatory bodies 6D rule, usually include drop loops in their designs particularly when faced with complicated piping runs. One such drop is presented in figure 1.14. This particular piping run is an extract from a system the author had the pleasure of working on in Ireland during the late 90's. The project required that a 2.7 million euro USP water purification system be designed, installed and commissioned for a Dublin based pharmaceutical company.

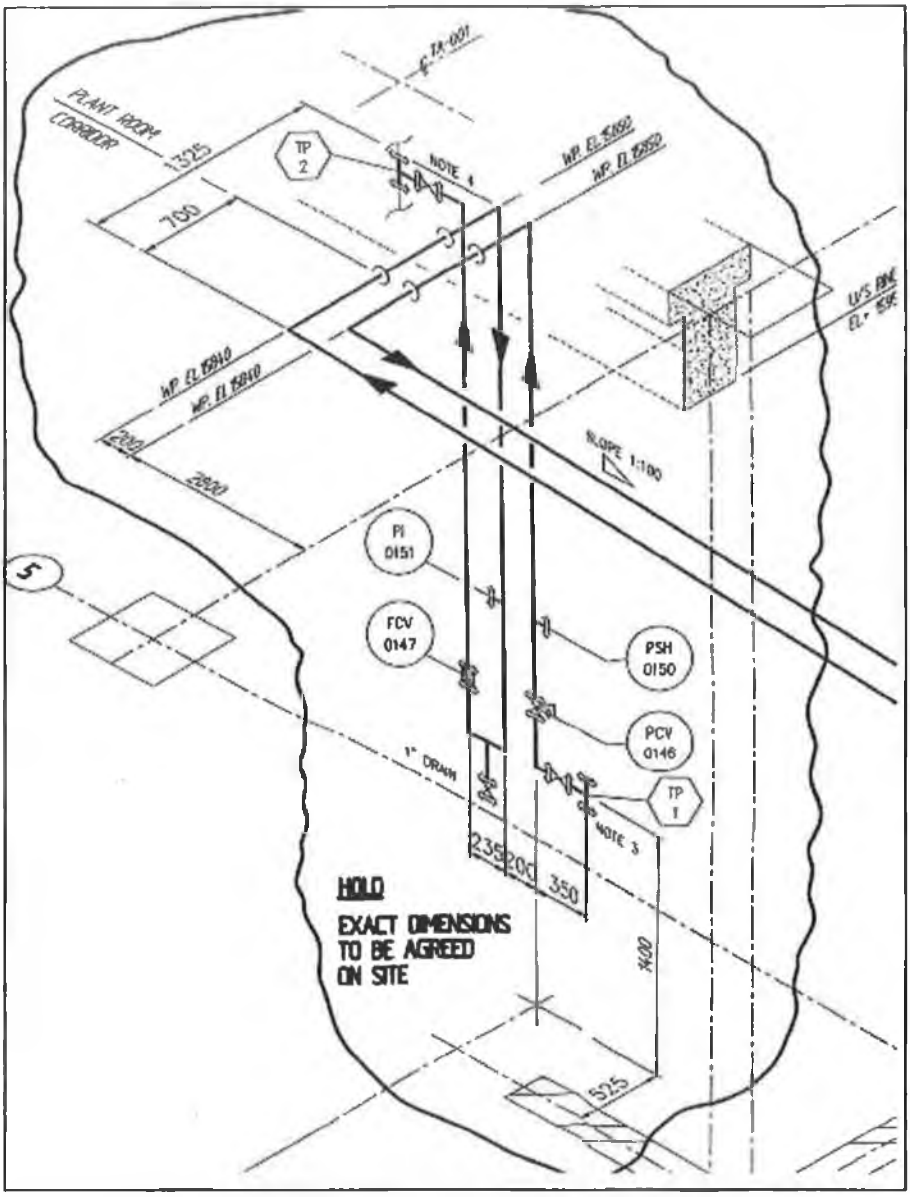

Figure 1.14: A typical industrial drop loop used to comply with the 6D rule

During the design phase of the distribution network it was necessary to include a number of drop loops in the system in order to comply with GMP regulations and the FDA 6D rule. It was at this point that the authors interest in dead-leg began. It was clear the designers were going to significant lengths to comply with the 6D rule. Hours were being spent routing pipes around existing installations in order to ensure compliance. Numerous attempts were made by the author to find publications on this topic. However these failed to produce any research of significant interest. Indeed the conclusion reached by the project team was that this was a rule-of-thumb rather than a sound engineering judgment. However failure to comply would leave the client open to citations and therefore it was better to be safe than sorry. One thing that was not discussed by the team was the considerable cost passed on to the client for the hour spent during the design and installation of the system complying with this 'rule-of-thumb'.

The loop presented in figure 1.14 was used to drop from an elevation of 15,850mm to 1400mm on a line distributing purified water to a production vessel. Compliance with the 6D rule is clearly visible between PI 0151 and FCV 0147 ensuring that the isolation valve between these two points fell well within the regulator guidelines.

It is not always possible to use a drop loop to full advantage. Figure 1.15 presents another piping run from the same project. During the design of this supply line it was clear that an array of existing pipework around the production vessel would prevent compliance with the 6D rule even with the use of a drop loop. Many hours were spent by the author, design engineers and draughts persons investigating methods to ensure compliance. Following days of research and reviews of other facilities with similar problems a decision was reached to install a flexible coupling between the production vessel isolation valve and the loop isolation valve. This immediately rendered the coupling a dead-leg which meant that special attention to cleaning and sterilisation of this section of pipework would be required under regulatory requirements and the client would be required by the regulatory authority to have documented evidence of compliance. This meant that the operators would have to implement a special SOP (standard operating procedure) and show records of performance over the lifetime of the installation. To assist the client with compliance a nitrogen supply was added to the coupling to allow blanketing of the section and a sample port installed at the tank isolation valve to allow microbial sampling of the water before every production run.

1.11.2 Continuously re-circulating distribution loops. The primary purpose of systems using a continuously circulating loop for purified water distribution is to reduce the chance of microbial growth and attachment to the surface of the pipe wall. It is generally believed that a velocity of 1.2 m/s or a Reynolds number between 10,000 to 20,000 will inhibit bacteria attachment [Vanhaecke, 1990] It is also believed that a turbulent condition (no figures given) is maintained in short dead legs if the length of the leg is limited to 6 branch pipe diameters.

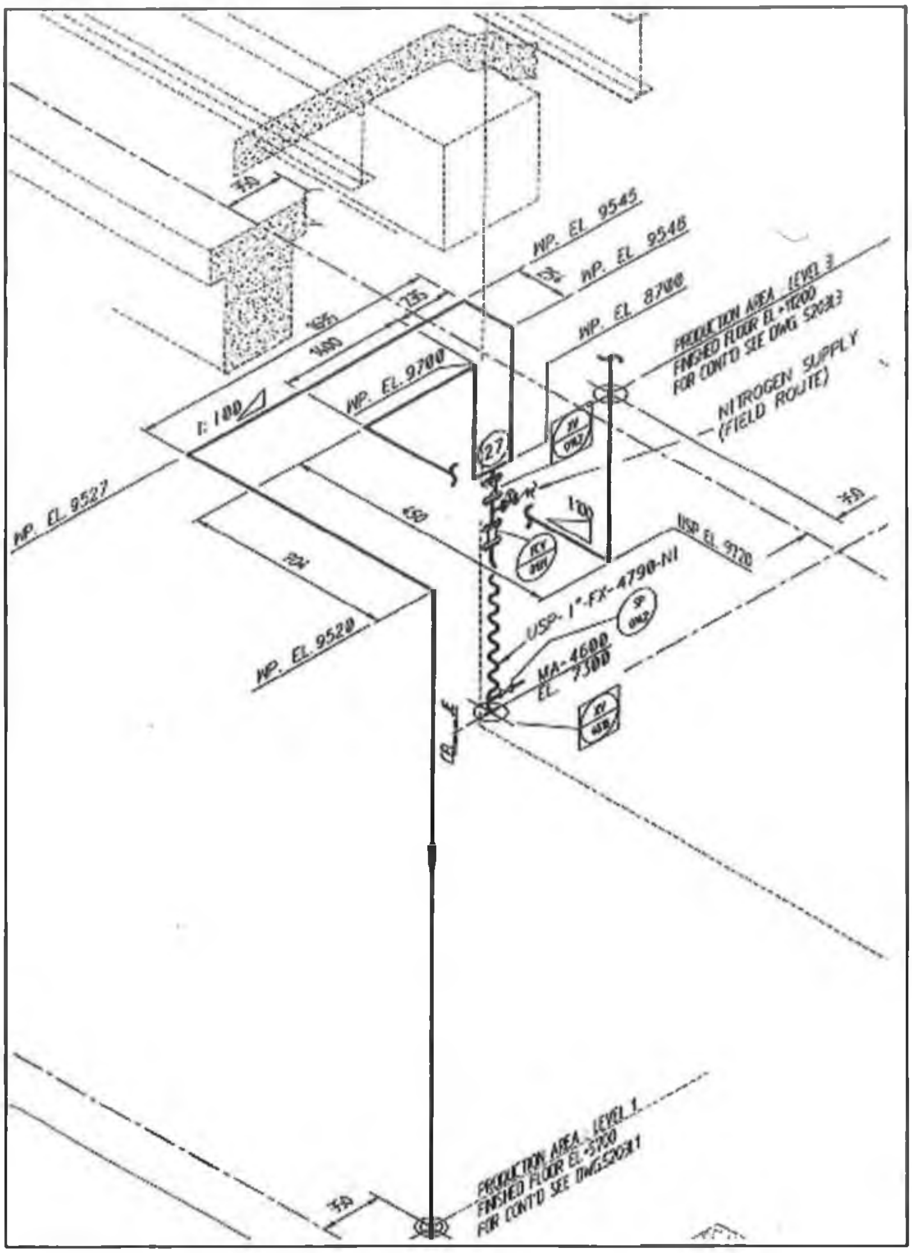

Figure 1.15: A modified industrial drop loop used to comply with the 6D rule

Husted (1991) suggested that flowing water would promote contact with and adsorption of organic material from the wall surface of a pipe. Given this outlook it is difficult to explain why dead legs should be conducive to organism growth. It is the authors view that the industry is assuming sufficient circulation and possible turbulent flow within the dead leg branch.

It is generally accepted that dead legs are particularly hazardous in high purity water systems as bacteria and contaminants accumulate in these areas [Young, 1993; Young, et al. 1995]. They are seen as difficult to clean, difficult to sterilise, as breeding grounds for microbes and following chemical cleaning they may retain chemicals creating a possible source of additional contamination. It is therefore recommended that the distribution loop circulate at a velocity of 0.8 to 1.2 m/s. It is *assumed* in the industry that at this velocity some benefit (be it flushing or prevention of Bio-film build up) will be achieved in dead legs up to the 6D rule. To date the author has found no valid information or research to back up this assumption. Many end users consider the 6D rule to be unacceptably high, particularly on critical processes and special adjustments are made which create minimal or even zero dead legs at points of use, particularly at the design stage, with little engineering justification for the additional expense incurred due to these modifications.

The 6D rule is an industrial guideline that emerged in the late 70's and which to date has not been placed on a well researched scientific footing. Typical guidelines for high purity water systems, extracted from Meyrick (1989), read as follows;

- Pipe networks in high purity water systems should be designed as a recirculating loops (figure 1.16). Long dead-legs should be avoided.
- Maximum length of dead-legs should be limited to 6 pipe diameters.

- Flow velocities should be in the range 1 – 1.2m/sec.
- The line supplying water to and returning from points-of-use must form a drop loop.

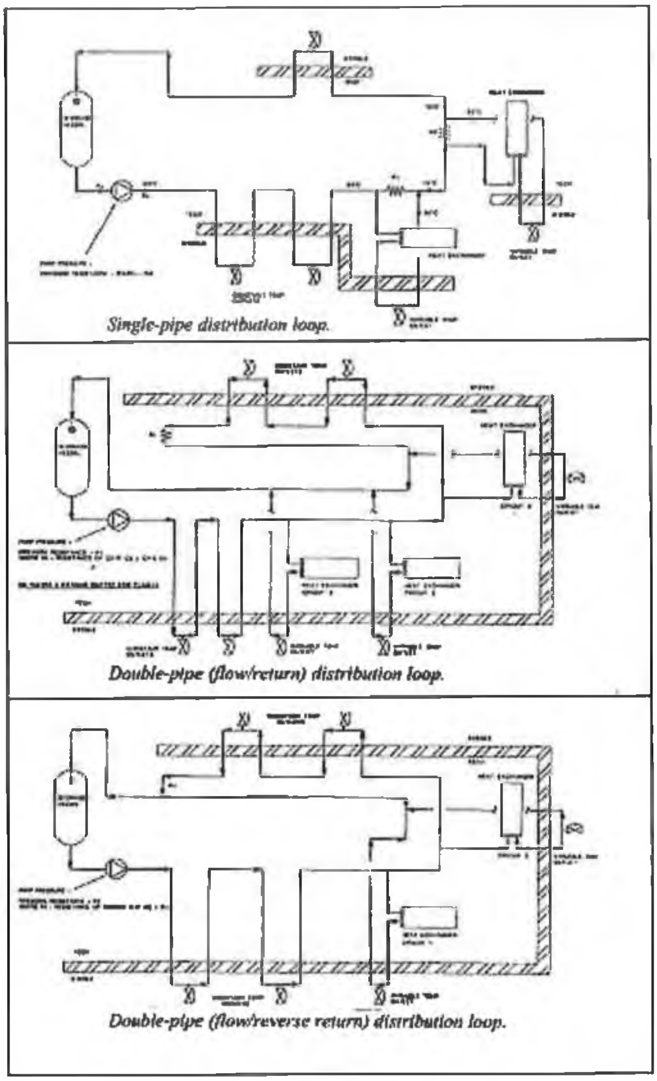

Figure 1.16: Various Configurations of a Purified Water Distribution Loop

Nobel (1994) attempted to put these guideline on a stronger scientific footing noting that dead-legs represent the weak point of these systems. He divided the dead leg into three regions. A turbulent zone, a free convection zone and a diffusive transport zone due to the fact that his analysis considered CIP (cleaning in place) on the dead-leg pipework. However he failed to address the underlying problem of how far into the dead-leg the turbulent action of flow within the distribution loop will penetrate. He suggested that at the entrance to the dead-leg one would expect that mixing created by turbulence would dominate and that at the end on the dead-leg one would expect stagnation. He suggested this without due consideration of the geometry of the tee or the implications of changing velocity within the distribution loop.

His analysis concluded by suggesting that the turbulent domain must occupy a large fraction of the dead-leg to allow the guideline of 6D to apply in practice. He noted that Seigerling (1987) suggested a guideline of 1.5D for dead-legs that are to receive CIP and noting that CIP must rely solely on turbulent transport to effectively clean dead-legs he concluded that the turbulent domain is circa. 2D in practice. Other conclusions include

- It should be expected that different types of fittings will have varying ability for turbulent transport into the dead-leg and that there is potential for improvement in transport through re-design.
- For CIP operations all dead legs should be insulated and those that cannot should be reduced to no more than 2D.
- Dead-legs should be kept as short as possible particularly during scale-up.

- When geometric similarity essentially remains the same increase the distribution loop velocity at least linearly with scale-up.

The FDA's recommendations in relation to dead-legs and the 6D rule has arisen from their observation that 'any drop or unused portion of pipework in the distribution loop has the potential for formation of bio-film and should be minimised were possible.' To date companies are assuming that dead-legs are resistant to the turbulent action of the main distribution loop and that following on from this assumption that the stagnant water found in these dead legs are breading grounds for bacteria. To avoid contamination of valuable product during production some companies continually dribble water from the dead-leg or install automatic timed valves to flush dead-legs before production starts. The result is a waste of expensive highly polished ultra pure water. Other companies assume that dead-leg stagnation is unavoidable and choose to disregard the problem running the risk of contaminated products and citations from the regulatory bodies.

It should be clear from the two loop drops presented in figures 1.14 and 1.15 that compliance with the 6D is far from easy. These designs incur cost from design and installation through to the end of the plants life cycle. These include design, installation and commissioning fees, additional pipework components (many of which are highly expensive), operating costs and daily testing and analysis all of which add up to numerous man hours over the life time of a project/plant. It is the author's opinion that considerable research into this problem will be of major benefit to the pharmaceutical and semi-conductor industry and that the work presented in the thesis will represent a corner stone on which further scientific research into this highly complex , multidisciplinary problem can be based.

1.12 OBJECTIVES OF THIS THESIS

The authors interest in the field began following a number of years working as a consultant engineer in the Pharmaceutical Industry in Ireland and Europe. During this time I had the pleasure of working on the design, installation and commissioning of high purity water systems. During the installation of one such system I noted that considerable time and effort was spent on compliance with the 6D dead leg rule. This particular installation was taking place in a compact area of a pharmaceutical plant which already had considerable quantities of pipe work and vessels associated with existing processes. The main difficulty was in routing of the distribution loop around existing plant while maintaining compliance.

During this time I began to investigate the 6D rule and found there was very little scientific detail related to the regulation. Indeed to date the author has found no significant research within this area and it is hoped that this thesis will encourage a multi-disciplined investigation of this problem that will lead to a better understanding of this area. Since the late 1990's the author at the school of Mechanical and Manufacturing Engineering at Dublin City University has been modelling flow in pharmaceutical pipework using state of the art commercial CDF codes. The main objective of this thesis is the investigation of loop flow velocity on Pharmaceutical pipe dead legs. This research offers the possibility to analyse interesting hydrodynamic problems such as separation, reattachment and reverse/backflow and discussion of these areas will be a key objective of this thesis. The experimental discussion will be based around the following areas of investigation

1) The fully developed region upstream of the tee junction
2) The entrance to the branch of the tee junction
3) Movement and patterns within the branch (dead leg)

The investigation will begin with a study of divided flow in a branch tee as most of the scientific and engineering data currently available is related to this field. The research will then concentrate on the move from divided flow (with the branch valve open) to dead-leg flow where the branch valve is fully closed. The effect of round and sharp entry tees will also be investigated along with the effect of reducing branch diameters on dead-leg configurations. Finally the results will be compared with two flow visualization techniques, a dye injection method and a hydrogen bubble technique.

CHAPTER 2. COMPUTATIONAL FLUID DYNAMICS

2.1 COMPUTATIONAL FLUID DYNAMICS AND COMPUTING

When industrial historians look back on the events of the latter part of the 20th century they may record that these were the decades which saw a revolution in the design of engineering equipment. The agent of this revolution was the digital computer and its ability to perform millions of calculations quickly and cheaply. In particular the design of process plant equipment has been greatly influenced by the recent advent of computational fluid dynamics.

Computational Fluid Dynamics or CDF is the analysis of systems involving fluid flow, heat transfer and associated phenomena by means of computer based simulation. The technique is very powerful and spans a wide range of industrial and non-industrial applications from lift and drag on aircraft to blood flow is arteries. From the early 1960's the aerospace industry had integrated CFD techniques into the design and manufacture of aircraft and jet engines. More recently these methods have been applied to design of internal combustion engines, gas turbines etc and CFD has become a vital tool in the design of industrial products and processes [Launder, 1989(b)].

All CDF codes are structured around a numerical algorithm used to model fluid flow problems [Daly and Harlow, 1970. Dhaubhadel, 1996]. These codes irrespective of supplier contain three main elements: a pre-processor, a solver and a post processor.

1) Pre-processor: The pre-processor consists of the input of a flow problem to the CFD program by means of a user-friendly interface and the subsequent

transformation of this input into a form suitable for the solver. Activities at the pre-processing stage include definition of the geometry (the computational domain), grid generation, definition of fluid properties and specification of boundary conditions [Matus, et al. 1999].

2) Solver: This is the numerical method used to solve the flow problem. The solver is used to approximate the unknown variables by means of simple functions, to discretise by substitution these approximations into the governing equations and to solve the algebraic equations.

One of the best understood and most highly validated techniques is the Finite Volume Method [Ferzieger and Peric, 1996] which is used by four of the five commercially available CFD codes namely FLUENT, PHOENICS, FLOW3D and STAR-CD. This numerical algorithm consists of the following steps:

- Integration of the governing equations of the flow field over the control volume of the solution domain.
- Discretisation of these integral equations into a system of algebraic equations.
- Solution of the algebraic equations by an iterative method.

3) Post-processor: This is a method of analysing and presenting data computed by the solver. Modern post-processing may include grid display, velocity plots, contour plots, particle tracking and animation.

2.2 TURBULENT FLOW AND CFD

Turbulent flow is a highly complex phenomenon. Although researchers have studied the phenomenon for many years, it is not yet possible to characterize turbulence from a purely theoretical standpoint [Thakre and Joshi, 2000. Bradshaw, et al. 1981]. Many important characteristics of turbulence are well-known and these include,

- Turbulence is time-dependent, three-dimensional, and highly non-linear.
- Fully-developed turbulent motion is characterized by entangled eddies of various sizes. The largest eddies arise from hydrodynamic instabilities in the mean flow field.
- The largest eddies break down into smaller eddies which, in turn, break down into even smaller eddies. This process of eddy break-down transfers kinetic energy from the mean flow to progressively smaller scales of motion. At the smallest scales of turbulent motion, the kinetic energy is converted to heat by means of *viscous dissipation*.
- The dynamic and geometrical properties of the largest eddies are closely related to the corresponding properties of the mean flow field.
- The time and length scales of the smallest turbulent eddies are many orders of magnitude greater than the time scales and free paths of molecular motion. As a result, the processes of viscous dissipation are statistically independent of molecular motion.
- Turbulent motion is not a random phenomenon. As a consequence, turbulent fields possess definite spatial and temporal structures.

For computers to provide accurate and realistic simulations of flow processes they must be supplied with a set of instructions which embody the implications of the conservation laws of momentum, mass and energy. While reliable computer programs are available for two dimensional and some three dimensional flows particularly for laminar flow situations, the same is not generally true for turbulent flow [Launder and Spalding, 1974. Guo, et al. 2002].

In principle there is no reason to adopt special practices for turbulent flow processes over laminar as the Navier-Stokes equations apply equally in both cases. The reason why this is not possible is that important details related to turbulent flow are small scale in character e.g. eddies responsible for the decay of turbulence in some flow problems are typically 0.1mm. To accurately calculate the equations of motion for such eddies is beyond the capacity of existing computers. Speziale (1991) states that the direct simulation of turbulent pipe flow at a Reynolds number of 500,000 requires a computer which is 10 million times faster than current generation supercomputers.

Fortunately there is no need for an engineer to consider the details of such eddies. They are primarily concerned with time-averaged effects even when the mean flow is unsteady. By predicting turbulent flow only on the time averaged properties of turbulence and since these vary gradually in space, no excessively fine grids are necessary. This avoids the need to predict the effects of each and every eddy in the flow field. Engineers and CFD users are almost always satisfied with information about the time averaged properties of the flow (mean velocities, mean pressures and mean stresses). The process of time averaging is not without its problems as it causes statistical correlation's involving fluctuating velocities to appear in the conservation equations. There is no direct way of knowing the magnitude of these terms and we must therefore approximate or 'model' their effects. The result of this approach has been the development and use of various 'models of turbulence'.

2.3 TURBULENCE MODELLING

The crucial difference between visualisation of laminar and turbulent flow is the appearance of eddying motions of a wide variety of length scales in turbulent flows. A typical flow domain of 0.1 by 0.1 m with a high Reynolds number turbulent flow may contain eddies down to 10 to 100um. Such eddies would require computing meshes of 10^9 to 10^{12} points to accurately describe processes at all length scales (Speziale 1991).

The computing requirements for direct solutions of time averaged Navier-Stokes equations of fully developed turbulent flow must await major developments in computer hardware. Meanwhile engineers require computational procedures that can supply adequate information about turbulent processes without the need to predict the effects of each and every eddy in the flow field (Reynolds, 1987. Mocikat, et al.2003). They are almost always satisfied with information about time-averaged properties of the flow (mean velocity, mean pressure etc.). In performing time averaging six additional unknowns are obtained, namely the Reynolds Stresses. The main task of turbulence modelling is to develop computational procedures of sufficient accuracy to allow prediction of the Reynolds Stresses and other scalar transport terms.

A turbulence model is a computational procedure used to close the system of mean flow equations so that a variety of flow problems may be calculated. For a turbulence model to be useful in a general purpose CFD code it must have a wide field of use, be accurate, simple and economical to run. Large eddy simulations are turbulence models where the time-dependent flow equations are solved for the mean flow and the largest eddies and where the effects of the smaller eddies are modelled. This approach results in a good model of the main effects of turbulence, however the calculations are very costly and seldom used on industrial applications [Abbott and Basco 1989]. Of the classical turbulence models the Mixing Length and k-ε models are presently by far the most widely used and validated. These models are based on the presumption that an analogy exists between the action of the viscous stresses and the Reynolds stresses on the mean flow [Shih, et al. 1995].

2.3.1 TURBULENCE AND THE k-ε MODEL

In k-ε eddy-viscosity models, the turbulence field is characterized in terms of two variables:

- Turbulent kinetic energy, k
- Viscous dissipation rate of turbulent kinetic energy, ε

The *k*-ε model is an eddy-viscosity model in which the Reynolds stresses are assumed to be proportional to the mean velocity gradient with the constant of proportionality being the Turbulent Viscosity μ_t. [Bradshaw, et al. 1981). This assumption, known as the Boussinesq hypothesis, provides the following expression for the Reynolds stresses

$$\rho \overline{u_i' u_j'} = \rho \frac{2}{3} k \delta_{ij} - \mu_t \left(\frac{\partial u_i}{\partial x_j} + \frac{\partial u_j}{\partial x_i} \right) + \frac{2}{3} \mu_t \frac{\partial u_i}{\partial x_i} \delta_{ij}$$

where 'k' is the turbulent kinetic energy. The turbulent viscosity μ_t is obtained by assuming that it is proportional to the product of a turbulent velocity scale and a length scale. In the k- ε model, these velocity and length scales are obtained from two parameters: k the turbulent kinetic energy and ε the dissipation rate of k. The velocity scale is taken to be the $\sqrt{k}$ and the length scale to be $\frac{\sqrt{k^3}}{\varepsilon}$. Hence, μ_t is given by

$$\mu_t = \rho C_\mu \frac{k^2}{\varepsilon}$$

where C_μ is an empirically derived constant of proportionality (typically set to 0.09). The value of k *and* ε are obtained by solution of the conservation equations:

$$\frac{\partial}{\partial t}(\rho k) + \frac{\partial}{\partial x_i}(\rho u_i k) = \frac{\partial}{\partial x_i}\left(\frac{\mu_t}{\sigma_k} \frac{\partial k}{\partial x_i} \right) + G_k + G_b - \rho \varepsilon$$

$$\frac{\partial}{\partial t}(\rho \varepsilon) + \frac{\partial}{\partial x_i}(\rho u_i \varepsilon) = \frac{\partial}{\partial x_i}\left(\frac{\mu_t}{\sigma_k} \frac{\partial \varepsilon}{\partial x_i} \right) + C_{1\varepsilon} \frac{\varepsilon}{k}\left(G_k + (1 - C_{3\varepsilon}) G_b\right) - C_{2\varepsilon\varepsilon} \rho \frac{\varepsilon^2}{k}$$

In words these equations are:

The 'Rate of change of k *or* ε plus 'Transport of k *or* ε by conduction' equals 'Transport of k *or* ε by diffusion' plus 'Rate of production of k *or* ε' minus the

'Rate of destruction of k or ε'. The equations contain five empirical constants and the standard 'k-ε model' employs values for these constants arrived at via comprehensive data fitting over a wide range of turbulent flows (Patel et al, 1985. Tekriwal, 1994):

$$C_{1\varepsilon} = 1.44 \qquad C_{2\varepsilon} = 1.92 \qquad C_{\mu} = 0.09 \qquad \sigma_k = 1.0 \qquad \sigma_e = 1.3$$

The k-ε model is the most widely used and validated turbulent model. It has achieved considerable success in modelling a wide variety of flows without the need for case by case adjustment of the model constants. The model performs particularly well for confined flows which embrace a wide variety of industrial engineering applications.

ADVANTAGES

- Simplest turbulence model for which only initial and/or boundary conditions need to be supplied
- Excellent performance for a range of industrial applications
- Well established and the most widely validated of all models
- Economical

DISADVANTAGES

- More expensive to implement than simpler mixing length models
- Poor performance in a variety of important cases
    1) complex flows with large strains (swirling flows)
    2) rotating flows
    3) unconfined flows
- Isotropic description of turbulence

Table 2.1: Advantages and disadvantages of the k - ε *model*

This alone accounts for its popularity of use and the fact that it is the most widely used industrial model. The model is robust, economical and its strengths and weaknesses well documented. A summary of the performance assessment of the k-ε model is given in table 2.1 above.

2.3.2. THE REYNOLDS STRESS MODEL

One major limitation of the k-ε model is that μ_t is isotropic. This implies that the velocity and length scales are the same in all directions. In complex flows the velocity and length scales can vary considerably with direction. For such flows the k-ε model is inadequate and can produce inaccurate results. The RSM, which computes the individual Reynolds Stresses, provides a better alternative in these cases (Speziale, 1991., Lauder, 1989. Murakami, 1998). This is the most complex classical turbulence model and can account for directional effects within the Reynolds stress field. The modelling strategy originates from work reported by Launder et al in 1975.

The RSM involves solving the transport equations for Reynolds stresses which are derived from the momentum equations and the following set of equations are used within FLUENT software to provide closure (Bates et al, 1995).

Reynolds Stress Transport equations: $$\rho U_k \frac{\partial \overline{u_i u_j}}{\partial x_k} = P_{ij} + \phi_{ij} - \varepsilon_{ij} + \frac{\partial J_{ijk}}{\partial x_k}$$

Generation $$P_{ij} \equiv \overline{u_i u_k} \frac{\partial U_j}{\partial x_k} + \overline{u_j u_k} \frac{\partial U_i}{\partial x_k} \quad \textit{(computed)}$$

Pressure Strain Redistribution $$\phi_{ij} \equiv -\overline{p'\left(\frac{\partial u_i}{\partial x_j} + \frac{\partial u_j}{\partial x_i}\right)} \quad \textit{(modeled)}$$

Dissipation $$\varepsilon_{ij} \equiv 2\mu \frac{\partial u_i}{\partial x_k}\frac{\partial u_j}{\partial x_k} \qquad \textit{(related to } \varepsilon\textit{)}$$

Turbulent Diffusion $$J_{ijk} = \overline{u_i u_j u_k} + \overline{p'\left(\delta_{jk} u_i + \delta_{ik} u_j\right)} \qquad \textit{(modeled)}$$

The Reynolds Stress Models are clearly quite complex, but it is generally accepted that they are the simplest type of model with the potential to describe all mean flow properties and Reynolds stresses [Lauder, et al. 1975. Kumar, et al 1999). The RSM is by no means as well validated as the *k*- ε model and because of its high computational cost is selectively used on industrial problems [Horiuti, 1990]. A summary of the performance assessment of the *Reynolds stress Model* is given in table 2.2 below.

ADVANTAGES • Potentially the most general of all classical turbulent models • Only initial and/or boundary conditions need to be supplied • Very accurate calculation of mean flow properties and all Reynolds stresses for complex flows • The history, transport and anisotropy of turbulent stresses completely accounted for.
DISADVANTAGES • Very high computing costs (six additional PDE's) • Not as widely validated on industrial flows • Difficulty modelling jets and unconfined flows

Table 2.2: Advantages and disadvantages of the Reynolds Stress Model

2.4 NEAR WALL TREATMENTS FOR WALL-BOUNDED FLOWS

Turbulence models are largely valid for the turbulent core of the flow. When the flow to be computed involves walls, turbulent flows in these regions are affected by the presence of these walls. The mean velocity field is affected by the no-slip condition which must be satisfied [Chen and Patel, 1988. Wakes, 1997]. Very close to the wall turbulence is dampened due to the presence of the wall. Towards the outer part of the near-wall region turbulence is rapidly augmented by the production of turbulent kinetic energy due to Reynolds Stresses and the large gradient of mean velocity.

The near-wall modeling significantly impacts the fidelity of numerical solutions, inasmuch as walls are the main source of mean vorticity and turbulence [Kim and Choudhury, 1995]. After all, it is in the near-wall region that the solution variables have large gradients, and the momentum and other scalar transports occur most vigorously. Therefore, accurate representation of the flow in the near-wall region determines successful predictions of wall-bounded turbulent flows. The k- ε models, and the RSM are primarily valid for turbulent core flows (i.e., the flow in the regions somewhat far from walls). Consideration therefore needs to be given as to how to make these models suitable for wall-bounded flows and how they can be applied throughout the boundary layer, provided that the near-wall mesh resolution is sufficient [Durst, et al. 1995].

When simulating turbulent flows it is particularly challenging to model the viscosity affected near-wall regions [Launder and Shima, 1989] that is, regions adjacent to solid boundaries which contain the viscous sub-layer. The difficulty arises for the following reasons.

- In order to resolve the sharply varying flow variables in near-wall regions, a disproportionately large number of grid points are required in the immediate vicinity of the solid boundary. For most typical flow scenarios, this leads to prohibitively expensive computations.
- Standard models employed in commercial packages (eg Fluent) are of the high-Reynolds number type and, therefore, cannot be used in the near-wall regions.

A number of techniques have been developed to model the effect of the viscous sublayer on the mean flow field. The well-known "*law-of-the-wall* " approach has been the technique most commonly adopted in the field of applied CFD. Although it is a popular and practical tool, this approach possesses a number of inherent weaknesses and drawbacks which become more apparent and pronounced as the complexity of the problem increases. For example, the "wall functions" that are used to apply appropriate boundary conditions for the various flow variables at the edge of the computational domain become less appropriate when there is significant departure from local one-dimensionality in the near-wall region. Such circumstances arise near points of separation, reattachment and stagnation, and in other situations involving strong acceleration, retardation or body forces (Chen and Patel, 1988).

As stated previously near wall modelling significantly impacts the fidelity of the numerical solution and therefore accurate representation of the flow in this region greatly enhances successful prediction of wall-bounded turbulent flows such as pipe dead-legs. Numerous experiments have shown that the near-wall region can be divided into three layers:

1) Viscous Sub-Layer: The flow in this layer is laminar and viscosity plays a dominant role.
2) Outer-Layer: Also known as the fully turbulent layer. In this region turbulence pays a major role.
3) Buffer-Layer: This is the interim region between the viscous sub-layer and the fully developed turbulent layer where the effects of viscosity and turbulence are of equal importance. (See Fig 2.1)

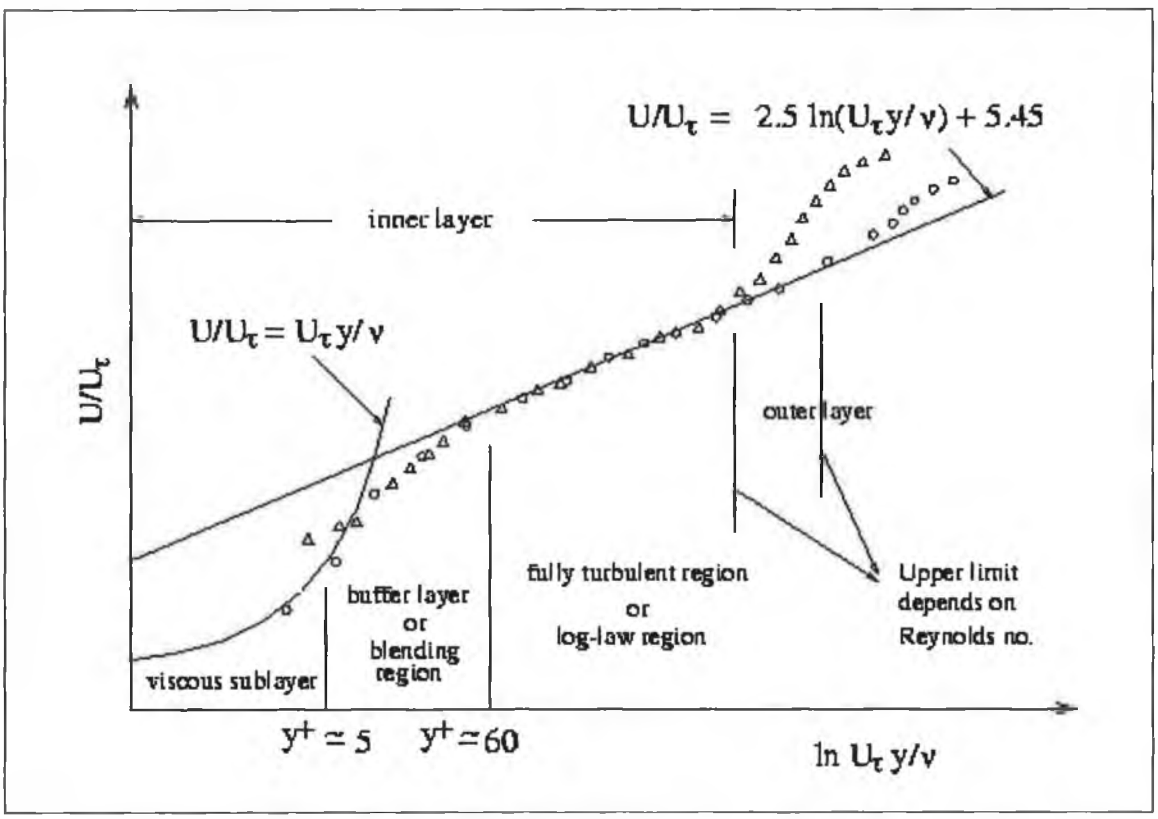

Figure 2.1: Subdivisions of the Near Wall Regions

For straight pipe flows these wall functions have been widely validated. Durst et al. (1995) have measured with detail the velocity in the near wall region of a fully developed turbulent pipe flow confirming agreement with the log law.

2.4.1. WALL FUNCTIONS VERSUS NEAR-WALL MODELS

Traditionally, there are two approaches to modeling the near-wall region. In one approach, the viscosity-affected inner region (viscous sublayer and buffer layer) is not resolved. Instead, semi-empirical formulas called ``wall functions" are used to bridge the viscosity-affected region between the wall and the fully-turbulent region. The use of wall functions removes the need to modify the turbulence models to account for the presence of the wall.

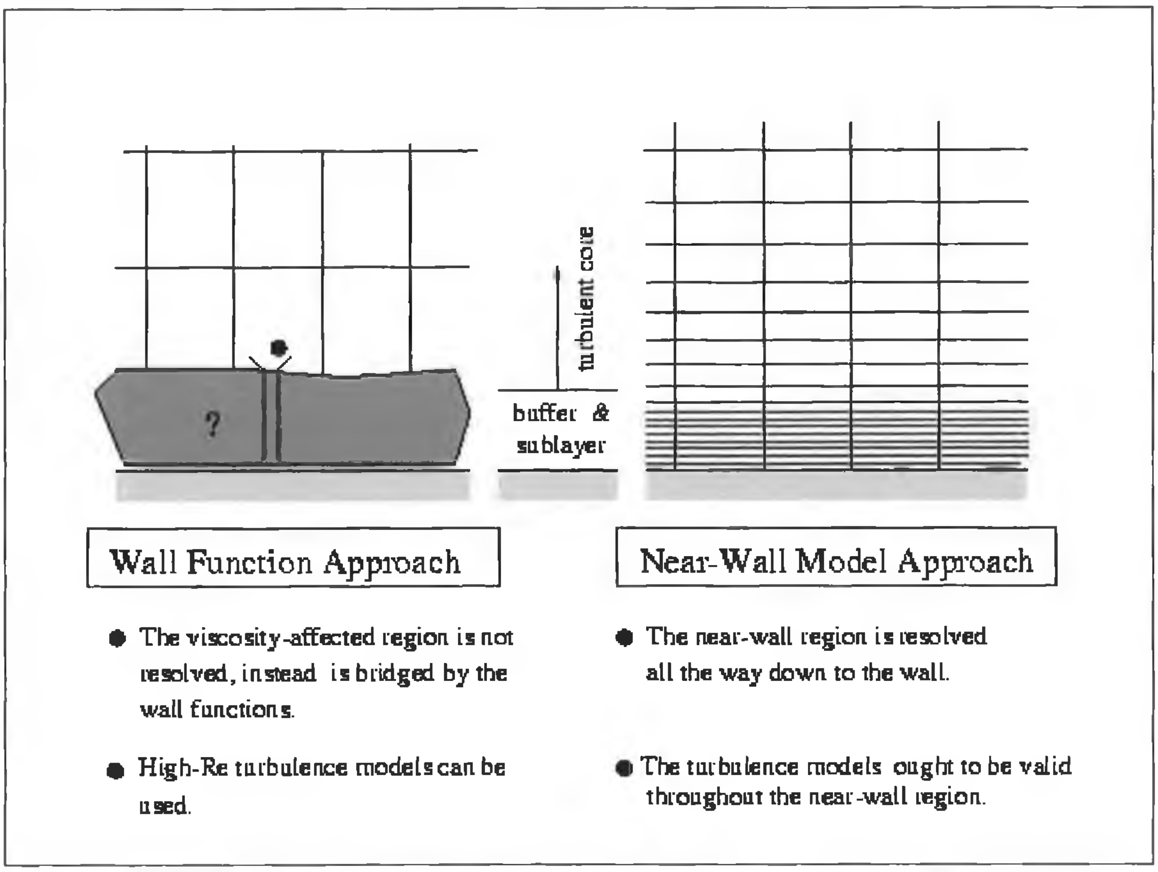

Figure 2.2: Near-Wall Treatments in FLUENT

In another approach, the turbulence models are modified to enable the viscosity-affected region to be resolved with a mesh all the way to the wall, including the viscous sublayer. For purposes of discussion, this will be termed the ``near-wall modeling" approach. These two approaches are depicted schematically in Figure 2.2.

In most high-Reynolds-number flows, the wall function approach substantially saves computational resources, because the viscosity-affected near-wall region, in which the solution variables change most rapidly, does not need to be resolved. The wall function approach is popular because it is economical, robust, and reasonably accurate. It is a practical option for the near-wall treatments and has been embraced as the most widely used approached for industrial flow simulations. The wall function approach, however, is inadequate in situations where the low-Reynolds-number effects are pervasive in the flow domain in question, and the hypotheses underlying the wall functions cease to be valid. Such situations require near-wall models that are valid in the viscosity-affected region and accordingly can be integrated all the way to the wall.

Because of the capability to partly account for the effects of pressure gradients and departure from equilibrium, the non-equilibrium wall functions are recommended for use in complex flows involving separation, reattachment, and impingement where the mean flow and turbulence are subjected to severe pressure gradients and change rapidly. In such flows, improvements can be obtained, particularly in the prediction of wall shear (skin-friction coefficient) and heat transfer (Nusselt or Stanton number).

Experimental data shows that the flow is predominantly laminar and has a linear velocity profile, in the region of the viscous sublayer $\left(y^+ < 5\right)$, transitional and intermittent with a log-linear velocity profile in the region of the transitional or buffer layer $\left(5 < y^+ < 30\right)$, and is fully turbulent with a logarithmic velocity profile in regions where $y^+ < 30$. Although y^+ is a normalized distance, it is also very helpful to think of it as a local Reynolds number that characterizes the state of the flow in the near-wall region. Thus the flow in the vicinity of the wall is laminar if the local Reynolds number is less than 5, is transitional between 5 and 30, and is fully turbulent if the Reynolds number is greater than 30.

2.4.2 STANDARD WALL FUNCTIONS

The standard wall functions available in FLUENT are based on the work of Launder and Spalding (1974). These are the most widely used of all wall functions and have been validated on numerous industrial flows. The law-of-the-wall for mean velocities yields:

$$U^* = \frac{1}{k}\ln\left(Ey^*\right)$$

where

$$U^* \equiv \frac{U_p C_\mu^{\frac{1}{4}} k_p^{\frac{1}{2}}}{\frac{\tau_w}{\rho}}$$

$$y^* \equiv \frac{\rho C_\mu^{\frac{1}{4}} k_P^{\frac{1}{2}} y_P}{\mu}$$

The logarithmic law for mean velocity is known to be valid for y* > 30 – 60. In FLUENT the log-law is employed when y* > 11.225. When the mesh is such that y* < 11.225 at the wall adjacent cells FLUENT applies the laminar stress-strain relationship,

$$U^* = y^*$$

2.4.3. NON-EQUILIBRIUM WALL FUNCTIONS

In addition to the standard wall function a two-layer based non-equilibrium wall function is also available. The key differences between this and the standard wall functions are:

- Launder and Spalding's log-law for mean velocity is sensitised to pressure gradient effects.
- The two –layer based concept is adopted to compute the turbulent kinetic energy in the wall-neighbouring cells.

The log-law for mean velocity sensitised to pressure gradient is given by:

$$\frac{\tilde{U} C_\mu^{\frac{1}{4}} k^{\frac{1}{2}}}{\frac{\tau_w}{\rho}} = \frac{1}{k} \ln\left(E \frac{\rho C_\mu^{\frac{1}{4}} k^{\frac{1}{2}} y}{\mu} \right)$$

where

$$\tilde{U} = U - \frac{1}{2}\frac{dp}{dx}\left[\frac{y_v}{\rho k^* k^{\frac{1}{2}}}\ln\left(\frac{y}{y_v}\right) + \frac{y - y_v}{\rho k^* k^{\frac{1}{2}}} + \frac{y_v^2}{\mu}\right]$$

where y_v is the physical viscous sublayer thickness and is computed from:

$$y_v \equiv \frac{\mu y_v^*}{\rho C_\mu^{\frac{1}{4}} k_p^{\frac{1}{2}}}$$

where $y_v^* = 11.225$. A summary of the performance of the *standard and non-equilibrium wall functions* is given in table 2.3 below.

Type of Function	**Strengths**	**Weaknesses**
Standard Wall Function	Robust Economical Reasonably Accurate Well Validated	Poor for low *Re* flows Does not account for pressure gradient
Non-equilibrium Wall Function	Pressure Gradient sensitive Accurate for -separation -reattachment -impingment	Poor for low *Re* flows Limited advantages with severe pressure gradients

Table 2.3: Performance of the standard and non-equilibrium wall functions

2.4.4 WALL BOUNDARY ELEMENTS CHECKLIST

The following sections present a checklist for the specification of wall boundary elements and recommendations that apply to flow and turbulence models with high Reynolds Number based on current research trends.

1. For ***high-Re*** k-ε models, the mesh should be created such that the first layer of elements is thick enough to completely contain the viscous sublayer and transition region in the near wall region.

2. The velocity components on wall boundaries should be set just as they would be set for non-turbulent analyses, that is, fixed walls are defined with all velocity components set to zero and moving walls have the appropriate velocity component set to a specified velocity.

3. Nodes on a WALL boundary do not require the specification of any kinetic energy or dissipation boundary conditions.

After the solution, to assure that the first layer of elements is thick enough to completely contain the viscous sublayer and transition region, the YPLUS command is used to plot the y^+ values at the WALL boundaries. If the value of y^+ for the momentum layer is greater than 30 for all elements then these elements are thick enough. Values of y^+ lower than 30 for the momentum layer may be safely tolerated provided these are not occurring in wall regions of crucial importance to the overall flow process [Kim and Choudhury, 1995. Kim, et al. 1997].

In flow problems involving subtle separation phenomena, such as separation occurring on gently sloping surfaces or on curved surfaces (for example, flow in turning ducts or U-bends), the predicted flow field will be sensitive to the y^+ values upstream of the separation point. In these situations the most accurate predictions were obtained if the y^+ values upstream of regions of potential flow separation are kept in the range $30 < y^+ < 100$. If after obtaining a solution y^+ values in these regions are found to be outside the above range, then a further run with a modified mesh in the near-wall region may have to be performed. If the y^+ values were too large, then a finer mesh in the near-wall region should be employed. Conversely, if y^+ values are less than 30, a mesh with thicker near-wall elements should be employed.

2.5 SEGREGATED SOLVER SOLUTION METHOD

Using the segregated solver solution algorithm the governing equations are solved sequentially (i.e., segregated from one another). Because the governing equations are non-linear (and coupled), several iterations of the solution loop must be performed before a converged solution is obtained. Each iteration consists of the steps illustrated in Figure 2.3 and are outlined below:

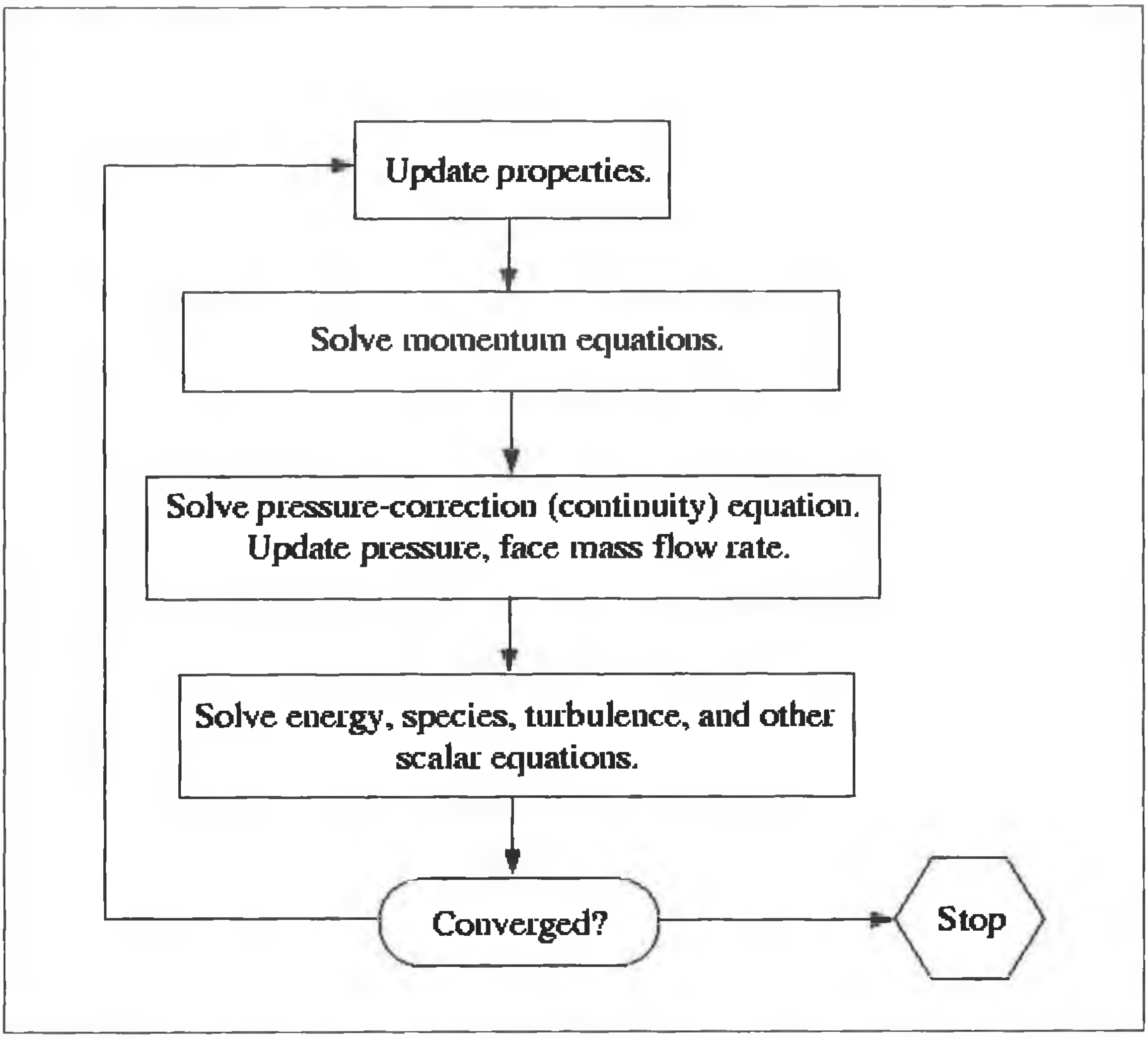

Figure 2.3: Overview of the Segregated Solver Solution Method

1. Fluid properties are updated, based on the current solution. (If the calculation has just begun, the fluid properties will be updated based on the initialized solution.)
2. The *u*, *v*, and *w* momentum equations are each solved in turn using current values for pressure and face mass fluxes, in order to update the velocity field.
3. Since the velocities obtained in Step 2 may not satisfy the continuity equation locally, a ``Poisson-type" equation for the pressure correction is derived from the continuity equation and the linearized momentum equations. This pressure

correction equation is then solved to obtain the necessary corrections to the pressure and velocity fields and the face mass fluxes such that continuity is satisfied.

4. Where appropriate, equations for scalars such as turbulence, energy, species, and radiation are solved using the previously updated values of the other variables.

5. When interphase coupling is to be included, the source terms in the appropriate continuous phase equations may be updated with a discrete phase trajectory calculation.

6. A check for convergence of the equation set is made.

These steps are continued until the convergence criteria are met.

2.5.1 THE COUPLED SOLVER SOLUTION METHOD

The coupled solver solves the governing equations of continuity, momentum, and (where appropriate) energy and species transport simultaneously (i.e., coupled together). Governing equations for additional scalars will be solved sequentially (i.e., segregated from one another and from the coupled set) using the procedure described for the segregated solver above. Because the governing equations are non-linear (and coupled), several iterations of the solution loop must be performed before a converged solution is obtained. Each iteration consists of the steps illustrated in Figure 2.4 and outlined below:

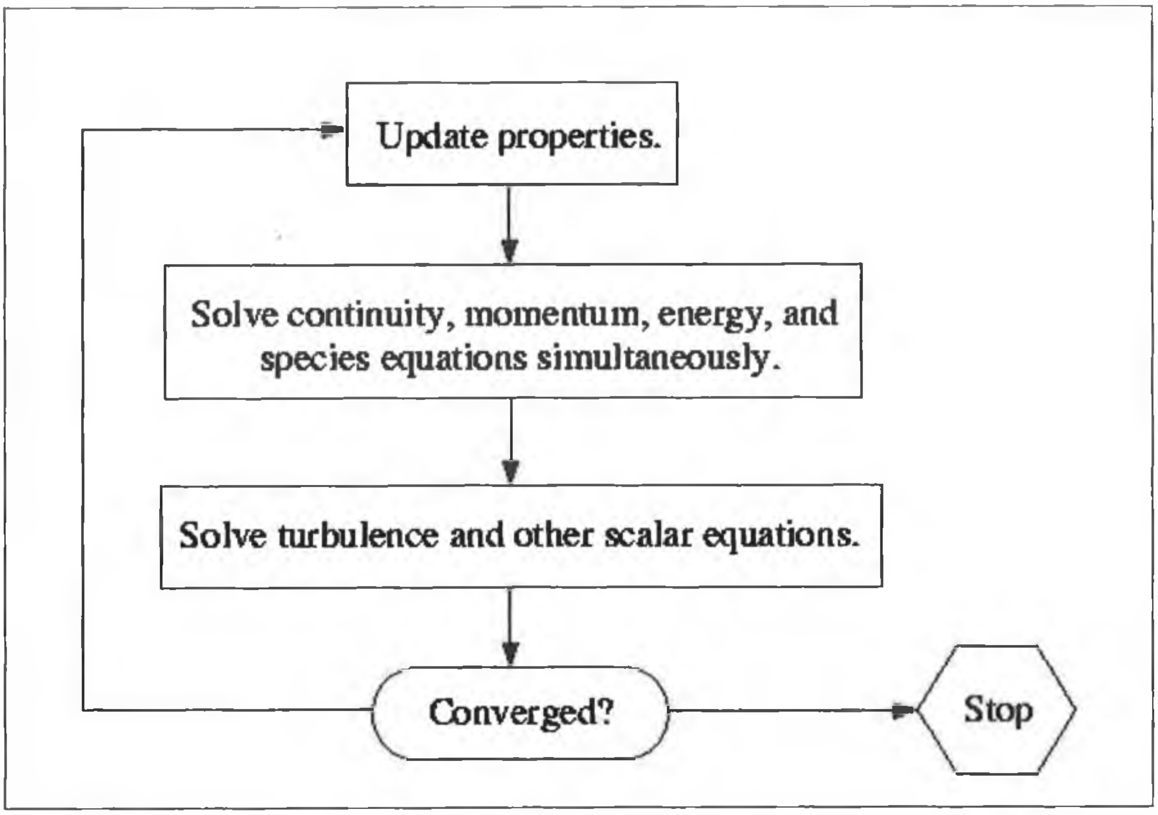

Figure 2.4: Overview of the Coupled Solution Method

1. Fluid properties are updated, based on the current solution. (If the calculation has just begun, the fluid properties will be updated based on the initialized solution.)
2. The continuity, momentum, and (where appropriate) energy and species equations are solved simultaneously.
3. Where appropriate, equations for scalars such as turbulence and radiation are solved using the previously updated values of the other variables.
4. When interphase coupling is to be included, the source terms in the appropriate continuous phase equations may be updated with a discrete phase trajectory calculation.
5. A check for convergence of the equation set is made.

These steps are continued until the convergence criteria are met.

2.5.2 LINEARIZATION: IMPLICIT VERSUS EXPLICIT

In both the segregated and coupled solution methods the discrete, non-linear governing equations are linearized to produce a system of equations for the dependent variables in every computational cell. The resultant linear system is then solved to yield an updated flow-field solution (Weiss et al., 1997).

The manner in which the governing equations are linearized may take an 'implicit' or 'explicit' form with respect to the dependent variable (or set of variables) of interest.

- Implicit: For a given variable, the unknown value in each cell is computed using a relation that includes both existing and unknown values from neighboring cells. Therefore each unknown will appear in more than one equation in the system, and these equations must be solved simultaneously to give the unknown quantities.
- Explicit: For a given variable, the unknown value in each cell is computed using a relation that includes only existing values. Therefore each unknown will appear in only one equation in the system and the equations for the unknown value in each cell can be solved one at a time to give the unknown quantities.

In summary, the segregated approach solves for a single variable field (e.g., p) by considering all cells at the same time. It then solves for the next variable field by again considering all cells at the same time, and so on. There is no explicit option for the segregated solver.

In the coupled solution method you have a choice of using either an implicit or explicit linearization of the governing equations. This choice applies only to the coupled set of governing equations. Governing equations for additional scalars that are solved segregated from the coupled set, such as for turbulence, radiation, etc., are linearized and solved implicitly using the same procedures as in the segregated solution method. Regardless of whether you choose the implicit or explicit scheme, the solution procedure is as outline previously (Wilcox, 1998).

2.5.3 FIRST ORDER VERSUS SECOND ORDER DISCRETIZATION

When the flow is aligned with the grid (e.g., laminar flow in a rectangular duct modeled with a quadrilateral or hexahedral grid) the first-order upwind discretization may be acceptable. When the flow is not aligned with the grid (i.e., when it crosses the grid lines obliquely), however, first-order convective discretization increases the numerical discretization error (numerical diffusion). For triangular and tetrahedral grids, since the flow is never aligned with the grid, more accurate results will generally be obtained by using the second-order discretization. Quad/hex grids will also give better results using the second-order discretization, especially for complex flows (Grant et al. 2001)

In summary, while the first-order discretization generally yields better convergence than the second-order scheme, it generally will yield less accurate results, especially on tri/tet grids. Convergence can be hindered by a number of factors. Large numbers of computational cells, overly conservative under-relaxation factors, and complex flow physics are often the main causes.

2.6. SOLUTION STRATEGIES FOR TURBULENT FLOW SIMULATIONS

Compared to laminar flows, simulations of turbulent flows are more challenging in many ways. For the Reynolds-averaged approach, additional equations are solved for the turbulence quantities. Since the equations for mean quantities and the turbulent quantities are strongly coupled in a highly non-linear fashion, it takes more computational effort to obtain a converged turbulent solution than to obtain a converged laminar solution. The fidelity of the results for turbulent flows are largely determined by the turbulence model used. Factors that can enhance the quality of turbulent flow simulations include Mesh Generation, Accuracy, Convergence and Solution strategies (Yakhot et al., 1989). Accuracy has been found to be influenced by the turbulence model used and the use of higher order schemes for the convective terms. Current research suggests that convergence may be enhanced by the use of conservative (small) under-relaxation parameters which can be gradually increased as the iterations proceed and the solution settles down. It was also found that convergence was faster when a reasonable initial guess for the k and ε was included in the model. When using the RNG k-ε model it is better to obtain a solution with the standard k-ε model before switching on the RNG model (Yakhot and Orszag, 1986).

2.6.1 GRID CONSIDERATIONS FOR TURBULENT FLOW SIMULATIONS

Successful computations of turbulent flows require some consideration during the mesh generation. Since turbulence (through the spatially-varying effective viscosity) plays a dominant role in the transport of mean momentum and other scalars for the majority of complex turbulent flows, one must ascertain that turbulence quantities are properly resolved, if high accuracy is required. Due to the strong interaction of the mean flow and turbulence, the numerical results for turbulent flows tend to be more susceptible to grid dependency than those for laminar flows. It is therefore recommended to resolve, with sufficiently fine meshes, the regions where the mean flow changes rapidly and there are shear layers with a large mean rate of strain. This is generally done using values of y +, y *, and Re_y, which are all available in the postprocessing panels

The distance from the wall at the wall-adjacent cells must be determined by considering the range over which the log-law is valid. The distance is usually measured in the wall unit, y + which is known to be valid for y + > 30 to 60.

- Although FLUENT employs the linear (laminar) law when y + < 11.225, using an excessively fine mesh near the walls should be avoided, because the wall functions cease to be valid in the viscous sublayer.

- The upper bound of the log-layer depends on, among others, pressure gradients and Reynolds number. As the Reynolds number increases, the upper bound tends to also increase. y + values that are too large are not desirable, because the wake component becomes substantially large above the log-layer.

- A y + value close to the lower bound $(y^+ = 30)$ is most desirable.

- Using excessive stretching in the direction normal to the wall should be avoided.

- It is important to have at least a few cells inside the boundary layer.

2.6.2 PROVIDING AN INITIAL GUESS FOR k and ε

For flows using one of the k-ε models or the RSM, the converged solutions or (for unsteady calculations) the solutions after a sufficiently long time has elapsed should be independent of the initial values for k and ε. For better convergence, however, it is beneficial to use a reasonable initial guess for k and ε. Guidelines include,

- Where possible specify reasonable boundary conditions at the inlet.
- For complex flows (e.g., flows with multiple inlets with different conditions) it may be better to specify the initial values in terms of turbulence intensity. 5-10% is enough to represent fully-developed turbulence. k can then be computed from the turbulence intensity and the characteristic mean velocity.
- Specify an initial guess for ε so that the resulting eddy viscosity is sufficiently large in comparison to the molecular viscosity. In fully-developed turbulence, the turbulent viscosity is roughly two orders of magnitude larger than the molecular viscosity.

2.6.3 DETERMINING TURBULENCE PARAMETERS

When the flow enters the domain at an inlet, outlet, or far-field boundary, FLUENT requires specification of transported turbulence quantities. A turbulence intensity of 1% or less is generally considered low and turbulence intensities greater than 10% are considered high. For internal flows, the turbulence intensity at the inlets is totally dependent on the upstream history of the flow. If the flow upstream is under-developed and undisturbed, a low turbulence intensity is used. If the flow is fully developed, the turbulence intensity may be as high as a few percent. The turbulence intensity at the core of a fully-developed duct flow can be estimated from the following formula derived from an empirical correlation for pipe flows:

$$\text{Turbulence Intensity } I = 0.16(\text{Re})^{-\frac{1}{8}}$$

The turbulence length scale, ℓ, is a physical quantity related to the size of the large eddies that contain the energy in turbulent flows. In fully-developed duct flows, ℓ is restricted by the size of the duct, since the turbulent eddies cannot be larger than the duct. An approximate relationship between ℓ and the physical size of the duct is

$$\text{Turbulence Length Scale } l = 0.07L$$

where L is the relevant dimension of the duct. The factor of 0.07 is based on the maximum value of the mixing length in fully-developed turbulent pipe flow, where L is the diameter of the pipe. In a channel of noncircular cross-section, you can base L on the hydraulic diameter.

2.6.4 RSM-SPECIFIC SOLUTION STRATEGIES

Using the RSM creates a high degree of coupling between the momentum equations and the turbulent stresses in the flow, and thus the calculation can be more prone to stability and convergence difficulties than with the k- ϵ models. Base on current research the following strategies are generally recommended to assist with convergence,

- Begin the calculations using the standard k- ϵ model. Turn on the RSM and use the k- ϵ solution data as a starting point for the RSM calculation.

- Use low under-relaxation factors for highly swirling flows or highly complex flows.

CHAPTER 3. COMPUTATIONAL MODELLING AND CFD VALIDATION

3.1 GAMBIT: FLUENTS PRE-PROCESSOR SOFTWARE

Gambit is a single integrated pre-processor package for CFD analysis. The package allows geometry to be constructed using bottom-up or top-down techniques or geometry to be imported from alternate packages. Its capabilities include:

- ACIS solid modelling capabilities.
- IGES import, cleanup and modification.

GAMBIT allows the construction and meshing of models by means of its graphical user interface (Figure 3-1).

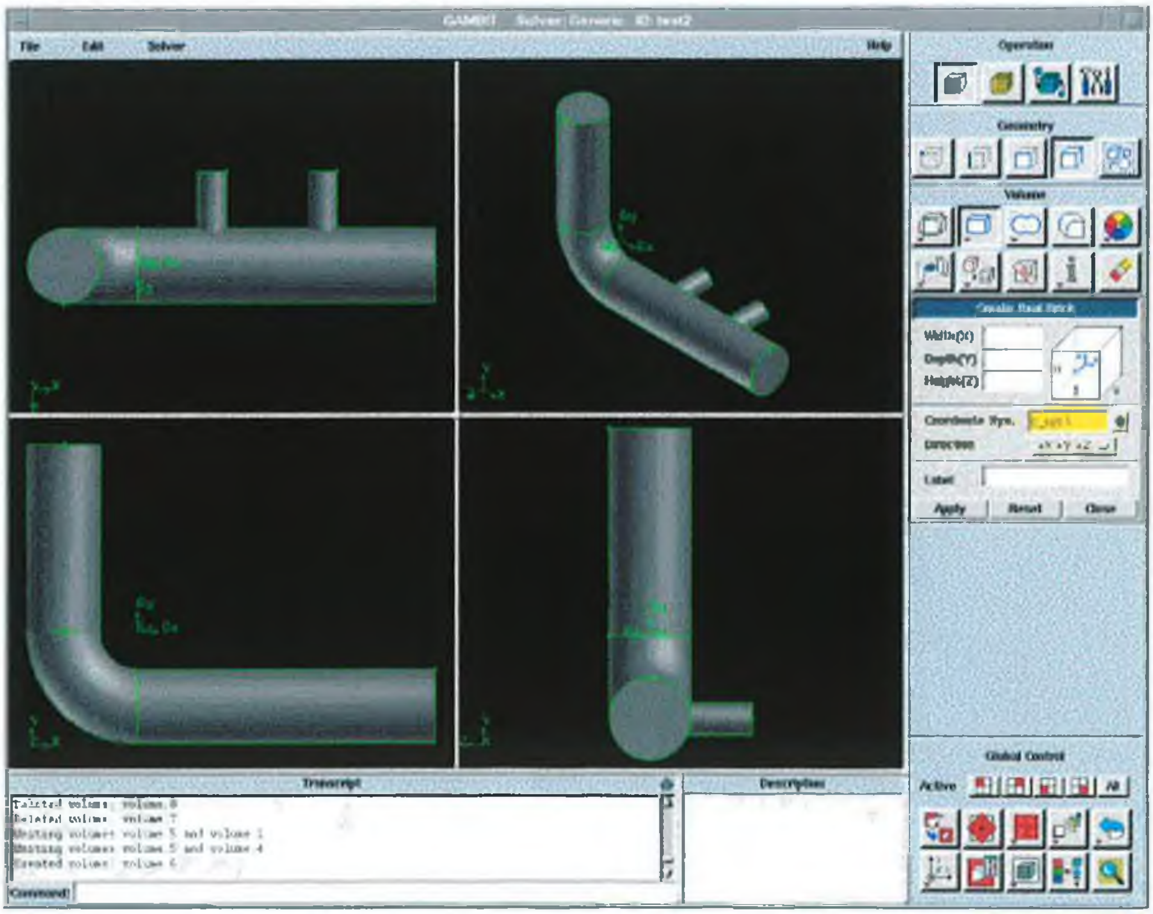

Figure 3.1: Gambits graphical user interface (GUI)

Gambit is used to generate meshes for all Fluents solvers and it offers a wide range of elements and schemes including structured and unstructured hexahedral, tetrahedral, pyramid and prisms. Once generated the mesh quality may be analysed and modified if necessary. The general sequence of operations for geometry construction and meshing is as follows:

1) Initial set-up: This includes solver selection, mesh size specification and defaults settings.
2) Geometry creation: Full geometry creation or decomposition into meshable sections.
3) Meshing: Edge and boundary local meshing or face and volume global meshing.
4) Mesh Examination: Mesh quality analysis and modification
5) Zone assignment and mesh export.

3.2 INITIAL SET-UP AND DEAD-LEG TEE GEOMETRY CREATION

Many studies are available for modelling of divided flow through a pipe-tee junction, a problem of considerable interest throughout the pharmaceutical, semi-conductor, food and process industries. Many process applications may be found which require flow to be diverted in part or in full from the ring main pipe through the tee branch. However, following extensive investigations using industrial contacts, literature surveys and library searches, little if any research has been found to date investigating the problem of dead-leg flow, a configuration that renders the branch of the tee stagnant. To ensure a sound bases for dead-leg flow investigation the author decided to take the most recent research available on divided flow, apply best current practice in relation to the generation and meshing of a tee for divided flow investigation and simply prevent flow through the branch to impart a dead-leg condition on the branch [Sierra-Espinosa, et al. 2000(a)].

Recent studies of modelling of divided flow of water through a tee junction include those of Bates et al (1995) and Sierra-Espinosa et al (1997). This tee consisted of a 50mm equal tee with a 12.5 mm radius between the main pipe and the branch. This type of tee is typical of those found in the distribution loops of high purity water systems apart from the fact that the tees would have a sharp edge branch. Due to the high cost of production and the problems of contamination following treatment distribution loop pipe diameters seldom exceed 50mm. Bates investigation was conducted using a computational grid of 230x14x49 cells. Espinosa constructed a grid using 100x18x59 cells reducing the number of cells and representing the domain through 106,000 control volume elements. Both authors stressed the importance of cell skewness and its direct relation to convergence. Considerable attention was paid by the author to the above mentioned conditions and the final grid refined on numerous occasions to ensure grid independence [Sierra-Espinosa, et al. 2000(a and b)]. For example the final grid (see fig 3.4) used for a 50mm equal tee with a dead-leg of 3D was constructed using a grid of 90x24x72 cells representing the domain with 155,520 elements.

Direct numerical simulation by Le et al (1997) stressed the importance of cell spacing which they found to have a detrimental effect on several flow characteristics. The main constraint associated with spacing is that of correct modelling of near wall turbulence. Le et al found a 10% reduction in reattachment length when they increased the spacing of cells in a streamwise direction. However this result was for direct numerical simulation with no wall laws applied. Spencer et al (1995) compared the simulation of fully developed turbulent pipe flow across a range of research groups and found discrepancies among them for similar problems. They concluded that making the computational cell attached to the wall closer than y+ = 12 produced poor results when using wall functions. They suggest that the near wall nodes be significantly further from the wall (y+ >25) unless wall laws are not applied. These facts were taken into account during the meshing of near wall regions. Within the current models all y+ values were above 30.

Initial developments of the dead-leg tees used in this thesis were found to have a high degree of grid dependence. Following detailed analysis of numerous models the curved entrance regions of the branch were found to be causing the problem.

Figure 3.2: Decomposition of the Geometry

To account for misalignment of the flow and to control skewness and local cell variation the geometry was decomposed a shown in figure 3.2. This detailed decomposition allowed accurate control of cells throughout the tee. The majority of the areas generated by this decomposition maintained 100% grid alignment with the flow. This technique is known to reduce numerical diffusion and result in a robust model. Decomposition also allowed detailed control of skewness at entry to the branch of the tee a region in which it was not possible to maintain grid alignment. By controlling local cell variation in this region it was possible to overcome grid dependence and to accurately model flow through the branch details of which are outlined in the validation studies presented later in this chapter.

3.3 MESHING OF THE DEAD-LEG TEES WITHIN GAMBIT

General meshing characteristics available within Gambit include edge, face and volume direct meshing. Pre-meshing of edges and faces is also available and is used to control cell distribution on face and volumes respectively. Edge meshing distribution may be controlled through spacing and grading using single and double sided meshing and interval size and count. Face meshing offered a range of element/scheme type combinations;

1) Quad: map, submap, tri-primative and pave
2) Quad/Tri: map, pave, wedge
3) Tri: pave.

The preference when volume meshing is to use a high quality hex mesh in order to reduce discretization errors. Therefore complicated geometries are generally decomposed into simpler volumes (Jones and Galliera, 1998). Some geometries may be too complex and decomposition for hex meshing impractical. The use of tet/hybrid is normally the preferred choice in these cases. Upon selection of a volume for meshing Gambit automatically chooses a type of mesh based on the solver selected and the type of faces available to act as sources. Options include hex, hex/wedge and tet/hybrid.

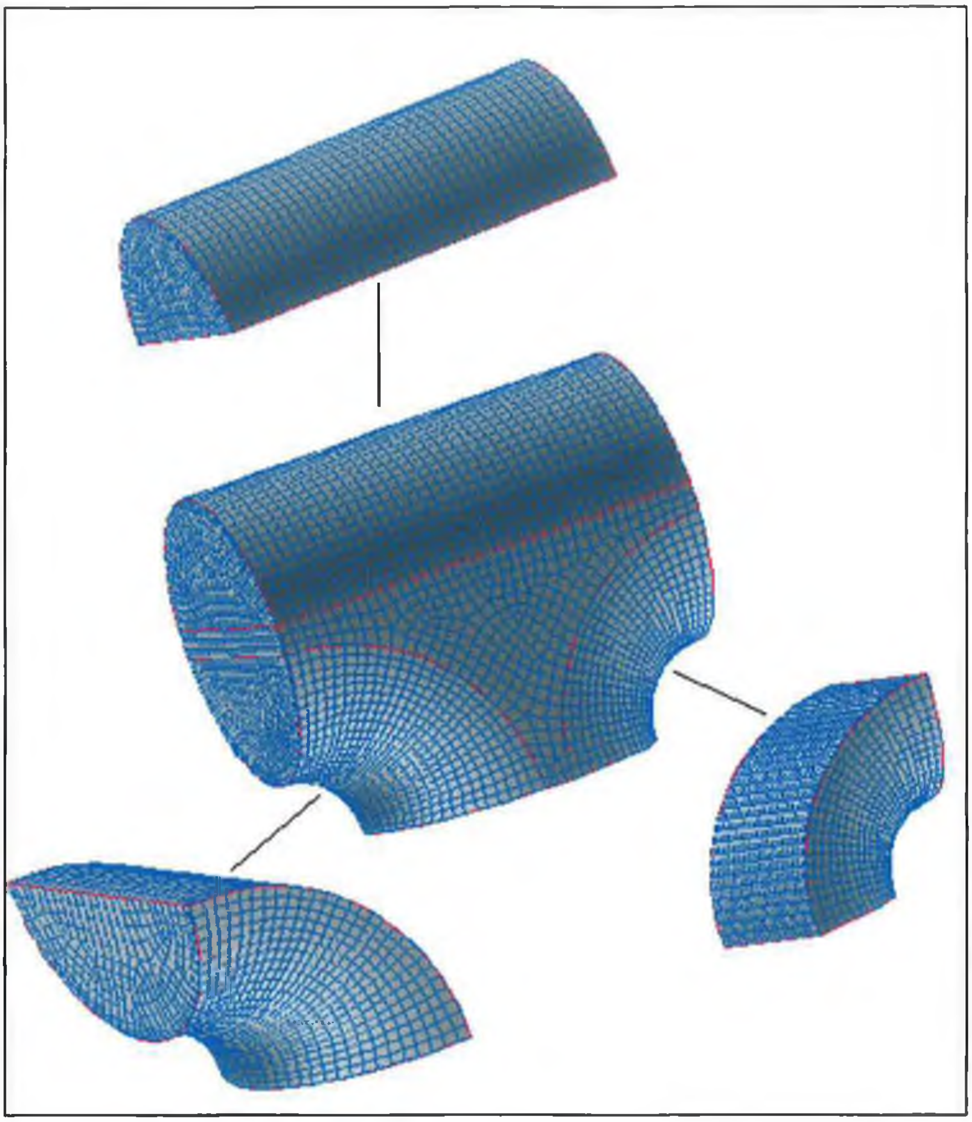

Figure 3.3: Meshing of the Curved Branch of the Dead-Leg Tee

The cooper scheme, a powerful meshing tool available within gambit, projects or extrudes a face mesh from one end of a volume to another, dividing the extruded mesh along the line of action of the volume to form a volume mesh. This scheme was extensively used to mesh both round entry and sharp entry tees used in this thesis. The results presented for round entry tees were generated using the refined mesh shown in figure 3.3 and 3.4 taking into account the complexity of the flow raised by the presence of curved boundaries at entry to the branch.

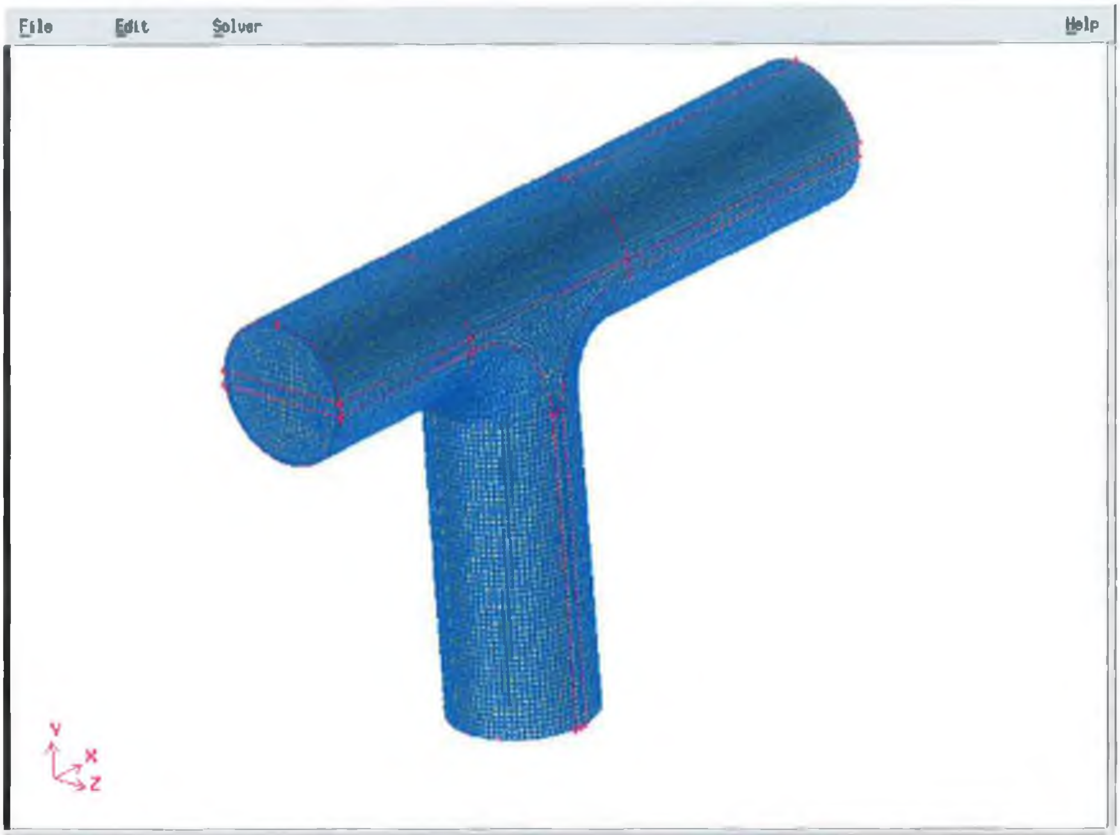

Figure 3.4: Overview of final mesh for a 50mm diameter equal dead-leg tee

As stated previously to achieve this mesh the tee was decomposed into a series of blocks and the mesh refined to achieve equal spacing and parallel topology were possible. This was noted by many researchers as a means of reducing numerical diffusion and thus improved the accuracy of the computation (Jones et al, 1993). The generation of the tee involved the use of bottom up techniques such as edge, face and sweep along with top down methods involving face and volume primitives. Boolean operations such as unite, subtract and intersect along with volume decomposition allowed for accurate generation of the complex geometries involved.

An outline of the meshing approach adapted for a sharp entry tee is shown in fig 3.6. A simple wedge decomposition was used for this configuration which reduced the complexity of the meshing and decreased the number of cells required. Cell spacing was off-set in the direction of the branch to overcome problems with skewness and this had the effect of concentrating cells in the branch region. It also had the effect of reducing equi-angle skew and reducing cell size variation.

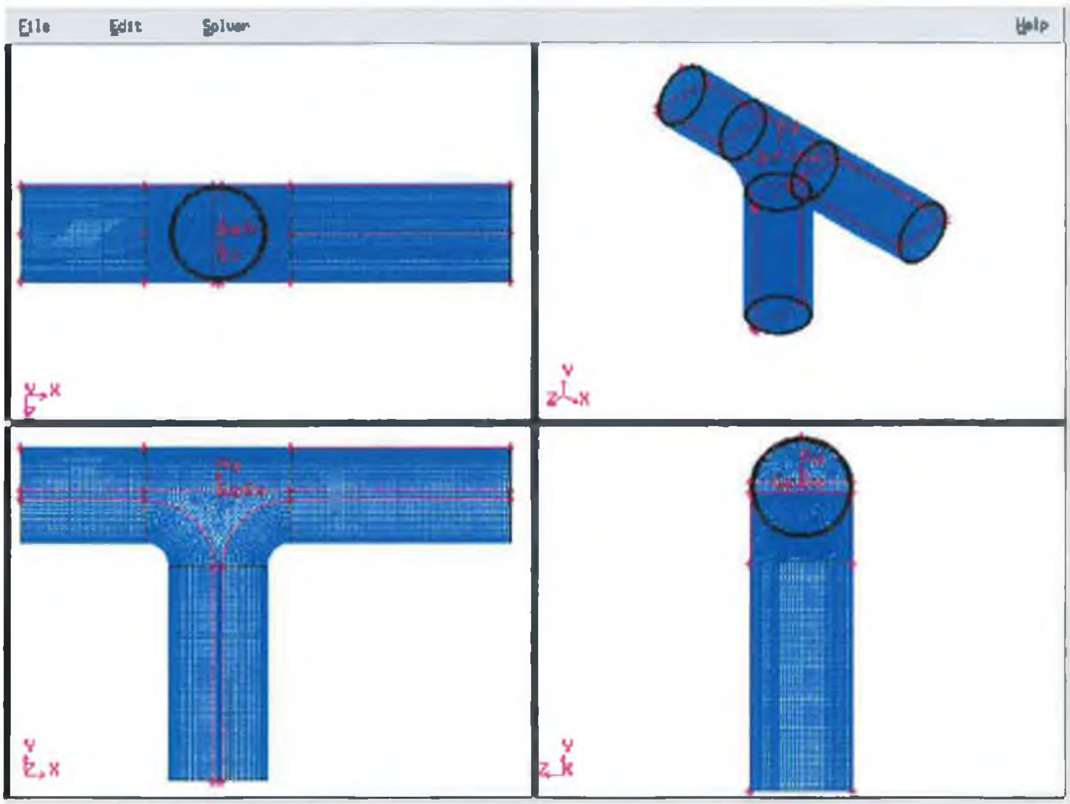

Figure 3.5: Final round entry model including boundary layer

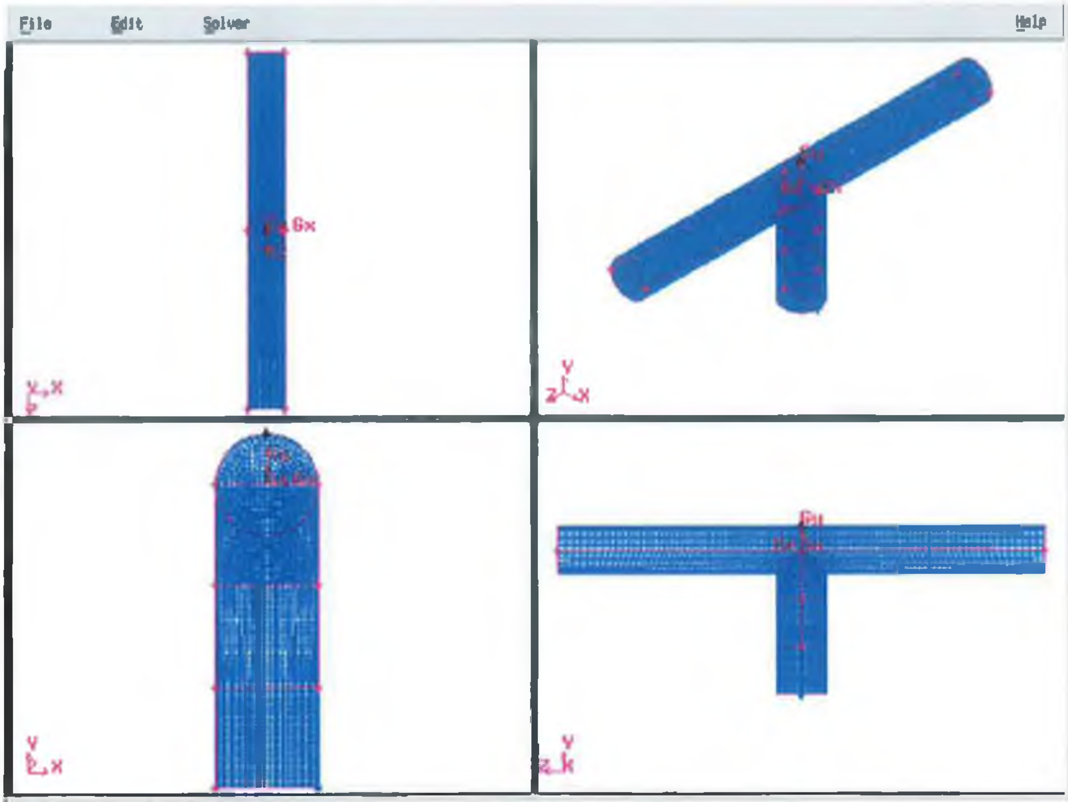

Figure 3.6: Example of sharp entry model including boundary layer

3.4 MESH QUALITY ANALYSIS

One measure of mesh quality, the default used by Gambit, is based on Equi-angle skew. This may be defined as:

$$\max\left[\frac{\theta_{\max}-\theta_e}{180-\theta_e},\frac{\theta_e-\theta_{\min}}{\theta_e}\right]$$

where $\theta_{\min}$ = the smallest angle in a face or cell, $\theta_{\max}$ = the largest angle in a face or cell and θe the angle for a equiangular face or cell (60 for triangles and 90 for square). The range of skewness offers zero as the best event and one as the worst. The mesh examine software offers a range of display and quality types. In striving for a quality mesh it must be remembered that a poor quality grid will cause inaccurate solutions and/or slow convergence. To overcome these effects a range of researchers offer the following words of advice:

1) *Minimise equi-angle skew*: skewness should not exceed 0.85

2) *Minimise local variation in cell size:* adjacent cells should not have a size ratio greater than 20%.

3) If these variations occur it is recommended that the mesh be deleted, the volume decomposed and the domain re-meshed.

Initial trials with various meshes failed one or both of the above recommendations and showed clear signs of grid dependence. Highly skewed elements were also found to adversely affect numerical calculations. Size function was used to specify the rate at which the mesh elements change size in relation to one another thereby controlling the element skewness. Figure 3.7 presents data in relation to size ratio. Following several readjustments the local variation in cell size was found to be well below the maximum recommendation of 20%. The maximum cell size variation found throughout the domain of the final model used for a 50mm round entry tee was 12%. 85% of the entire range of cell used in the mesh had a size ratio of 5% or less. For a similar sharp entry tee the maximum variation found was 14% and 85% of the entire range found to have a mesh size ration of less than 8% (fig 3.9).

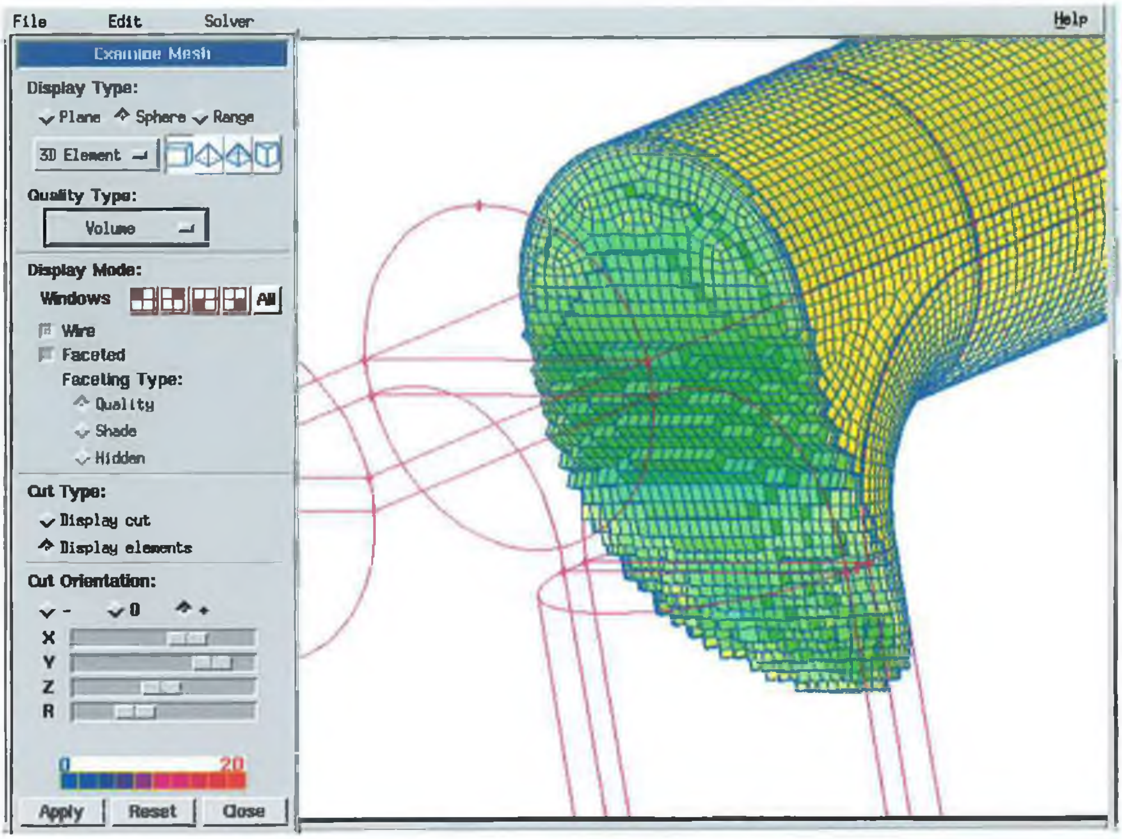

Figure 3.7: Local variation in model cell size

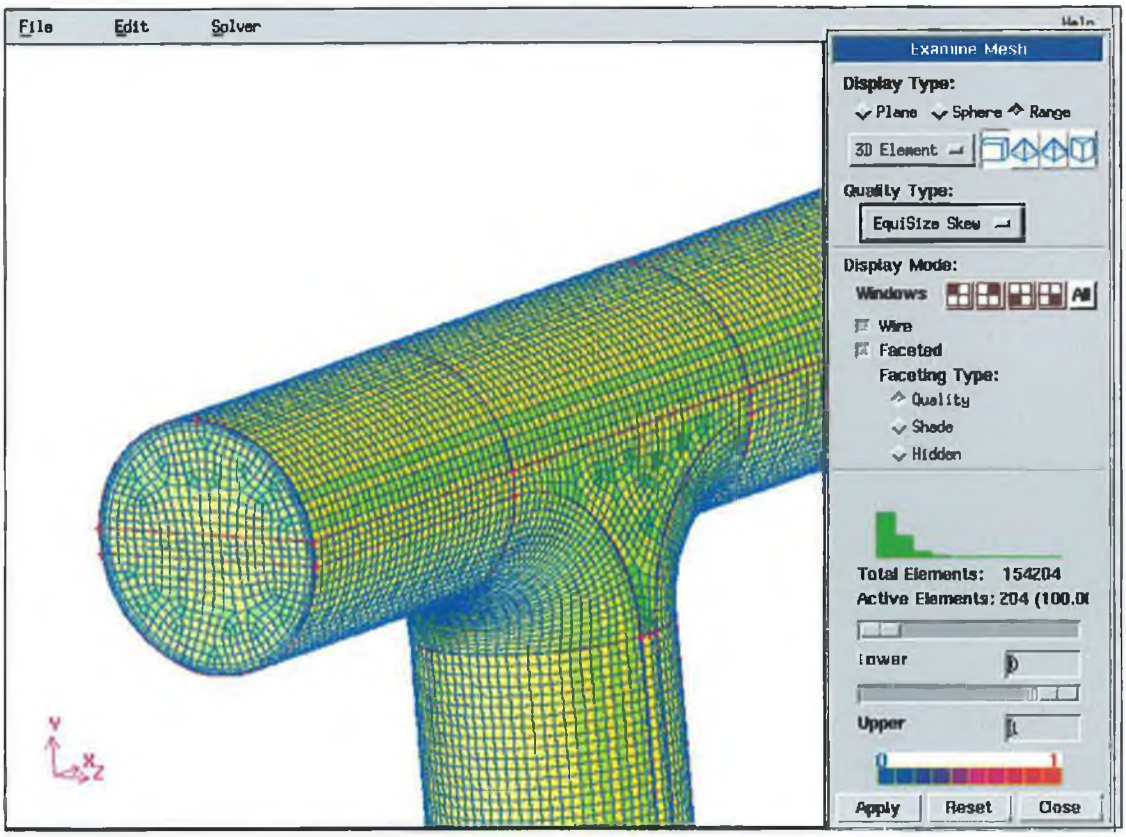

Figure 3.8: Elements within a specified quality range. Equi-angle skew 0 to 1

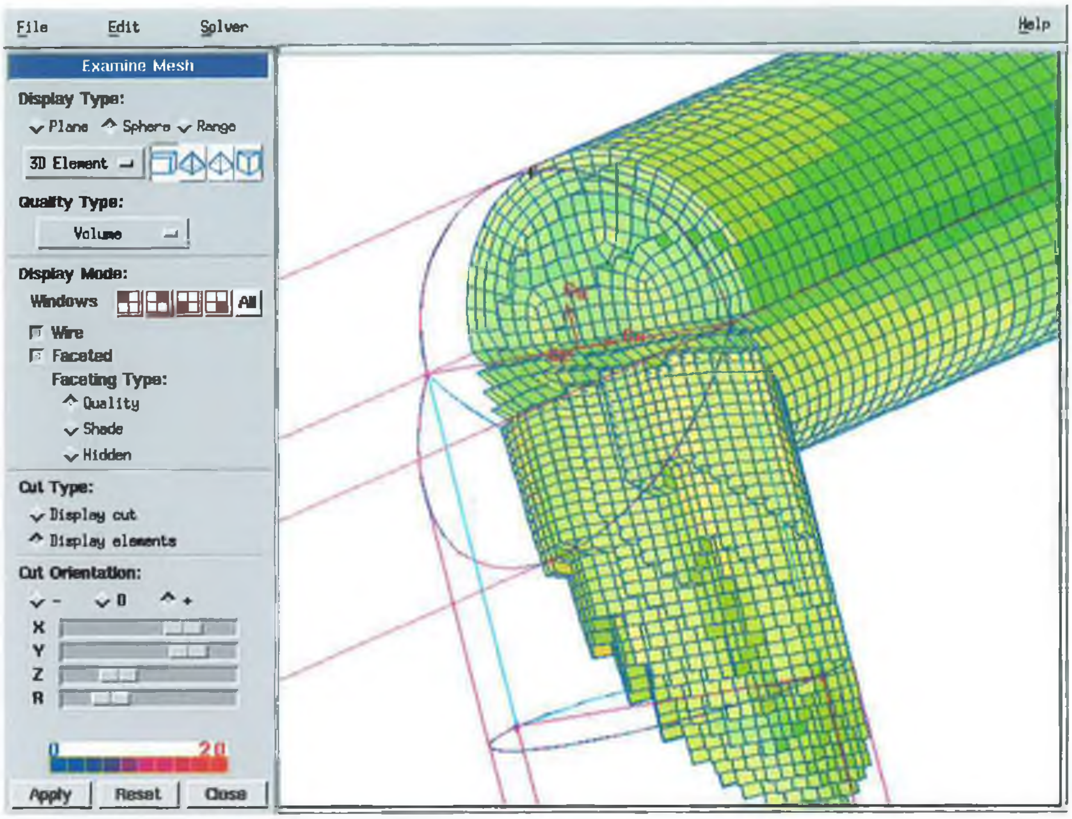

Figure 3.9: Local variation in model cell size for sharp entry tee

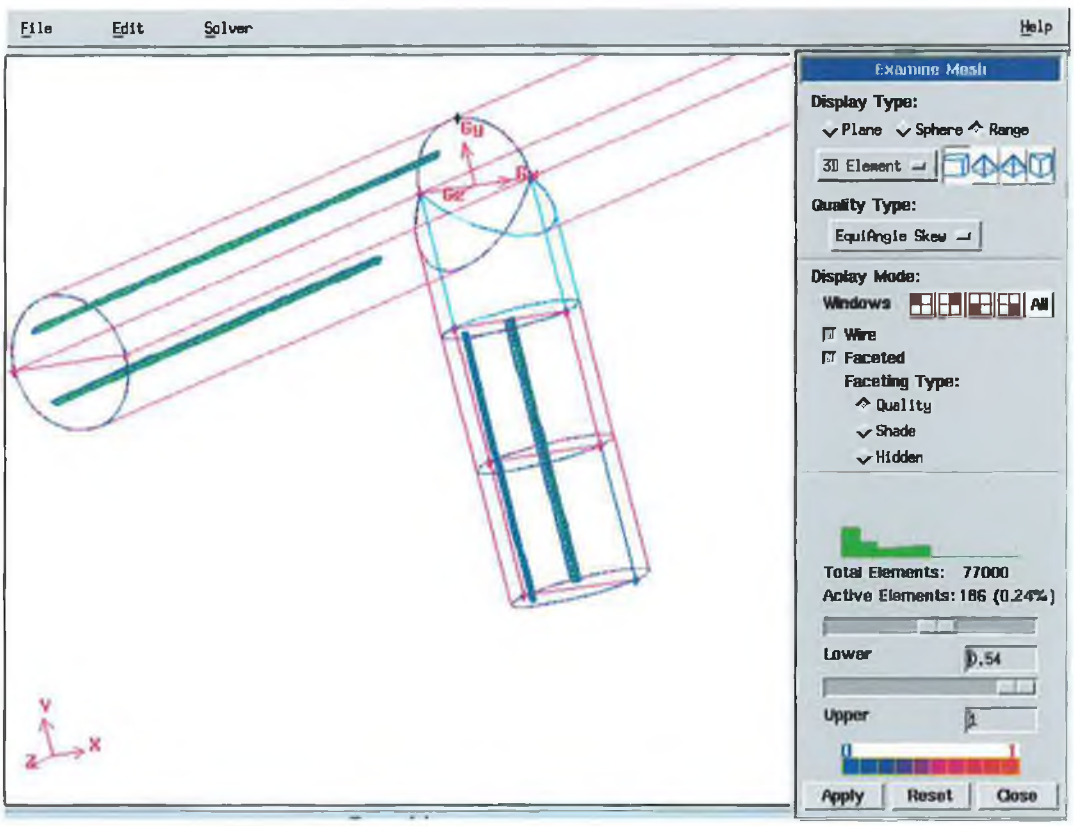

Figure 3.10: Equi-angle skew for a sharp entry 50mm tee

The elements presented in figure 3.8 give an insight into the quality of the mesh based on equi-angle skew. The histogram consists of a bar chart representing the statistical distribution of the mesh elements with respect to the specified quality type. Each bar corresponds to a unique set of upper and lower quality limits. The low values indicate that the mesh is of extremely high quality and fall well within the accepted range of cell skewness of less than 0.85. For the mesh presented no cell ever exceeded a skewness of 0.65 and 92% of all cells had a skewness value below 0.48. It is important to check the quality of the resulting mesh, because properties such as skewness can greatly affect the accuracy and robustness of the CFD solution. For a sharp entry tee (fig 3.10) the histogram is more evenly distributed up to a skewness of 0.5. However at this point only 0.24% of cell were found to have a skewness of 0.54 and above this value no cells were found indicating an excellent quality mesh. It can be noted from the diagram that problem cells were in the upstream region of the tee and deep within the branch well away from the branch where most of the activity was found to take place.

3.5 FLUENT SOLVERS

The current version of Fluent (Fluent 5.4) offers the use of two numerical methods when solving flow problems, the segregated solver method or the coupled solver method. Using either method Fluent will solve the governing integral equations for conservation of mass and momentum and when appropriate energy using a control-volume-based technique which consists of:

- Division of the domain into discrete control volumes using a computational grid.

- Integration of the governing equations on the individual control volumes to construct algebraic equations for the discrete dependent variables (unknowns) such as velocity, pressure, temperature etc.
- Lineraisation of the discrete equations and solution of the resultant equation system to yield updated values of the dependant variables.

The two numerical methods employ a similar discretization process(finite volume), but the approach used to linearise and solve the discretized equations are different. With the Segregated Solution Method the governing equations are solved sequentially i.e. segregated from each other. Because the governing equations are non-linear several iterations of the solution loop must be performed before a converged solution is obtained. Using the Coupled Solution Method the governing equations are solved simultaneously i.e. coupled together. In both the segregated and coupled solution methods the discrete, non-linear governing equations are linearized to produce a system of equations for the dependent variables in every computational cell. The manner in which these equations are linearized may take an implicit or explicit from with respect to the dependent variable. The coupled solvers are recommended if a strong inter-dependence exists between density, energy, momentum and/or species. In general the coupled implicit solver is recommended over the explicit as it runs roughly twice as fast. However it required twice as much memory. The coupled explicit solver should only be used for unsteady flows when the characteristic time scale of the problem is of the same order as that of acoustics (e.g. tracking transient shock waves).The segregated implicit solver is generally preferred in all other cases as it has lower memory requirements and provides flexibility in solution procedures.

3.6 IMPORT AND SET UP OF MODEL IN FLUENT

Once the various models used in this thesis were developed and analysed in Gambit (as outlined previously) they were imported into Fluent 5.5 and conditioned to allow each model to be solved. The following paragraphs outline the settings applied within Fluent before the models were solved.

a) Each mesh was read into Fluent and checked to ensure the quality of the domain. The mesh was then adjusted using Fluents smooth and swop, which can be used to improve the quality of an imported mesh. Any cells that may cause problems during solving within Fluent are adjusted in order to aid convergence. Once problem cells have been adjusted the mesh may then be scaled and units applied. The mesh may then have a model applied.

b) The solver settings applied to each model were selected based on best current practice. The solver employed through this investigation was the segregated implicit solver. The viscous models applied included k-ε, realisable k-ε, and the Reynolds Stress Model (RSM). These viscous models were selected based on the fact that they are robust and the most widely validated models currently available. The constants employed for the range of models investigated were the default models used within the Fluent package A non-equilibrium wall function was selected over the standard wall functions approach. This type of wall function is recommended for use with complex flows were separation and reattachment may exist. Recent research has shown improvements in wall shear stress and skin friction coefficient analysis when the non-equilibrium wall function is applied. To obtain the same accuracy by means of direct numerical simulation which include points within the laminar sublayer the near wall grid spacing must be so fine as to be uneconomical. All walls within the tee were declared as a non-slip wall boundary condition. Using the material specification sheet water at ambient temperature (with a density of 998.2 kg/m^3 and a viscosity of 0.001 kg/ms) was specified throughout the current study.

c) Boundary conditions were applied to the inlet, outlet and branch of the tee. For divided flow conditions an inlet velocity profile based on LDA measurements (Espinosa et al, 1997) was specified (table 3.1). As stated previously it has been found that convergence was faster when a reasonable initial guess for the k and ε was included in the model. This applies to all models used in this thesis and in particular major advantages have been found using this technique with the RSM model. An overview of these profiles are presented in table 3.2 for an average inlet velocity of 1.85 m/s

y	**0**	**2.5**	**5.25**	**8**	**10.5**	**13**	**15.57**	**18.5**	**21**	**23.75**	**25**
I	0.06	0.063	0.069	0.078	0.094	0.1	0.132	0.173	0.251	0.323	0.4
k	0.018	0.02	0.0224	0.03	0.044	0.049	0.086	0.148	0.311	0.516	0.791
ε	0.016	0.018	0.024	0.034	0.06	0.072	0.166	0.374	1.14	2.43	4.62

Table 3.1: Inlet boundary conditions for a 50mm rounded tee

For dead-leg flow conditions it was assumed that the inlet velocity profile entering the tee was fully developed and a velocity profile was generated based on the one 7th

power law model. This model was used to generate profiles of inlet velocity from 0.5 to 2 m/s in steps of 0.25m/s and initial data for k and ε generated using these profiles to aid convergence. A summary of some of the profile data used during dead-leg analysis is outlined in table 3.2 below

Umax	**R=0**	**5**	**10**	**15**	**20**	**21**	**22**	**23**	**24**	**25**
0.5	0.5	0.4843	0.4648	0.4386	0.3972	0.3847	0.3692	0.3484	0.3155	0
1.0	1.0	0.9685	0.9295	0.8772	0.7944	0.7695	0.7385	0.6968	0.6311	0
1.5	1.5	1.4527	1.3942	1.3158	1.19	1.15	1.1077	1.0452	1.9466	0
2.0	2.0	1.937	1.859	1.7544	1.588	1.539	1.477	1.393	1.262	0

Table 3.2: Velocity profiles for a 50mm dead-leg tee

d) Initialisation controls and monitoring of residual was used to check progression of the models. At the end of each solver iteration the residual sum for each of the conserved variables was computed and stored thus recording the convergence history. This history was saved in a data file.

e) Validation of results: A key component of any CFD simulation is the validation of results generated by the software package. A number of steps were taken throughout the course of this study to ensure the quality of results. These included the use of LDA data from previously published work as boundary conditions for newly developed models and the comparison of simulated results with LDA plots. A number of trips were made to Fluent Europe with CFD models to have them evaluated by

Property	Slice Location	Position	k-e size interval 4	k-e size interval 2	Realisable k-e	RSM 2^{nd} order
Velocity Magnitude	X line –50	-25	0.3	0.42	0.225	0.25
		+25	0.6	0.475	0.275	0.6
	Y line -25	-25	1.2	1.2	1.2	1.2
		-30	0.2	0.2	0.2	0.2
Dynamic Pressure	X line –25	-35	1050	1100	1100	1100
		+35	1000	1000	700	1000
	X line -50	-25	50	80	80	80
		+25	180	110	110	110
	Y line –25	+20	700	750	750	750
		-30	100	100	100	100
	Y line -95	+25	780	787.5	787.5	787.5
		-25	780	787.5	787.5	787.5
Turbulent Intensity	X line –50	+20	0.26	0.31	0.24	0.25
		-25	0.07	0.12	0.12	0.12
	X line –100	+20	0.12	0.14	0.24	0.14
		-25	0.06	0.07	0.14	0.07
	Y line +75	0	0.34	0.475	0.31	0.31
	Y line -25	0	0.0525	0.06	0.0425	0.525
Skin Friction Co-efficient	X line –25	-25	15	25	25	25
		+25	16	20	20	20
	Y line –95	-25	37.5	32.5	35	35
		+25	37.5	32.5	35	35
	Y line -25	-25	8	6	6	6
		+25	16	18	18	18

Table 3.3: Sample of validation studies evaluating grid independence

senior CFD engineers. These trips proved invaluable in terms of practical tips and in keeping up to date with current best practice. Grid independence studies were carried out on a range of models to ensure that the grid was not affecting the final results. A sample chart of data collected during one such trial is presented in table 3.3. The final chapter of this thesis highlights two rigs used for flow visualisation studies. The first, a dye injection rig, was designed in the early stages of the research to give an insight into flow patterns within a dead-leg branch. The second, a hydrogen bubble visualisation rig, was purchased shortly before completion of this thesis and offered an opportunity to study dead-leg patterns at higher flowrates than those available from the dye injection tests.

CHAPTER 4. RESULTS AND DISCUSSION

Part A. The move from divided flow to dead-leg flow conditions

4.1 DIVIDED FLOW PROFILES FOR A 50MM EQUAL TEE

Divided flow contours of velocity magnitude are presented in figure 4.1. Analysis of these contours indicate that the original inlet turbulent velocity profile is maintained along the length of the tee up to the inlet radius of the branch at x/D = -1.0. At x/D = -0.75 a separation region emanating from the upstream branch wall can be identified, as highly strained fluid flows into the branch. This point (x/D = -0.75) corresponds with the start of the radius of curvature of the bend. The effect of this separation point is to accelerate the fluid in the lower half of the tee in anticipation of the branch.

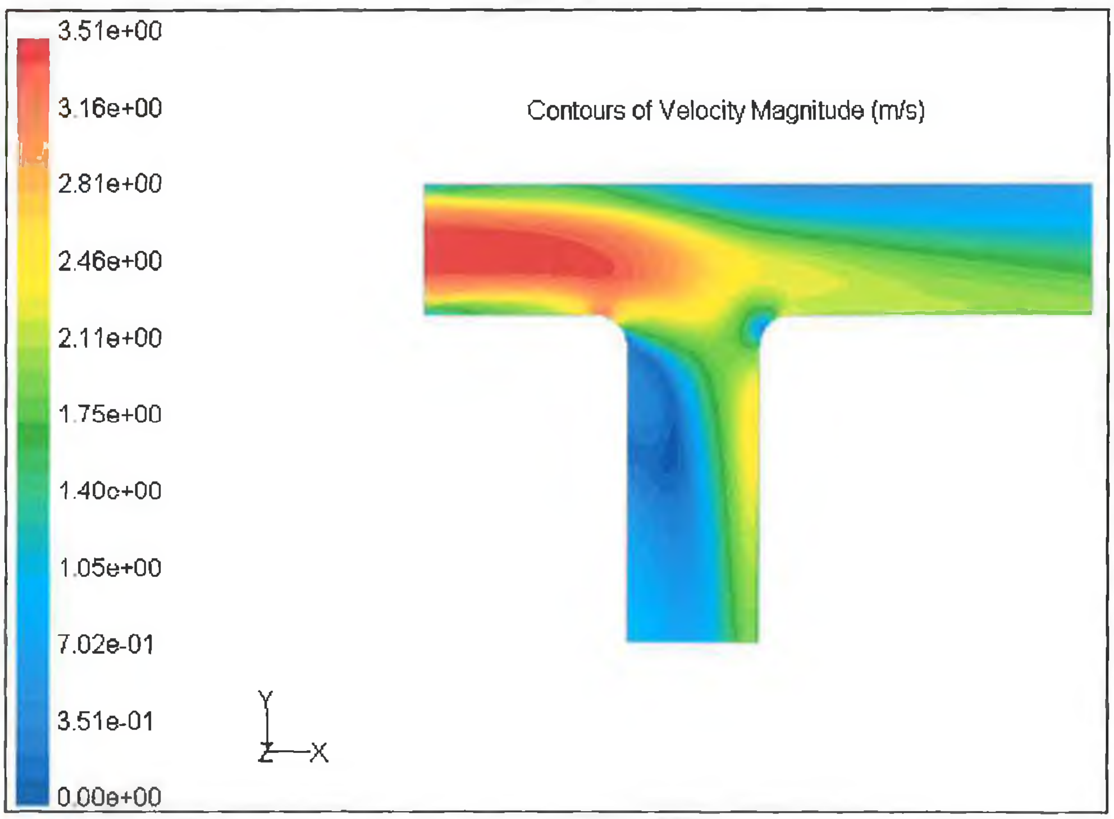

Figure 4.1: Divided flow velocity magnitude contours

By the time the fluid has reached half way across the branch (x/D = 0) the main flow has begun to divide and separate and the initial velocity profile changes rapidly (figure 4.2).

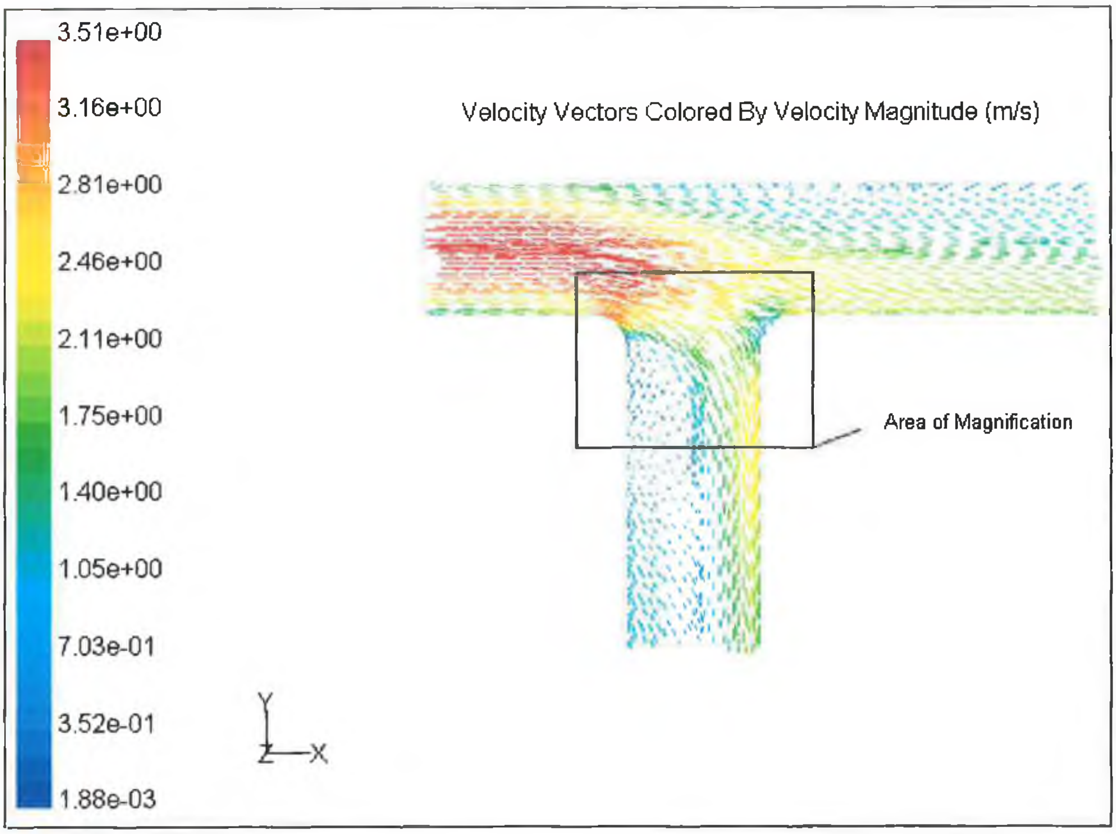

Figure 4.2 Divided flow velocity vectors

The mainstream flow was found to separate around a stagnation point on the down-stream wall of the branch at x/D = 0.6. The mainstream flow across the top of the tee was drawn down towards the bottom of the pipe following separation. This concentrated the mainstream flow in this region into an area covering ¾ of the pipe diameter. An area of low flow velocity was also noted in this region which began as a narrow strip at x/D = 0 and continued to expand until it covered ¼ of the flow area at the outlet from the straight through branch of the tee. The velocity range in this region was from 0.2 to 1.0 m/s. The potential for bio-film formation in this region would increase due to the low velocities encountered. However this would be dependant on the length of time the flow is diverted into the branch as a return to full flow would return this region to a turbulent flow profile negating the potential for build up. A similar configuration was noted along the upstream wall of the branch of the tee. The potential for bio-film build up was considered to be even greater in this area due to the very low velocities and wall shear stresses encountered. A re-circulation region occupied an area up to half the width of the tee branch. This resulted from a separation point at y/D = -0.75 (i.e. at the base of the inlet radius of the branch) on the upstream wall of the branch (figure 4.3).

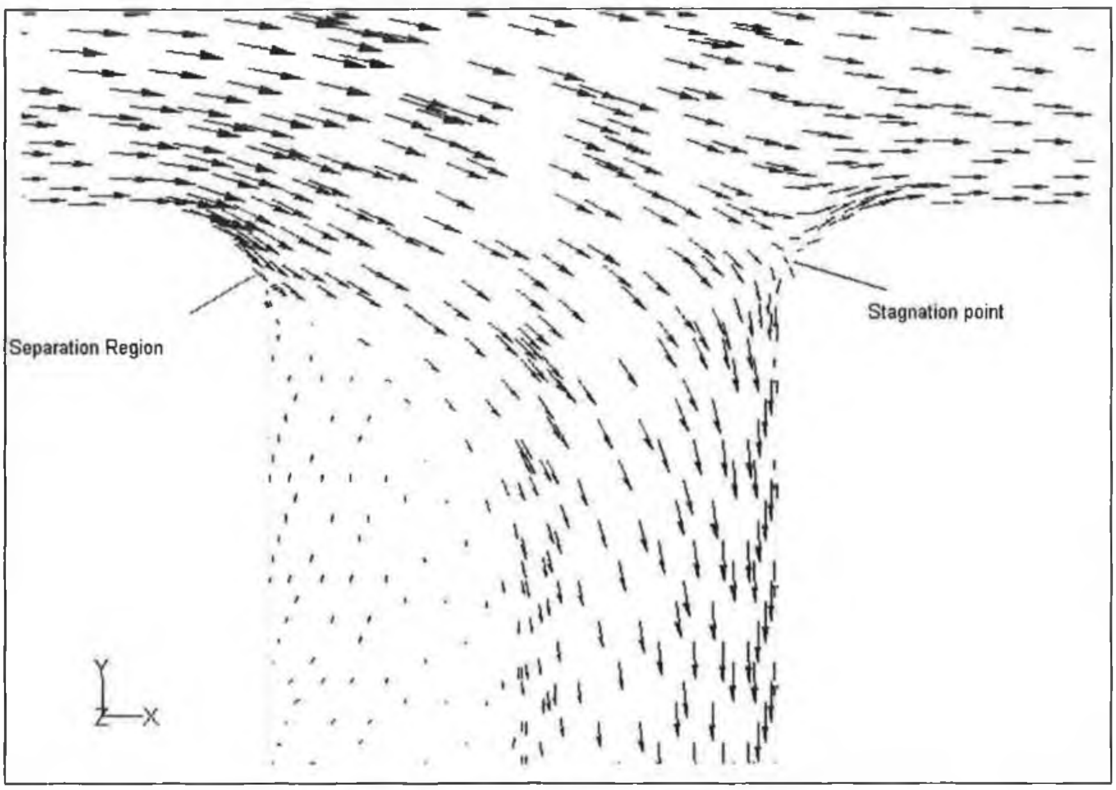

Figure 4.3: Divided flow stagnation and separation points

The velocity magnitude within the re-circulation area was found to be zero close to the centre and along the wall increasing to 0.7 m/s at the outer edge along the branch centreline. Bacteria entering this re-circulating region would find a safe haven with the potential for passage to the wall laminar sub-layer. Low wall shear stresses in this region would enhance the potential for attachment and propagation. This area is of considerable interest in the fight against bio-film formation as a return to dead-leg flow, (i.e. full flow across the top of the tee and the branch closed off) when the branch valve is closed will not increase the velocity profile in this region. Once bacteria had established itself it would be extremely difficult to dislodge through the conventional methods of increasing flowrate and increased wall shear stress. It is clear from figure 4.2 that the downstream wall of the branch, apart from the separation region, is well scoured by the fluid during divided flow while the same section of the upstream wall remains relatively undisturbed. Velocities of up to 2.5 m/s were not uncommon along the downstream wall. It is clear from the magnified view of the entrance to the tee branch (figure 4.3) that the separation point on the upstream side of the branch and the stagnation point on the downstream side were almost aligned. This view also clearly indicates an acceleration of fluid on the downstream wall of the branch with tightly packed velocity vectors while the upstream wall is only exposed to the slow moving re-circulating region noted by previous researchers.

4.2 DEAD LEG FLOW PROFILES FOR A 50MM EQUAL TEE

Dead leg contours of velocity magnitude are presented in figure 4.4 for a round entry 50mm equal tee. This configuration was achieved by preventing flow into the branch. This is a common set up which regularly occurs in pharmaceutical and semi-conductor plants when the branch valve is in a closed (isolated) position. This dead-leg configuration results in full flow across the top of the tee. Analysis of the velocity contours indicates that the original upstream turbulent velocity profile is reasonably well maintained across this top portion of the tee. Up to x/D = -0.75 the profile remains undisturbed. The change in the radius of curvature of the tee at entry to the branch does influence the velocity profile. Some of the fluid flow across the top of the branch penetrates the branch at this point to a depth of 6.25mm. However, the effect of this penetration is felt to a depth equal to the radius of curvature of the branch i.e. 12.5mm.

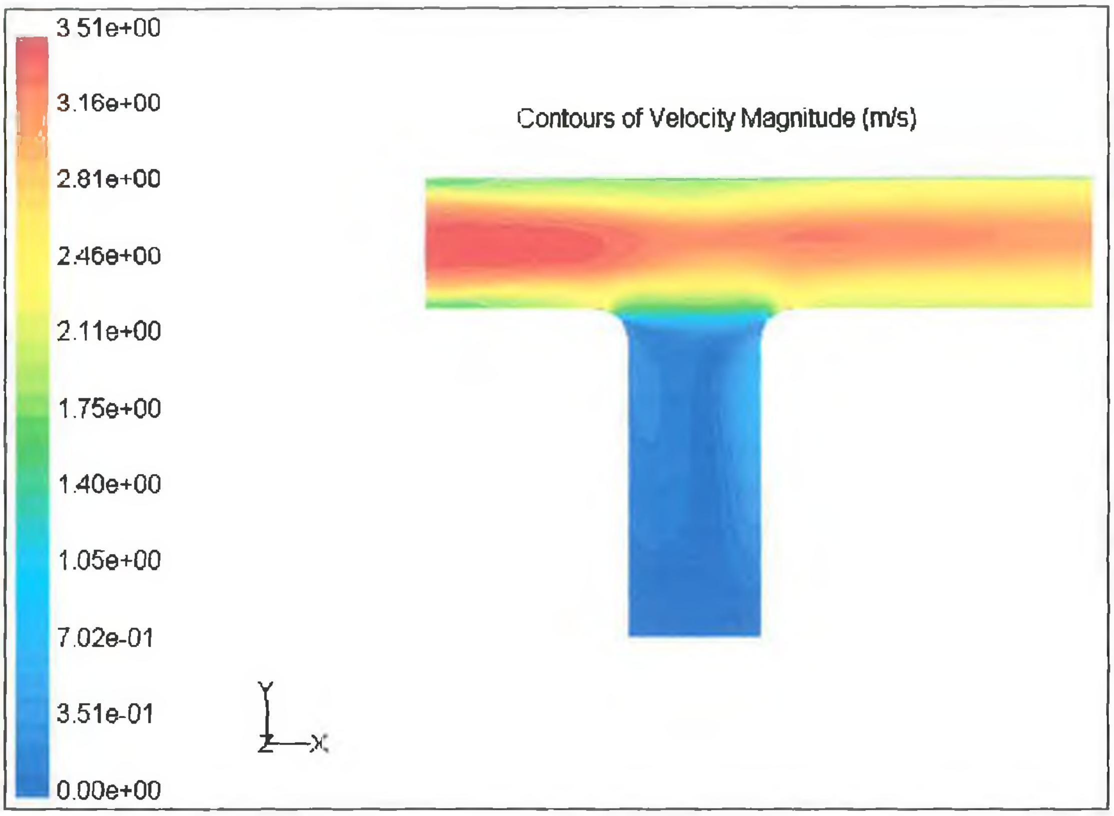

Figure 4.4. Dead-leg flow velocity magnitude contours

The main effect of this penetration into the branch due to dead-leg flow is a fall off in centreline velocity magnitude. A 25% drop off in velocity along the centreline of the straight through portion of the tee was noted from inlet to outlet. This penetration of fluid from the top of the tee into the branch had a significant influence on activity within the dead-leg. At entry to the branch on the upstream wall the fluid was again highly strained as fluid flowing up the upstream wall of the branch attempts to re-attach itself to the high-speed fluid flowing across the branch.

This fast flowing fluid, while attempting to enter the branch due to the radius of curvature, is prevented from doing so due to the blockage presented by fluid already within the dead-leg. The result is a flow induced rotating cell. As the fluid flows quickly across the top of the branch the plug of fluid trapped in the dead-leg prevents mainstream fluid from exiting the branch. The result is a rotating cell in which the trapped fluid is forced to rotate in a clockwise direction down the downstream wall of the branch across the base and back up the upstream wall. This is a slow rotating cell with an average velocity of 0.2 m/s.

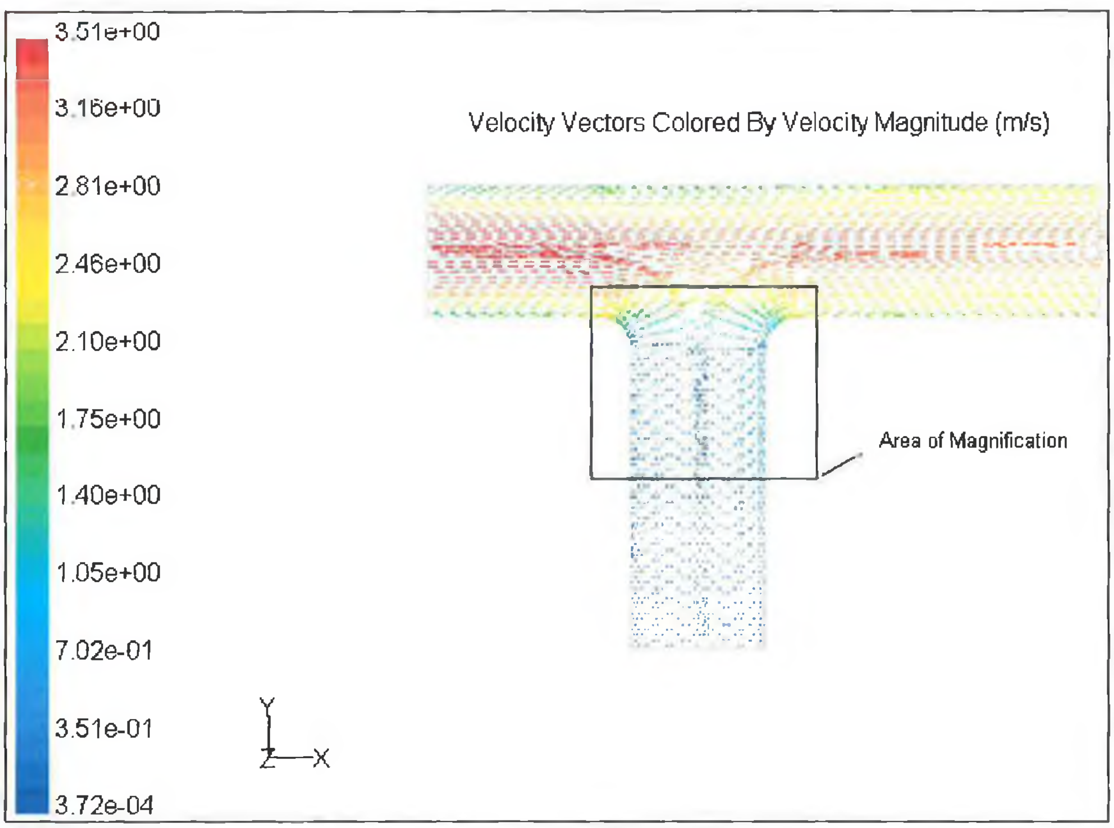

Figure 4.5. Dead-leg flow velocity vectors

Analysis of the velocity vectors in figure 4.5 offers an interesting insight into the flow patterns of the dead-leg tee. Vectors in the straight through section of the tee run smoothly from right to left. The maximum centerline velocity is 3.5m/s. The radius of curvature at entry to the branch offers a wider flow area to the fluid and the vectors clearly show an attempt to enter the branch and a fall in velocity magnitude as the flow is retarded by fluid already in the dead-leg of the branch. The region affected by this retarded flow ranges from x/D = -0.75 to x/D = +0.75. The max velocity in this region of the tee was found to have fallen to 1 m/s.

A reattachment point was noted on the upstream radius of the branch at x/D = -0.625. At this point fluid flowing up the upstream wall of the branch attempts to recombine with fluid flowing across the top of the branch. On closer examination of this region (figure 4.6) a stagnation point was identified on the downstream radius of the branch. This was found to be located at x/D = +0.625. The fluid was found to separate around this point with fluid above prevented from entering the branch and fluid below being forced down the downstream wall of the dead-leg into the branch. It was at this point that the rotating cavity was induced. Maximum velocities of 0.58 m/s were noted along the downstream wall of the branch while upstream wall velocities peaked at 0.23 m/s. The momentum of the fluid across the top of the branch, developed by the speed of the flow in the straight through section of the tee, was carried well into the branch along the downstream wall.

This motion continued down to the base of the dead leg (y/D = -3) with the velocity decreasing the further into the branch the fluid travelled. The fluid then slowly travelled across the base of the dead-leg from x/D = +0.5 to x/D = -0.5 and up the opposite wall albeit at a very slow pace. The difference in velocity between these two walls and the impact of the fluid around the stagnation point resulted in a region of circulation between the centreline of the branch and the downstream wall (figure 4.6). The center of this region was located at x/D = +0.2 and y/D = -0.8. Maximum velocities on the downstream side of this small circulation region of 0.23 m/s were noted while the upstream side peaked at 0.2 m/s.

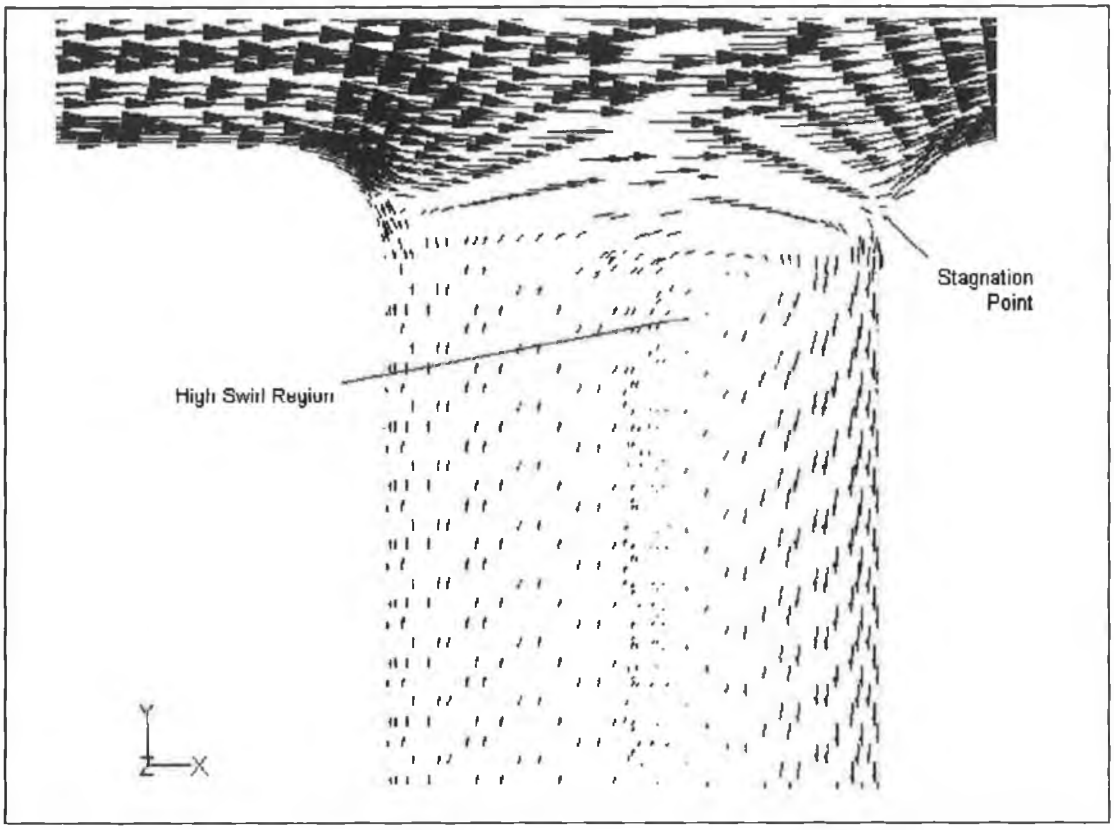

Figure 4.6: Dead-leg flow reattachment and stagnation points

The higher values of velocity on the downstream side of the branch may be attributed to the impact of the fluid on the wall of the branch below the separation point. Following detailed analysis of the high swirl region the author concluded that the fluid in this region, driven on by the speed of the flow above the separation point, impinged on the branch wall and was reflected back towards the center of the branch.

This resulted in the skewed shape of the vortex visible in figure 4.6. Once reflected from the wall the fluids velocity and turbulent intensities dissipated the further into the branch the fluid progressed. Velocities at the base of the dead-leg were found to be of the order 0.0003 m/s indicating little, if any, fluid movement 3D into the branch.

4.3 MAINSTREAM ANALYSIS OF DIVIDED AND DEAD-LEG FLOW

The fully developed turbulent profile used in this analysis is presented in figure 4.7. This model was found to match well with the 'one 7th power law model' and was used by Espinosa (1997) in his analysis of flow in pipe tees. He compared this profile with that measured using Laser Doppler techniques and found an excellent correlation between both profiles. As stated previously this profile was maintained along the length of the tee up to the inlet radius of the branch at x/D = -1.0.

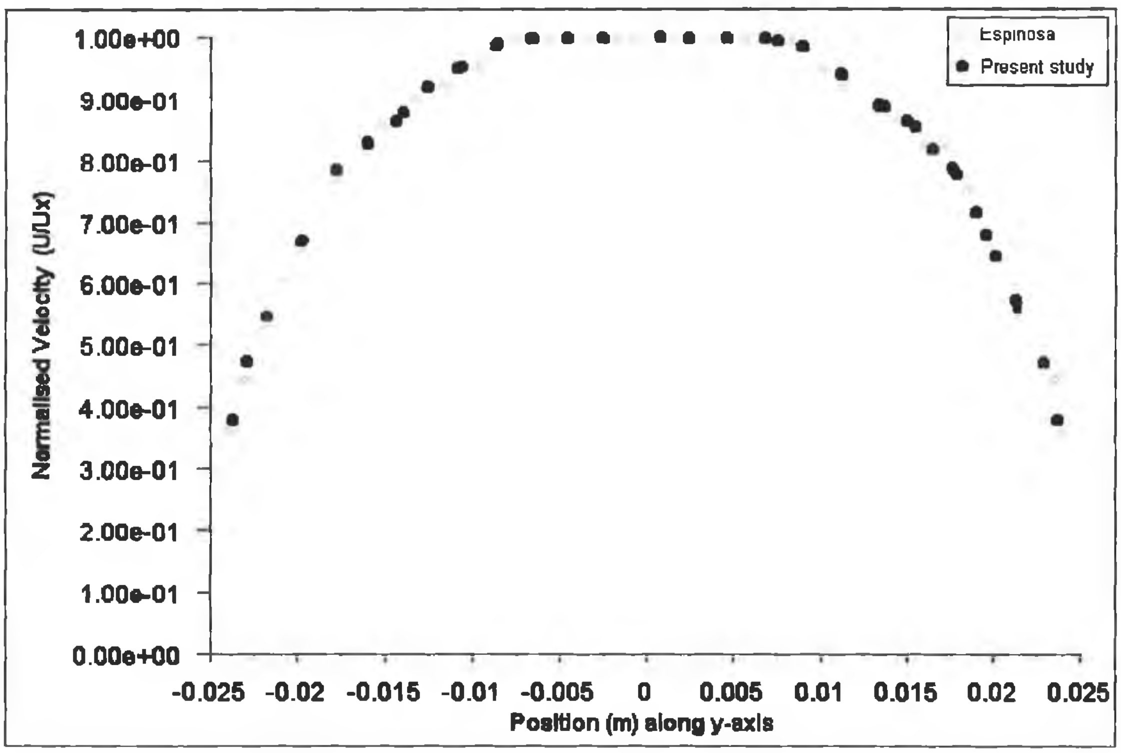

Figure 4.7: Initial turbulent velocity profile

Analysis of the velocity profile for divided flow beyond x/D = -1.0 indicate that a degree of realignment of the flow in anticipation of the branch begins to occur. As the fluid approaches the branch (x/D = -0.75) is begins to accelerate in the region y/D = -0.2 to +0.4 changing the initial profile and a new profile emerges which is presented in figure 4.8. The overall effect of this realignment is a decrease in velocity in the upper half of the straight through branch and an acceleration of the fluid in the lower half as the highly strained fluid is forced into the branch of the tee.

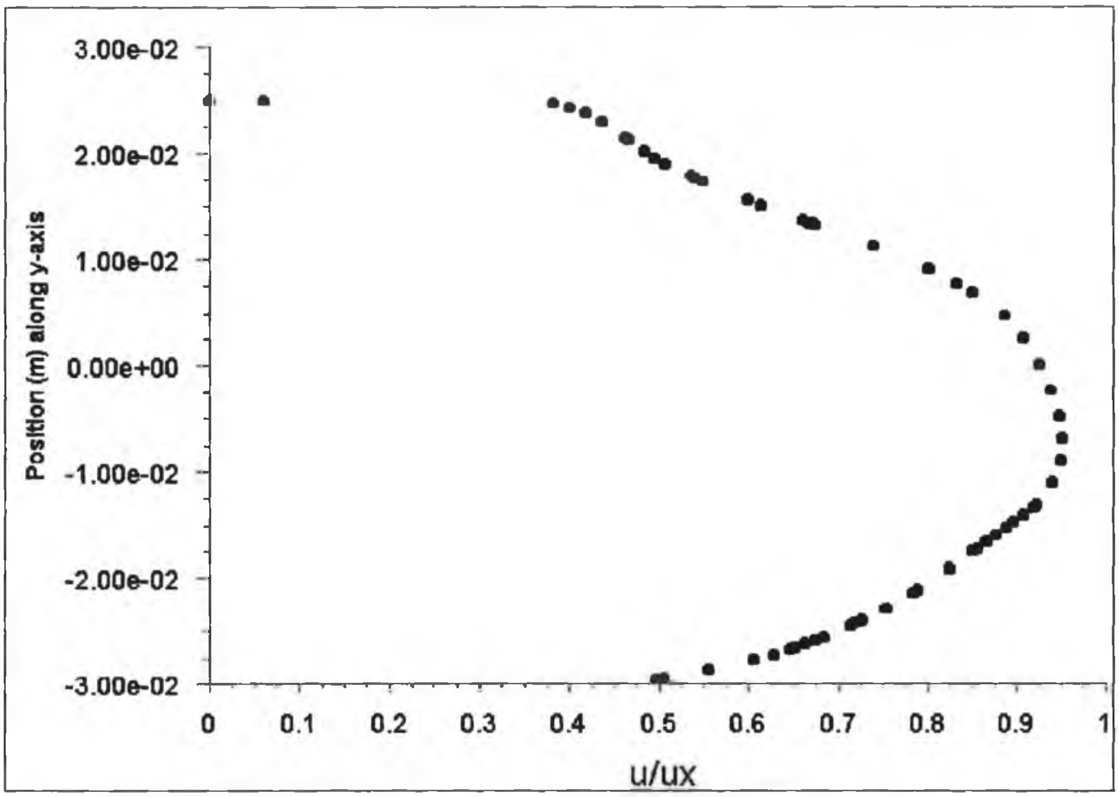

Figure 4.8: Divided flow velocity profile at entry to the branch

When dead-leg flow conditions were induced, by preventing flow through the branch, the initial inlet velocity profile was maintained with only a slight disturbance in the branch wall region. The profile retained its symmetry around the centreline of the straight through branch (figure 4.9). This retention of the initial velocity profile indicates little disturbance of the flow along the straight through section of the tee during dead-leg conditions with the bulk of the fluid remaining unaffected by the body of fluid in the branch dead-leg. It would appear that the dead-leg fluid is no more than a solid boundary preventing flow into the branch with little more effect than to slightly retard the flow along the top of the tee branch.

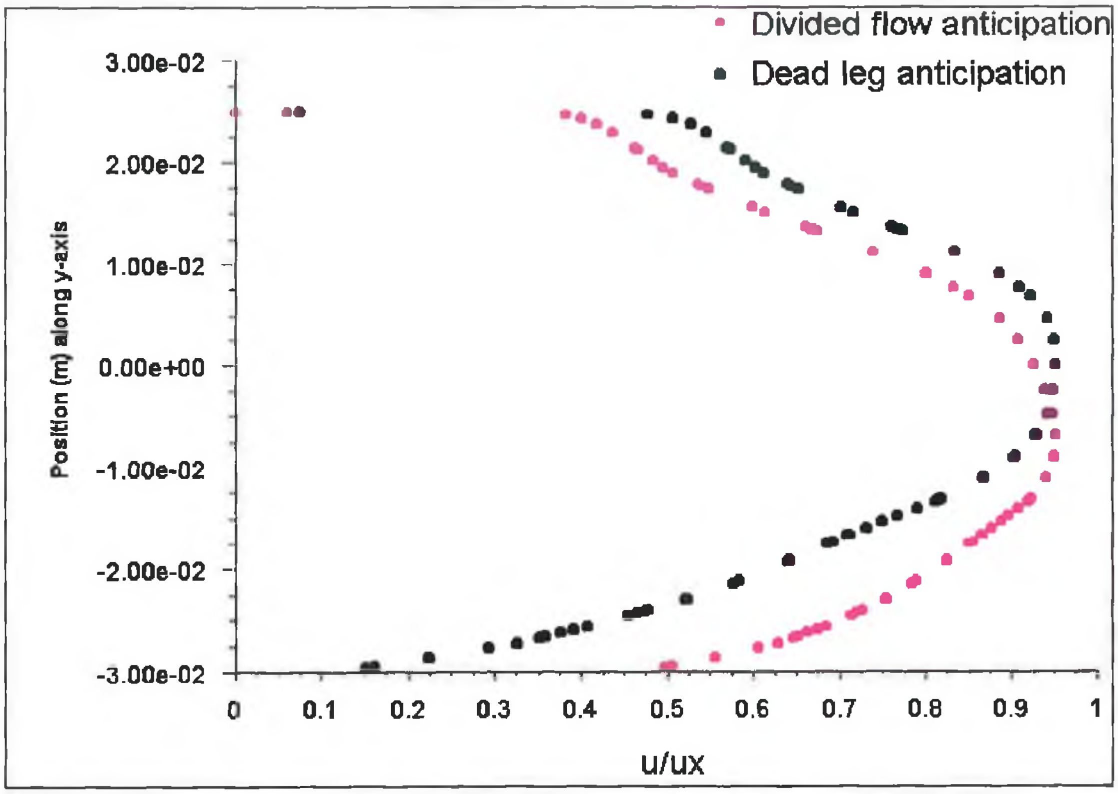

Figure 4.9: Dead-leg and Divided flow velocity profiles at entry to the branch

4.4 DIVIDED FLOW BRANCH VELOCITY PROFILES

Contours of branch velocities are presented in figure 4.10 for divided flow on planes 10mm upstream (x/D = -0.2), 10 mm downstream (x/D = +0.2) and on the centreline of the branch. Examinations of these slices, taken within the branch of the tee, clearly indicate the symmetrical nature of the velocity profiles. An increase in velocity and flow activity is clearly visible at x/D = +0.2 when compared with the same plane at x/D = -0.2. A region of low activity was noted around the centreline of all three planes coinciding with the separation area mentioned earlier.

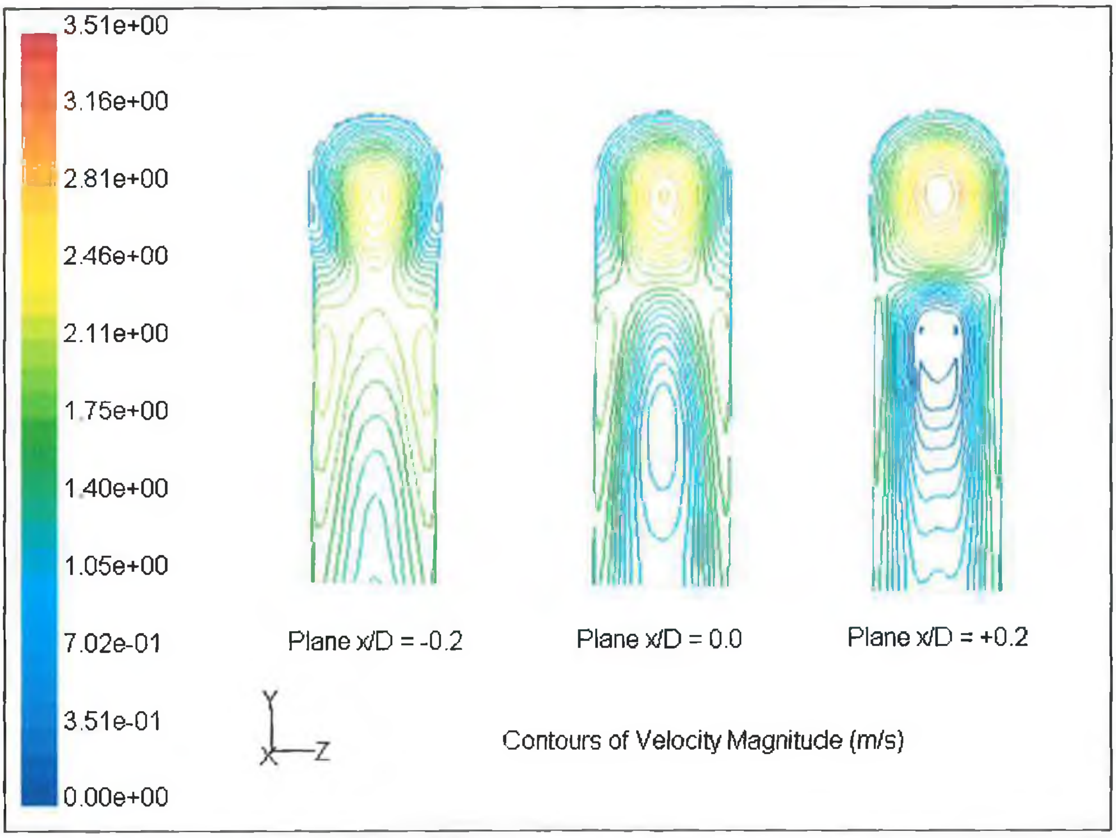

Figure 4.10: Divided flow velocity planes within the tee branch

One thing not captured by the above contour plots is the 3D nature of the flow within the branch. The vector plot presented in figure 4.11 highlights this by magnifying the upper portion of the contours at entry to the branch of the tee. The complex nature of the flow is clearly evident from the flow patterns. The fluid is divided between the upper and lower half of the branch entry region. In the upper half the fluid attempts to remain with the bulk flowing fluid of the mainstream flow section of the tee. In the lower half the fluid is forced into the branch around the separation point (see fig 4.3)

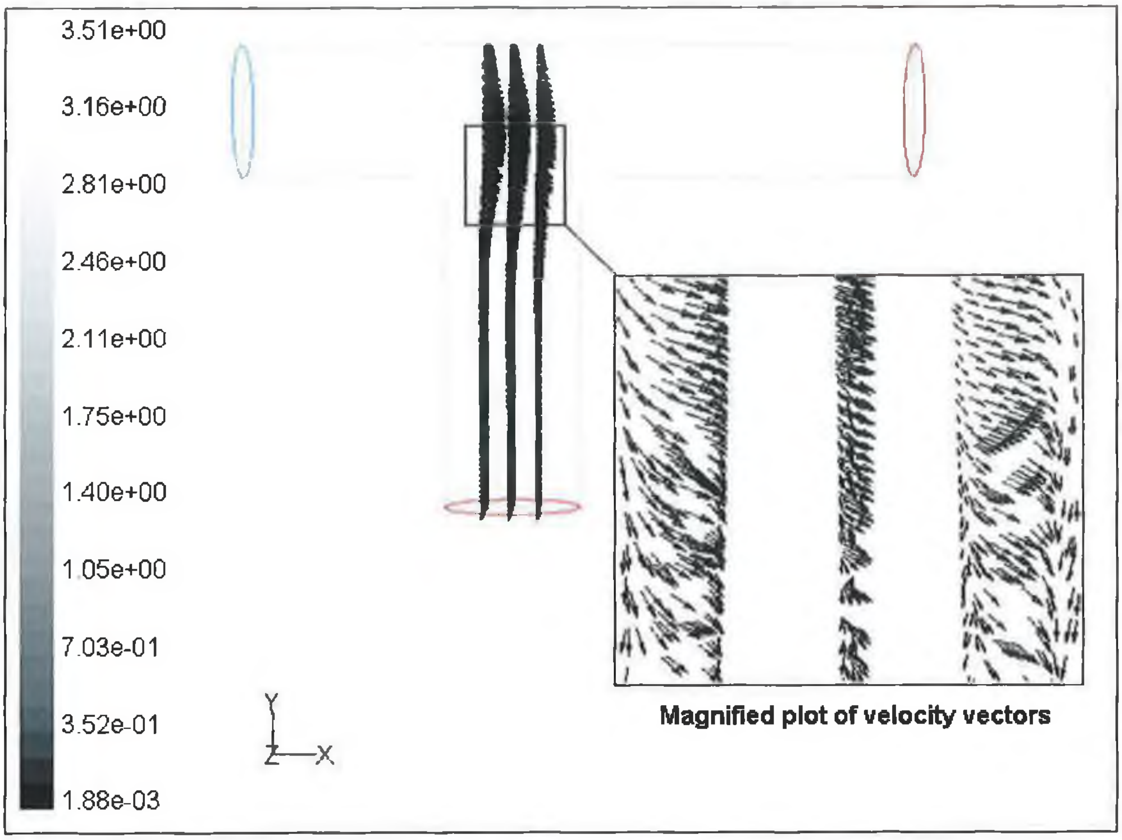

Figure 4.11: Magnified divided flow velocity planes within the tee branch

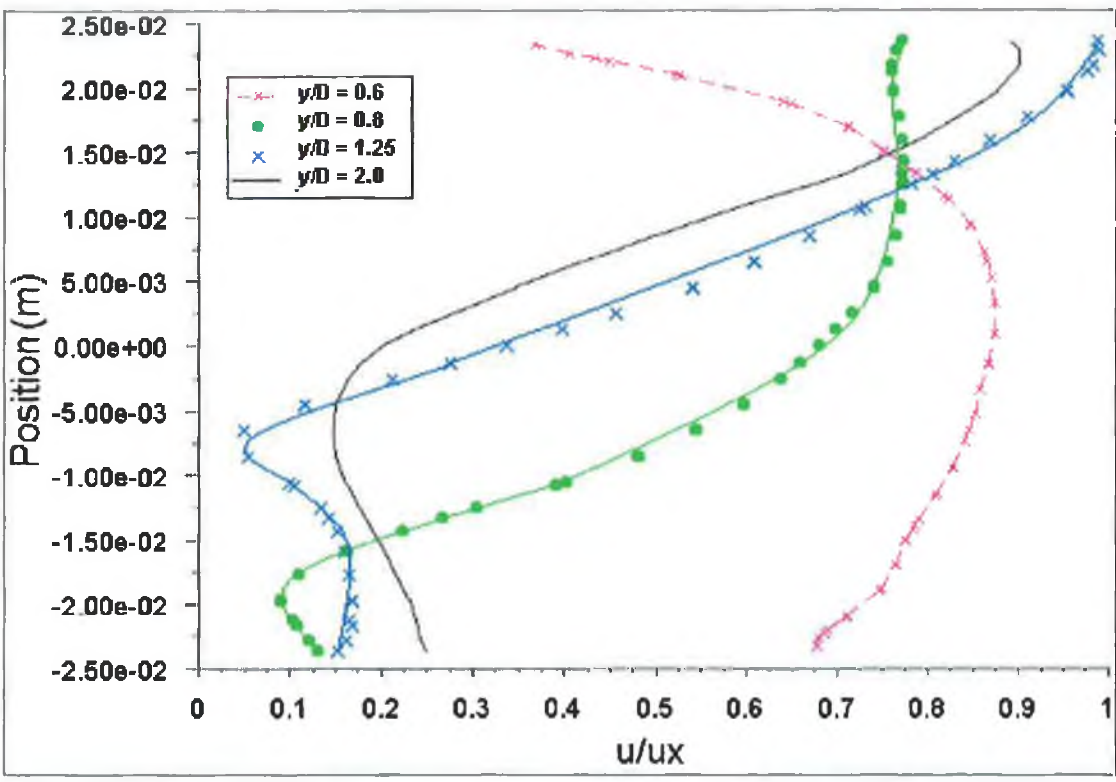

Figure 4.12: Divided flow velocity profiles within the branch

and is influenced by the radius of curvature of the bend. The most complex flow patterns are visible on plane x/D = +0.2 on the downstream side of the branch as the fluid makes a 90 degree change in direction to enter the branch.

Velocity profiles within the branch of the divided flow tee are presented in Figure 4.12 at 30, 40, 62 and 102mm from the centreline of the straight through leg of the branch. These values correspond to y/D values of 0.6, 0.8, 1.24 and 2.04 respectively. It is evident that the flow separates at entry to the branch creating a reverse flow region. Outside of this reverse flow region the flow accelerates from the free shear boundary layer of the reverse region to a maximum velocity of 2.5 m/s. The fluid decelerates again on the downstream wall of the branch exit of the tee. Due to the high acceleration encountered in the branch the flow is almost one-directional in this area outside of the reverse flow region. The separation region expands from the upstream wall of the branch until it almost reaches the centreline of the branch at y/D = 2.04. Le et al (1997) states that profiles with similar characteristics have been observed by other authors (Sierra-Espinosa, et al. 1997. Bradshaw, 1981).

It is worth noting at this point that the fall off in velocity in the separation region from 2.5m/s to 0.1 m/s would be a cause for concern even with divided flow through the branch when using high purity water. The potential for bio-film formation in this region is high as at no point will the wall of the branch in this region be adequately flushed. Under standard operating conditions the branch valve will be opened to allow flow into a production tank (divided flow conditions) and then closed when an adequate amount of fluid has passed leaving the branch in a dead-leg configuration.

The upstream wall of the branch in both cases sees little in terms of scouring from the fluid within the branch.

4.5 DIVIDED FLOW WALL SHEAR STRESS

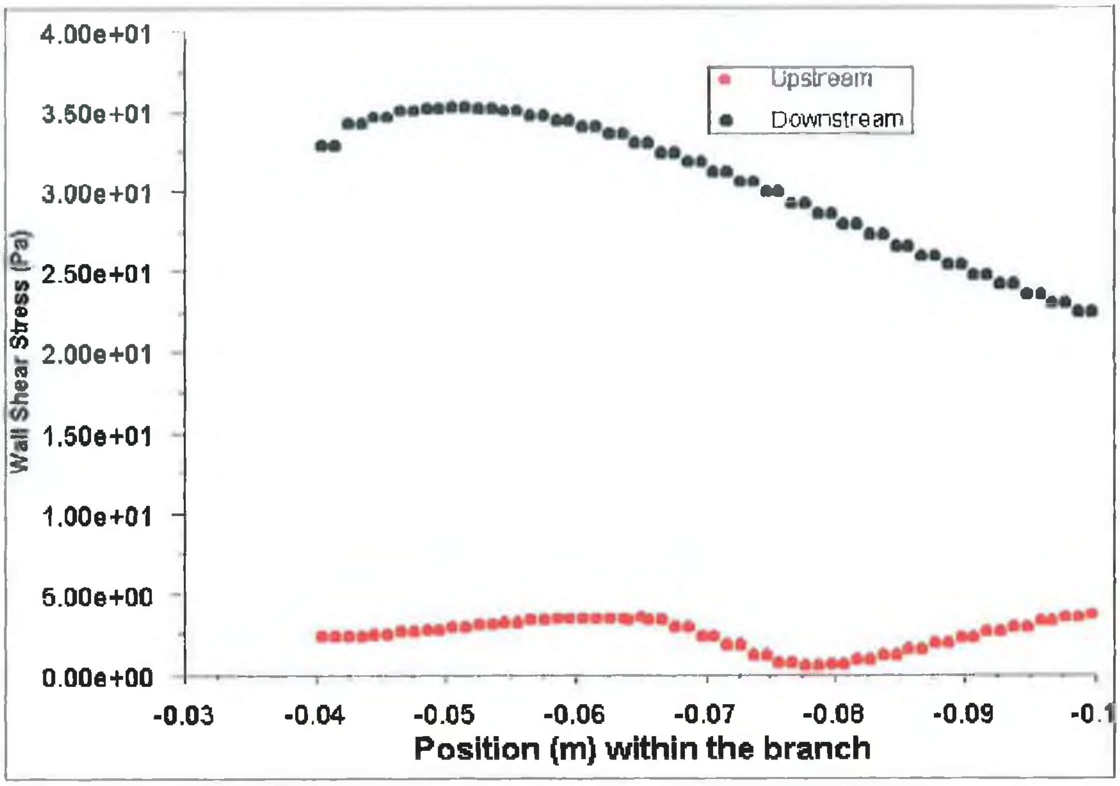

Figure 4.13: Divided flow upstream and downstream wall shear stress within the branch

Figure 4.13 presents wall shear stress values within the branch of the tee for both the upstream and downstream walls. Analysis of the data indicates that the maximum values of wall shear stress are to be found on the downstream wall of the branch for divided flow. A maximum value of 35 pascals was noted approximately 25 mm into the branch. This high value was maintained over a distance ranging form y/D = -0.9 to y/D = -1.1. The shear stress was found to decrease as the fluid flowed further into the branch. A 30% decrease in wall shear stress was noted on the downstream wall 100 mm into the branch.

The wall shear stress on the upstream side of the branch was found to have a maximum value of 7.5 pascals, an 80% decrease in comparison to that found on the downstream side. This value remained relatively constant over the range y/D = -0.75 to y/D = -1.3 and suddenly dipped to a low of almost zero at y/D = 1.55 before recovering back to its original maximum value. As stated previously wall shear stress is of considerable interest in the study of bio-film formation. The fact that a values of zero shear stress are to be found on the upstream wall of a divided flow tee is of major concern as these conditions favour bio-film attachment and growth.

4.6 DEAD-LEG FLOW BRANCH VELOCITY PROFILES

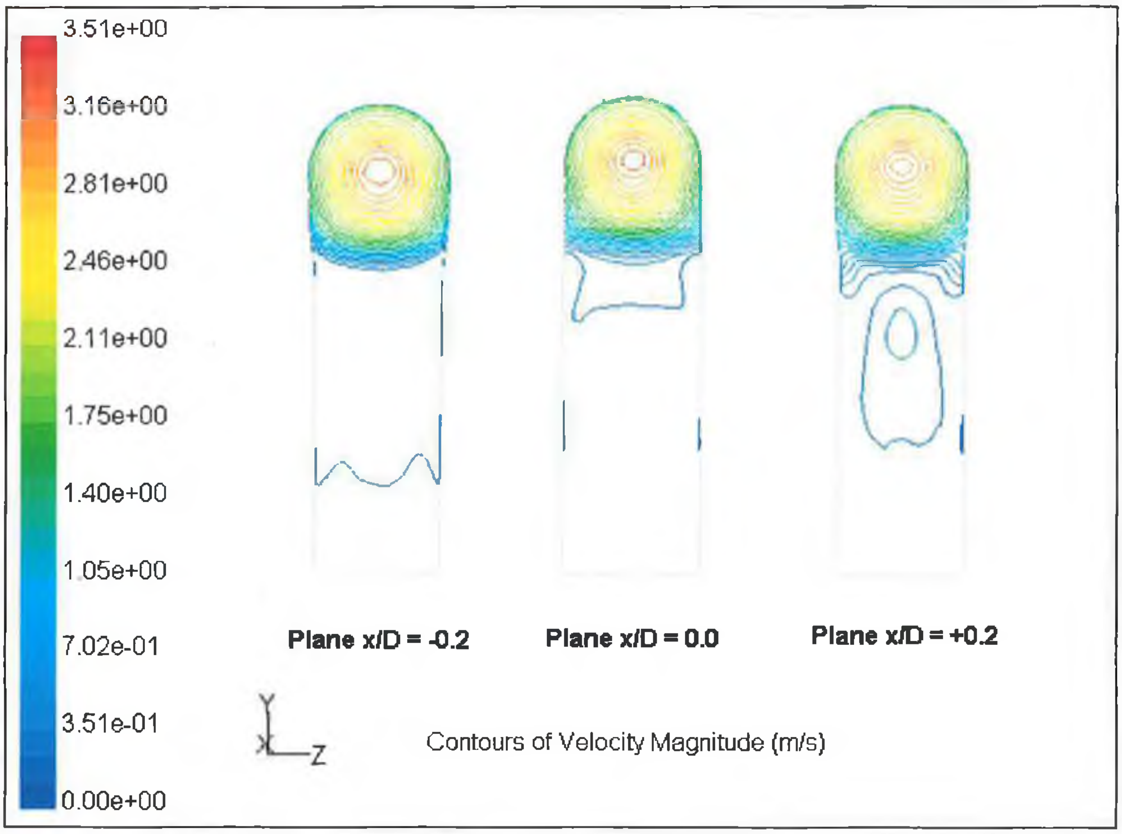

Figure 4.14: Dead-leg flow velocity planes within the tee branch

Contours of branch velocities are presented in figure 4.14 for dead-leg flow on planes 10mm upstream ($x/D = -0.2$), 10 mm downstream ($x/D = +0.2$) and on the centreline of the branch. Examination of these slices highlights symmetry in the flow patterns for dead-leg flow. Most of the activity in this configuration occurs in the upper straight through section of the tee. A key feature is the ability of the flow to maintain the inlet velocity profile across the dead –leg branch. The core of the flow remains undisturbed by any activity associated with the dead-leg. Following the introduction of the dead-leg configuration the separation region observed during divided flow was eliminated at entry to the branch. Fluid from the main straight through pipe entered the branch to a depth of the half the radius of curvature of the branch.

A ripple effect was noted across the top of the branch as fluid was prevented from entering the branch by fluid already within the dead-leg. This ripple effect coupled with separation within the branch around the stagnation point induced a region of swirl (a vortex) outlined in fig 4.6 between the centreline of the branch and the downstream wall. Figure 4.15 clearly highlights two separate regions of flow encountered during dead-leg conditions. The bulk of the fluid in the upper region of the tee remains fixed on flowing in the positive x-direction straight across the branch. The complex 3D flow patterns noted during divided flow are now replaced by a simple separation of the flow above and below the stagnation point and the slow rotating vortex previously mentioned. The area of maximum activity within the dead-leg ranges from the centre of the branch ($x/D = 0.0$) to the downstream wall and from $y/D = -0.65$ to $y/D = -1.0$ along the downstream wall. Maximum velocities on the downstream side of the branch were found to be 0.23m/s and on the upstream wall 0.117m/s. Velocities at the base of the branch during dead-leg flow were found to be

0.003m/s indicating little if any movement in this region. The slow rotating cavity within the dead-leg was made up of fluid already present in the branch. Once in the branch it would be difficult for fluid to escape with only a small exchange of fluid occurring in and around the stagnation point.

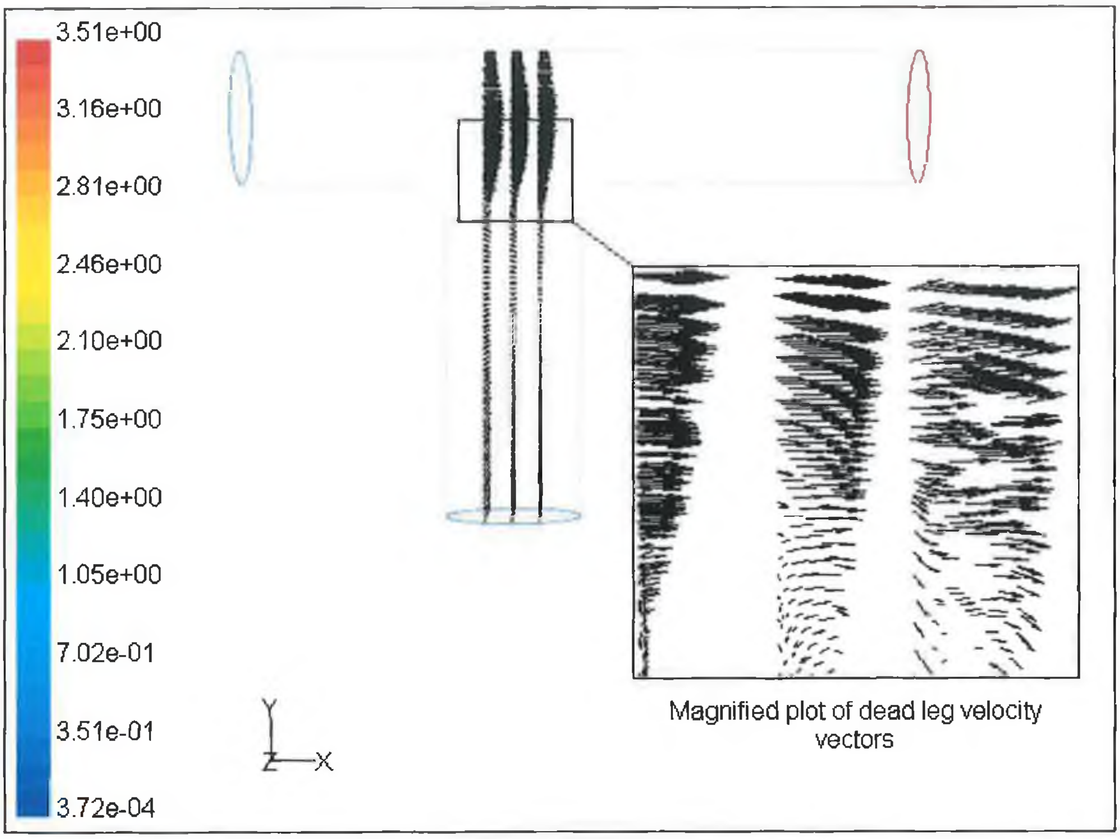

Figure 4.15: Magnified dead-leg flow velocity planes within the tee branch

A comparison between divided flow and dead-leg flow branch velocity profiles is offered in figure 4.16. It is evident that the dead-leg profiles differ considerably from those presented for divided flow in figures 4.12. The y/D = -0.6 highlights the attempt of the mainstream fluid to enter the branch without much success. Apart from this entry region all other plots within the branch show two distinct flow regions. The reverse flow regions for the dead-leg branch is offset towards the downstream wall by 5-10mm. Maximum velocities were noted along the downstream wall. These values decreased with increasing depth into the branch while upstream wall velocities were found to be very low irrespective of depth within the branch.

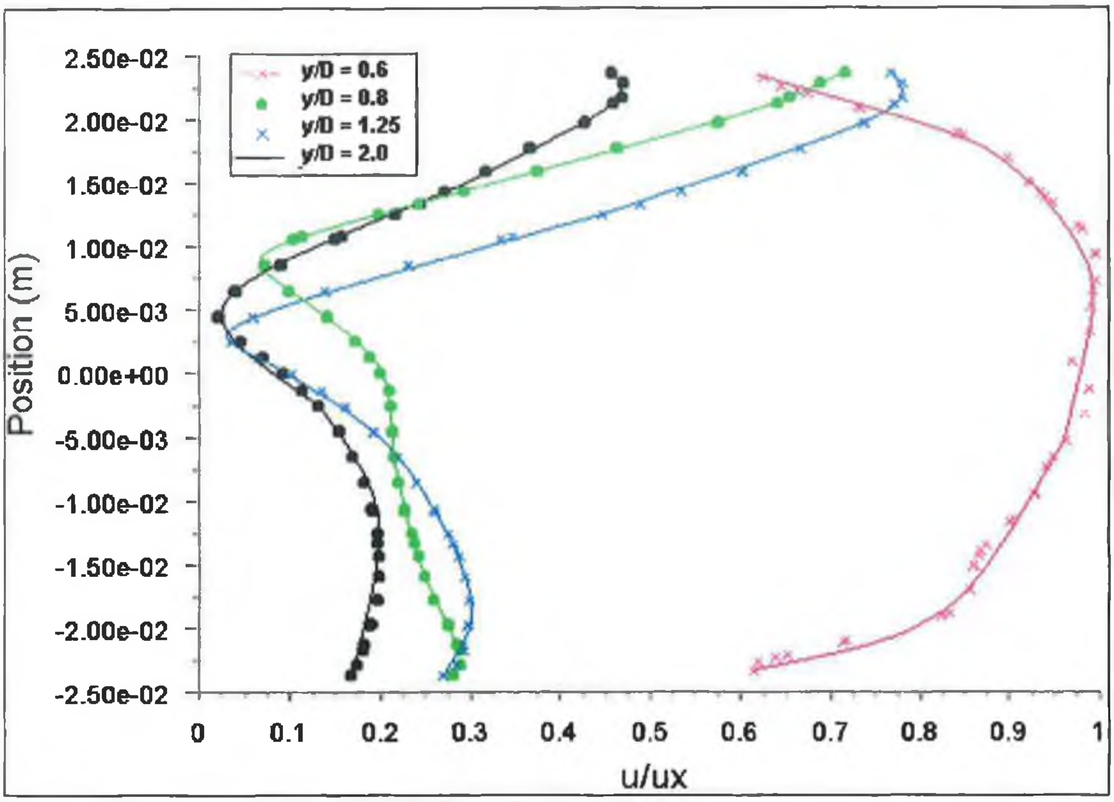

Figure 4.16: Dead-leg flow velocity profiles within the branch

4.7 DEAD-LEG FLOW WALL SHEAR STRESS

A comparison of divided flow and dead-leg flow wall shear stress for both upstream and downstream branch walls are presented in figure 4.17. A considerable drop in wall shear is evident for both wall in dead-leg flow conditions. A maximum wall shear was found on the downstream wall of 7.5 Pa which decreased with increasing penetration into the branch. Of particular concern was the trend found for upstream wall values. These values were almost constant irrespective of depth and low values of 0.5 Pa were considerably lower than those found for divided flow configurations.

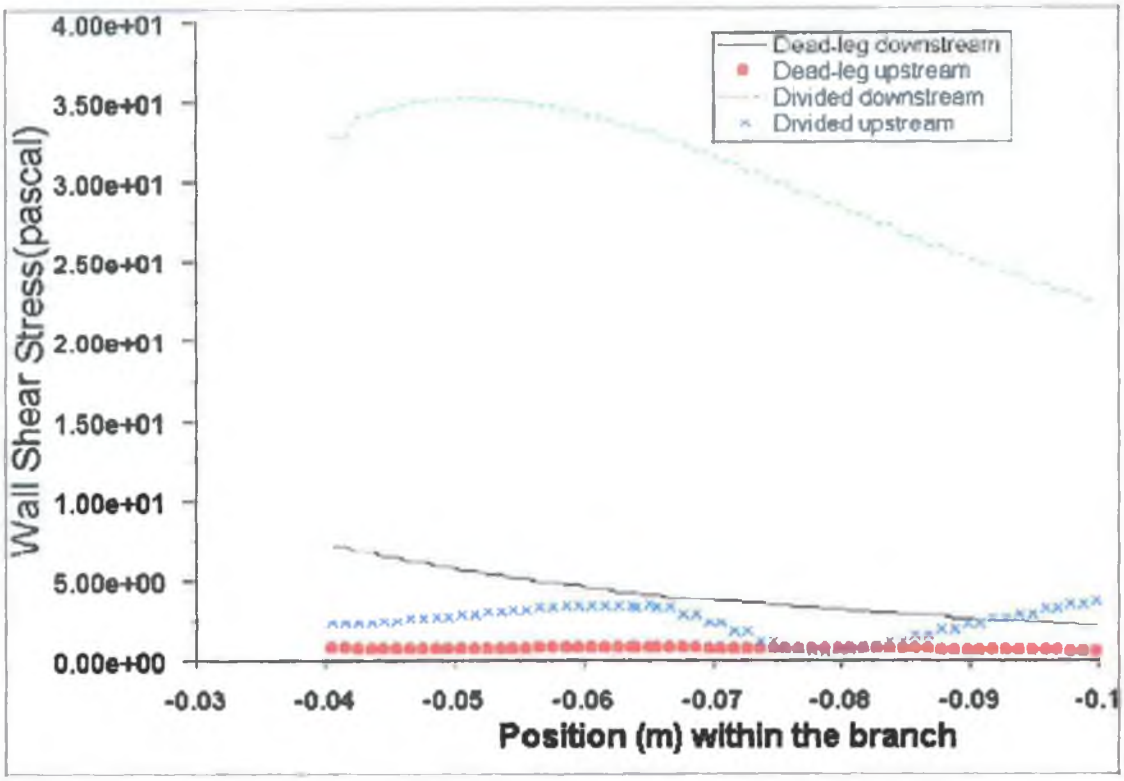

Figure 4.17: Dead-leg flow upstream and downstream wall shear stress within the branch

The information presented to date gives a clear insight into the key features found when moving from divided flow conditions to dead-leg flow configurations for a 50mm equal tee. The following section investigates the effect of mainstream velocity and dead-leg depth on flow profiles within the branch of a dead-leg tee.

PART B: ANALYSIS OF MAINSTREAM VELOCITY AND DEAD-LEG DROP ON A 50MM EQUAL TEE

4.8 1D VELOCITY PLOTS FOR DEAD-LEG FLOW CONDITIONS

Velocity vectors for a 50 mm diameter 1D dead-leg tee junction are presented in figures 4.18 to 4.21. The data presented in these plots relate to a velocity range of 0.5 m/s to 2 m/s in steps of 0.5m/s. Initial examination of these plots revealed that the initial velocity profile upstream of the tee remained undisturbed over the entire range of velocities. Branch anticipation and a consequent disturbance of the initial velocity profiles was only found to occur at entry to the branch ($x/D = -0.75$) in all cases. At this point the mainstream pipe flow separated from the wall of the branch at both high and low velocities. At this separation point fluid from within the branch, driven by the mainstream flow across the top of the branch, reattached itself by turning through 90 degrees following time spent within the rotating cavity of the branch.

This rotating cavity was a feature of each configuration irrespective of mainstream velocity profile and a magnified section of the velocity vectors are highlighted in each vector plot. Fluid from the mainstream pipe is prevented from entering the branch by fluid already present in the branch. However the speed of the flow across the top of the branch causes the branch fluid to slowly rotate in a clockwise direction. This slow rotation in the branch in turn decelerates the mainstream flow across the top of the branch. A second separation point was noted on the downstream wall of the branch. This point was further into the branch than the upstream point and the depth of penetration into the branch was related to the mainstream velocity.

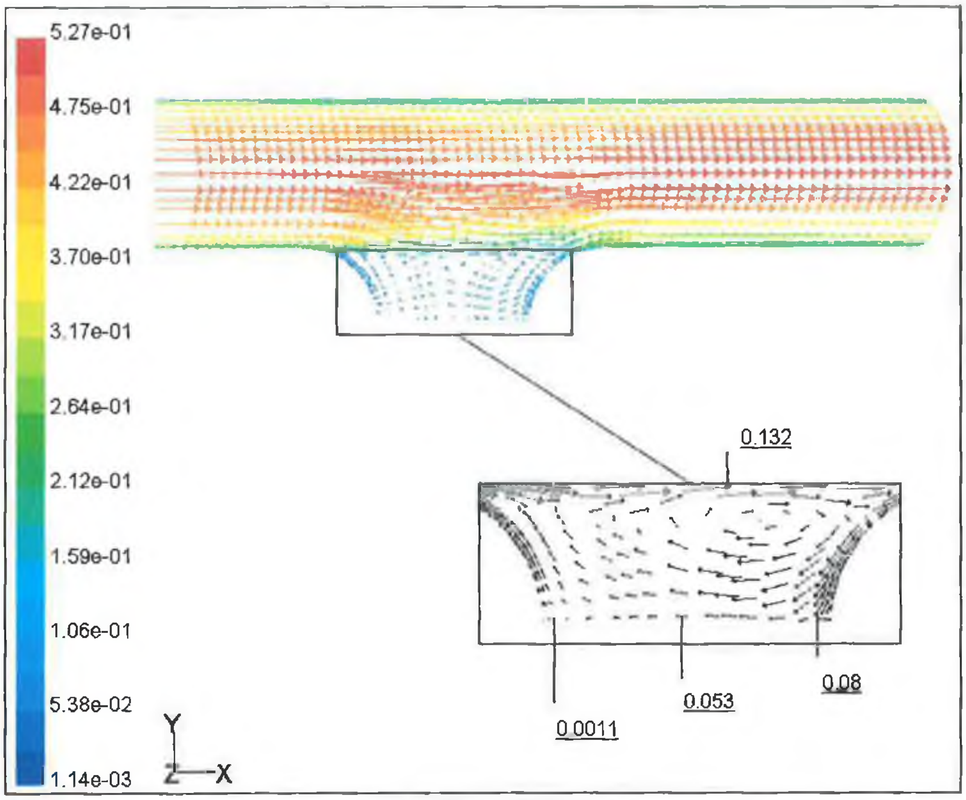

Figure 4.18: Velocity Vectors for a 1D tee at 0.5 m/s

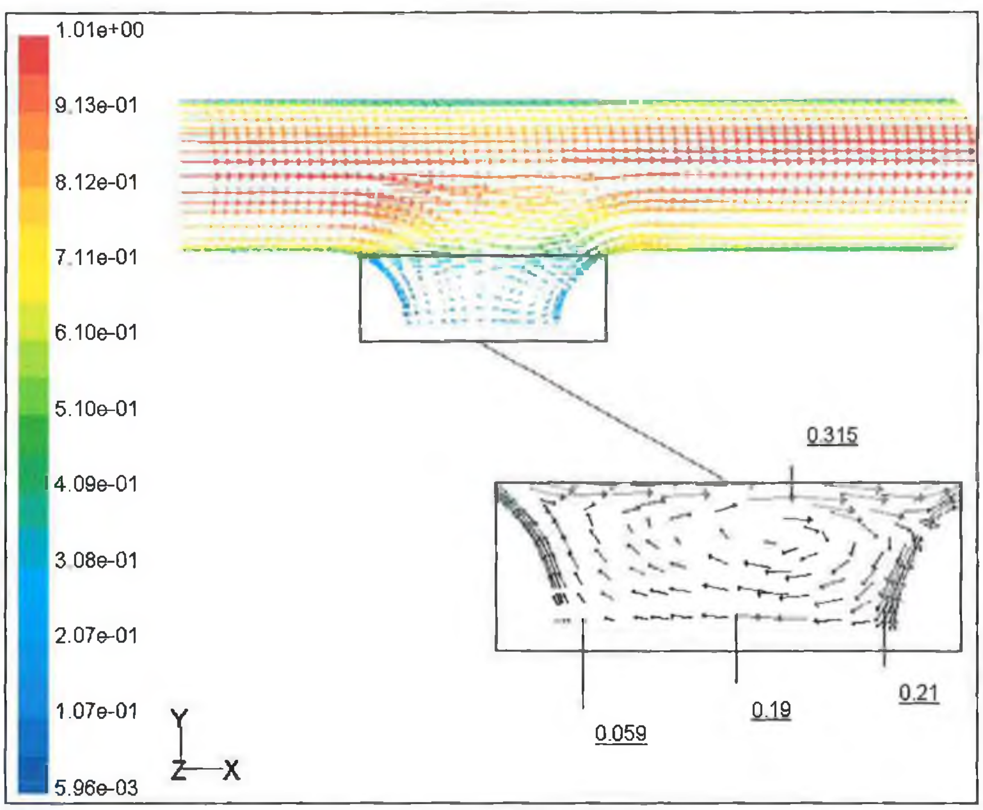

Figure 4.19: Velocity Vectors for a 1D tee at 1.0 m/s

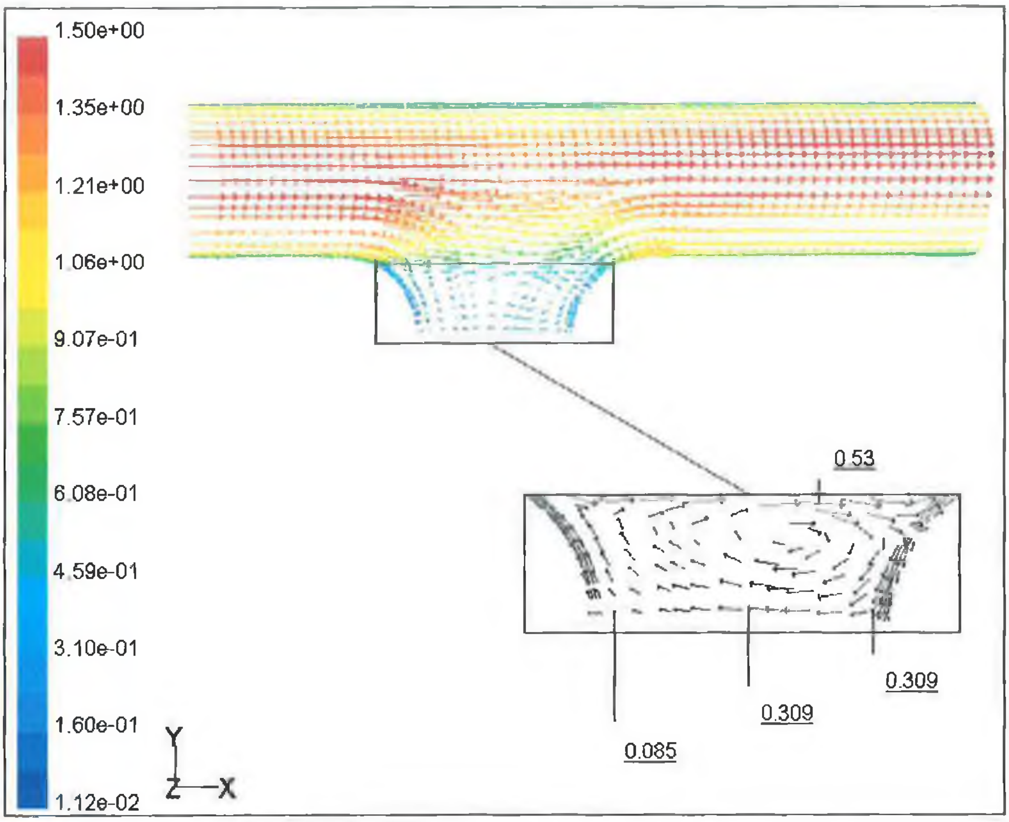

Figure 4.20: Velocity Vectors for a 1D tee at 1.5 m/s

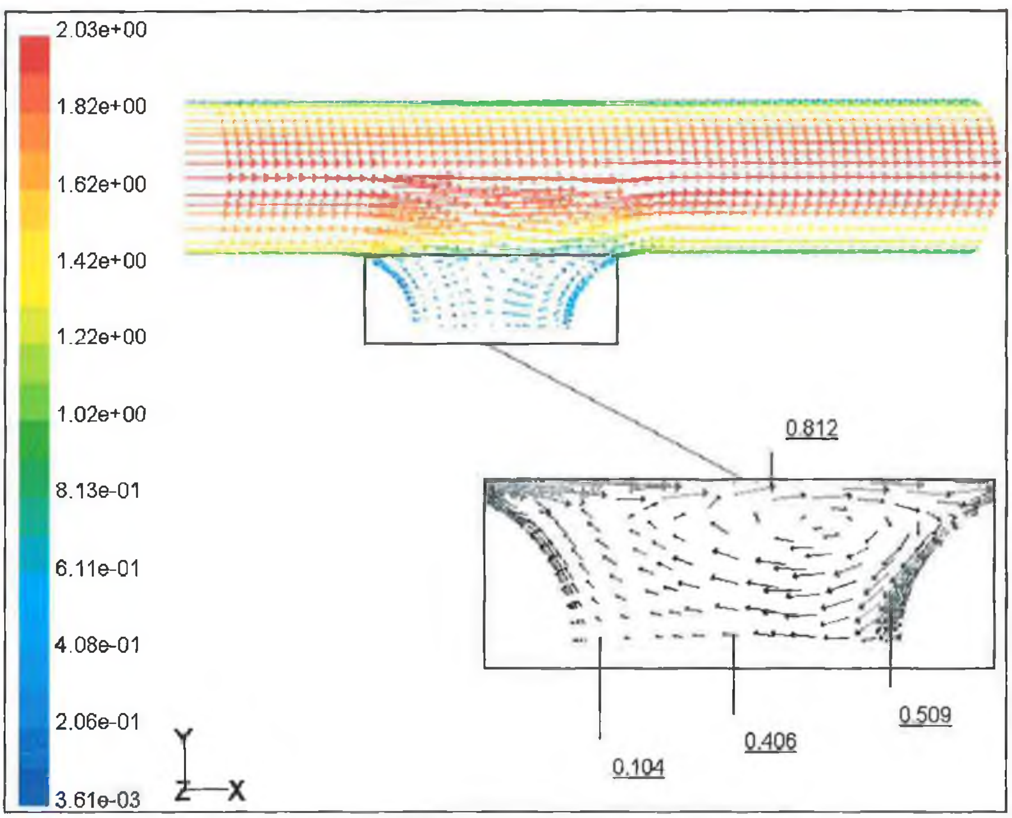

Figure 4.21: Velocity Vectors for a 1D tee at 2.0 m/s

The downstream separation point was pushed further into the branch with increasing velocity. At 2.0 m/s this trend was reversed as the separation point moved further up the downstream wall of the branch. The author believes this to be due to lack of penetration into the branch by the mainstream flow due to the high velocity across the top of the branch.

As stated previously, the speed of rotation of the rotating cavity within the branch is related to the mainstream velocity. To highlight this fact four points were selected within the branch for detailed analysis of velocity. Bearing in mind recent FDA statements relating increased turbulence in the mainstream flow to increased turbulence within the branch, these point offer an interesting insight into activity within the branch of the 1D dead-leg. At 0.5 m/s the velocity across the top of the branch was found to be 0.132 m/s while at the base of the branch dead-leg the velocity ranges from 0.08 to 0.0011 m/s from right to left respectively. These figures highlight the lack of turbulent flow within the branch and are in direct conflict with the industrial held norms. An increase in velocity across the top of the branch improves activity within the dead-leg but areas of concern still remain. Consistently across the range of velocities investigated the upstream corner at the base of the branch ($x/D = -0.5$ and $y/D = -1.0$) is a region of extremely slow flow. At a mainstream velocity of 2 m/s the maximum velocity found in this region was 0.1 m/s. At these levels the potential for bio-film formation is extremely high. A 50% decrease in mainstream velocity results in a decrease of almost 50% in branch velocity (figure 4.21).

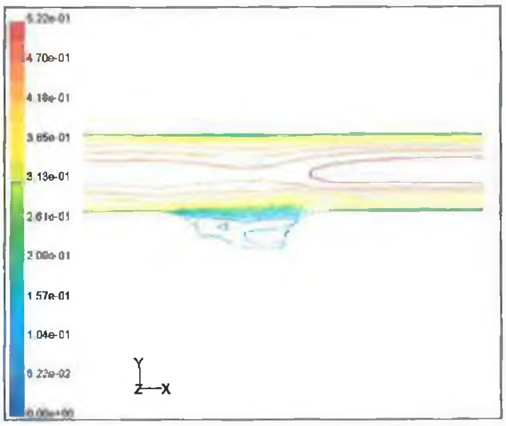

Figure 4.22: Velocity Contours 1D at 0.5 m/s

- Mainstream contours undisturbed
- Compact contours across top of branch
- Contours slightly skewed downstream
- Little disturbance within the branch

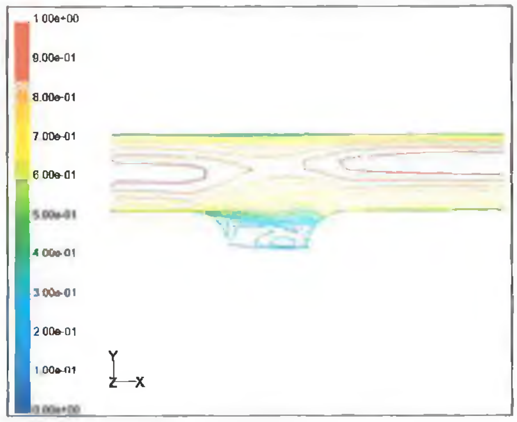

Figure 4.23: Velocity Contours 1D at 1.0 m/s

- Mainstream contours disturbed
- Less contours across top of branch
- Contours highly skewed downstream
- Some penetration into branch

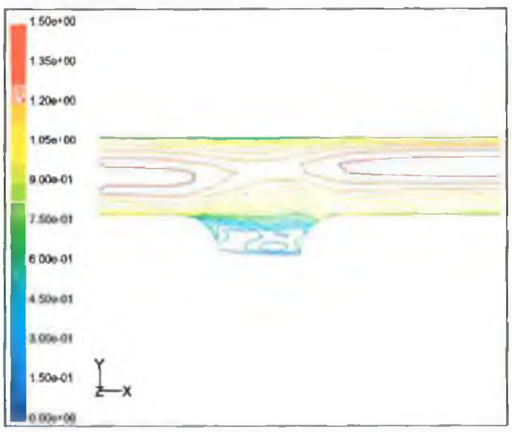

Figure 4.24: Velocity Contours 1D at 1.5 m/s

- Similar trends to 1.0m/s runs
- Compact contours on upstream wall
- Contours highly skewed downstream
- Some disturbance of branch fluid

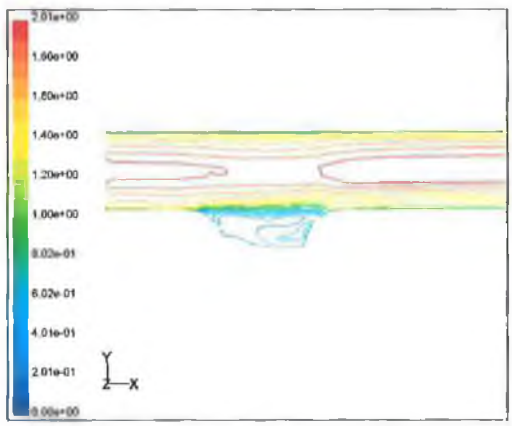

Figure 4.25: Velocity Contours 1D at 2.0 m/s

- Mainstream contours undisturbed
- Compact contours across top of branch
- Contours slightly skewed downstream
- Overall return to 0.5m/s trends

The slow rotating vortex highlighted during initial investigations (fig 4.6) was present in all cases irrespective of inlet velocity. The location of the centre of this region remained relatively undisturbed by mainstream velocity however the speed of rotation around this point was highly dependent of mainstream velocity. Other regions of interest include the downstream wall of the branch that, on average, experienced velocities 500% higher that those of the upstream branch walls. Low velocity regions within the branch include the base of the branch and the entire upstream wall region.

4.9 CONTOURS OF VELOCITY FOR A 1D DEAD-LEG

Figures 4.22 to 4.25 present contours of velocity magnitude for a 1D pipe dead-leg at various mainstream velocities. At 0.5 m/s little disturbance of the mainstream flow was noted. Compact contours exist across the top of the branch and these are skewed towards the downstream wall of the branch. Within the branch there is little change in velocity taking place. Figures 4.23 and 4.24 present contours at 1.0 and 1.5 m/s respectively. At these velocities compact contours were found to penetrate further into the branch and further into the mainstream flow. A ripple effect (see dye visualisation studies) was noted half way across the inlet pipe. The contours were again skewed towards the downstream wall of the branch. Increased contours were also noted within the dead-leg at these velocities.

A considerable change in profile was found when the mainstream velocity was increased to 2 m/s (figure 4.25). The pattern reverted back to that found at 0.5 m/s. The contours were once again compact across the top of the branch with little penetration in either direction into or out of the branch. Again the contours were skewed towards the downstream wall of the branch.

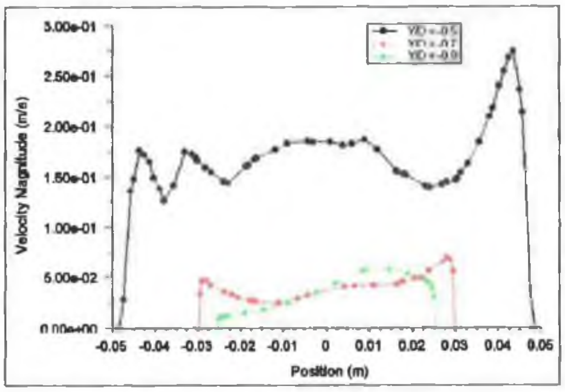

Figure 4.26: 1D velocity profiles at 0.5 m/s

- Mainstream average velocity 0.5m/s
- Max branch velocity 0.275m/s
- Min branch velocity 0.01m/s
- Base and upstream wall problem region

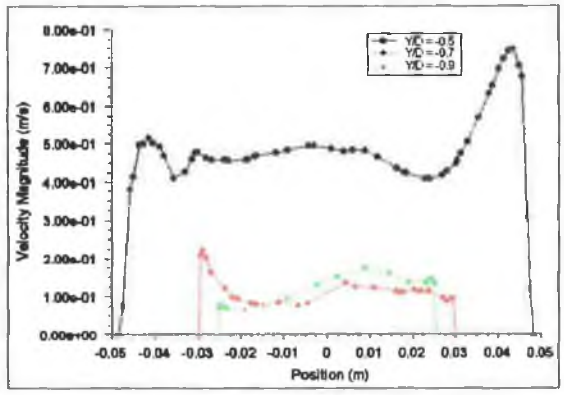

Figure 4.27: 1D velocity profiles at 1.0 m/s

- Mainstream average velocity 1.0m/s
- Max branch velocity 0.725m/s
- Min branch velocity 0.075m/s
- Peak on upstream wall at y/D = -0.7

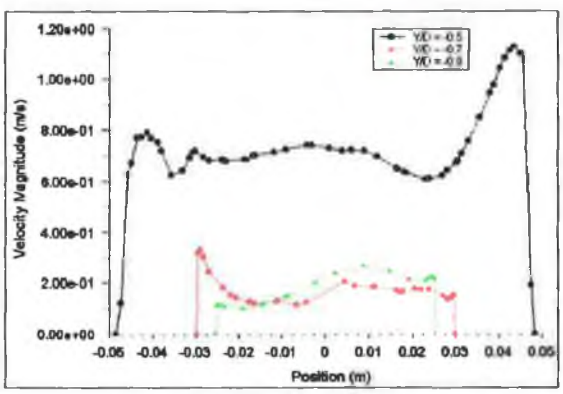

Figure 4.28: 1D velocity profiles at 1.5 m/s

- Mainstream average velocity 1.5m/s
- Max branch velocity 1.6m/s
- Min branch velocity 0.1m/s
- Low velocity region along base of branch

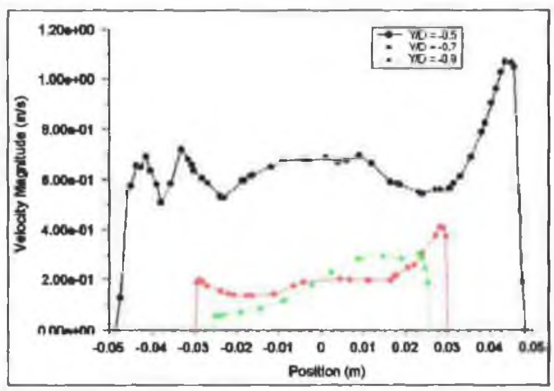

Figure 4.29: 1D velocity profiles at 2.0 m/s

- Mainstream average velocity 2.0m/s
- Max branch velocity 1.4m/s
- Min branch velocity 0.075m/s
- Considerable decrease along y/D = -0.9

Following detailed investigation of these patterns the author concludes that they occur due to lack of penetration of the mainstream flow into the branch. At low velocities the fluid lacks momentum around the separation point on the downstream wall to force its way into the branch and to overcome the resistance presented by the fluid already present in the branch. On the other hand at high velocities a similar pattern was found due to the fact that the mainstream fluid is travelling so fast it simply passes across the top of the branch (at high speed) with little time for separation on the downstream wall of the branch. This may also explain why the separation point of the downstream wall of the branch was found to move up the branch wall at higher mainstream velocities. The outcome is a higher rotational speed of the fluid trapped within the branch while the mainstream velocity profile is maintained at high velocities.

4.10 BRANCH VELOCITY PROFILES FOR A 1D DEAD-LEG

Graphs of velocity profiles within the branch of a 1D 50mm equal tee dead-leg are presented in figures 4.26 to 4.29. Plots are presented at $y/D = -0.5, -0.7, -0.9$ (25, 35 and 45mm) from the centreline of the mainstream flow into the dead-leg branch.

Maximum velocities at entry to the branch ($y/D = -0.5$) are found along the radius of curvature of the downstream wall. This is due in part to separation as the mainstream fluid impinges on the wall of the branch and is separated into two streams the upper portion of which accelerated out of the branch. The average velocity noted in this region for all flow conditions is at times half that of the mainstream flow. Some high and low values are present along the upstream wall and these may be attributed to reattachment in this region where slow flowing branch fluid meets with high-speed mainstream flow causing a disturbance. These conditions generally occur in the region x/D = -1.0 to -0.5. Little disturbance was noted directly across the branch form x/D = -0.5 to +0.5 indicating most of the activity is along the upstream and downstream walls of the branch.

At y/D = -0.7 the velocity decreased considerably across the entire flow range. Once again the highest value of velocity were noted on the upstream and downstream wall of the branch. At minimum and maximum mainstream velocities peaks in velocity profile were noted on the downstream wall of the dead-leg while the reverse was true for 1.0 and 1.5 m/s conditions. Outside of these regions the velocity profile was found to relatively stable across the diameter of the branch. The average drop in velocity in moving from y/D = -0.5 to y/D = -0.7 (a 10mm drop into the branch) was found to be 70%. This is a considerable decrease when one considers the industrial objective is to promote turbulence in order to prevent stagnation.

Further into the branch (y/D = -0.9) a more stable profile was found. At this point the profile was measured 5 mm from the base of the branch and these measurements identified two regions of interest. Downstream of the centreline of the branch the highest velocities were found with a maximum profile occurring when the mainstream velocity was set to 2 m/s. At this velocity the maximum velocity found 5 mm from the base of the branch was 0.3 m/s. This resulted in an 85% decrease from mainstream flow. A similar trend was noted across the entire range of flows investigated. The minimum velocities were found upstream of the centreline of the branch adjacent to the upstream wall. A gradual fall off in velocity was noted for all y/D = -0.9 profiles from high values on the downstream wall to low on the upstream wall however this decrease was most notable at maximum mainstream velocities. This is a worrying trend as the perception is that an increase in mainstream velocity will increase turbulence within the branch and while this may be true along the downstream wall it is not true for the upstream wall. Table 4.1 gives a summary of the maximum and minimum velocities found at various points within the 1D dead-leg under varying increasing mainstream flow conditions.

Mean Pipe Velocity	Y/D = -0.5 Max / Min		Y/D = -0.7 Max / Min		Y/D = -0.9 Max / Min	
0.5 m/s	0.275	0.125	0.07	0.025	0.06	0.01
1.0 m/s	0.725	0.425	0.225	0.075	0.175	0.075
1.5 m/s	1.60	0.620	0.32	0.10	0.28	0.10
2.0 m/s	1.40	0.50	0.33	0.15	0.3	0.075

Table 4.1: Max/Min velocities (m/s) within the branch of a 1D Dead-Leg

Taking the average velocity (U) at 25, 35 and 45mm into the branch and dividing by the maximum mainstream velocity (Umax) gives a clear insight into the rapid fall off in mainstream velocity within the branch of the tee. This normalised velocity (U/Umax) is plotted against branch location in figure 4.30 for a 50mm equal tee with a 1D dead-leg. The average branch velocity was found to have fallen by 50% at entry to the branch for a mainstream velocity of 2m/s and to 35% at 0.5m/s. 35mm into the branch the drop average drop off in velocity was 80% and 45mm into the branch only 10% of the mainstream velocity was available to drive the flow.

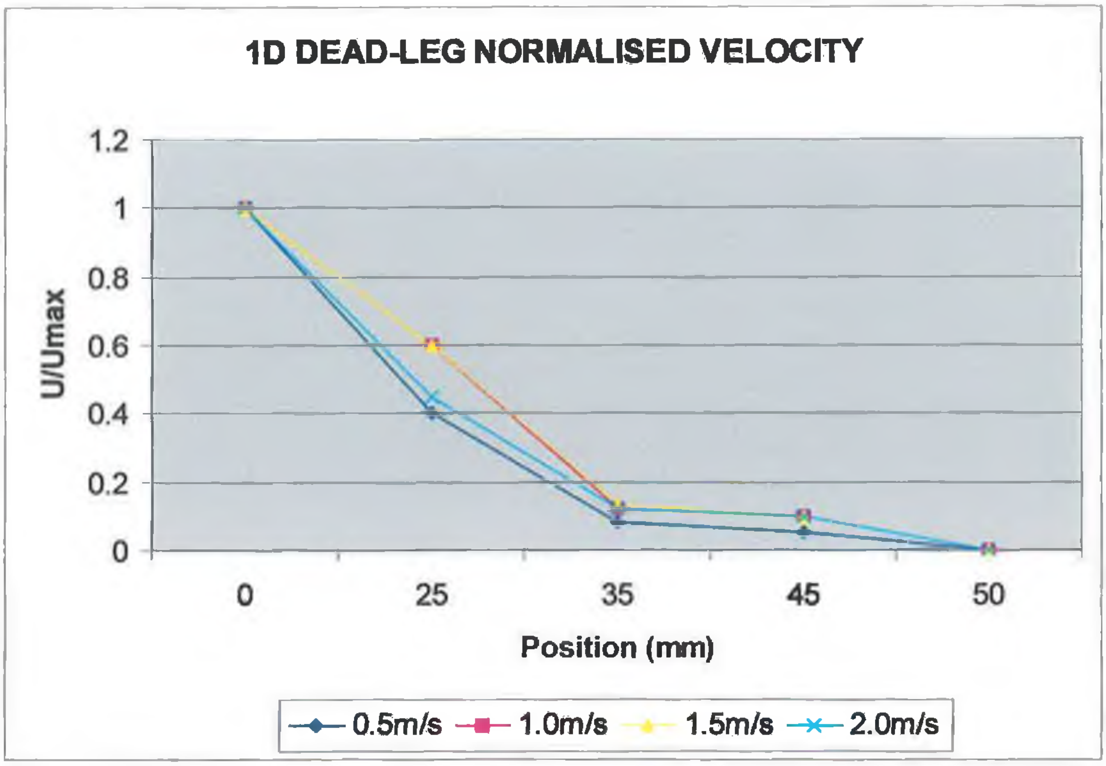

Figure 4.30: Branch normalised velocity for a 50mm equal tee with a 1D dead-leg

4.11 INCREASING DEAD-LEG LENGTH

Figures 4.31-4.34 above present velocity vectors for a 50mm equal tee with a mainstream velocity of 0.5 m/s. The mainstream flow remains relatively undisturbed irrespective of dead leg drop. Apart from a slight penetration across the top of the branch in each configuration (already noted in earlier tests) it would appear that dead-leg drop has little influence on fluid outside of the branch at this velocity. At entry to the branch for each dead-leg drop a slow rotating vortex area was noted. This area was offset towards the downstream wall of the branch. The motion of fluid around this area was responsible for branch re-circulation, all-be-it slow, in both the 1D and 2D dead-leg configurations.

For 4D and 6D configurations the motion of fluid around the re-circulation zone was soon dissipated, as the fluid in the branch was forced further into the dead-leg. The effect of this dissipation was to decelerate the already slow moving fluid and to generate regions of no flow or regions of stagnation deep within the dead-leg. For a 4D dead-leg the base of the branch was found to be stagnant and at 4D into the 6D dead-leg the same conditions existed. This level of decay within the branch was considered by the author to be of considerable interest in the investigation of dead-leg flow. Some benefit was to be gained by the separation of fluid on the down stream wall of the branch for 1D, 2D and to a limited extent 3D configurations as the fluid would be forced to flow down the wall and as long as it maintained sufficient momentum would be forced along the base of the dead-leg and re-circulate up the opposite wall of the branch. This level of circulation would possibly encourage the exchange of fluid from the mainstream flow into the branch and vice-versa. However for a 3D dead-leg configuration at low flowrates limited motion was noted on the

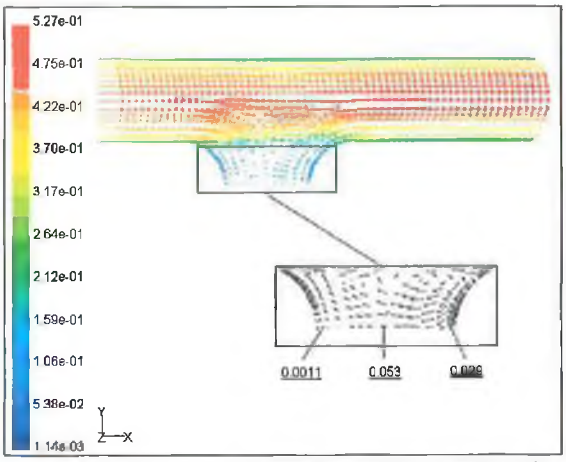

Fig 4.31: Velocity Vectors for a 1D tee at 0.5m/s

- Little disturbance of the main stream flow
- Flow patterns in the branch well defined
- Slow rotating vortex towards the top of the branch
- Motion noted throughout the branch to a depth of 1D

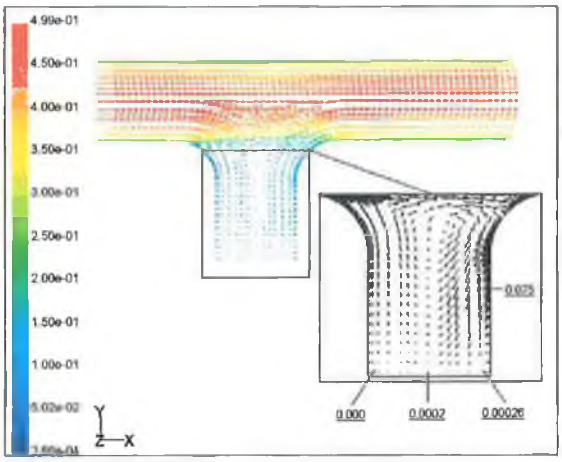

Fig 4.32: Velocity Vectors for a 2D tee at 0.5m/s

- Little disturbance of the main stream flow
- Flow patterns extended beyond 1D
- Slow rotating vortex towards the top of the branch elongated further into the branch
- Motion noted in the branch to a depth of 1.5D beyond which velocity is very slow

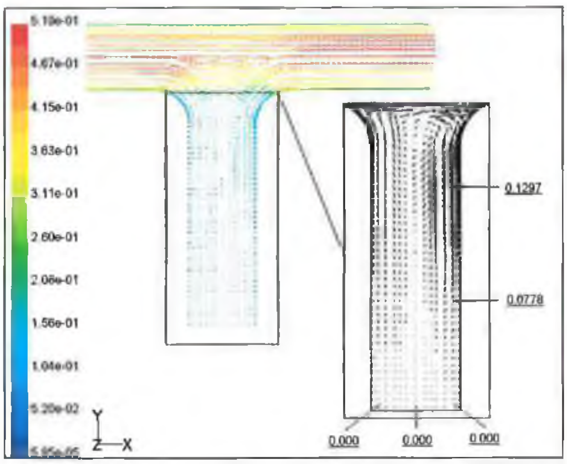

Fig 4.33: Velocity Vectors for a 4D tee at 0.5m/s

- Little disturbance of the main stream flow
- Flow patterns established to a depth of 3D
- Slow rotating vortex still visible and effects noted to a depth of 3D
- Beyond 3D little motion of the fluid and at 4D velocity is zero throughout

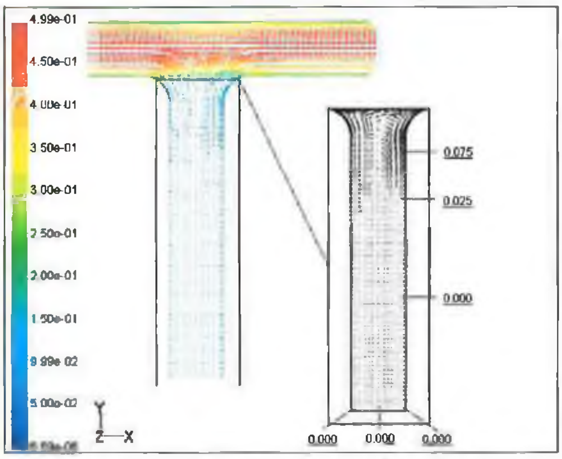

Fig 4.34: Velocity Vectors for a 6D tee at 0.5m/s

- Little disturbance of the main stream flow
- Flow patterns established to depth of 3D
- Vortex less clearly defined and effects less well established in the branch
- Motion noted to a depth of 3D with the remainder of the branch stagnant

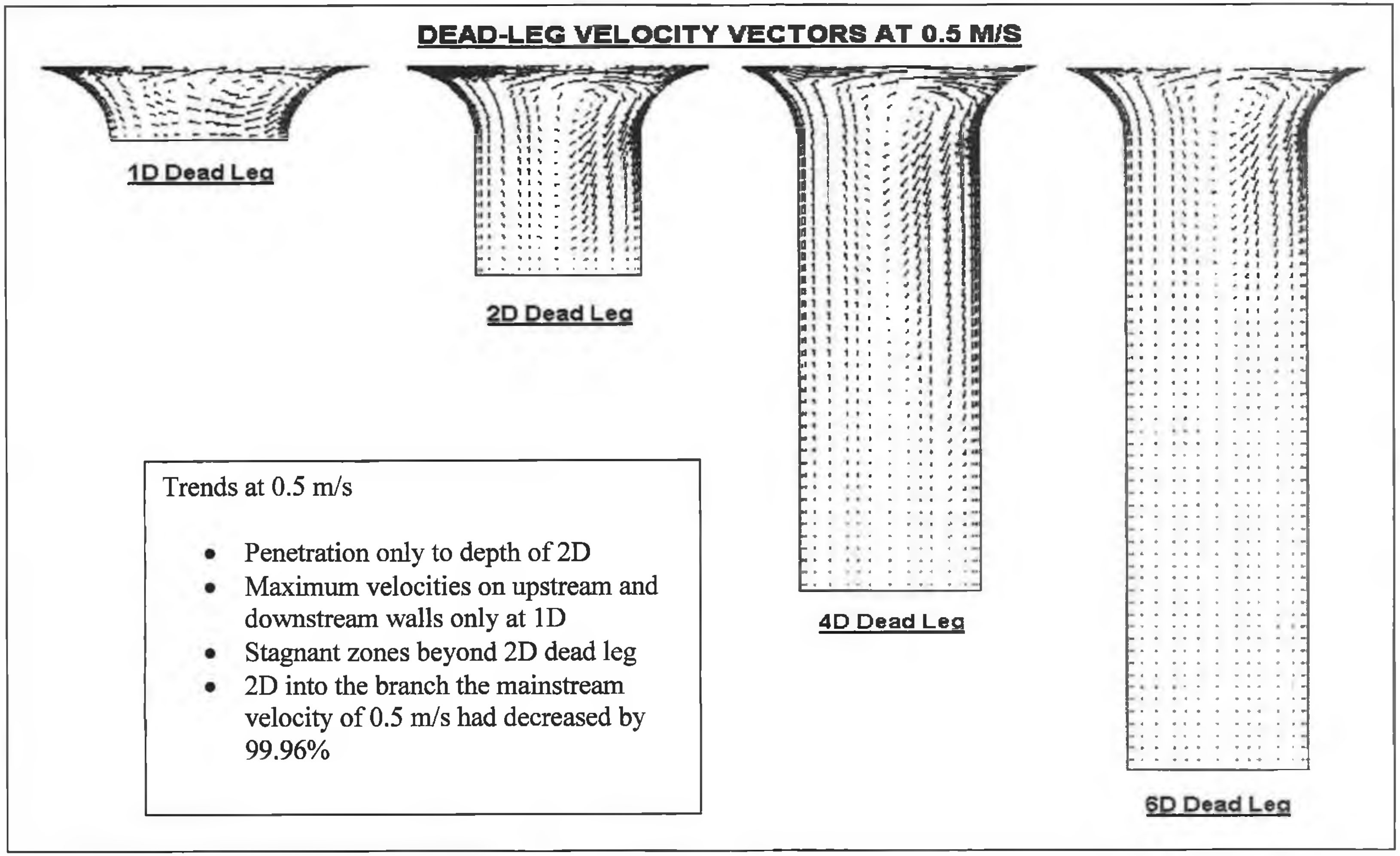

Figure 4.35: Velocity Vectors for a 50mm tee with various dead-leg drop

upstream wall of the branch and the base of the branch was almost stagnant. These conditions were also noted to worsen for 4D and 6D dead-legs. For 6D configurations the level of decay of motion was highest and this was highlighted by a lack of motion along the upstream wall of the branch. Stagnant conditions were at a level of 3D into the 6D dead-leg and re-circulation was limited to 2D within the branch. Table 4.2 below highlights some of the more interesting velocities found in the branch of various dead-legs at a main stream velocity of 0.5 m/s.

	Downstream Branch Wall				**Dead leg base**		**Dead leg centre**	
	1D	**2D**	**4D**	**6D**	**Mid**	**Left**	**Mid**	**Left**
1D 0.5m/s	0.027	----	----	----	0.053	0.0011	0.053	0.029
2D 0.5m/s	0.075	0.0002	----	----	0.0002	0.0000	0.0002	0.025
4D 0.5m/s	0.129	0.0778	0.0000	----	0.0000	0.0000	0.0000	0.000
6D 0.5m/s	0.075	0.025	0.0000	0.000	0.0000	0.0000	0.0000	0.000

Table 4.2: Velocity measurements within dead-leg branches at 0.5 m/s

Figure 4.35 presents an exploded view of the dead-leg regions for a mainstream velocity of 0.5 m/s and outlines the trends present at this velocity. It is clear from these vector profiles that for 1D configurations the re-circulation zones within the branch are well established. However it is also important to note that the maximum velocity at the base of this dead leg is 0.053 m/s and that velocities much lower than this are also present. It would be difficult to envisage much exchange of fluid from the main stream into the branch at these velocities. The separation points for all configurations from 1D through to 6D are around the same point on the downstream wall. For the 2D dead-leg rotation around the slow moving vortex is sufficient to force fluid to reach the base of the branch. This motion is absent at the base of the upstream wall and this region is effectively a stagnation zone. For the 4D and 6D configurations there is no re-circulation beyond the 3D zone but motion above this point for the 4D dead-leg is sufficient to encourage slow motion of fluid along the upstream wall of the branch. However below the 3D zone this region is also a stagnation zone. The worst configuration is the 6D dead-leg. Poorly defined re-circulation around the ever-present vortex, due to the length of the branch and the fact that any motion is dissipated the further into the branch the fluid moves, is reflected in the very low flowrates along the upstream wall of the branch. Below the 3D zone the fluid is completely stagnant with little hope of exchange of fluid from the mainstream flow.

The effect of increasing the velocity of the mainstream flow across the top of the branch from 0.5 m/s to 2 m/s in steps of 0.5 m/s is outlined in the range of figures and tables now presented. Figures 4.36 – 4.39 present velocity vectors at 1.0 m/s. The velocities along both the upstream and downstream walls were found to increase slightly compared to those generated for 0.5 m/s flow conditions. An average of 20% of the mainstream velocity was maintained to a depth of 1D for all configurations. However at 2D this had fallen to 0.1% at the base of the branch. Between 4D and 6D stagnant zones were present throughout the branch. For the 6D configuration the velocity was found to be 0.05 m/s at a depth of 75 mm into the branch representing a dead leg depth of 2D. Some improvement in penetration into the branch was noted at this velocity over 0.5 m/s but only to a depth of 3D at which point the fluid became stagnant again. The effect of increasing dead-leg length on velocity profiles for a mainstream velocity of 1.0m/s is shown in figure 4.40. Similar plots and trends are presented in figures 4.41 through to 4.50 representing mainstream velocities of 1.5 to 2 m/s respectively. For both only 15% of the mainstream velocity was present in the branch at a depth of 1D along the downstream wall irrespective of dead-leg drop. However at a depth of 2D into the branch for a mainstream velocity of 1.5 m/s the average branch velocity was 0.001 m/s and at 2.0 m/s mainstream velocity the average branch velocity was 0.002 m/s. Only 5% of the average mainstream velocity was noted along the upstream wall of the branch to a maximum depth of 2D and again stagnant zones were noted beyond 3D for both 1.5 and 2 m/s velocities. The 5% average of mainstream velocity was a key feature of each velocity examined by the author. For all tests run the maximum velocity noted on the upstream wall at a depth of 2D was always 5% of the average mainstream velocity. An alternative way of looking at this is irrespective of mainstream velocity examined at a depth of 2D into a dead leg the mainstream velocity value had fallen by 95% in all cases.

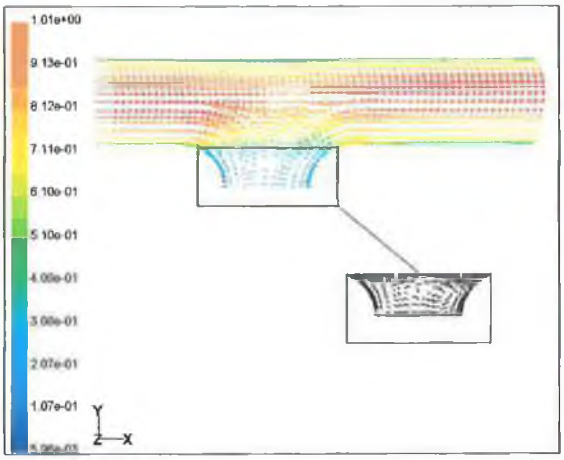

Fig 4.36 Velocity Vectors for a 1D tee at 1.0m/s

- Little disturbance of the main stream flow
- Increased flow in the branch over 0.5m/s
- Velocity in the vortex region increased resulting in higher rotational speed
- Improvement in velocity along the upstream wall of the branch

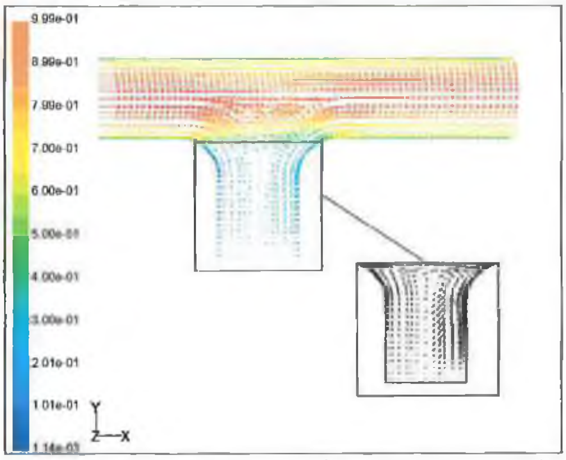

Fig 4.37 : Velocity Vectors for a 2D tee at 1.0m/s

- Slight acceleration of main stream flow across the top of the branch
- Minor flow noted to a depth of 2D
- Elongation of the slow rotating vortex to a depth of 2D into the branch
- Minor improvement in penetration into the branch

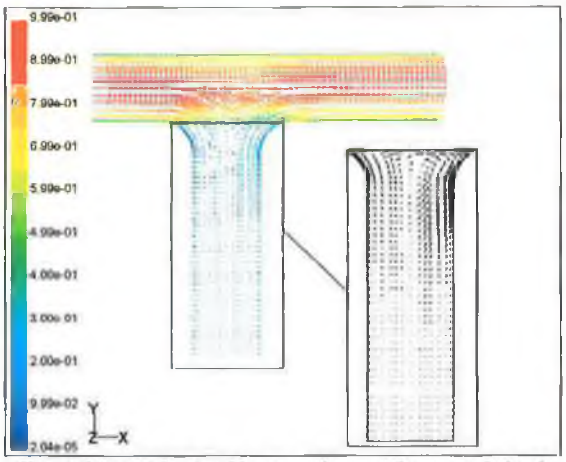

Fig 4.38 : Velocity Vectors for a 4D tee at 1.0m/s

- Similar trend to that of 2D configuration
- Flow patterns established to a depth of 3D
- Slow rotating vortex still visible and effects noted to a depth of 2D
- Beyond 3D little motion of the fluid and at 4D velocity is zero

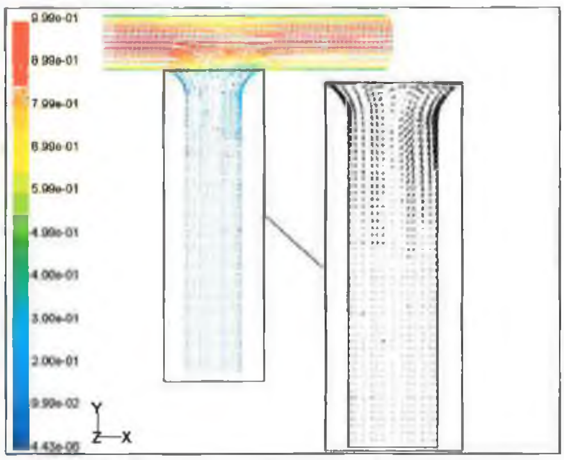

Fig4.39 : Velocity Vectors for a 6D tee at 1.0m/s

- Similar trend to that of 4D configuration
- Flow patterns established to depth of 3D
- Vortex effects noted to the same depth as 4D configuration
- Diminished influence noted along both the upstream and downstream walls

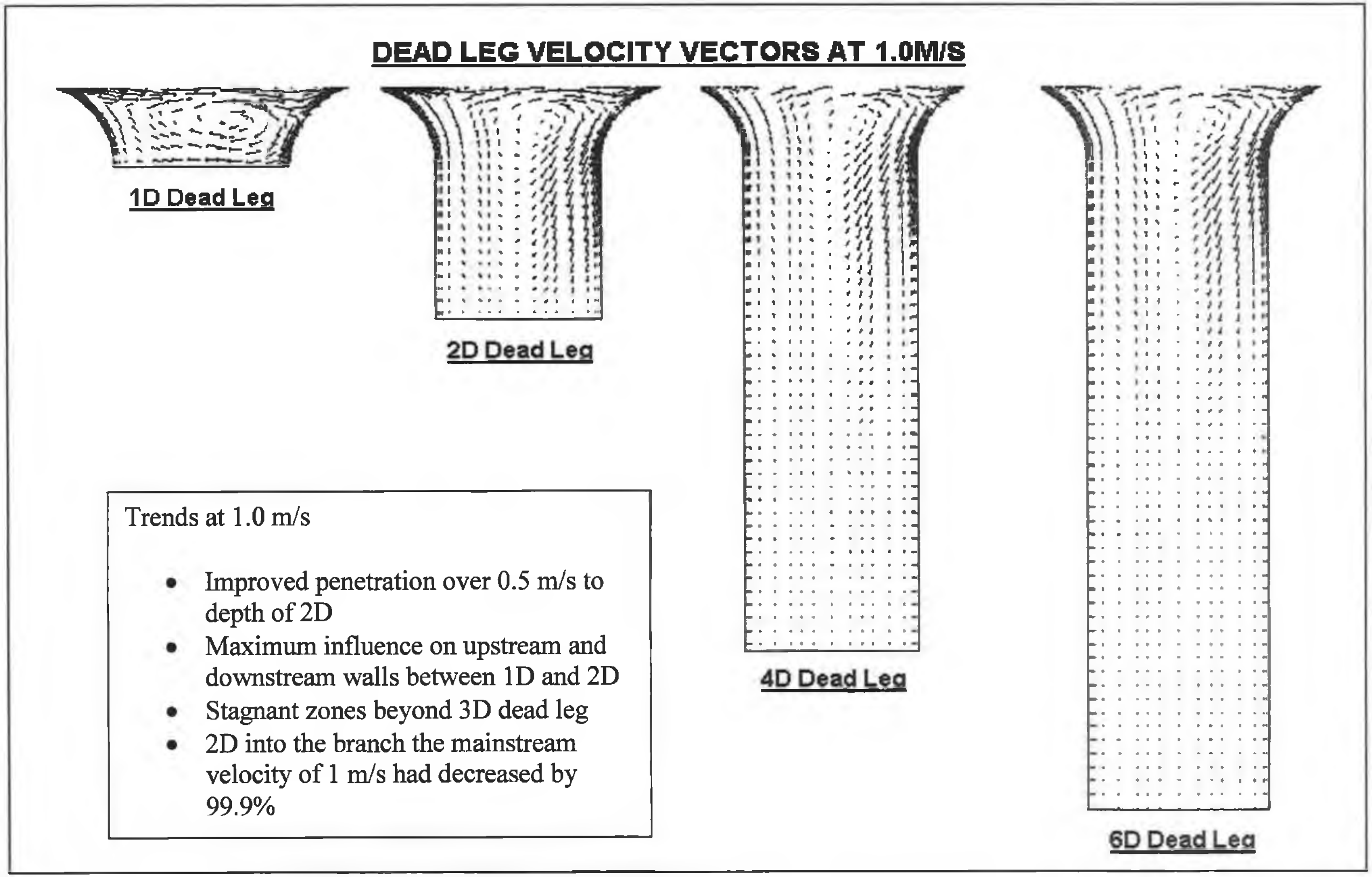

Figure 4.40: Velocity Vectors at 1.0 m/s for a 50mm tee with various dead-leg drop

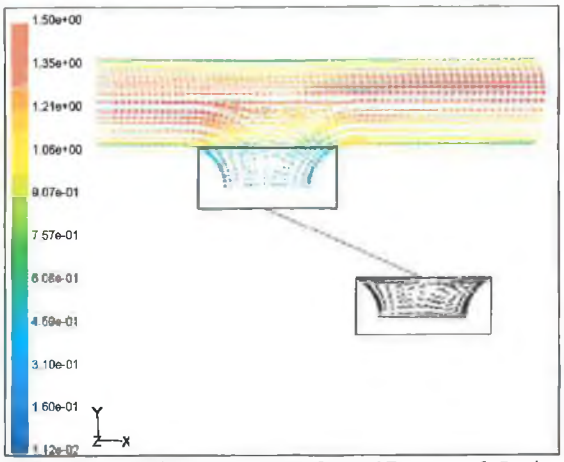

Fig 4.41: Velocity Vectors for a 1D tee at 1.5m/s

- Main stream flow trend similar to 1.0m/s
- Improved penetration into the branch
- Increase in velocities surrounding the rotating vortex
- Improved velocities noted throughout the branch to a depth of 1D

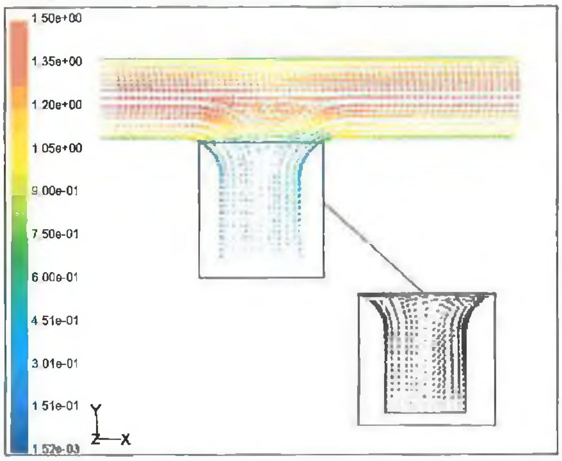

Fig 4.42 : Velocity Vectors for a 2D tee at 1.5m/s

- Little disturbance of the main stream flow
- Flow patterns extended beyond 1D
- Vortex elongated further into the branch
- Motion noted in the branch to a depth of 1.5D beyond which velocity is very slow

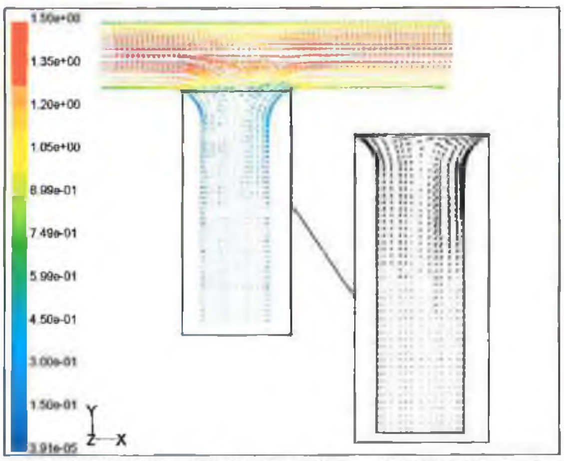

Fig 4.43: Velocity Vectors for a 4D tee at 1.5m/s

- Lack of main stream flow penetration
- Flow patterns established to a depth of 2D
- Slow rotating vortex still visible and effects noted to a depth of 2D
- Beyond 3D little motion of the fluid and at 4D velocity is zero

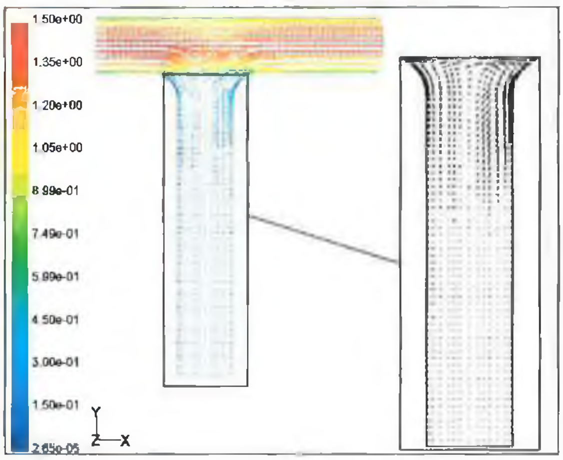

Fig 4.44: Velocity Vectors for a 6D tee at 1.5m/s

- Little disturbance of the main stream flow
- Flow patterns established to depth of 2D
- Vortex still confined to the upper 2D of the branch
- Motion noted to a depth of 3D with the remainder of the branch stagnant

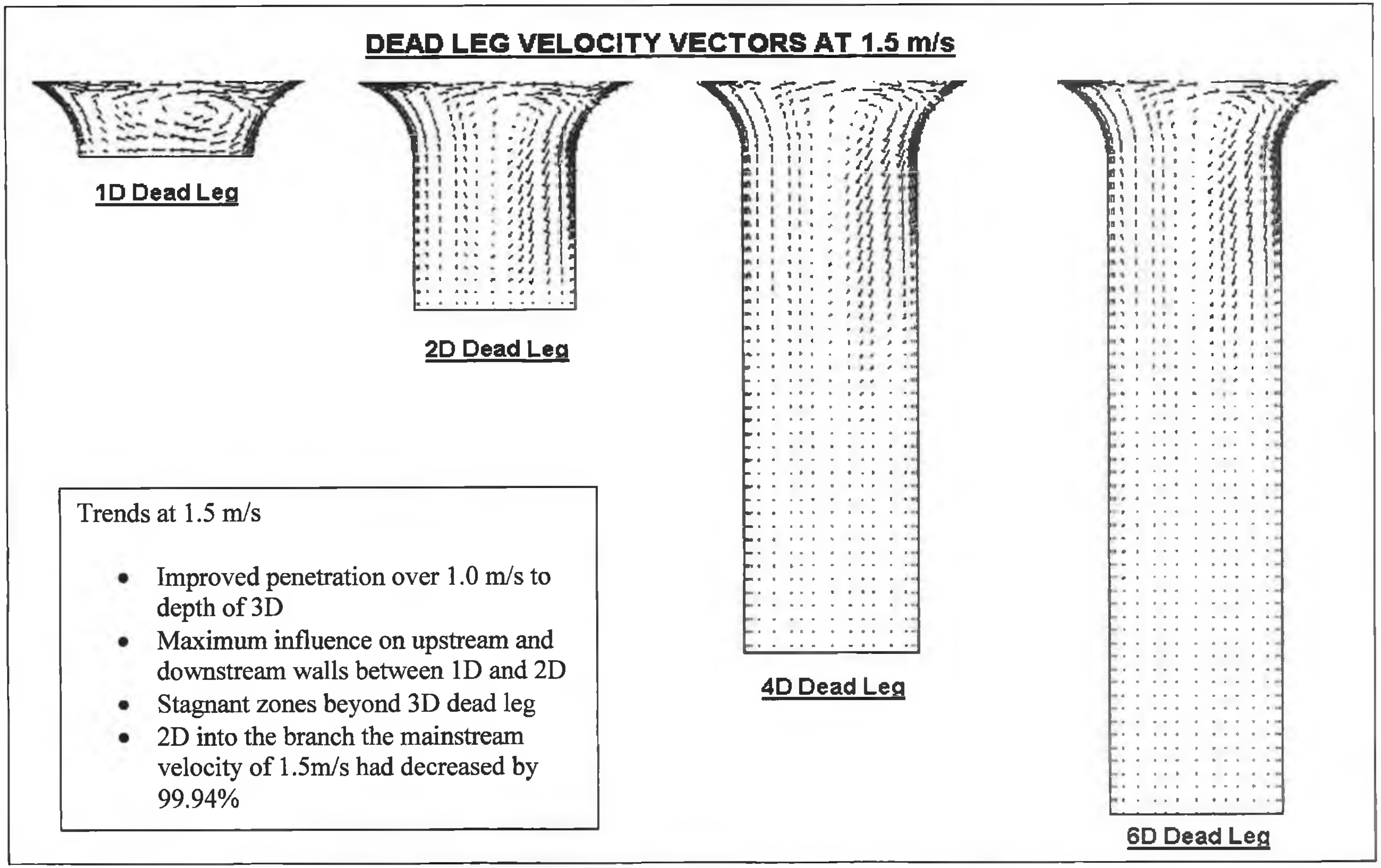

Figure 4.45: Velocity Vectors at 1.5m/s for a 50mm tee with various dead-leg drop

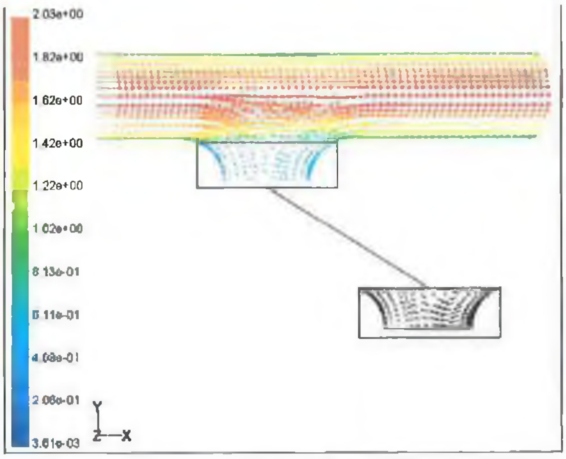

Fig 4.46 : Velocity Vectors for a 1D tee at 2.0m/s

- Main stream fluid uniform across top of branch
- Flow patterns in the branch well defined
- Vortex established towards downstream wall of branch
- Motion noted throughout the branch and along the base of the dead leg

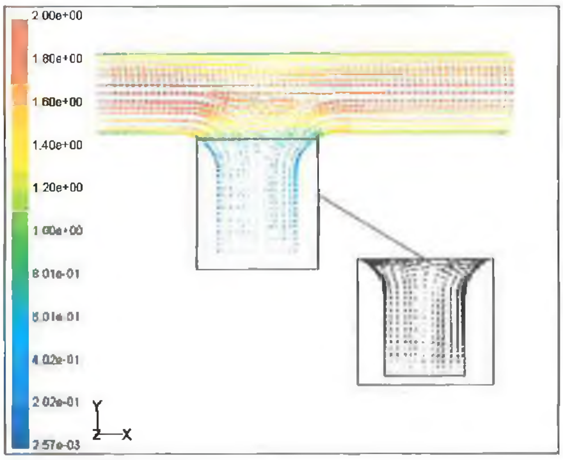

Fig 4.47 : Velocity Vectors for a 2D tee at 2.0m/s

- Little disturbance of the main stream flow
- Flow patterns extended further into the branch
- Drop off in velocity around the rotating vortex
- Base of the branch has low velocities

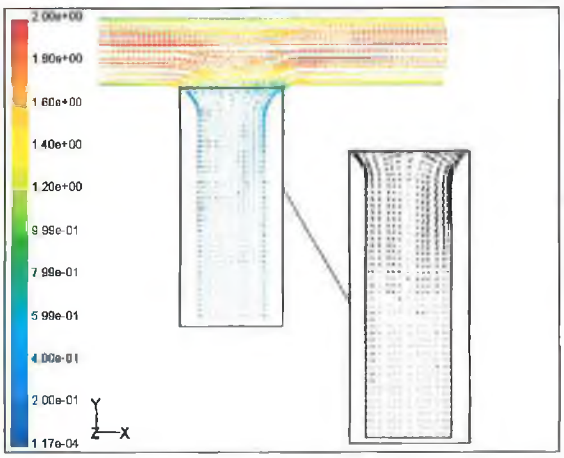

Fig 4.48 : Velocity Vectors for a 4D tee at 2.0m/s

- No change in mainstream configurations
- Flow patterns established to a depth of 3D
- Little change in vortex configuration
- Beyond 3D little motion of the fluid and at 4D velocity is zero

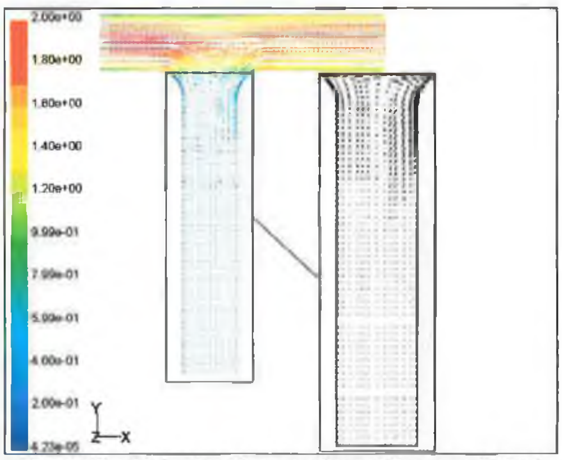

Fig 4.49 : Velocity Vectors for a 6D tee at 2.0m/s

- Little disturbance of the main stream flow
- Flow patterns established to depth of 3D
- Vortex isolated between 1D and 2D
- Motion noted to a depth of 3D with the remainder of the branch stagnant

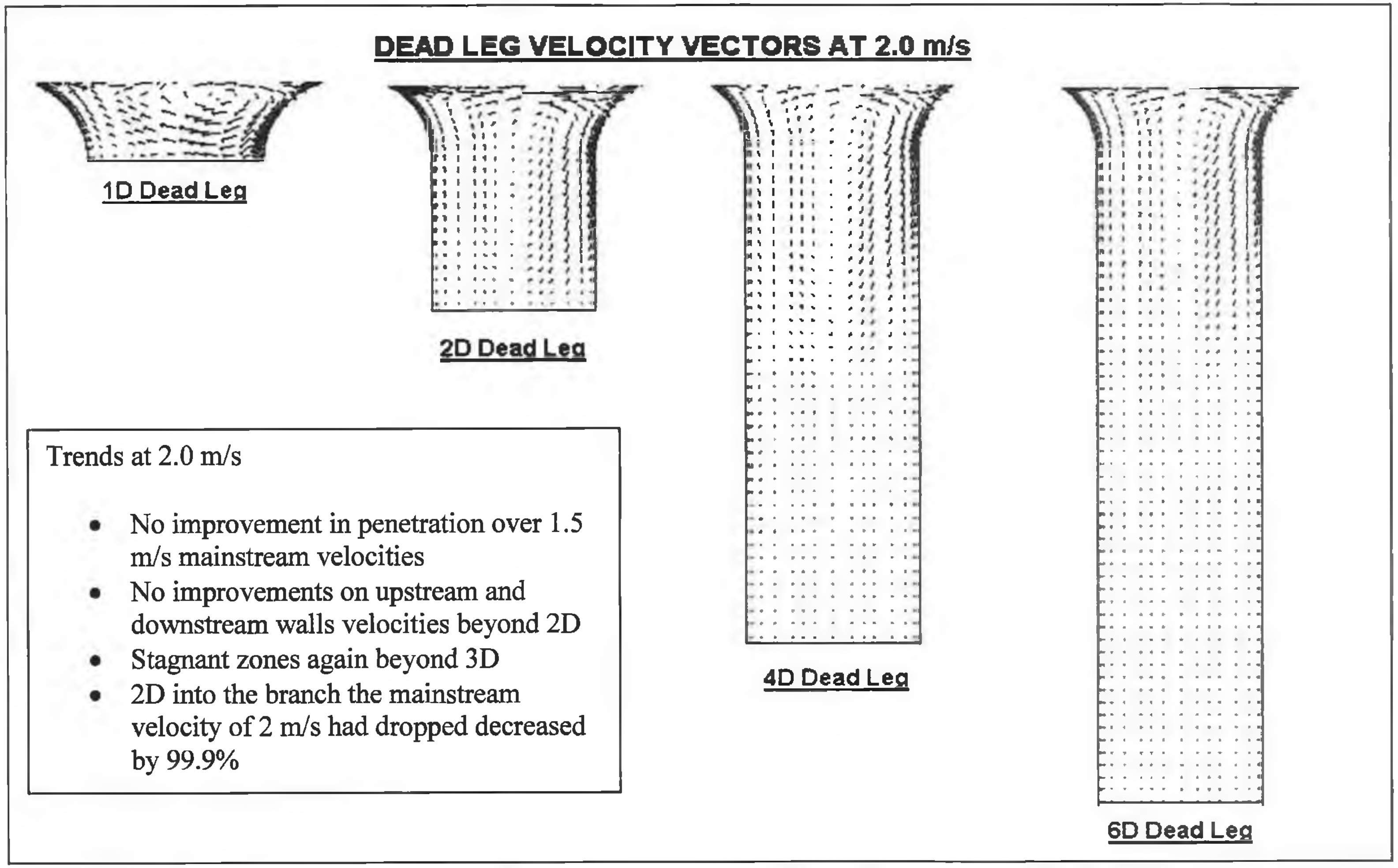

Figure 4.50: Velocity Vectors at 2.0m/s for a 50mm tee with various dead-leg drop

	Downstream Branch Wall				Dead leg base		Dead leg centre	
	1D	**2D**	**4D**	**6D**	**Mid**	**Left**	**Mid**	**Left**
1D 1.0m/s	0.157	----	----	----	0.107	0.005	0.257	0.207
2D 1.0m/s	0.200	0.001	----	----	0.001	0.001	0.001	0.051
4D 1.0m/s	0.200	0.000	0.0000	----	0.0000	0.0000	0.0000	0.000
6D 1.0m/s	0.200	0.050	0.0000	0.000	0.0000	0.0000	0.0000	0.000

Table 4.3: Dead-leg branch velocities at 1.0m/s mainstream velocity

	Downstream Branch Wall				Dead leg base		Dead leg centre	
	1D	**2D**	**4D**	**6D**	**Mid**	**Left**	**Mid**	**Left**
1D 1.5m/s	0.16	----	----	----	0.16	0.085	0.45	0.45
2D 1.5m/s	0.226	0.001	----	----	0.001	0.001	0.001	0.076
4D 1.5m/s	0.229	0.000	0.0000	----	0.0000	0.0000	0.0000	0.000
6D 1.5m/s	0.225	0.075	0.0000	0.000	0.0000	0.0000	0.0000	0.000

Table 4.4: Dead-leg branch velocities at 1.5m/s mainstream velocity

	Downstream Branch Wall				Dead leg base		Dead leg centre	
	1D	**2D**	**4D**	**6D**	**Mid**	**Left**	**Mid**	**Left**
1D 2.0m/s	0.40	----	----	----	0.205	0.003	0.71	0.80
2D 2.0m/s	0.30	0.002	----	----	0.002	0.002	0.002	0.10
4D 2.0m/s	0.30	0.100	0.0000	----	0.0000	0.0000	0.0000	0.000
6D 2.0m/s	0.30	0.2	0.0000	0.000	0.0000	0.0000	0.0000	0.000

Table 4.5: Dead-leg branch velocities at 2.0m/s mainstream velocity

4.12 DEAD-LEG VELOCITY MAGNITUDES FROM 1D TO 6D

Tables 4.3 to 4.5 present detailed measurements of velocity magnitude in dead-legs ranging from 1D to 6D and over a range of mainstream velocities 0.5 to 2.0 m/s. An overview of the data clearly indicated a lack of penetration into the dead-leg irrespective of mainstream velocity. While some benefit is gained by increasing the velocity across the top of the branch it is limited to the 1D to 2D range. At 2 m/s and a depth of 1D 40% of the average velocity is retained along the upstream wall of the branch indicating a reasonable level of re-circulation. The only difficulty with this evidence is that it is unclear from the present study if this is retained fluid in closed loop re-circulation or if it is exchange of fluid from the mainstream into and out of the branch. Flow visualisation studies later in this thesis will attempt to answer this question, which is of considerable importance in the investigation of dead-leg flow. Tables 4.6 to 4.8 present dead-leg velocities as a percentage of mainstream velocities. Examination of these tables will show that the transfer of mainstream velocity to the branch, a property that the author considers very important in order to encourage exchange of fluid between the mainstream distribution loop and the dead-leg, is at a maximum when a loop velocity of 2 m/s is applied. This is particularly true to a depth of 1D. However at 2 to 3D in each range studied the branch velocity had decreased by 95% or more irrespective of initial loop velocity. Beyond 3D little if any evidence of circulation was noted within the dead-leg. The average velocity found on the downstream wall of the branch for the FDA recommended 6D dead-leg rule was 15% of the loop velocity but only to a depth of 1D into the branch. Investigations at 2D found that this figure averaged 5% and beyond 3D have moved to 0%. These figures are alarming and in direct contradiction of the widely held belief that turbulent flow within the distribution loop will penetrate the dead-leg to a depth of 6D. Base on this investigation this is simply untrue.

	Downstream Branch Wall				Dead leg base		Dead leg centre	
	1D	2D	4D	6D	Mid	Left	Mid	Left
1D 1.0m/s	15%	----	----	----	10%	0.5%	25%	20%
2D 1.0m/s	20%	0.1%	----	----	0.1%	0.1%	0.1%	5%
4D 1.0m/s	20%	0.000	0.0000	----	0.0000	0.0000	0.0000	0.000
6D 1.0m/s	20%	5%	0.0000	0.000	0.0000	0.0000	0.0000	0.000

Table 4.6: Dead-leg branch velocities as a percentage of 1.0m/s mainstream velocity

	Downstream Branch Wall				Dead leg base		Dead leg centre	
	1D	2D	4D	6D	Mid	Left	Mid	Left
1D 1.5m/s	10%	----	----	----	10%	5%	30%	30%
2D 1.5m/s	15%	0.06%	----	----	0.06%	0.06%	0.06%	5%
4D 1.5m/s	15%	0.000	0.0000	----	0.0000	0.0000	0.0000	0.000
6D 1.5m/s	15%	5%	0.0000	0.000	0.0000	0.0000	0.0000	0.000

Table 4.7: Dead-leg branch velocities as a percentage of 1.5m/s mainstream velocity

	Downstream Branch Wall				Dead leg base		Dead leg centre	
	1D	2D	4D	6D	Mid	Left	Mid	Left
1D 2.0m/s	20%	----	----	----	10%	1.5%	35%	40%
2D 2.0m/s	15%	0.1%	----	----	0.1%	0.1%	0.1%	5%
4D 2.0m/s	15%	5%	0.0000	----	0.0000	0.0000	0.0000	0.000
6D 2.0m/s	15%	10%	0.0000	0.000	0.0000	0.0000	0.0000	0.000

Table 4.8: Dead-leg branch velocities as a percentage of 2.0m/s mainstream velocity

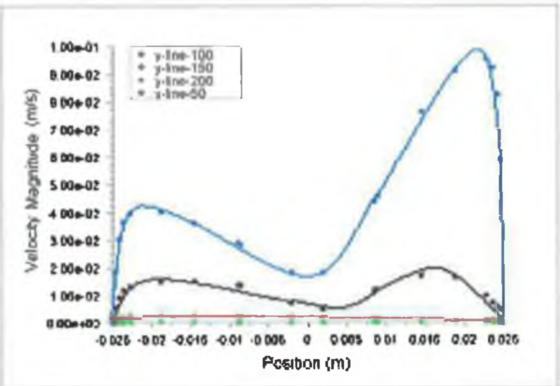

Fig 4.51: y-Velocity plots for a 6D tee at 0.5m/s

- 1D max 0.1 and min 0.02 m/s
- 2D max 0.02 and min 0.01 m/s
- 3D max 0.003 and min 0.001 m/s
- 4D max and min are zero
- Overall slight skew to downstream wall but all low velocities

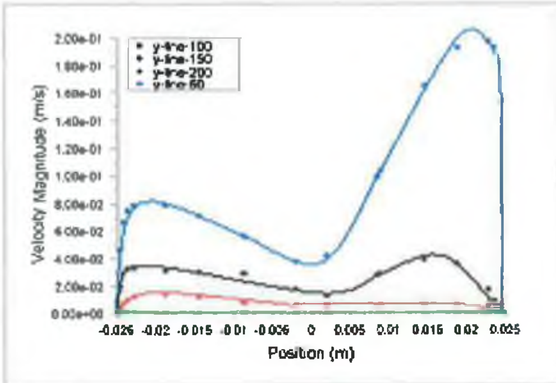

Fig 4.52: y-Velocity plots for a 6D tee at 1.0m/s

- 1D max 0.2 and min 0.05 m/s
- 2D max 0.04 and min 0.02 m/s
- 3D max 0.015 and min 0.005 m/s
- 4D max and min are zero
- Profiles become linear across branch from 3D

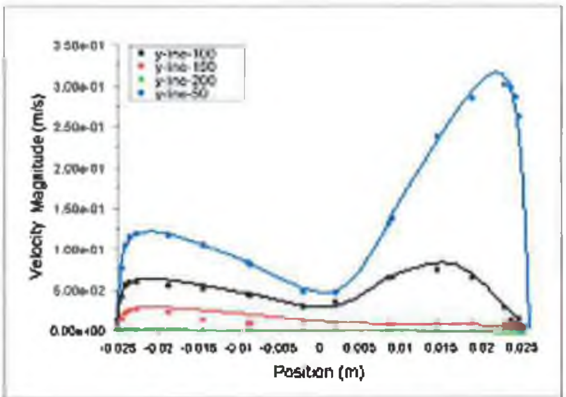

Fig 4.53: y-Velocity plots for a 6D tee at 1.5m/s

- 1D max 0.325 and min 0.05 m/s
- 2D max 0.075 and min 0.025 m/s
- 3D max 0.025 and min 0.01 m/s
- 4D max and min are zero
- Slight increase in velocities notes up to 3D along the downstream wall

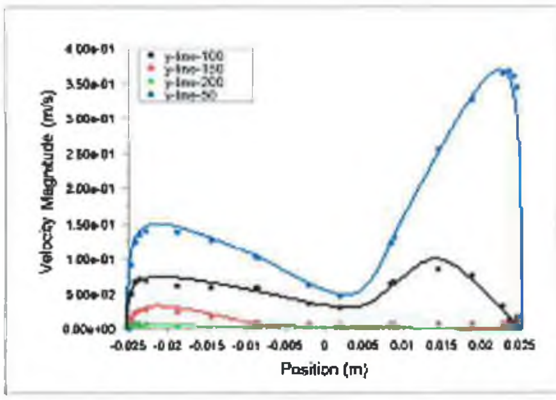

Fig 4.54: y-Velocity plots for a 6D tee at 2.0m/s

- 1D max 0.375 and min 0.05 m/s
- 2D max 0.1 and min 0.025 m/s
- 3D max 0.025 and min 0.000 m/s
- 4D max and min are zero
- Overall trends same but some improvement in upstream motion

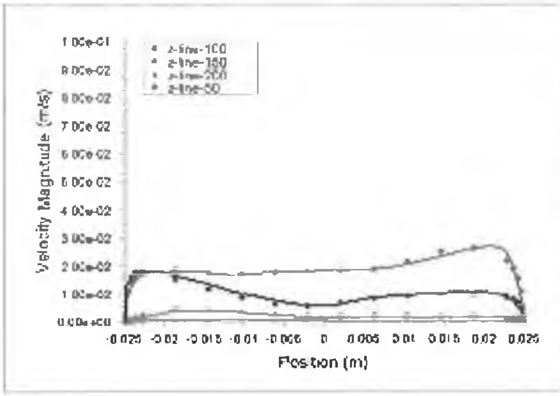

Fig 4.55: z-Velocity plots for a 6D tee at 0.5m/s

- 1D max 0.03 and min 0.018 m/s
- 2D max 0.02 and min 0.005 m/s
- 3D max 0.005 and min 0.005 m/s
- 4D max and min are zero
- Overall slight skew on the right and left wall but all low velocities

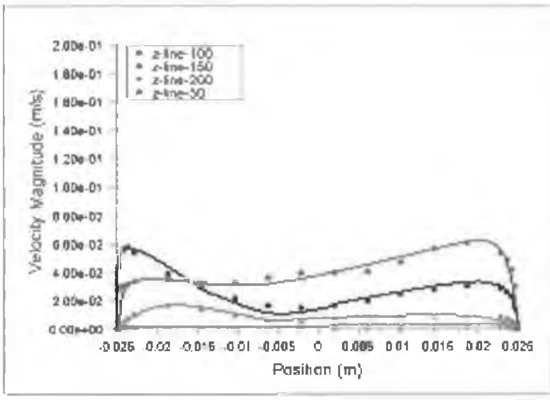

Fig 4.56: z-Velocity plots for a 6D tee at 1.0m/s

- 1D max 0.06 and min 0.04 m/s
- 2D max 0.06 and min 0.02 m/s
- 3D max 0.02 and min 0.01 m/s
- 4D max and min are zero
- Low velocities throughout , upstream wall skewed at 2D

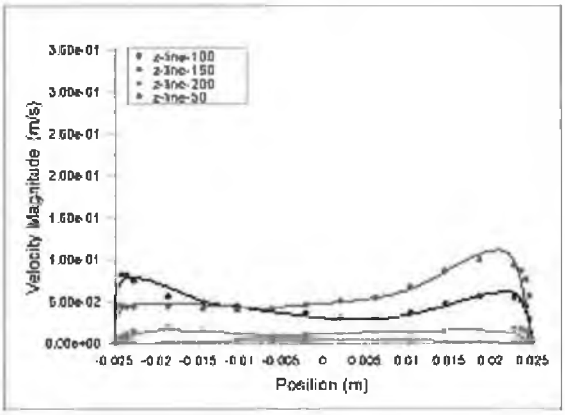

Fig 4.57: z-Velocity plots for a 6D tee at 1.5m/s

- 1D max 0.1 and min 0.05 m/s
- 2D max 0.075 and min 0.025 m/s
- 3D max 0.025 and min 0.01 m/s
- 4D max and min are zero
- Slight skew on the downstream wall

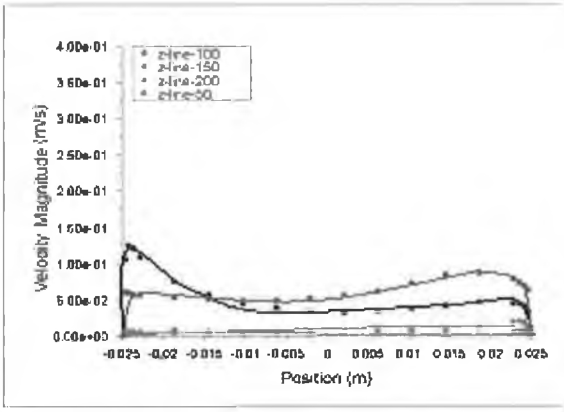

Fig 4.58: z-Velocity plots for a 6D tee at 2.0m/s

- 1D max 0.1 and min 0.05 m/s
- 2D max 0.125 min 0.04 m/s
- 3D max 0.025 and min 0.00 m/s
- 4D max and min are zero
- Low velocities throughout with little penetration into the branch.

Figures 4.51 to 4.54 above plots velocity within the branch along the y- axis and along the z-axis. It is clear from the data presented for the y-axis that the velocity plots within the branch are highly skewed along the downstream wall. This is only true in the upper regions of the branch at 1D and 2D only. At 3D the velocity profiles had levelled out to an almost linear profile. A steady increase in downstream wall velocity was noted with increasing mainstream velocity. This trend was only true to a depth of 2D after which little advantage was to be gained in downstream wall velocity by increasing mainstream velocity. At 4D irrespective of mainstream velocity the branch velocity profile was found to be zero in all cases. Some minor increases in upstream velocity were noted with increasing mainstream velocity. However the range of velocities involved were very low. For example 3D into the branch and at a mainstream velocity of 1m/s the upstream wall velocity was 0.015 m/s and for the same point at 2 m/s mainstream velocity this had increased to 0.025 m/s. These values will not promote removal of biofilm. Centerline velocities throughout the branch were at a minimum for all cases investigated. This indicated a region of very slow moving fluid around which the upstream and downstream wall fluid circulated at very low velocity. This circulation was only noted to a depth of 2D beyond which the remainder of the fluid became stagnant.

Examination of profiles along the z-axis highlights a trend of low velocity across the entire branch irrespective of dead-leg drop. These velocity profiles were found to be lower than their y-axis counterparts. At the maximum mainstream velocity of 2.0 m/s the maximum velocity recorded in the branch was 0.125 m/s at a depth of 2D. In comparison to the y-axis data, profiles along the z-axis were less skewed. In general these profiles were found to be slightly skewed in the positive z direction of the branch for all 1D plots and towards the negative z direction for 2D plots. Linear profiles were established in all cases at 3D into the branch and at 4D the profiles were zero indicating that the fluid was stagnant. Once again velocities within the branch were found to be very low irrespective of mainstream profiles.

4.13 TURBULENT KINETIC ENERGY AND DISSIPATION RATES

Examination of the graphs in figures 4.59 to 4.62 clearly indicate that turbulent kinetic energy in the branch is not dramatically affected by mainstream velocity. Overall trends are similar for all velocities examined and each dead-leg drop presents similar graphs irrespective of velocity. In all cases examined turbulent kinetic energy within the branch had dropped to very low levels from a dead-leg value of 3D and these low values persisted through to 6D. The maximum values on turbulent kinetic energy were noted in all cases at a depth of 1D into the branch. For each velocity examined the y-line-50 plot presented a similar trend. The plot was highly skewed from the centreline of the branch to the downstream wall. A maximum value of turbulent kinetic energy was noted 5 mm from the downstream wall and a sudden decrease occurred from this point through to the downstream wall at which point the value was found to be zero. Dead leg plots at 2D (y-line-100) show a similar trend of increasing turbulent kinetic energy from the centreline of the branch however this time the maximum values occur 12.5mm from the downstream wall. Each plot was still skewed between the centreline and the downstream wall however the maximum values are considerably less than those found 1D into the branch. This trend of falling turbulent kinetic energy values continued with increasing dead-leg drop into the branch and from 3D to 6D the values had decreased to almost zero.

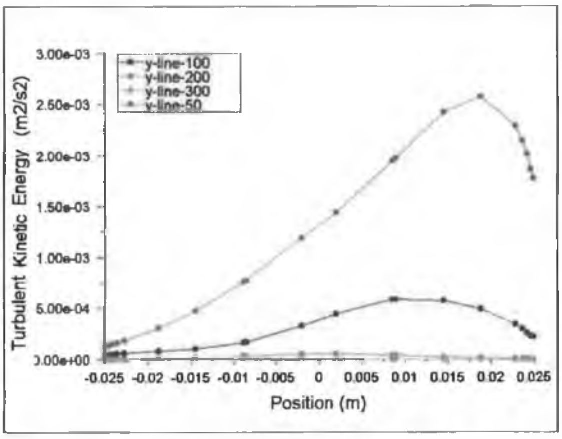

Fig 4.59: Turbulent Kinetic Energy Plotsfor a 6D tee at 0.5m/s

- Low value of turbulent kinetic energy throughout the branch
- Maximum value at 1D into the branch
- Values skewed between centreline of the branch and the downstream wall
- 3D into the branch the turbulent kinetic energy had reduced to zero

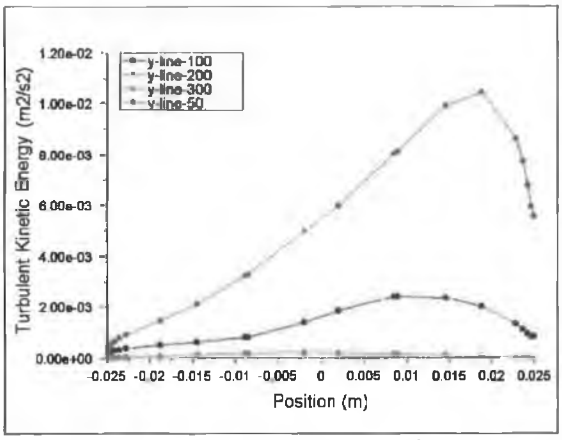

Fig 4.60: Turbulent Kinetic Energy Plots for a 6D tee at 1.0m/s

- Increasing velocity in the mainstream slightly increased the turbulent kinetic energy in the branch
- Trends are almost identical to those presented at a velocity of 0.5 m/s
- Values are skewed along the downstream wall for 1D and 2D plots
- Base of the branch has very low values of turbulent kinetic energy

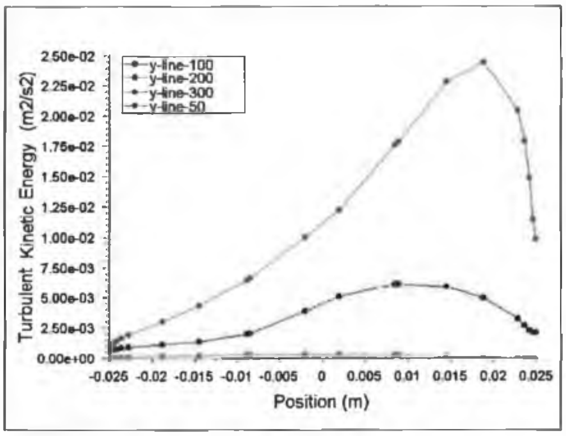

Fig 4.61: Turbulent Kinetic Energy Plots for a 6D tee at 1.5m/s

- No change in overall trends
- Maximum values noted on the along the downstream wall at a depth of 1D into the branch
- Slight improvement in values noted at a depth of 2D into the branch
- Beyond 3D value are generally zero

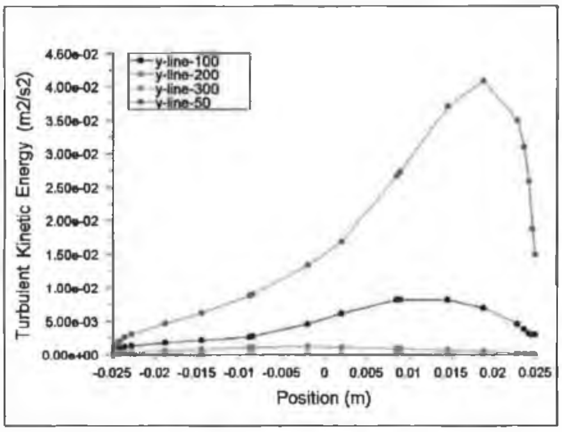

Fig 4.62: Turbulent Kinetic Energy Plots for a 6D tee at 2.0m/s

- Maximum value of turbulent kinetic energy noted at this velocity
- Plots still skewed for 1D and 2D although 2D profile less well defined
- Minor improvements for 3D and 4D conditions
- Very low values noted below 3D

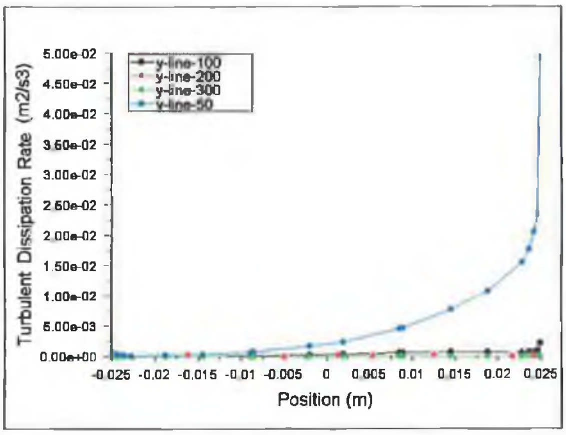

Fig 4.63: Turbulent Dissipation Plots for a 6D tee at 0.5m/s

- Dissipation max at 1D into the branch
- Maximum value noted for all depths along the downstream wall
- Maximum dissipation values of 0.05 and 0.0025 m^2/s^3 at 1D and 2D respectively
- Dissipation rate below 2D irrelevant

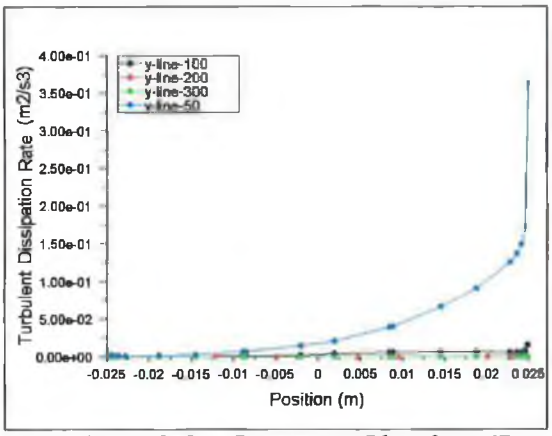

Fig 4.64: Turbulent Dissipation Plots for a 6D tee at 1.0m/s

- Small increase in dissipation at 1D
- Maximum value noted for all depths along the downstream wall
- Maximum dissipation values of 0.4 and 0.025 m^2/s^3 at 1D and 2D respectively
- Dissipation rate below 2D irrelevant

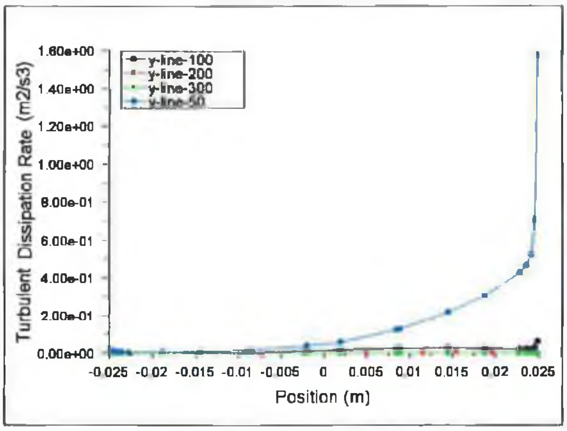

Fig 4.65: Turbulent Dissipation Plots for a 6D tee at 1.5m/s

- Maximum dissipation noted again at 1D
- Maximum value noted for all depths along the downstream wall
- Maximum dissipation values of 1.6 and 0.1 m^2/s^3 at 1D and 2D respectively
- Dissipation rate below 2D irrelevant

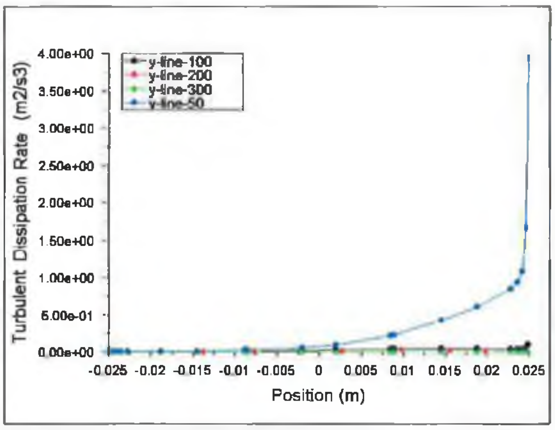

Fig 4.66: Turbulent Dissipation Plots for a 6D tee at 2.0m/s

- Dissipation max at 1D into the branch
- Maximum value noted for all depths along the downstream wall
- Maximum dissipation values of 4 and 0.5 m^2/s^3 at 1D and 2D respectively
- Dissipation rate below 2D irrelevant

Turbulent dissipation rates are presented in figures 4.63 to 4.66 for a range of velocities from 0.5 m/s to 2.0 m/s in steps of 0.5 m/s. The only trends noted for the range of data presented was a maximum value occurring at 1D into the branch along the downstream wall. For all other data from 2D through to 6D the values of turbulent dissipation was insignificant. The trend for 1D plots was similar for each velocity examined. Low values of dissipation were found along the upstream side of the branch. Maximum values ranged from 0.05 m^2/s^3 to $4m^2/s^3$ for mainstream velocities of 0.5 m/s to 2.0 m/s respectively. A gradual increase in dissipation was noted from the centreline of the branch through to the downstream wall of the branch in each case. This profile, at 1D into the branch, was found to be suppressed with increasing velocity. The overall effect of this was to diminish the dissipation rate in the upstream area of the branch and increase the dissipation rate in a limited area close to the downstream wall of the branch.

4.14 EFFECT OF MAINSTREAM VELOCITY ON BRANCH WALL SHEAR STRESS

Data related to branch wall shear stress is outlined in figures 4.67 to 4.70. Following extensive investigation of the wall shear stress throughout the branch the most interesting features once again appeared along the upstream and downstream walls. Wall shear is very important in the analysis of piping system dead-legs as it is a means of reducing bio-film and during cleaning-in-place operations a means of removing bio-film. Maximum values of wall shear were noted on the downstream wall of the branch for all cases. Above 1D into the branch a separation point was noted which resulted in a shear stress value of zero at the point of separation.

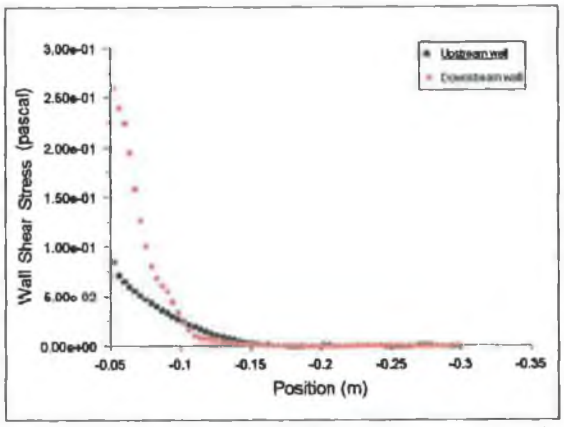

Fig 4.67: Wall Shear Stress for a 6D tee at 0.5m/s

- Maximum shear on downstream wall of 0.26 Pascal
- Considerable drop in downstream shear between 1D to 2D
- Upstream wall shear stress at a maximum towards the top of the branch
- Gradual decrease in upstream shear from 1D to 3D

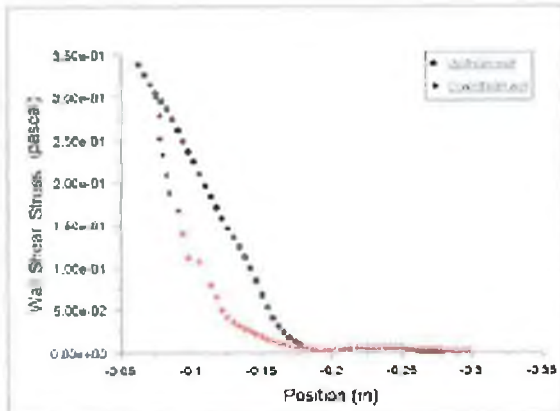

Fig 4.68: Wall Shear Stress for a 6D tee at 1.0m/s

- Slight increase in shear on downstream wall to 0.34 Pascal
- Linear drop in shear between 1D and 3D. At 4D shear stress falls to zero.
- Upstream wall shear stress profile higher than that of 0.5 m/s results
- Sharp decrease in upstream shear from 1D to 3.5D

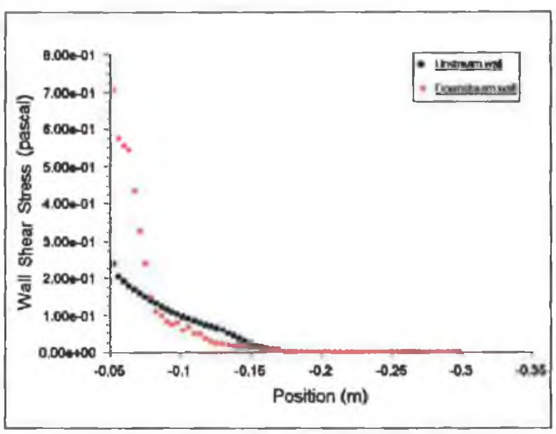

Fig 4.69: Wall Shear Stress for a 6D tee at 1.5m/s

- Increase in shear on downstream wall noted to a maximum of 0.7 Pascal
- Considerable drop in shear between 1D to 1.5D and a gradual drop up to 3D
- Upstream wall shear stress profile similar to that of 0.5 m/s results
- Decrease in upstream shear from 1D to 3.5D

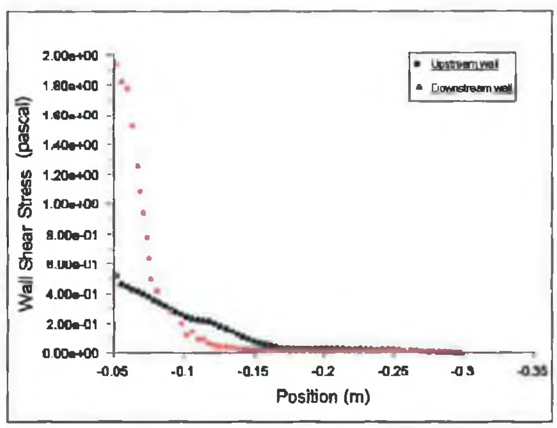

Fig 4.70 : Wall Shear Stress for a 6D tee at 2.0m/s

- Maximum shear on downstream wall of 1.95 Pascal
- Considerable drop in downstream shear between 1D to 2D. Zero at 3D
- Upstream wall shear stress at a maximum towards the top of the branch
- Almost linear decrease in upstream wall shear stress from 1D to 3D

Comparison of the data highlights a distinct difference between upstream and downstream results. The maximum wall shear stress occurred on the downstream wall of the branch in all cases. The maximum value was found at 1D into the branch and this high value of shear stress had fallen to zero 3D into the branch irrespective of mainstream velocity. The decrease in wall shear stress was found to be linear between 1D and 2D and 90% of the drop from maximum to zero also took place in this region. A more gradual decrease in stress took place between 2D and 3D and from 3D to 6D the wall shear stress was found to be zero again irrespective of velocity. Table 4.9 outlines the maximum wall shear stress found for both the upstream and downstream walls and also the position (measured from the centreline of the mainstream pipe) at which the shear stress reduced to zero for each case studied.

Mainstream Velocity	Maximum shear stress downstream (Pascal)	Downstream Zero position (mm)	Maximum shear stress upstream (Pascal)	Upstream Zero position (mm)
0.5 m/s	0.26	125	0.08	140
1.0 m/s	0.35	175	0.30	175
1.5 m/s	0.70	150	0.25	180
2.0 m/s	1.95	125	0.525	250

Table 4.9: Upstream and downstream wall shear stress for a 50mm 6D dead-leg

Upstream wall shear stress values were found to be considerably lower than those of the downstream wall over the range of velocities. A average decrease of 30% was found between maximum upstream and downstream wall shear stress. Figures 4.71 and 4.72 combine the plots for upstream and downstream wall shear stress over a mainstream velocity range of 0.5 to 2.0 m/s. It is clear from these plots that some benefit is to be gained from increasing the distribution loop velocity. With increasing velocity both the upstream and downstream wall shear stress values increased however the high values of wall shear stress on the downstream wall were rapidly diminished and almost eliminated 3D into the branch. Although the drop off in upstream wall shear stress was far more gradual it should be noted that the initial high values found on the upstream wall were on average 70% less than those on the downstream wall.

Irrespective of mainstream velocity both the upstream and downstream wall shear stresses had fallen to zero beyond 3D into the dead-leg. One practice commonly used during the cleaning of high purity water systems is to increase the velocity on the distribution loop to encourage scouring of the wall of the pipe-work. It is assumed that the increase in turbulence due to the increase in flowrate will dislodge loosely held bio-film that will be flushed to drain during the final stages of the cleaning process. While these conditions may prevail in the distribution loop it is clear from figures 4.71 and 4.72 that the dead-leg fluid has a detrimental affect on wall shear within the branch. While some increase in shear stress is noted near the entrance region of the tee the same is not true beyond 3D into the branch. Beyond this point low flow conditions exist irrespective of increasing mainstream velocity and the result is little if any wall shear. Such conditions are conducive to bio-film formation and dispel the myth that high loop flowrates will decrease branch bio-film formation.

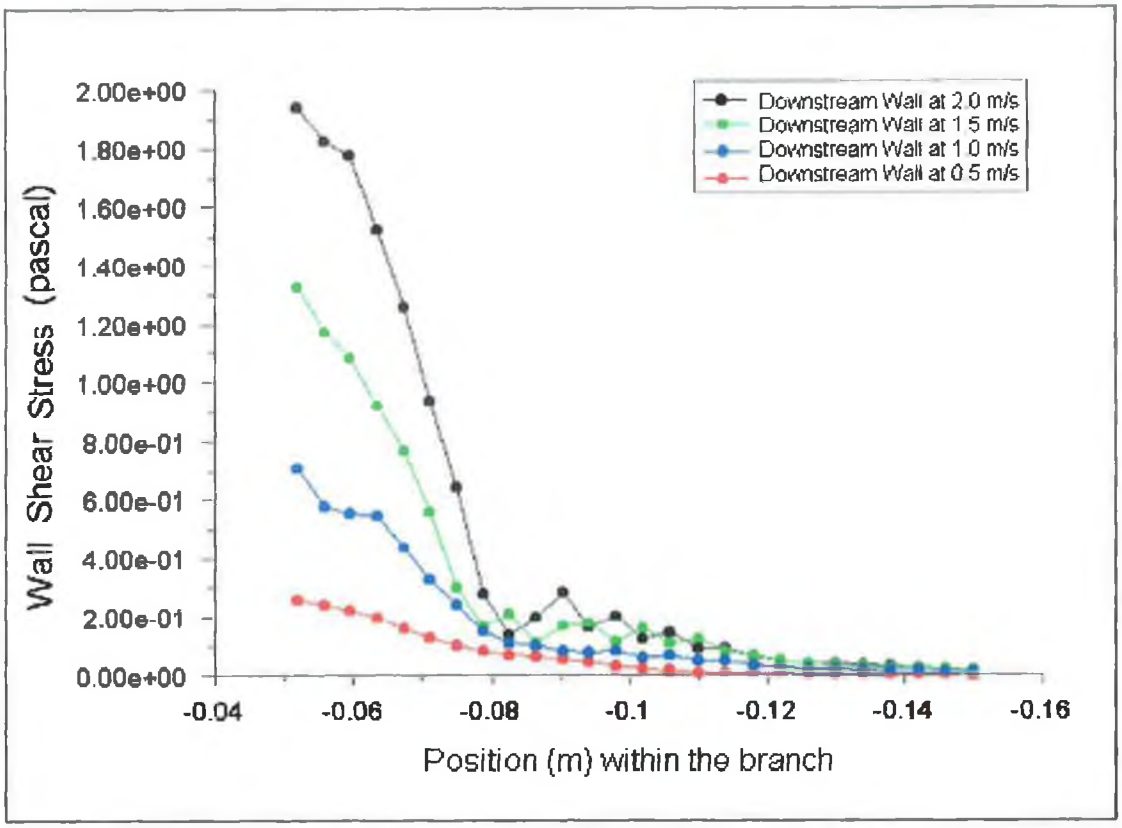

Fig 4.71: Downstream Wall Shear Stress plots for a 6D 50mm equal tee

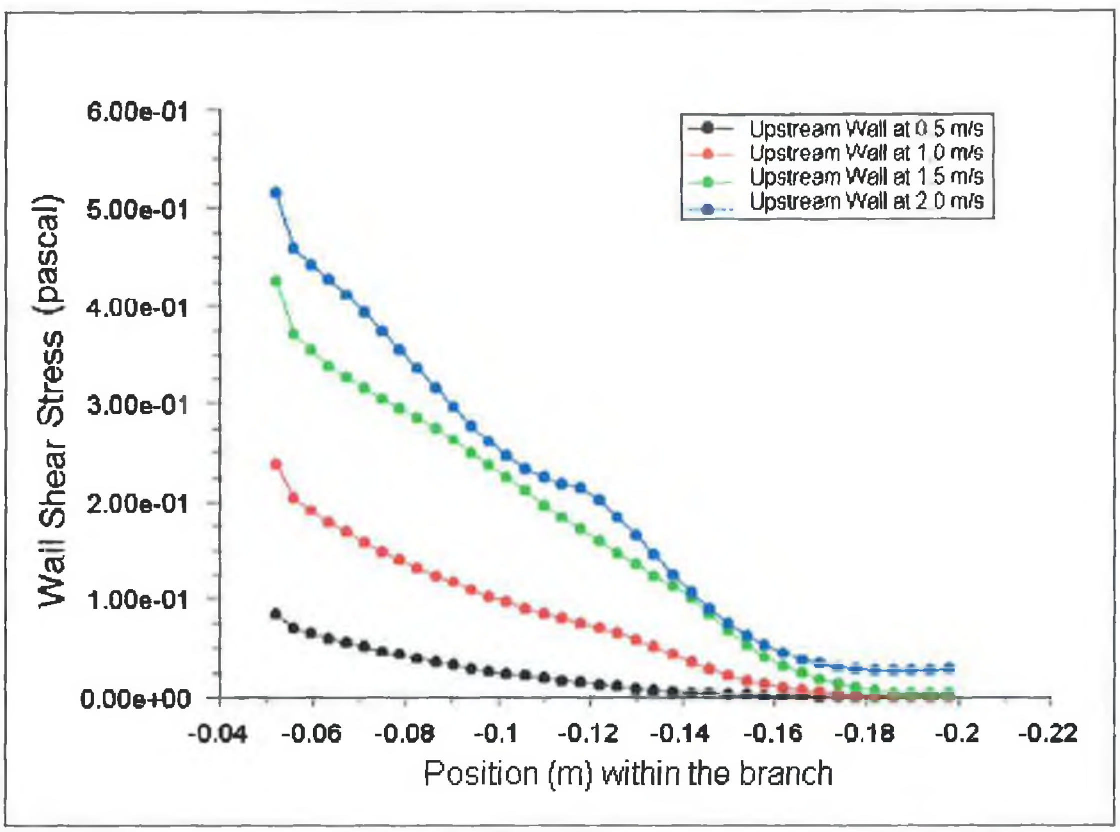

Fig 4.72: Upstream Wall Shear Stress plots for a 6D 50mm equal tee

To summarise the data presented for a 50mm round entry equal tee with a dead-leg drop from 1D to 6D the normalised branch velocity was plotted against dead-leg length for various loop velocities (figures 4.73a to 4.37e). The trend found was surprising for 6D dead-legs in that each loop velocity resulted in a similar drop off in branch velocity. A sharp drop in velocity was noted from the centreline of the distribution loop pipe 1D. This highlights the negative effect the branch fluid has on the mainstream flow and the difficulty in penetrating the branch with mainstream fluid. It is clear that at 4D no motion is present in the branch and this was identified as a cut-off point for this configuration although it should be noted that at 3D and 2D very low flowrates exist within the branch.

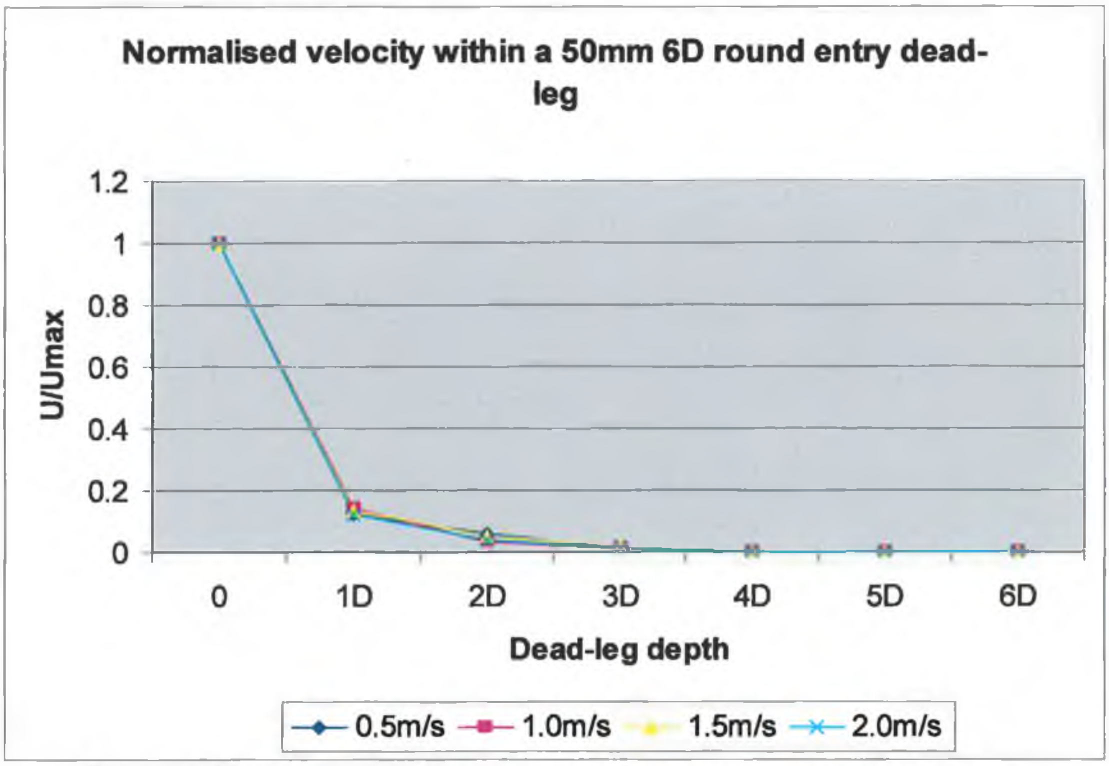

Figure 4.73a: Normalised branch velocities for a 50mm 6D dead-leg tee

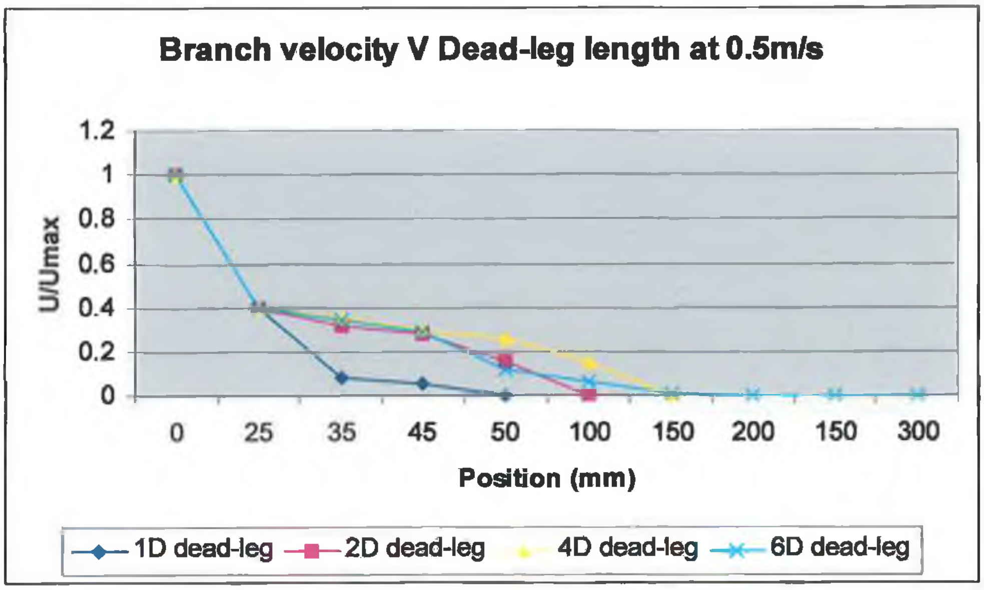

Figure 4.73b: Normalised velocity at 0.5m/s

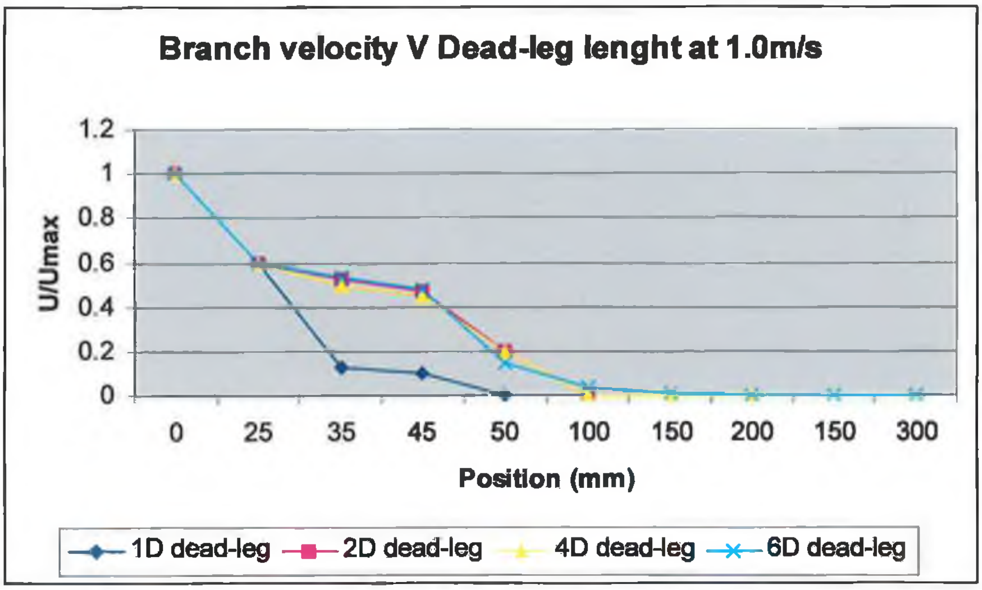

Figure 4.73c: Normalised velocity at 1.0m/s

Little advantage is to be gained from varying the dead-leg length, as the drop in branch velocity is similar across the range of dead-leg lengths examined. 2D, 4D and 6D branch configurations show signs of overlap from branch entry at 25mm through to the base of each dead-leg. 1D configurations highlight the sharp drop off in branch profiles between 25mm and the base of the dead-leg at 50mm.

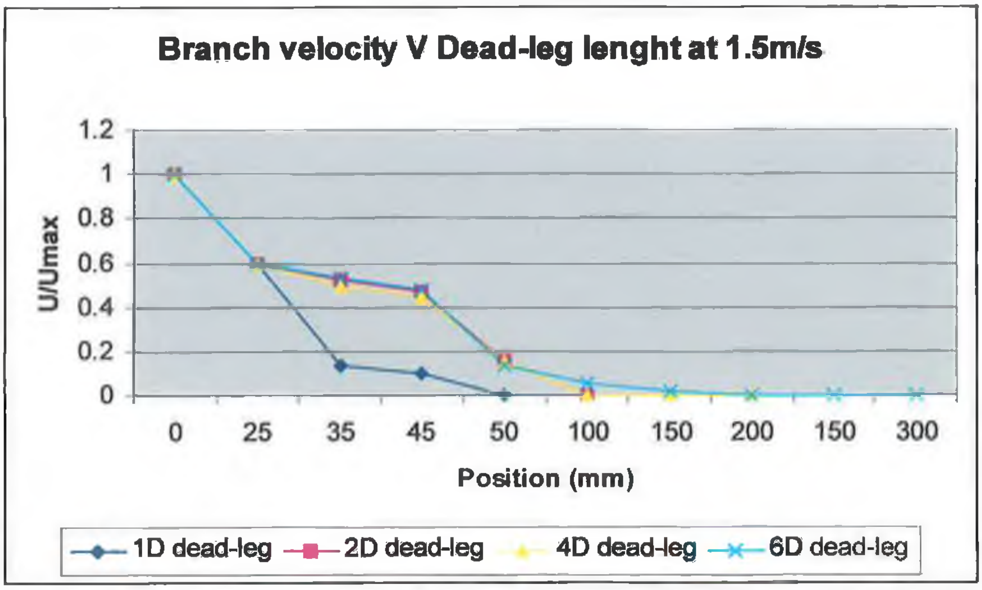

Figure 4.73d: Normalised velocity at 1.5m/s

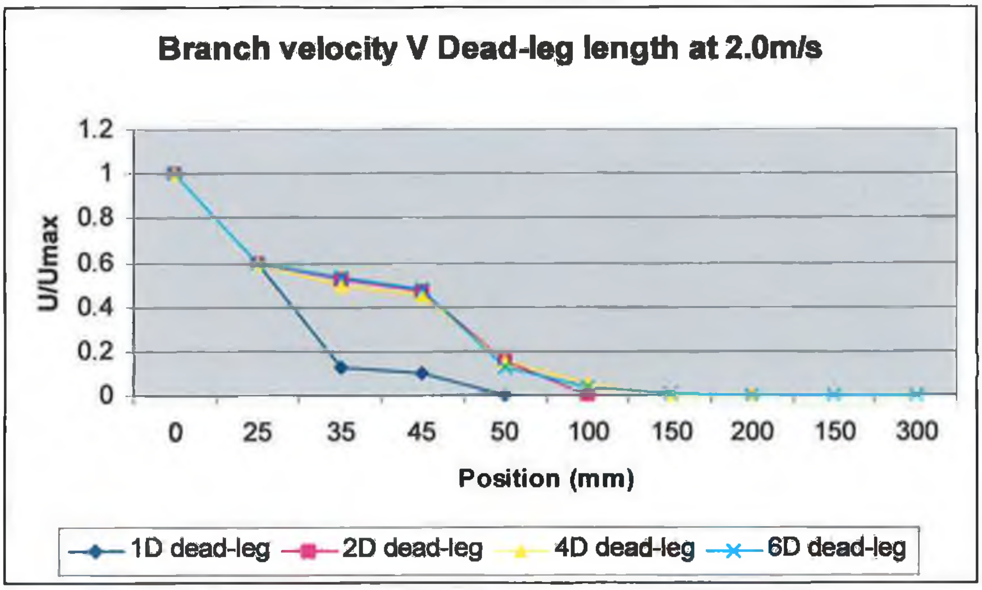

Figure 4.73e: Normalised velocity at 2.0m/s

Part C: INTRODUCTION OF A SHARP ENTRY TO THE BRANCH

4.15 SHARP TEE ANALYSIS

Most of the tees used in high purity water distribution networks are sharp entry tees. These tees are cheap to manufacture as they eliminate the need for complicated welding of the joint between the distribution loop and the branch. The data presented in this section is based on a 50*50mm equal tee (the most common tee found in high purity water systems) and a 3D dead-leg. Moving from a radius branch entry tee to a sharp entry gave rise to a number of important features.

The sharp edge interface between the upstream wall of the branch and the main distribution loop resulted in the steady passage of the mainstream fluid straight across the top of the branch of the tee. This was a feature of all cases examined. Once again the fluid within the branch section of the tee prevented fluid from the main distribution loop from entering the branch and the sharp joint between these pipes further reduced the possibility of penetration into the branch. The result of the sharp joint was a channelling of the fluid straight across the top of the branch until the fluid reached the downstream wall. A separation point was noted on the downstream wall of the branch around which the fluid above this point continued its passage across the top of the branch and remained part of the mainstream flow. However fluid below the separation point was forced into the branch following a collision with the downstream wall. The effect of this impact was to set up a region of low swirl between the centreline of the branch and the downstream wall. Some of the fluid was reflected back into the branch while the remainder flowed steadily along the down stream wall further into the branch.

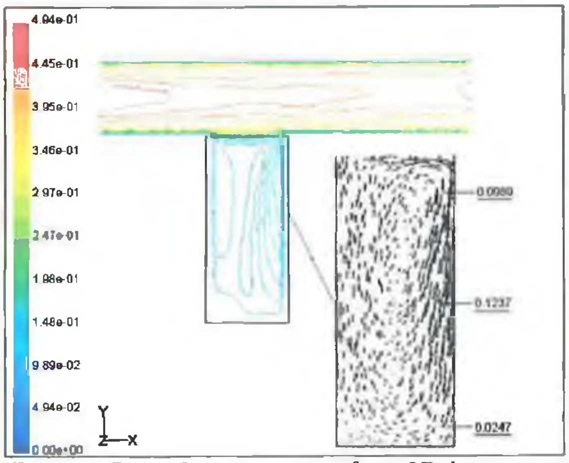

Figure 4.74: Velocity contours for a 3Dsharp tee at 0.5m/s

- At 1D fluid accelerates along the downstream wall of the branch
- At 2D downstream motion continues into the branch
- At 3D stagnant areas develop in each corner of the branch
- Overall trend is skewed towards the downstream wall and the development of a re-circulating cavity within the branch

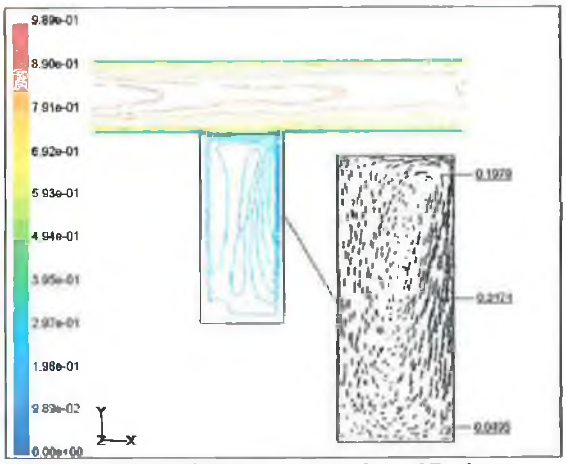

Figure 4.75: Velocity contours for a 3D sharp tee at 1.0m/s

- At 1D fluid again forced along the downstream wall of the branch
- At 2D downstream motion continues at a slightly higher velocity
- At 3D stagnant areas in each corner of the branch at slightly higher velocities
- Re-circulating cavity still evident with fluid motion increased around it

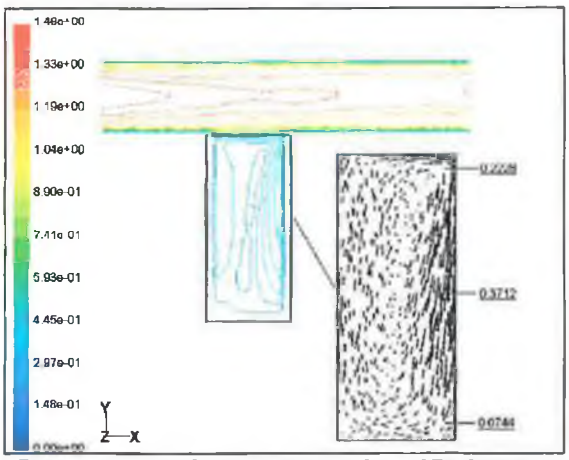

Figure 4.76: Velocity contours for a 3D sharp tee at 1.5m/s

- No major changes to 1 and 2D trends
- 3D stagnant zone visible on upstream wall
- Increased motion noted on the downstream wall
- Additional swirl around the rotating cavity

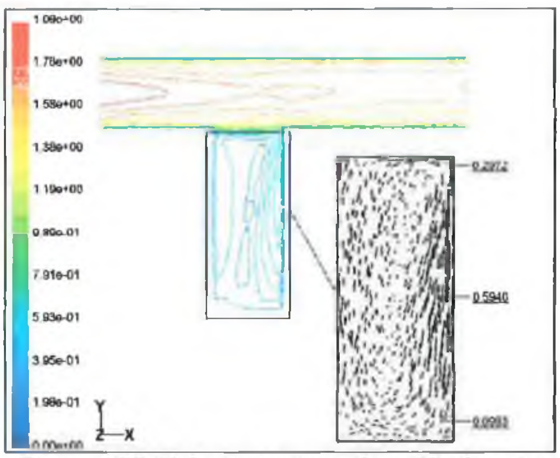

Figure 4.77: Velocity contours for a 3D sharp tee at 2.0m/s

- Higher velocities at 1 and 2D
- 3D stagnant zone on upstream wall
- Increased motion noted on the downstream wall
- Similar trend around the rotation cavity

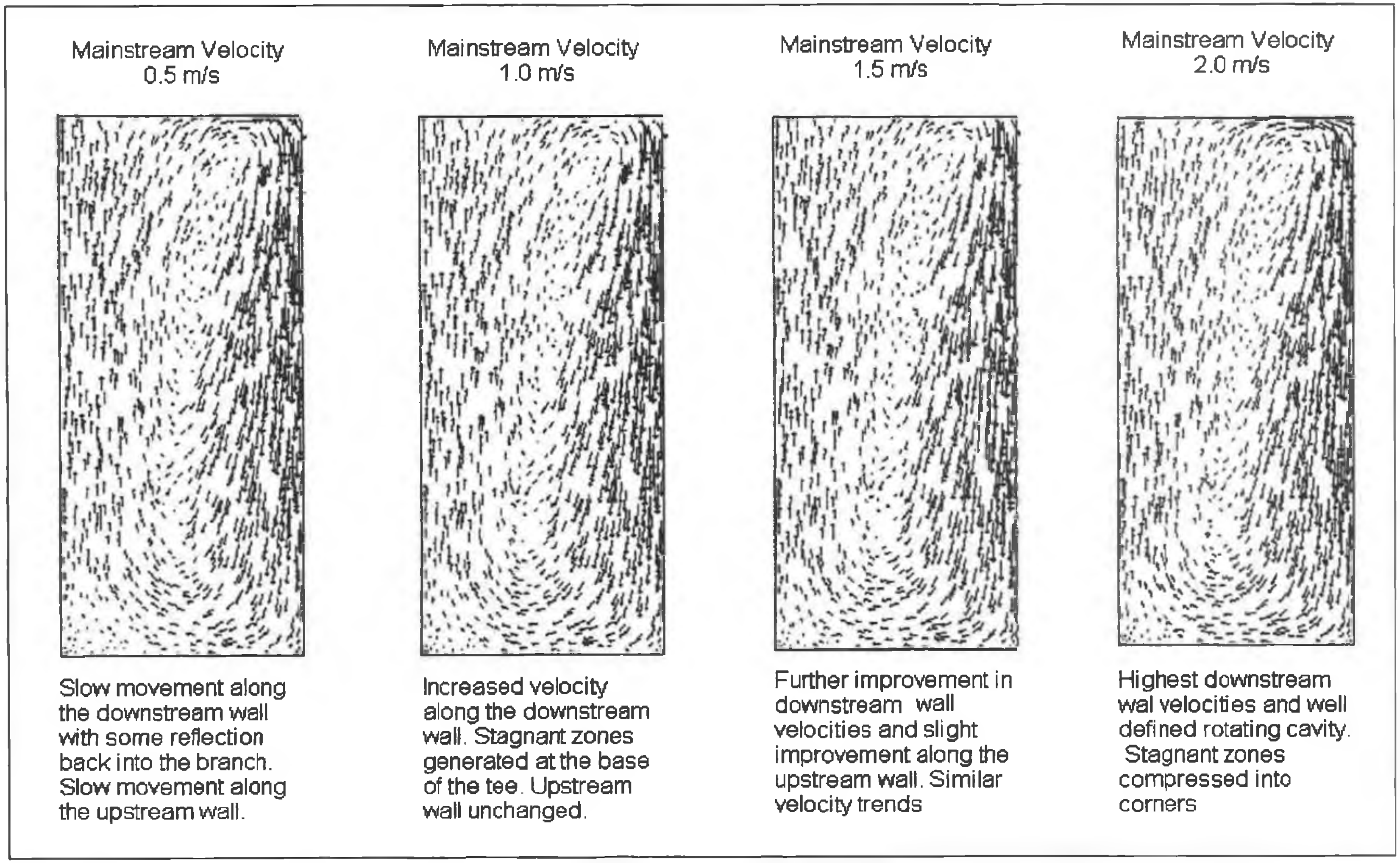

Figure 4.78: Velocity vectors in a 50mm sharp entry branch

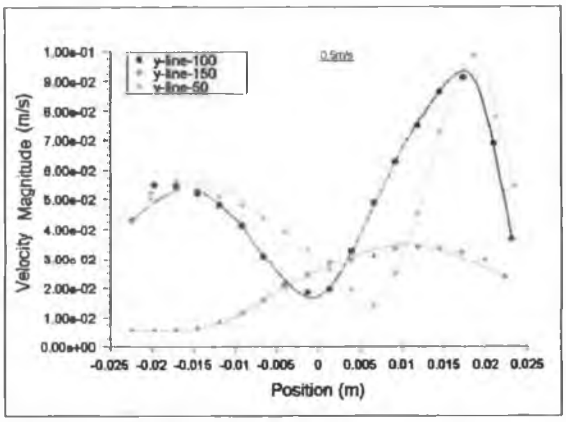

Figure 4.79: y-Velocity plots for a 3D sharp tee at 0.5m/s

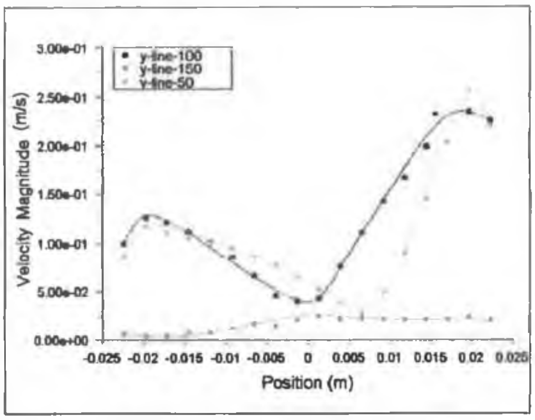

Figure 4.80: y-Velocity plots for a 3D sharp tee at 1.0m/s

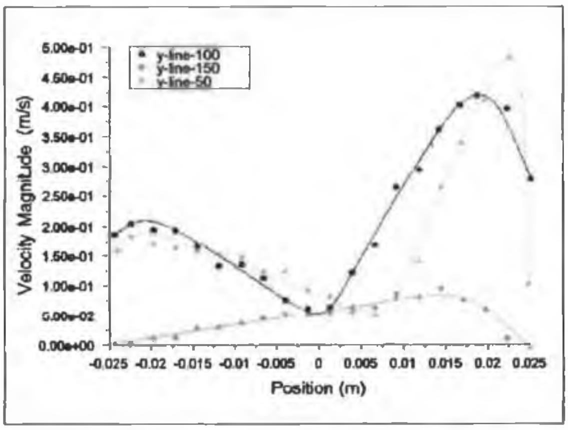

Figure 4.81: y-Velocity plots for a 3D sharp tee at 1.5m/s

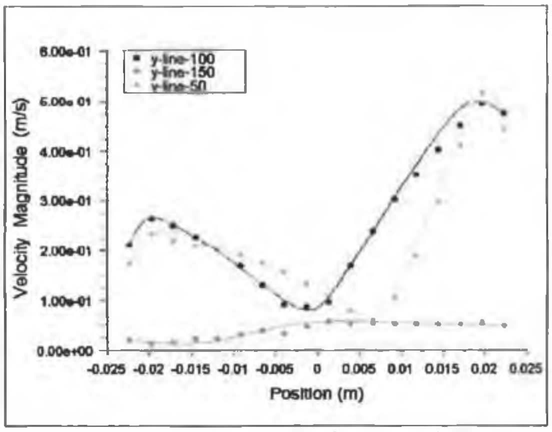

Figure 4.82: y-Velocity plots for a 3D sharp tee at 2.0m/s

4.16 SHARP ENTRY DEAD-LEG BRANCH VELOCITY PLOTS

Velocity plots for a 3D sharp entry dead-leg are presented in figures 4.79 to 4.82. Although the overall magnitude of velocity within the branch did not change considerably from those found in a rounded entry tee some notable effects can be identified on the upstream and downstream wall. For each velocity studied a region of increased velocity was noted on both the upstream and downstream wall irrespective of depth into the branch. At each mainstream velocity studied the maximum branch velocity was found to be close to the downstream wall similar to the skewed plots for rounded entry tees outlined in figures 4.51 to 4.54. At 1D into the branch (y-line-50) the maximum downstream velocity had increased in all cases when compared to those of the rounded tee. The minimum value at this depth was located downstream of the branch centreline at a distance of 7.5mm from the centreline. The location of this low velocity region was fixed even when the velocity increased. Overall the values of velocity noted on the upstream and downstream walls of the branch at this depth of 1D were higher than those found for a rounded entry tee. It is the author's opinion that the sharp entry contributes to the separation of fluid within the branch that results in higher (albeit slightly higher) values of velocity throughout the branch. Table 4.11 outlines the velocities found at various points within the branch.

	Downstream Wall			**Dead-leg Centre**			**Upstream Wall**		
	Top	**Mid**	**Base**	**Top**	**Mid**	**Base**	**Top**	**Mid**	**Base**
3D and 0.5m/s	0.098	0.123	0.024	0.024	0.000	0.000	0.049	0.049	0.000
3D and 1.0m/s	0.197	0.247	0.049	0.049	0.000	0.049	0.098	0.098	0.000
3D and 1.5m/s	0.222	0.371	0.074	0.074	0.000	0.074	0.148	0.148	0.000
3D and 2.0m/s	0.297	0.594	0.099	0.099	0.000	0.099	0.198	0.198	0.000

Table 4.11: Branch velocities found in a 3D 50mm sharp tee at various mainstream velocities

Considerable changes in velocity profile were found 2D into the branch for sharp entry. As shown previously the values of velocity found for rounded tees at a depth of 2D were very low and the downstream values almost a mirror image of the upstream around the centreline of the branch. However following analysis of the sharp entry tees it was found that the 2D velocity profile had changed considerably. In all cases the 2D profile mimicked those of the 1D apart from a slight decrease in value along the downstream wall and a slight increase on the upstream wall. The lowest velocity values were found along the centreline of the branch, a small shift of 7.5mm towards the upstream wall. This increase in velocity at 2D represents increased motion within the branch and this fact is consolidated when 3D data is analysed. Although all values of velocity are low some motion was found at the base of the sharp tee branch for both high and low mainstream velocities. In comparison to rounded tee values a sharp entry tee will encourage some motion at the base of a 3D branch. At 1 and 2 m/s values were found to increase from the upstream wall to the center of the branch at which point the values remained unchanged to the downstream wall. For 0.5 and 1.5 m/s maximum values were found on the downstream side of the branch. It is clear from the data presented that a sharp entry tee has advantages over a rounded entry tee in relation to dead-leg motion however there is still a considerable decrease in velocity 3D into the branch.

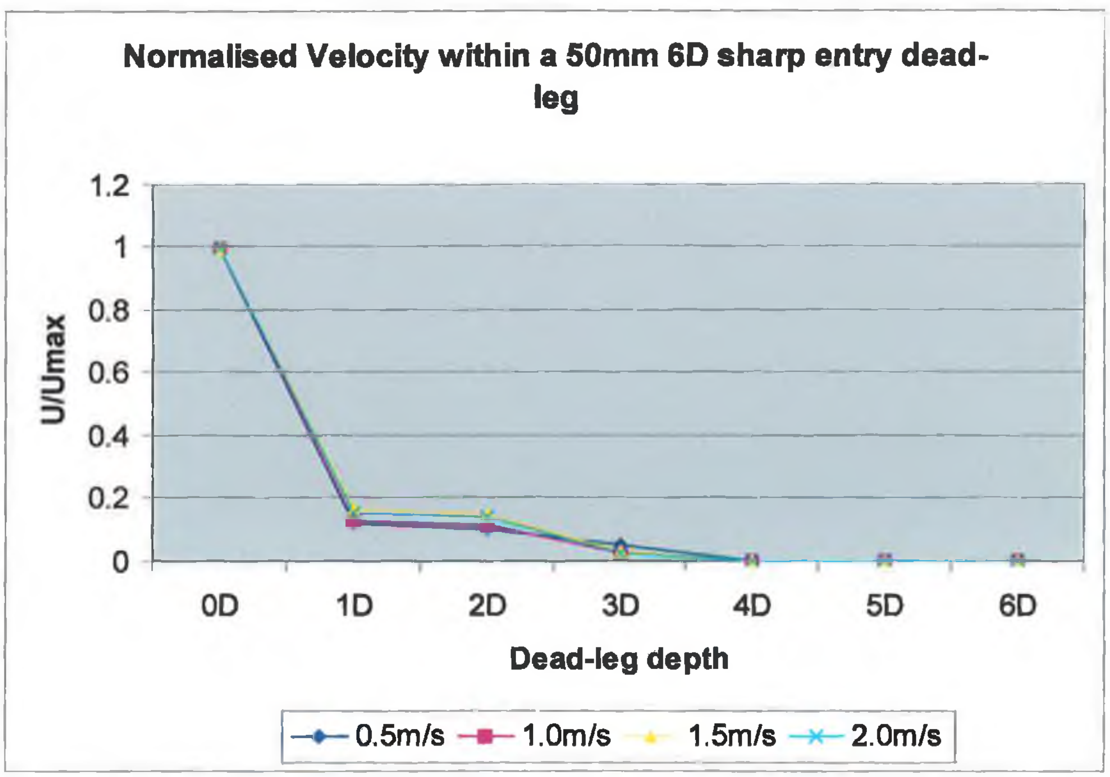

Figure 4.83: Normalised branch velocity for a 50mm sharp entry tee

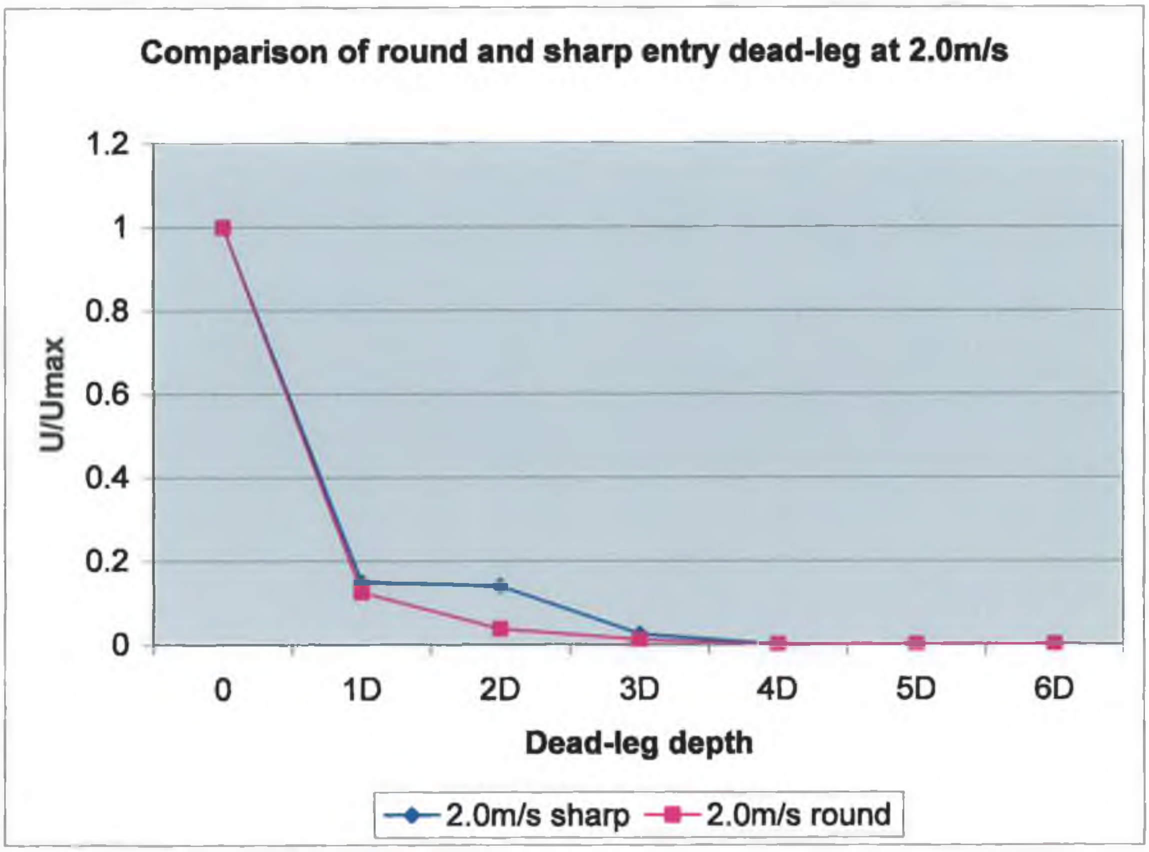

Figure 4.84: Comparison of round and sharp entry 50mm tee

For a sharp entry tee the normalised velocities within the branch were found to be higher than those of a round entry (fig 4.83 and 4.84). At high mainstream velocities a small increase in branch normalised velocity was noted at 1, 2 and 3D for a sharp entry tee. Once again the velocity in the branch fell to zero at 4D and very low values were also noted 3D into the branch. Figure 4.84 presents a comparison between round entry and sharp entry configurations for a 50mm equal tee with a mainstream velocity of 2m/s. This graph highlights the maximum velocity profiles within the branch. The only difference between the two graphs was found to be 2D into the branch where the sharp entry tee has a higher velocity than the round entry due to increased separation on the downstream wall of the branch. Table 4.12 highlights the maximum and normalised velocities found within each branch

Mainstream Velocity	Round Entry Tee		Sharp Entry Tee	
	Max Vel	U/Umax	Max Vel	U/Umax
0.5m/s	0.02	0.12	0.10	0.12
1.0m/s	0.05	0.14	0.275	0.125
1.5m/s	0.325	0.133	0.475	0.166
2.0m/s	0.375	0.125	0.55	0.15

Table 4.12: Maximum and normalised branch velocities for a sharp and round entry 50mm tee at 2m/s

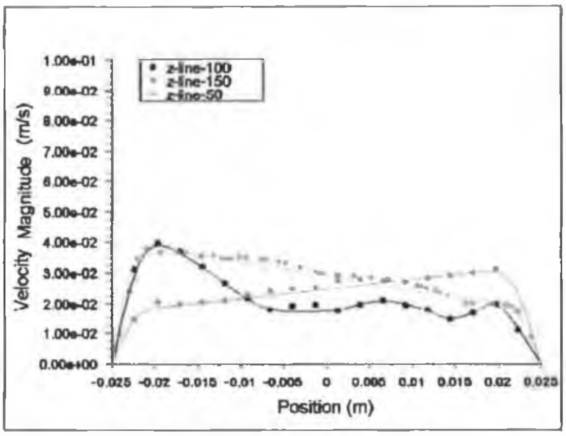

Figure 4.85: z-Velocity plots for a 3D sharp tee at 0.5m/s

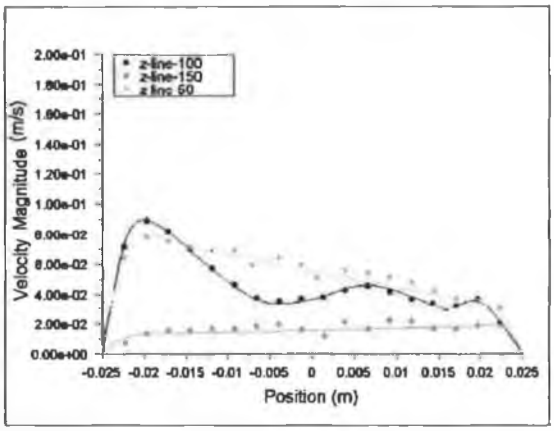

Figure 4.86: z-Velocity plots for a 3D sharp tee at 1.0m/s

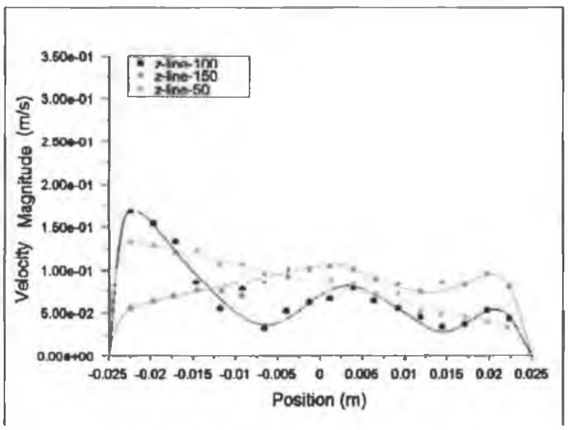

Figure 4.87: z-Velocity plots for a 3D sharp tee at 1.5m/s

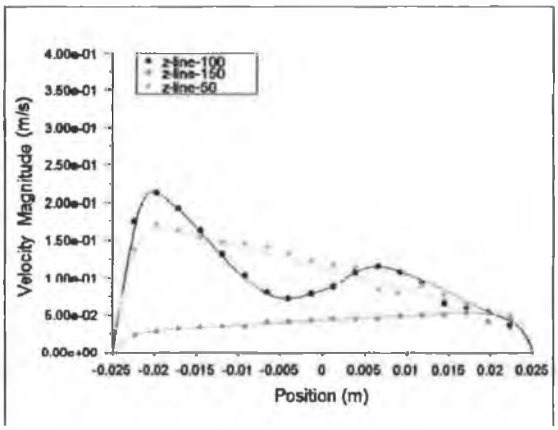

Figure 4.88: z-Velocity plots for a 3D sharp tee at 2.0m/s

The three dimensional nature of the flow in the branch is evident from the data presented in figures 4.85 to 4.88. These plots show the velocities in the z-plane and demonstrate high values on the upstream wall at z equal to -22.5mm at a depth of 1 and 2D. A steady decrease in velocity was noted from z = -25 to +25mm at 1D into the branch with the opposite occurring at 3D. Values for 2D undulate across the branch from a high at –22.5mm to a low at –5mm. This effect was associated with the region of low swirl identified earlier around which the fluid flows in complex patterns. In comparison to rounded entry data it is clear that the velocity patterns are more complex within the branch for sharp tee configurations. Smoother profiles were present in the rounded tee branch. At 1D the maximum values were noted at –22.5 mm while the opposite was found in a rounded tee configuration namely +22.5mm. 2D values undulated across the branch again peaking around the – 22.5 mm range. While the 3D values in all cases were the lowest value found they peaked in all cases at +22.5mm across the branch similar to conditions noted for the rounded entry tee at 2m/s.

4.17 TURBULENT KINETIC ENERGY AND DISSIPATION RATES

Figures 4.89 to 4.92 plot the turbulent kinetic energy profiles found for a 3D sharp entry tee. 1D values were found to peak towards the downstream wall of the branch 10 – 15mm from the centreline of the branch in all cases examined. 2 and 3D plots were found to be at a maximum 5mm upstream of the centreline. The maximum values ranged from 0.00125 m^2/s^2 at 0.5 m/s to 0.0225 m^2/s^2 at 2 m/s compared to 0.0025 and 0.04 m^2/s^2 for a rounded entry tee. Considerable differences were noted for 2D data in comparison to data presented for rounded entry tees. Sharp entry values were low in comparison throughout the range examined and maximum at 2 m/s mainstream velocities. 3D trends mimicked 2D profiles with higher values of turbulent kinetic energy values noted at 1, 1.5 and 2m/s.

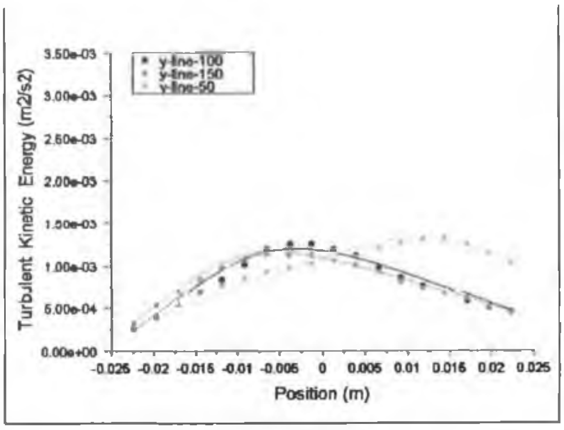

Figure 4.89: Turbulent Kinetic Energy plots for a 3D sharp tee at 0.5m/s

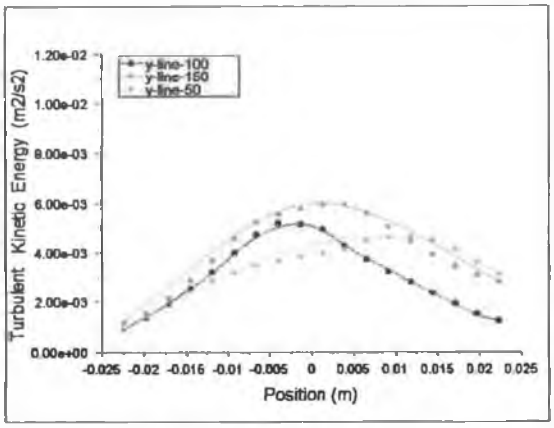

Figure 4.90: Turbulent Kinetic Energy plots for a 3D sharp tee at 1.0m/s

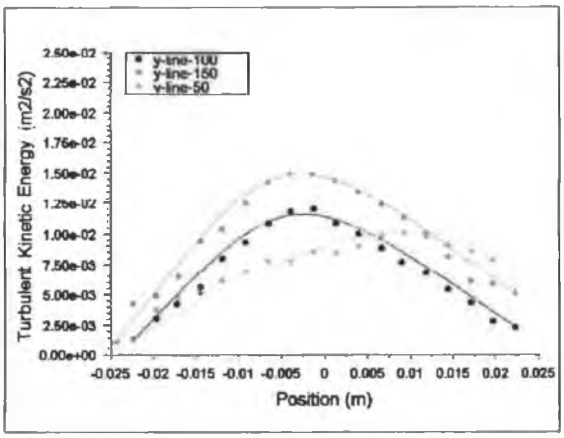

Figure 4.91: Turbulent Kinetic Energy plots for a 3D sharp tee at 1.5m/s

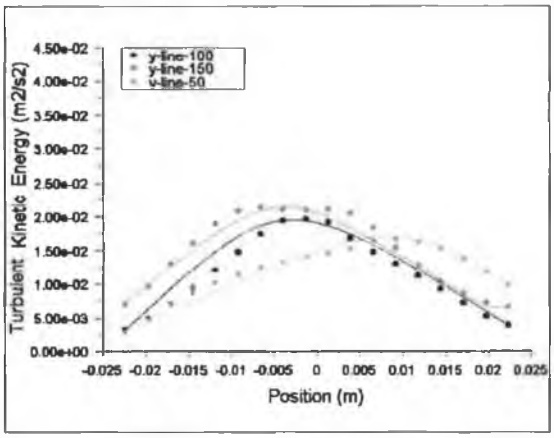

Figure 4.92: Turbulent Kinetic Energy plots for a 3D sharp tee at 2.0m/s

Turbulent dissipation rates were found to be at a maximum 1D into the branch for sharp entry tees along the downstream wall of the branch (Fig 4.93 to 4.96). The data was found to increase from the centreline of the branch to the downstream wall. The values ranged from $7.5*10^{-3}$ to $4.5*10^{-1}$ m^2/s^3 , values higher than those found for the rounded entry analysis. Profiles for 2D and 3D were spread across the branch peaking generally around the centreline. The higher the mainstream velocity the higher the dissipation rates found at 3D into the branch. The maximum value of dissipation at 0.5 m/s mainstream velocity was $1*10^{-3}$ m^2/s^3 while at 2 m/s this value had increased to $3.5*10^{-1}$ m^2/s^3.

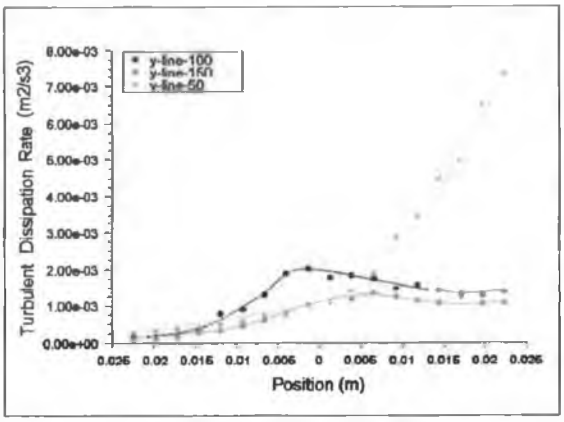

Figure 4.93: Turbulent Dissipation Rates for a 3D sharp tee at 0.5m/s

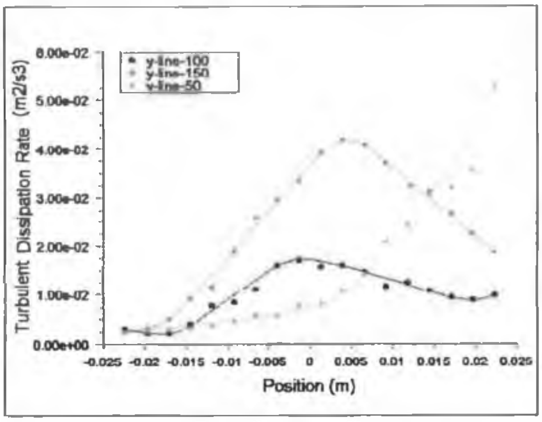

Figure 4.94: Turbulent Dissipation Rates for a 3D sharp tee at 1.0m/s

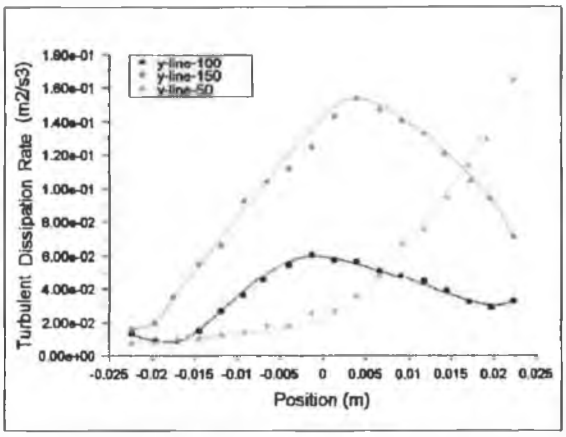

Figure 4.95: Turbulent Dissipation Rates for a 3D sharp tee at 1.5m/s

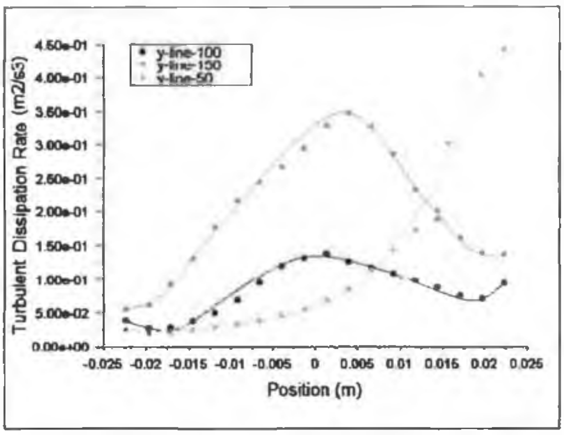

Figure 4.96: Turbulent Dissipation Rates for a 3D sharp tee at 2.0m/s

4.18 ROUND AND SHARP ENTRY WALL SHEAR STRESS VALUES

Analysis of the wall shear stress data related to a sharp entry tee shows that some advantage is to be gained by specifying a sharp entry tee over a round entry equivalent. Sharp entry analysis showed increasing upstream and downstream wall shear with increasing mainstream velocity (fig 4.97 and 4.98). Downstream wall shear stress was found to be approximately twice that of upstream wall shear over the entire range analysed. A maximum wall shear stress of 2.5 pascals was found at 2m/s. However the downstream wall shear fell to zero 3D into the branch (150mm depth) irrespective of mainstream velocity indicating a stagnant zone deep into the dead leg.

	Downstream Wall		**Upstream Wall**		
	Max Shear Stress	Zero Position	Max Shear Stress	Location	Zero Position
6D at 0.5 m/s	0.225 Pa	150 mm	0.100 Pa	90 mm	60 mm
6D at 1.0 m/s	0.725 Pa	150 mm	0.312 Pa	95 mm	65 mm
6D at 1.5 m/s	1.625 Pa	150 mm	0.625 Pa	100 mm	65 mm
6D at 2.0 m/s	2.522 Pa	150mm	1.245 Pa	100 mm	60 mm

Table 4.13: Upstream and downstream wall shear stress values for a sharp entry tee

The upstream wall shear stress ranged from 0.1 to 1.245 pascals increasing with increasing mainstream velocity. The location of the maximum wall shear stress was not fixed. Its position was forced further into the branch with increasing velocity. However the range was located between 90 – 100mm into the branch. The upstream wall shear stress fell to zero within a range of 60-65 mm as outlined in table 4.13. A comparison of rounded versus sharp entry tee and the effect on wall shear stress are presented in table 4.14 for both upstream and downstream branch walls. At high mainstream velocities the sharp entry tee showed a 50% increase in maximum wall shear stress over rounded entry. Indeed all values of velocity examined showed increased wall shear stress when using a sharp entry tee apart from 0.5 m/s data which resulted in a small decrease in shear. It is clearly advantages to have a sharp entry tee if wall shear stress is to be increased. Some advantages were also noted on the upstream wall when a sharp entry tee was used.

	Downstream Wall		Upstream Wall	
	Round Entry	Sharp Entry	Round Entry	Sharp Entry
6D at 0.5 m/s	0.265 Pa	0.225 Pa	0.095 Pa	0.100 Pa
6D at 1.0 m/s	0.352 Pa	0.725 Pa	0.252 Pa	0.312 Pa
6D at 1.5 m/s	0.712 Pa	1.625 Pa	0.425 Pa	0.625 Pa
6D at 2.0 m/s	1.955 Pa	2.522 Pa	0.532 Pa	1.245 Pa

Table 4.14: Comparison of round and sharp entry tee wall shear stress for a 50mm branch.

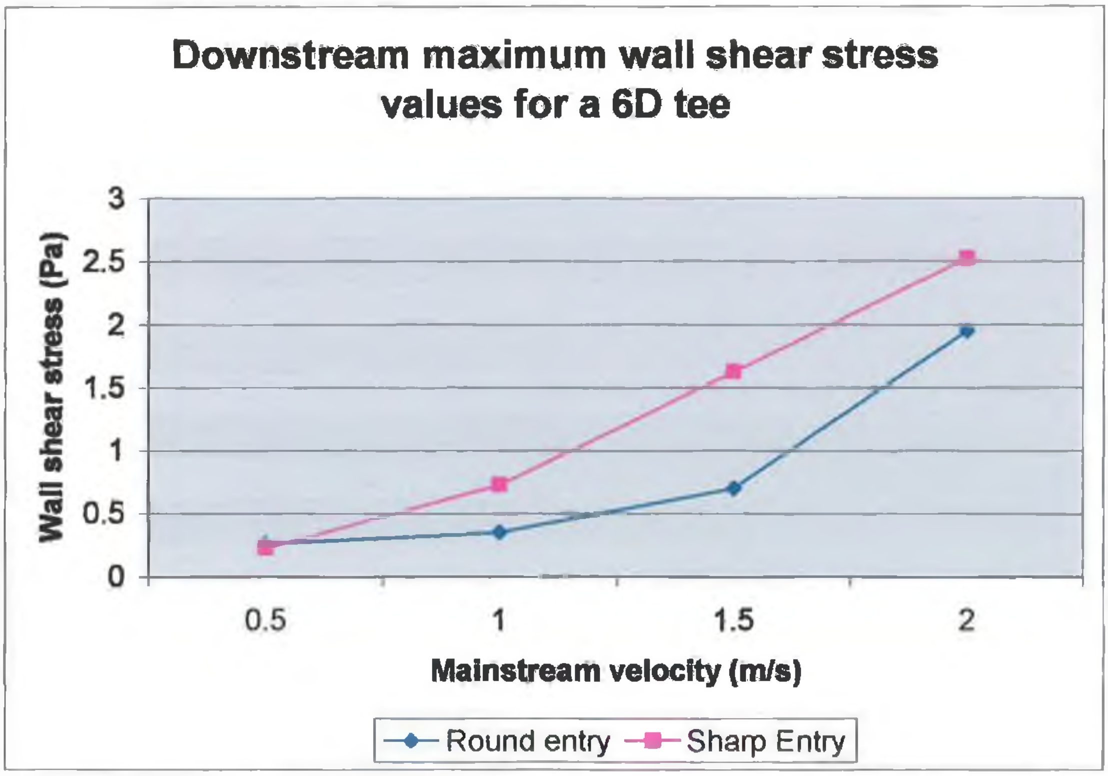

Figure: 4.97: Round and sharp entry downstream wall shear stress

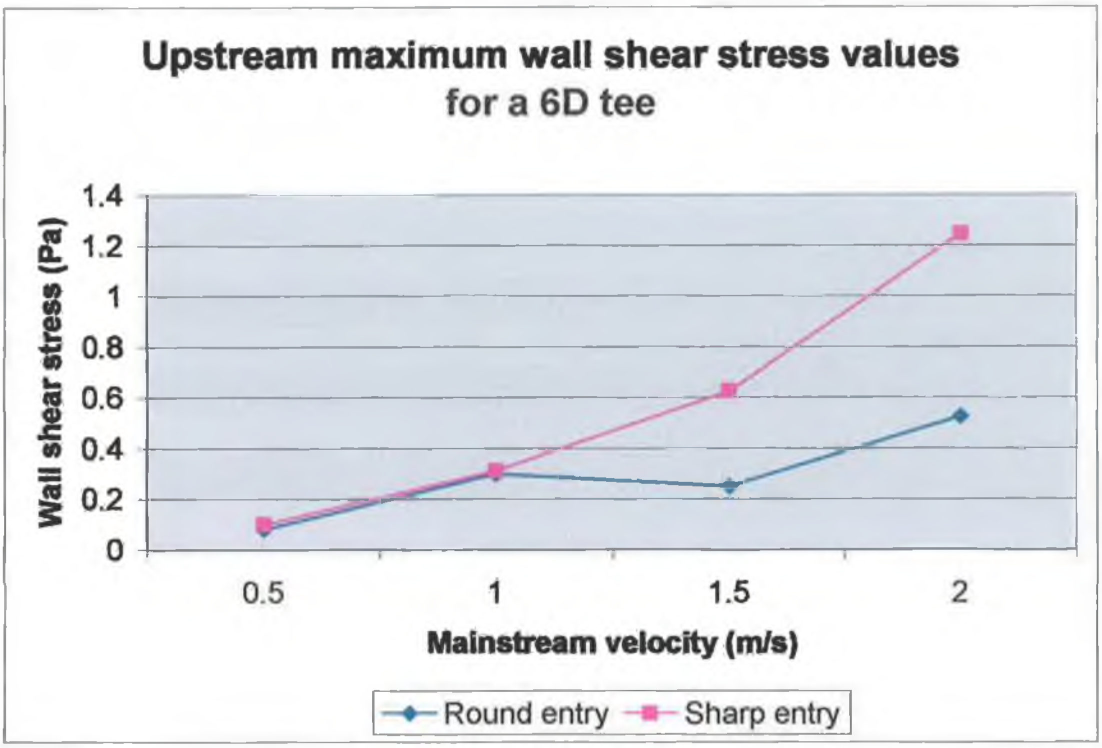

Figure: 4.98: Round and sharp entry upstream wall shear stress

Again the maximum benefit was noted at high mainstream velocity although values were considerably less than those on the downstream wall The maximum value of wall shear stress on the upstream wall was again found to be at 2 m/s, as outlined in table 4.14.

Part D: REDUCTION IN BRANCH TO DISTRIBUTION LOOP DIAMETER

4.19 EFFECT OF BRANCH TO LOOP DIAMETER ON DEAD-LEG FLOW

There are numerous examples in pharmaceutical and semi-conductor plant of reduced tee junctions. These reduced tees when used on high purity water systems are often found at points-of-use. Water is taken from the main distribution loop through a reduced pipe diameter to a processing tank. The general industrial standards for these reductions may be categorised as 1:1, 1:1/2 or 1:1/4 in respect of loop to branch ratios. For a 50mm distribution loop this will result in a 50:50mm equal tee, a 50:25 mm reduced tee and a 50: 12.5mm reduced tee. Below 12.5mm high purity water systems revert to lab based equipment and small-scale purification techniques. The remainder of this chapter will examine data related to reduced diameter tees and highlight the influence of such reductions on dead-leg patterns.

It is important to outline the effect of the 6D rule on these new configurations. Figure 4.99 highlights the overall dimensions established by the 6D rule for a 50mm distribution loop and a 1:1, 1:1/2 and 1:1/4 loop to branch ratio (branch A, B and C respectively). Examining positions related to the 6D rule for each tee offers an interesting insight into cross referencing between each configuration. For Branch A (50mm:50mm) 6D into the branch is 300mm from the loop centreline. However for Branch B (50mm:25mm) it is only 150mm and for Branch C (50mm:12.5mm) is has reduced to 75mm. For Branch C a position of 1D does not reach the branch at all. In fact it is still within the distribution loop.

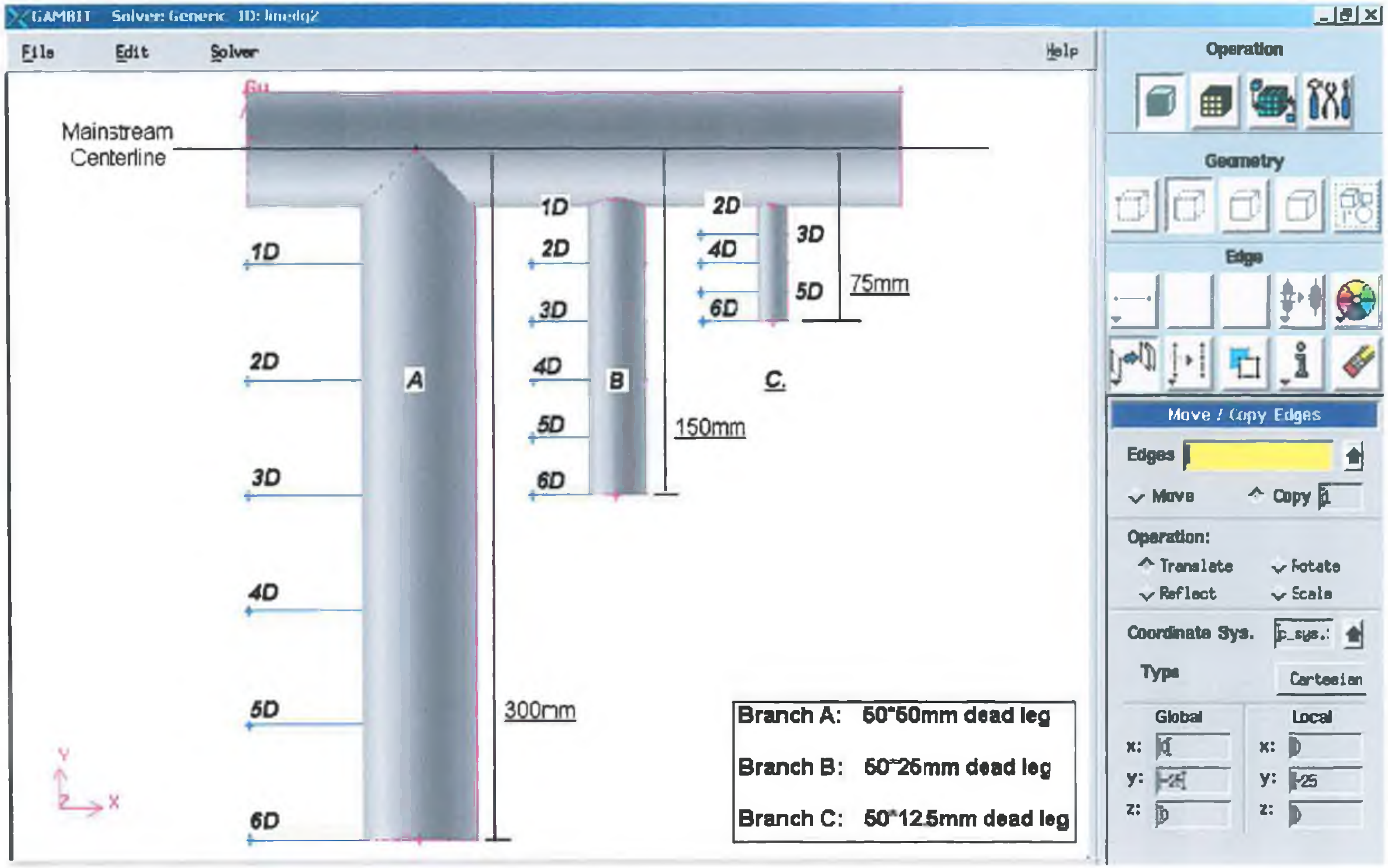

Figure 4.99: Reduced branch configurations for a 50mm distribution loop

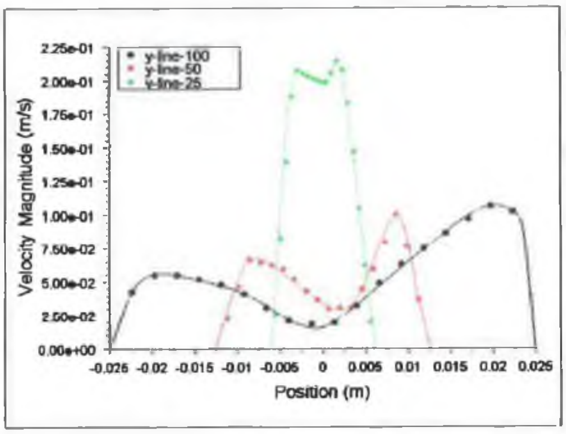

Figure 4.100: Combined branch 2D plots at 0.5m/s

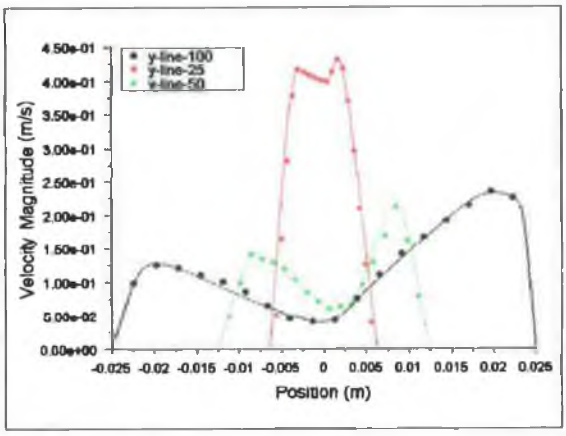

Figure 4.101: Combined branch 2D plots at 1.0m/s

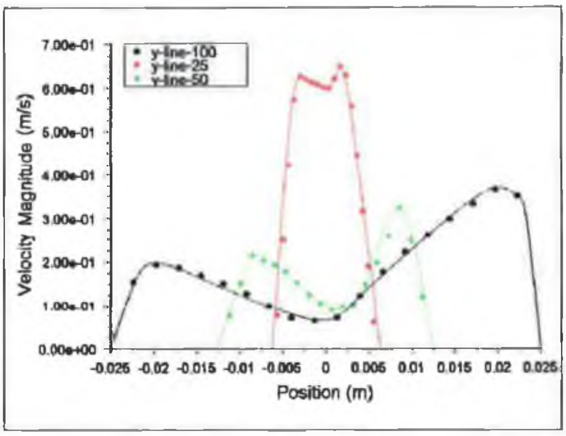

Figure 4.102: Combined branch 2D plots at 1.5m/s

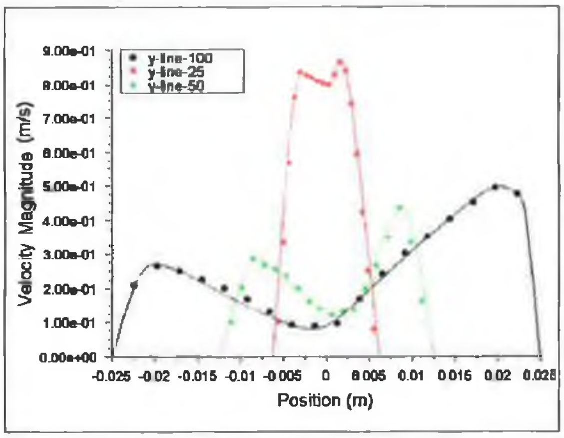

Figure 4.103: Combined branch 2D plots at 2.0m/s

It is clear from the data presented in figures 4.100 to 4.103 that over the range of mainstream velocities studied the velocity profiles within the dead-leg are similar apart from magnitude. 2D into the 50mm branch (y-line-100 plots) the maximum velocity was found along the downstream wall as noted previously. This trend was also present in both the 25mm and 12.5mm dead-legs. However the velocity profile was at a minimum around the centreline of the branch for the 50mm dead-leg while these minimum values were off set towards the downstream wall for both the 25 and

12.5mm branch. It should be noted that the peak values presented by each y-line-25 plot over the range of mainstream velocities investigated are highly influenced by the fact that this position represents the top (entry to) the dead-leg for a 12.5mm tee. The y-line 50 and y-line 100, both of which are also at 2D, are well inside the branch and show signs of a similar drop off in velocity at this depth. Therefore the current definition of a dead-leg based on measurement from the centreline of the mainstream pipe make it difficult to compare dead-leg drops particularly when the branch is small compared to the mainstream pipe. For the tee considered at this point (50mm * 12.5mm) a 1D position is outside the branch and a 2D located just at the entry to the branch (see figure 4.99).

Further into the branch at 3D (figures 4.104 to 4.107) it is clear that the velocity has decreased even further. Within the 50mm branch (y-line-150 plots) the profiles are no longer dipping at the center of the tee. The highest velocities are evident along the downstream wall for both the 0.5 and 1.0m/s runs while these peaks are suppressed when the mainstream velocities are increased to 1.5 and 2.0m/s. The drop in velocity previously noted at 2D for the 50mm branch is now evident 3D into the 25mm branch and is once again located on the centreline of the branch. Apart from the 0.5 m/s runs the maximum velocities for both the 25 and 12.5mm branches are almost identical. Peak values for both the 25 and 12.5mm branches were found close to the downstream wall.

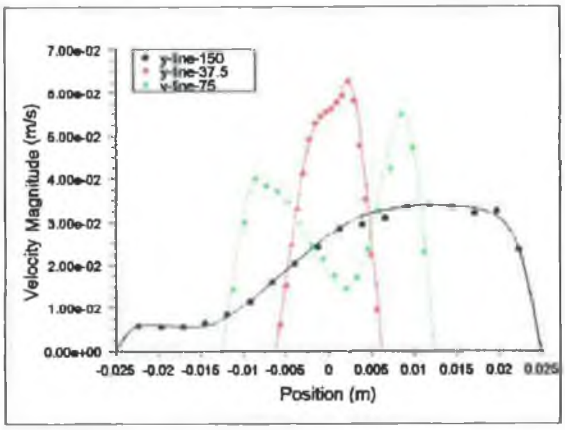

Figure 4.104. Combined branch 3D plots at 0.5m/s

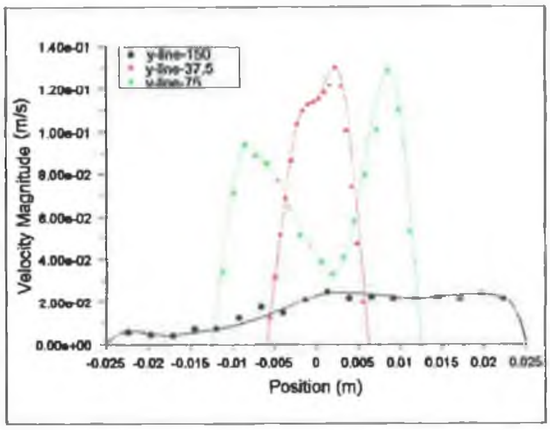

Figure 4.105. Combined branch 3D plots at 1.0m/s

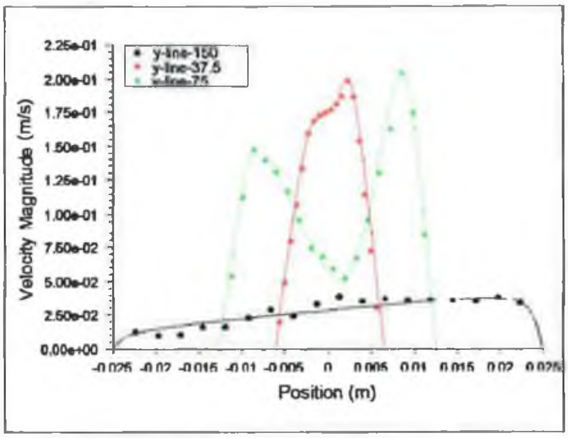

Figure 4.106. Combined branch 3D plots at 1.5m/s

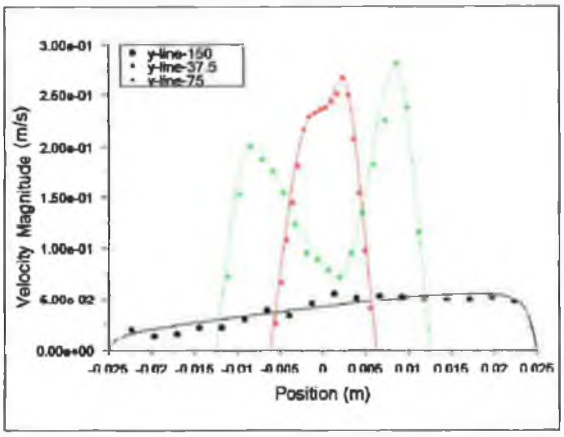

Figure 4.107. Combined branch 3D plots at 2.0m/s

4D branch investigations (figure 4.108 to 4.111) consolidate previous conclusions that below 3D into a 50mm branch there is little if any motion. This is clear from the y-line-200 plots which represent a position of 200mm into the branch. The branch velocities have dropped to zero over the range of mainstream velocities investigated. Again a minimum velocity was noted at the center of the 25mm tee with a maximum velocity along the downstream wall. This was the highest of all velocities found in any of the branches for 4D dead-leg investigations.

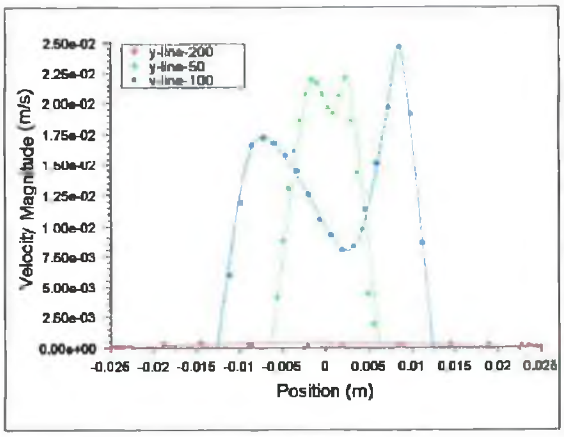

Figure 4.108. Combined branch 4D plots at 0.5m/s

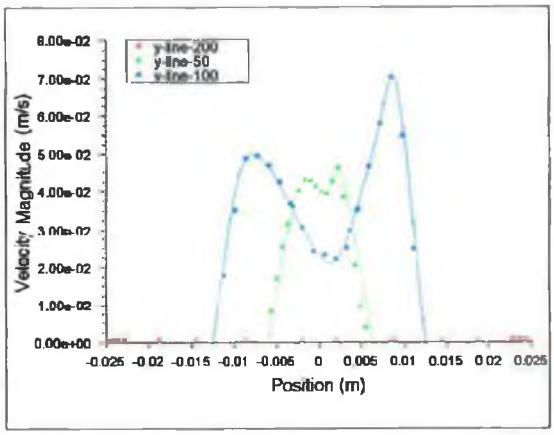

Figure 4.109. Combined branch 4D plots at 1.0m/s

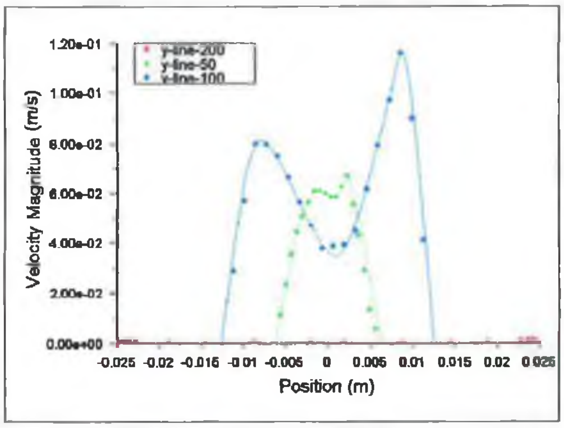

Figure 4.110. Combined branch 4D plots at 1.5m/s

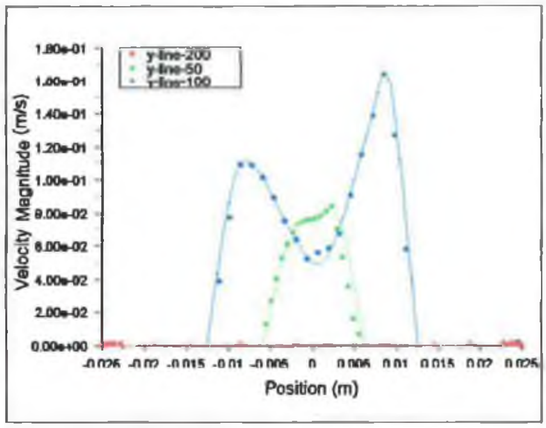

Figure 4.111. Combined branch 4D plots at 2.0m/s

It should be noted that although these are peak values they are still very low. The peak velocity found 4D into the branch was 0.17m/s from a mainstream velocity of 2m/s, a 92% decrease. The values noted for a 12.5mm branch were all less than those found in the 25mm branch at 4D. Trends were similar to those noted in 2D and 3D investigations.

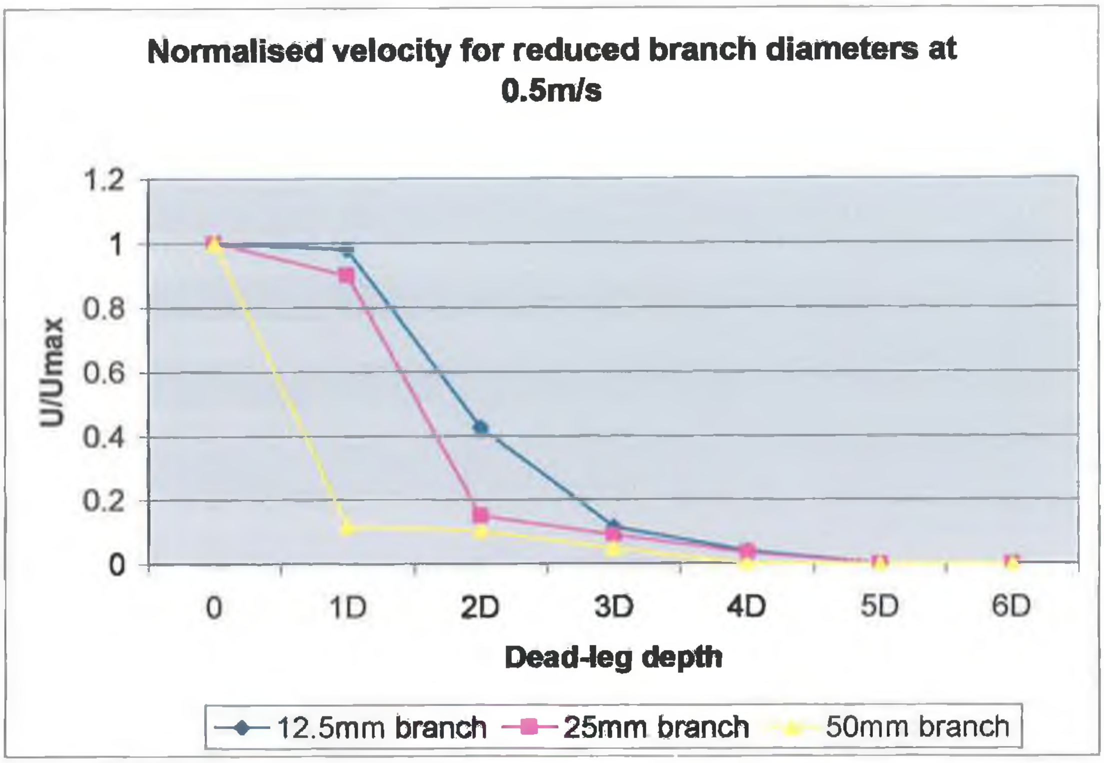

Figure 4.112: Reduced branch velocities at 0.5m/s

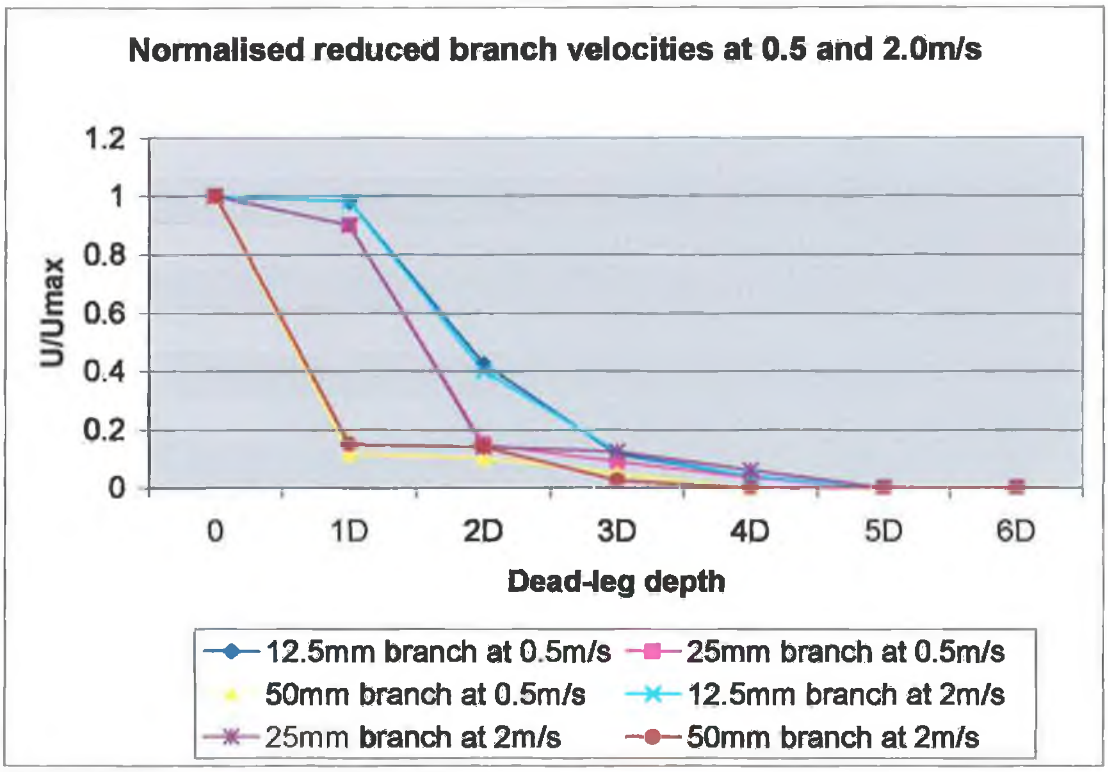

Figure 4.113: Comparison of reduced branch velocities at 0.5 and 2.0m/s

A comparison of branch velocities for various reduced branch diameters is presented in figures 4.112 and 4.113. It is evident from the data presented that some benefit is to be gained by reducing the branch diameter from 50mm to 12.5mm. Within the confines of the 6D-rule reducing the branch diameter has the result of reducing the length of the tee branch. Therefore 1D data is not a fair comparison across the board due to the fact that for a 12.5mm branch one is not inside the branch at this point. For a 25mm branch one is only entering the branch and hence the high values found. There is an increase in velocity at 2D for a 12.5mm branch that is retained up to 3D but then the velocity falls in line with 4D reading across the range of diameters studied. Between 4 and 6D no motion was noted even in a small (12.5mm) branch. An interesting overlap was identified when comparisons were made across the range of velocities studied. Figure 4.113 highlights this by comparing 0.5m/s with 2.0m/s data. Irrespective of mainstream velocity branch profiles overlap. This highlights the fact that for the 6D –rule, only a reduction in branch diameter will increase velocity within the branch.

An overview of key points noted during the investigation of varying branch diameters are outlined in table 4.15 below. These include vector plots, velocity investigations and z-plane velocity plots for each branch ratio.

Vector Plots 50:50	Vector Plots 50:25	Vector Plots 50:12.5
Recirculation zone clearly visible Stagnation zones in corners at base of the tee Reflection off the downstream wall evident	Recirculation zone not as clearly defined. Centred in branch Dead zones evident below 3D region Less reflection with motion in the branch concentrated along the downstream wall	Recirculation area not developed Stagnation zones visible below 4D Less room in the branch for reflection along the downstream wall
Velocity Plots 50:50	**Velocity Plots 50:25**	**Velocity Plots 50:12.5**
At 0.5m/s max velocity in the branch was 0.1m/s with minimum values skewed around 7.5 mm downstream at 1D and centred from 2D to 6D At 1.0m/s max velocity noted was 0.275m/s with similar trends to those noted for 0.5m/s runs At 1.5m/s penetration into the branch had increased and a max velocity of 0.5m/s was noted 1D into the branch. Maximum velocities noted along the downstream wall. At 2m/s only a slight improvement in branch velocities was noted with a max value of 0.55m/s. 3D profiles were found to decrease with increasing velocities.	At 0.5m/s the same maximum velocity was noted within the branch but the low points were skewed 2.5mm downstream of the branch centreline At 1.0m/s the maximum velocity was again the same but increased motion was found along the upstream wall At 1.5 m/s maximum branch velocity was 0.425m/s while the velocity fell to a minimum for each plot at 2.5mm downstream of the branch centreline At 2m/s the maximum velocity had fallen to 0.45m/s while increased motion was noted throughout the branch	At 0.5m/s a maximum velocity of 0.225 was noted at entry to the branch falling to 0.06m/s 3D into the branch At 1.0m/s the branch entry velocity was 0.5m/s however this value had fallen to 0.2m/s again at 3D into the branch At 1.5m/s no improvement was found for an increase in mainstream velocity and again a value of 0.2m/s was found 3D into the branch At 2m/s the branch entry velocity (2D) was 1.0m/s which fell to 0.3m/s at 3D into the branch. This sever drop off was a common feature of all 12.5mm branch analysis.
Z-Velocity Plots 50:50	**Z-Velocity Plots 50:25**	**Z-Velocity Plots 50:12.5**
At 0.5m/s the maximum velocity recorded was 0.04m/s At 1.0m/s the max value was 0.09m/s At 1.5m/s the value was 0.175m/s At 2.0m/s the max value was 0.225m/s Max values were always 2D into the branch	At 0.5m/s a slight decrease to 0.03m/s was noted At 1.0m/s the max value was 0.08 m/s At 1.5m/s the value was 0.125m/s At 2.0m/s the max value was 0.15 Max values were 2D into the branch and profiles flat	At 0.5m/s the velocity had decreased to 0.02m/s At 1.0m/s the peak value was 0.05m/s At 1.5m/s no change was noted within the branch At 2.0m/s the max value was 0.1m/s Profiles were not consistent and influenced by mainstream flow

Table 4.15: Comparison of 50mm, 25mm and 12.5mm branch data

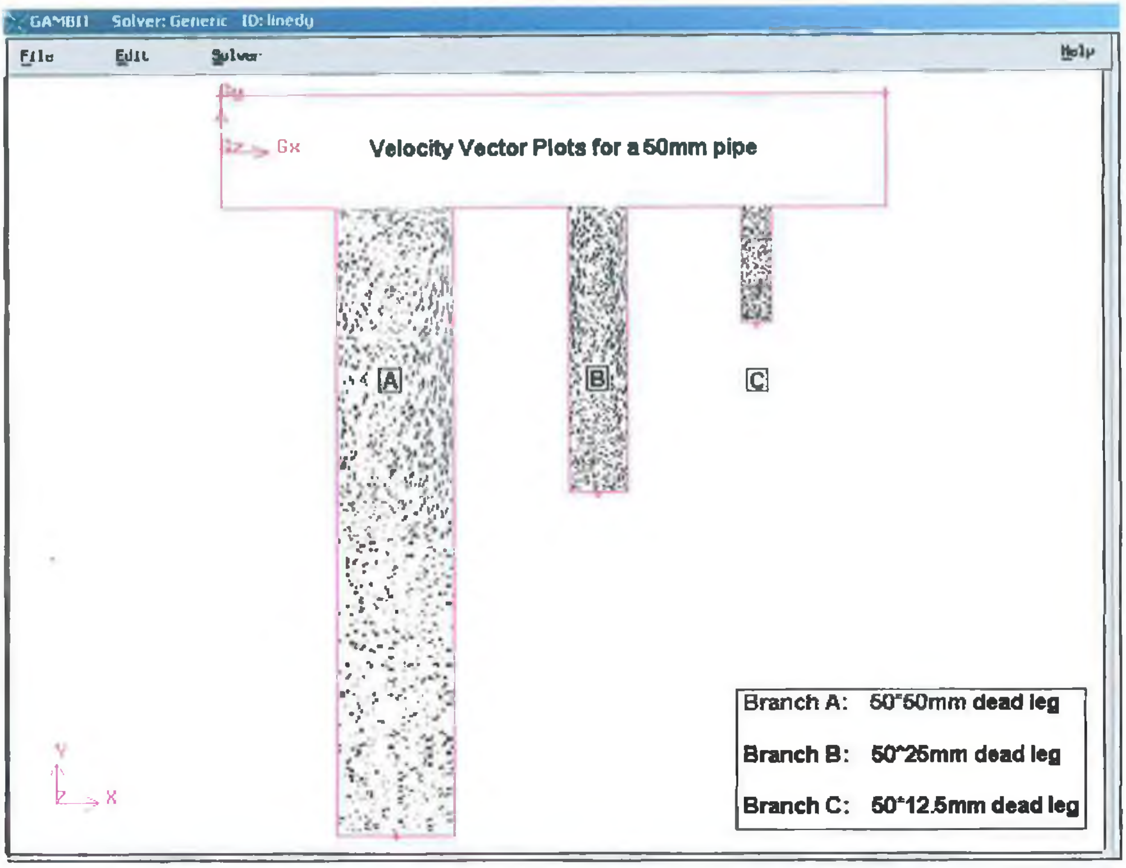

Figure 4.114: Reduced branch velocity vectors for a 50mm distribution loop

Figure 4.114 presents velocity vector plots for a 50mm distribution loop pipe and various branch diameters. As stated previously Branch A (50:50mm tee) has a clear separation point on the downstream wall of the branch above which fluid re-enters the mainstream flow and below which fluid flows into the dead-leg along the downstream wall. Penetration was found to a depth of 3D below which the fluid was found to be generally stagnant. A slow rotating cavity was also present. This cavity was not visible in Branch C (50:12.5mm tee) and although becoming visible in Branch B (50:25mm tee) was not as clearly developed as that found in Branch A. The developing cavity in Branch B was positioned around the centreline of the branch while that found in Branch A was off-set towards the downstream wall. It is the author's opinion that the development of this cavity and its location is directly related to the diameter of the branch. A small diameter branch restricts penetration from the distribution loop. The mainstream fluid rushes across the top of the branch imparting motion to the fluid already in the branch. There is no separation point evident within the branch of the 12.5mm tee. A separation point is present in the 25mm branch close to the top of the branch downstream wall and this point is pushed further into the branch for a 50mm branch. The result is no cavity in the 12.5mm branch, a developing cavity centred in the 25mm branch due to increased penetration from the mainstream fluid and a well developed swirl off-set along the downstream wall of the 50mm branch due to the cross-sectional area available and position of the separation point on the downstream wall of the branch. Motion across the 12.5mm branch is quickly dissipated into the branch fluid. The result is that the entire branch becomes a rotating cavity with less opportunity for exchange of fluid between the branch and mainstream flow. Wider branches are influenced by downstream wall penetration and upstream wall motion giving rise to a separate and distinct cavity high up within the branch. Narrowing of the branch from 50 to 25 mm results in repositioning of the cavity on the centreline of the 25 mm branch and a decrease in size of the cavity. Narrowing the branch further to 12.5mm eliminates the cavity.

4.20 COMPARISON OF REDUCED BRANCH WALL SHEAR STRESS

Tables 4.16 to 4.18 give an insight into the effect of loop to branch ratios on branch wall shear stress. The primary concern is the maximum wall shear stress found within the branch and this value was found to occur on the downstream wall of each branch. Trends similar to those already outlined for a 50mm sharp entry tee were found irrespective of branch ratio. The tables presented give an insight into the maximum upstream and downstream wall shear stress and also the location at which the wall shear stress fell to zero within each branch investigated. For an equal ratio tee (50:50mm) the maximum wall shear stress was found to be 2.522Pa. This value occurred for a mainstream velocity of 2.0m/s. The maximum upstream and downstream wall shear stress was found to increase with increasing mainstream velocity. However the downstream wall shear stress had fallen to zero 150mm into the branch for all cases investigated. The upstream wall shear stress also increased with increasing velocity influenced by reflection from the downstream wall and motion around the rotating cavity.

Downstream wall shear stress for both the 25mm and 12.5mm branch again increase with increasing mainstream flow. The range of maximum values for both branches were almost identical along the downstream wall while those on the upstream wall varied considerably. Higher upstream values were noted for the 12.5mm branch, which may be attributed to the branch rotating cavity effect outlined previously. For both branch diameters the downstream wall shear stress fell to zero much deeper into the branch.

	Downstream Wall		Upstream Wall		
	Max Shear Stress	Zero Position	Max Shear Stress	Location	Zero Position
6D at 0.5 m/s	0.225 Pa	150 mm	0.100 Pa	90 mm	60 mm
6D at 1.0 m/s	0.725 Pa	150 mm	0.312 Pa	95 mm	65 mm
6D at 1.5 m/s	1.625 Pa	150 mm	0.625 Pa	100 mm	65 mm
6D at 2.0 m/s	2.522 Pa	150mm	1.245 Pa	100 mm	60 mm

*Table 4.16: Wall shear stress values for a 50mm*50mm equal tee*

	Downstream Wall		Upstream Wall		
	Max Shear Stress	Zero Position	Max Shear Stress	Location	Zero Position
6D at 0.5 m/s	0.20 Pa	125 mm	0.075 Pa	90 mm	78 mm
6D at 1.0 m/s	0.70 Pa	125 mm	0.25 Pa	95 mm	78 mm
6D at 1.5 m/s	1.25 Pa	12 mm	0.50 Pa	100 mm	78 mm
6D at 2.0 m/s	2.0 Pa	125mm	0.80 Pa	100 mm	78 mm

*Table 4.17: Wall shear stress values for a 50mm*25mm tee*

	Downstream Wall		Upstream Wall		
	Max Shear Stress	Zero Position	Max Shear Stress	Location	Zero Position
6D at 0.5 m/s	0.28 Pa	55 mm	0.35 Pa	40 mm	36 mm
6D at 1.0 m/s	0.70 Pa	70 mm	0.50 Pa	42 mm	37.5 mm
6D at 1.5 m/s	1.25 Pa	50 mm	0.75 Pa	42 mm	40 mm
6D at 2.0 m/s	2.00 Pa	50mm	1.60 Pa	45 mm	40 mm

*Table 4.18: Wall shear stress values for a 50mm*12.5mm equal tee*

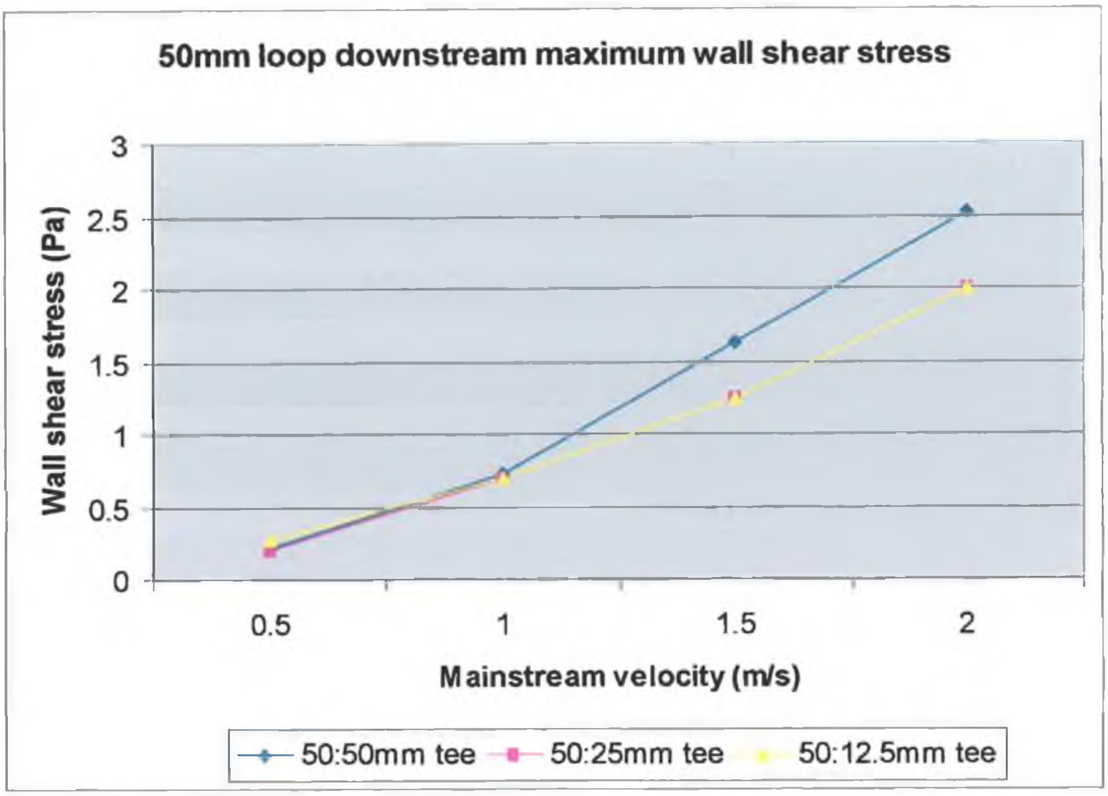

Figure 4.115: 50mm loop reduced branch downstream wall shear stress

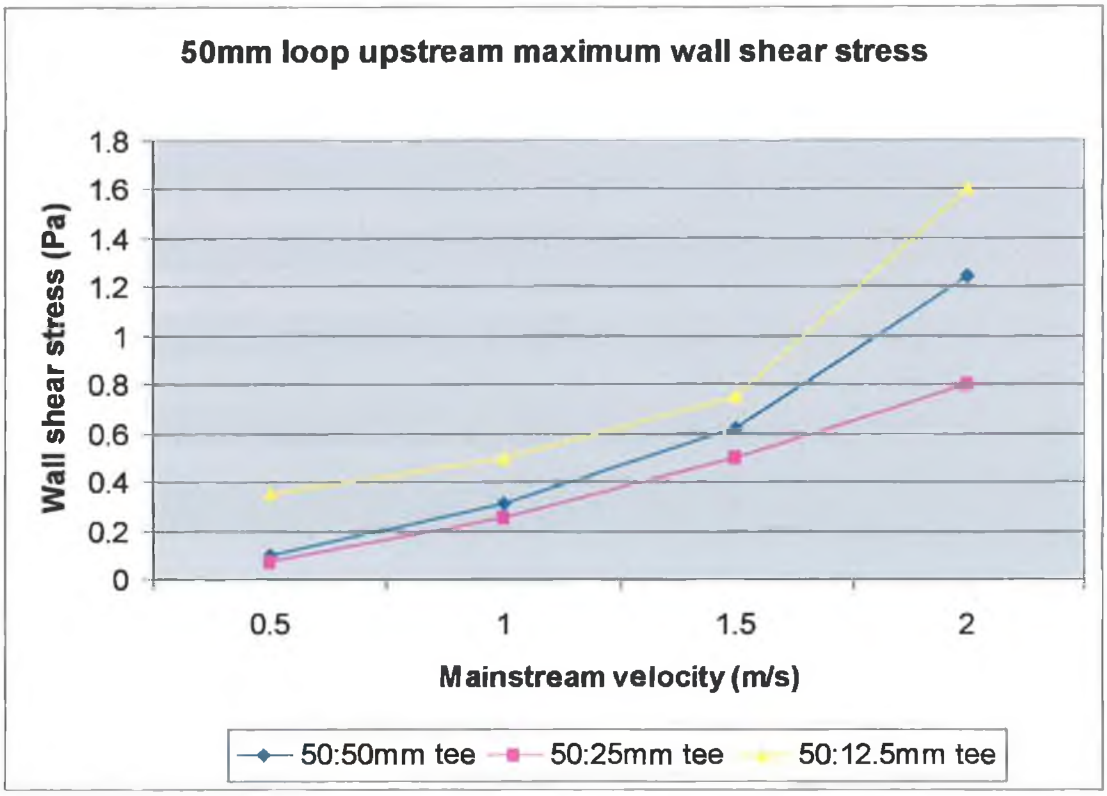

Figure 4.116: 50mm loop reduced branch upstream wall shear stress

The lowest upstream values were found for a 25mm branch, which could be attributed to less motion around the rotating cavity (figures 4.115 and 4.116). The unexpected high values of upstream shear for a 12.5mm branch may be due to suction on the upstream wall as the loop fluid rushes across the top of the tee.

4.21 ANALYSIS OF A 25MM DISTRIBUTION LOOP CONFIGURATION

Very few distribution loops within the pharmaceutical industry exceed 50mm in diameter due to the high cost of operating and maintaining such systems. Also very few high purity water systems, similar to those outlined during the literature survey of this thesis, fall below 25mm diameter distribution loops as these small systems covered by laboratory based systems or small turn-key skids. Therefore to investigate the effect of reducing the loop diameter from 50mm to 25mm a series of new models were developed for 25:25, 25:12.5 and 25:6.25mm loop to branch ratios.

In moving from a 50mm diameter tee to a 25mm diameter tee some interesting effects arose. Figure 4.117 offers an insight into the flow patterns found within the branch of each tee investigated. The plots are for 2m/s mainstream velocity as this has the maximum influence on the branch of each tee investigated. This velocity gave the clearest branch profiles although similar trends were noted at lower mainstream velocities. To clearly highlight the flow patterns only half of the 25mm branch is shown (ie 3D of the 6D branch). It is clear that the trends found for a 50mm tee are also applicable to a 25mm tee. For the equal tee (25:25) the slow rotating cavity identified previously was present. The cavity was again off-set towards the downstream wall however there was less reflection of the fluid from the downstream wall resulting in channelling of the fluid parallel to the wall and into the branch. In the

25:12.5 branch the cavity was still visible although again is was less well defined and centred in the branch due to the narrowing of the branch opening from 25mm to 12.5mm. The fluid was again channelled deep into the branch although beyond 4D little if any motion was evident. Centring of the cavity within the branch caused the entire branch to rotate driven by the flow of fluid across the top of the branch opening.

The smallest branch diameter of 6.25mm, which in the water purification industry would be considered a tube rather than a pipe, gave rise to an interesting profile at the base of the branch that was not seen for the 50:12.5 analyses. Two stagnant zones were clearly evident in each corner at the base of the tee. It would be difficult to see how bacteria could be removed from these regions should they establish themselves there. These regions were not visible during previous analysis and it is clear that there is a point beyond which the branch diameter cannot be reduced if these stagnant regions are to be avoided. It would appear that these zones result from a lack of penetration at the base of the tee. Following 3D analysis of this area it became clear that they were regions outside the rotating vortex and that the vortex was elongated in the centre of the small diameter branch (tube). This elongation prevented fluid from sweeping into the corner of the branch.

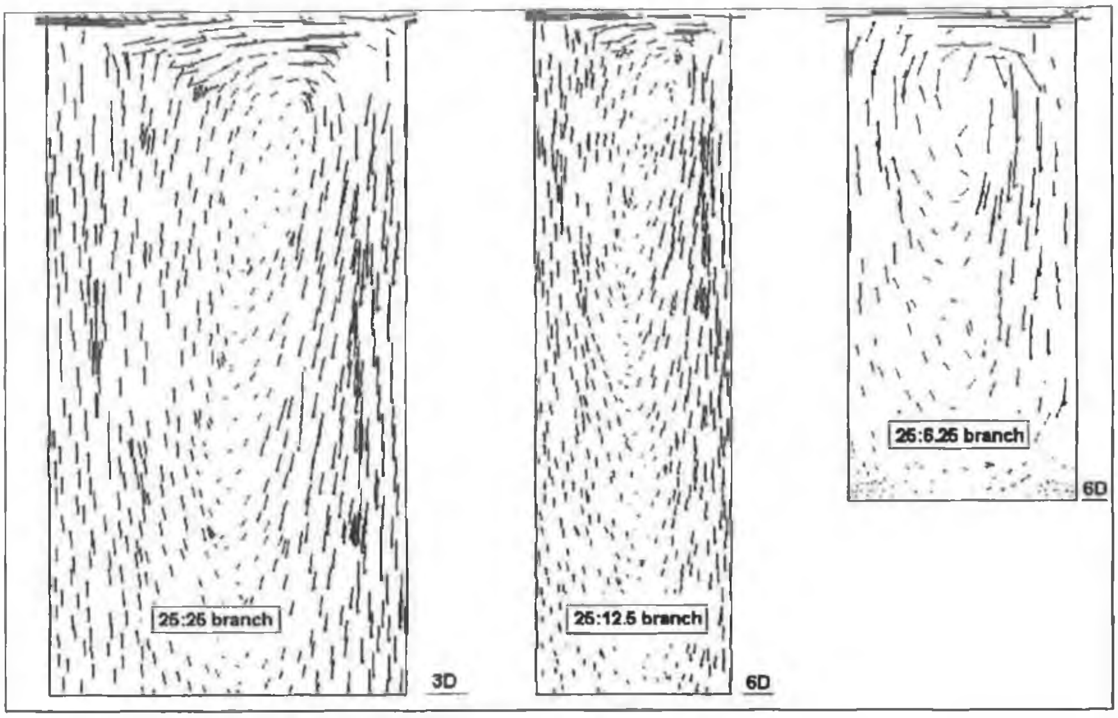

Figure 4.117: Velocity vector plots for a 25mm tee with various branch diameters

4.22 VELOCITY PROFILES FOR A 25MM DISTRIBUTION LOOP

Data related to velocity profiles found in the branch of various 25mm tees is presented in figures 4.118 to 4.121. Figures 4.118 and 4.119 present a comparison for a 25mm*25mm equal tee at 0.5m/s and 2.0m/s mainstream flow. It is clear from these graphs that the profiles throughout do not change much apart from magnitude. 4D into the branch at 0.5m/s the profile is flat and the velocities very low. At both 5D and 6D the velocity falls to zero indicating that although the mainstream to branch ratio (D/d ratio) is the same as that of a 50:50mm tee the smaller loop diameter slightly increases penetration into the branch (figure 4.118). Some benefit is to be gained by increasing mainstream velocity however this advantage is lost when the branch diameter is decreased. There is little consistency between data for the same D/d ratio. However 3D and 4D into each branch the advantages of a wider branch neck are less clear.

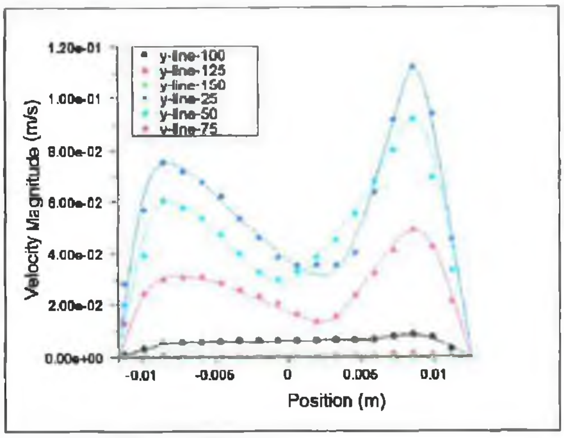

Figure 4.118: Velocity profiles for a 25mm equal tee at 0.5m/s

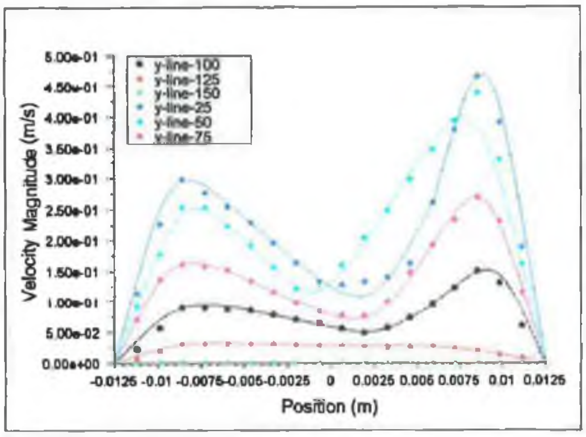

Figure 4.119: Velocity profiles for a 25mm equal tee at 2.0m/s

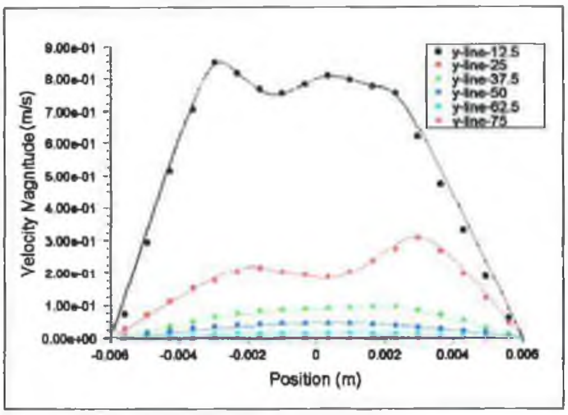

*Figure 4.120: Velocity profiles for a 25*12.5mm tee at 2.0m/s*

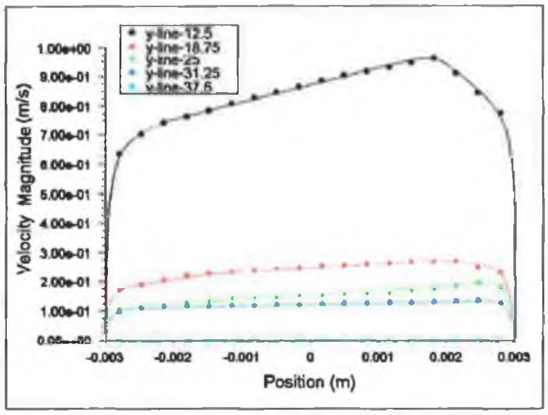

*Figure 4.121: Velocity profiles for a 25*6.25mm tee at 2.0m/s*

Narrowing of the branch was found to damp the velocity within the branch of a 25mm diameter loop. This is evident from figures 4.120 and 4.121 where profiles within the dead-leg are almost linear. Normalised velocities show that decreasing branch diameter increases penetration up to 3 and 4D. However care must be exercised with 1D readings because for a 6.25mm branch these values are outside the dead-leg. There is very little difference in dead-leg penetration for 25mm and 50mm diameter loops for equal tee configurations. There is a slight improvement at 3D and 4D for 25mm distribution loops at 2m/s (figures 4.122 to 4.123).

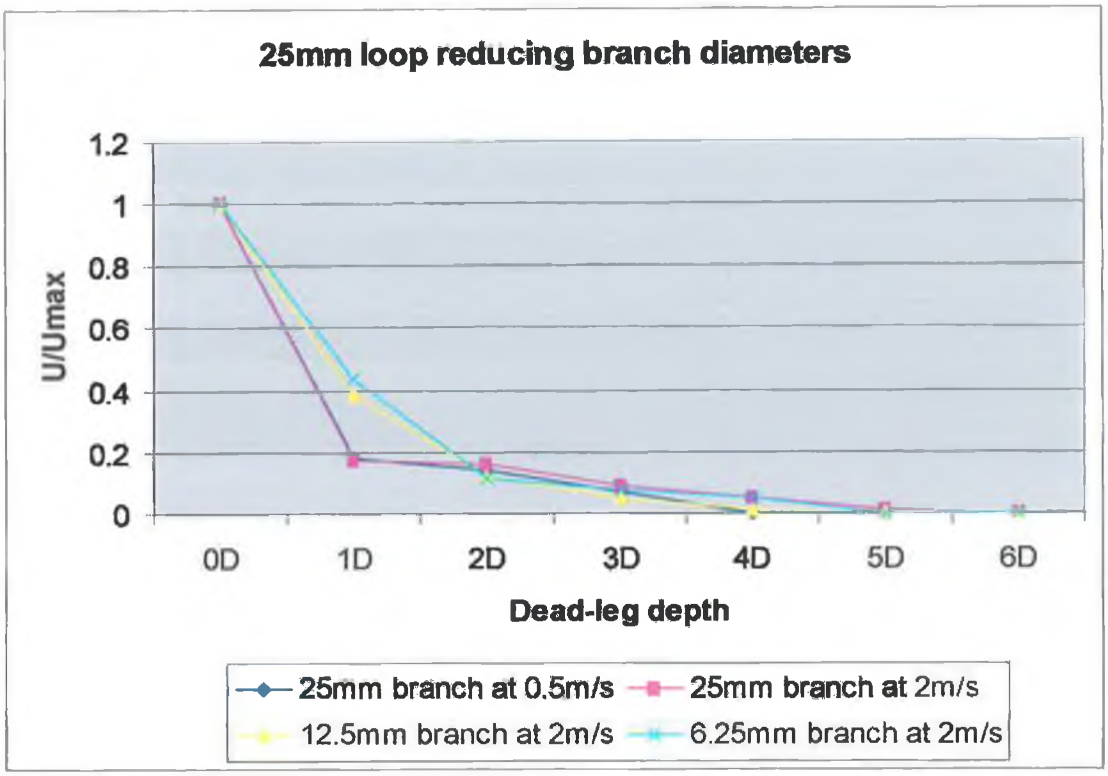

Figure 4.122: Flow profiles within a 25 mm distribution loop with various branch diameters

Figure 4.123: Comparison of flow profiles within 25mm and 50mm distribution loops

Comparison of these distribution loops using various tee configurations and a mainstream velocity of 2m/s are given in figure 4.124. For dead-leg tees with 1 to 0.25 ratios a 50mm loop is best up to 2D after which the remaining profiles quickly align themselves. The same is true for 1 to 0.5 tee ratios where there is some benefit in having a 50mm loop up to 1D but this advantage is lost 2D into the branch. For equal tee configurations (1:1) both loops are completely aligned and no benefit is to be gained by varying loop diameter. Based on these results it is very difficult to flush the branch. There is very little advantage to be gained from increasing distribution loop velocity, changing loop diameter or varying branch diameter.

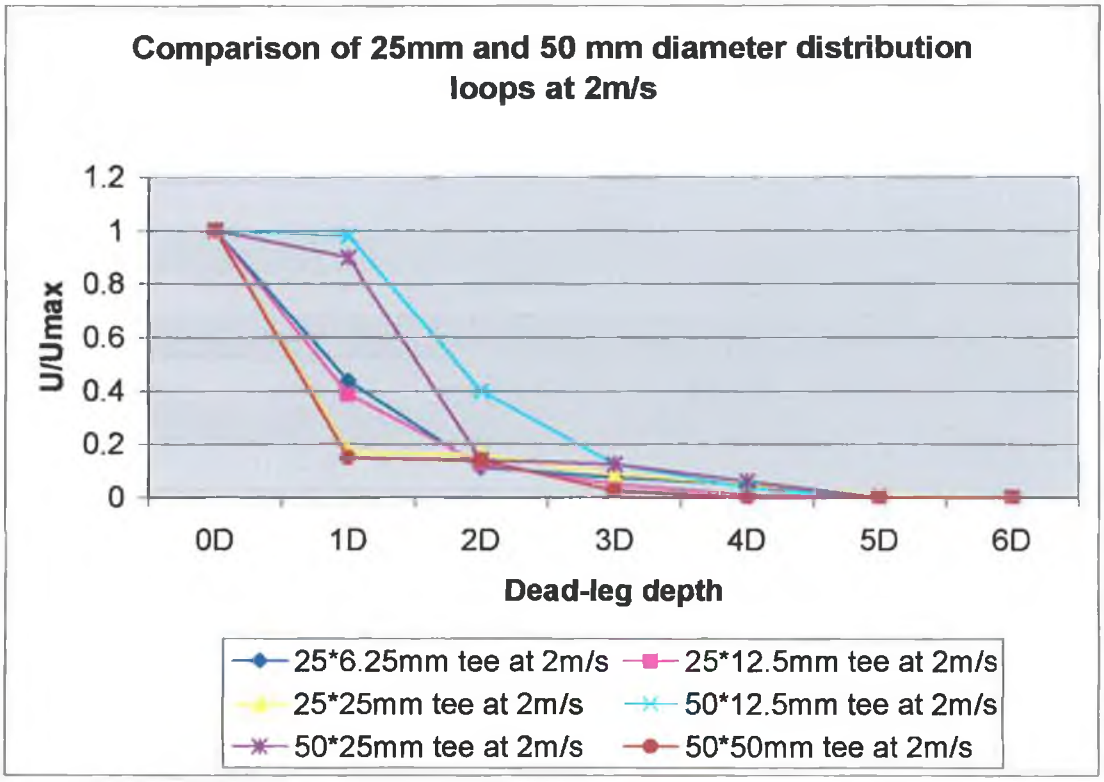

Figure 4.124: Comparison of 25mm and 50mm dead-leg penetration at 2m/s

4.23 25MM LOOP Z AND TURBULENT KINETIC ENERGY PROFILES

The move from a 50mm distribution loop diameter to a 25mm diameter influenced the z-plane velocity profiles within the branch and also the turbulent kinetic energy. The average velocity within a 25mm branch was found to be higher than that of its 50mm counterpart. Apart from slight variations and skewness in the upper portion of the branch the profiles were found to be reasonably linear (figures 4.125 and 4.126). At both high and low loop velocities values were highest at entry to the branch with an average value of $3.5*10^{-2}$ m/s for a loop velocity of 0.5m/s and $1.4*10^{-1}$ m/s at 2.0m/s. Both these values were higher than those found for similar ratios in a 50mm loop (figures 4.55 and 4.53).

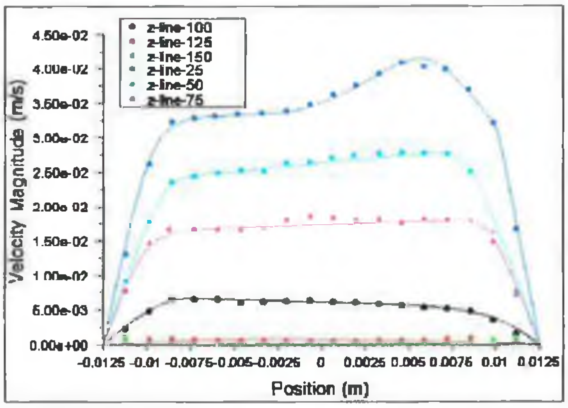

Figure 4.125: z-Velocity plots for a 25:25mm 6D tee at 0.5m/s

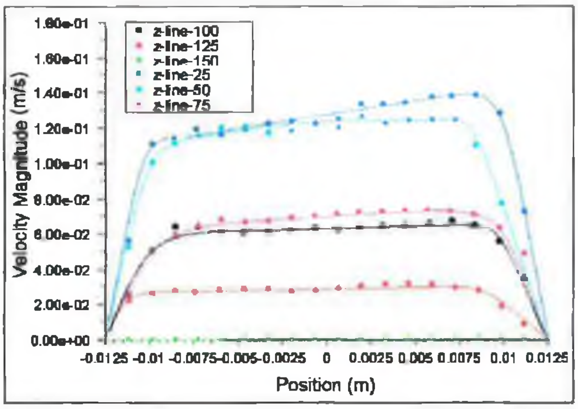

Figure 4.126: z-Velocity plots for a 25:25mm 6D tee at 2.0m/s

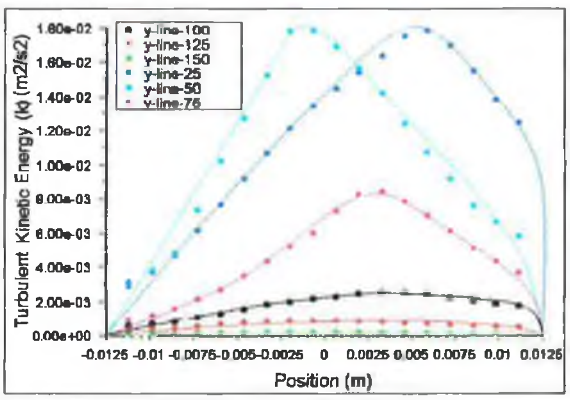

Figure 4.127: Turbulent Kinetic Energy plots for a 25:25mm 6D tee at 2.0m/s

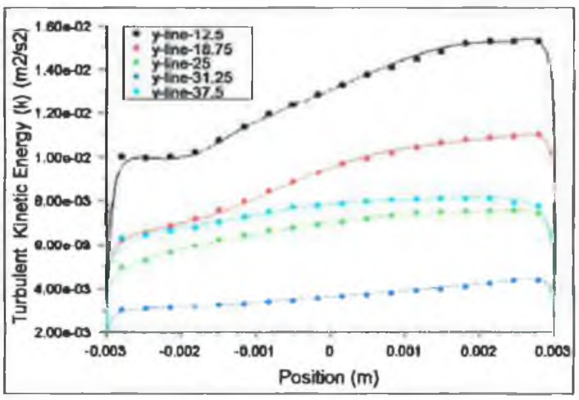

Figure 4.128: Turbulent Kinetic Energy plots for a 25:6.25mm 6D tee at 2.0m/s

Velocity throughout the 25mm branch was far more uniform than those found in a 50mm distribution loop. For sharp entry 50mm tee the average velocities found were similar to those for a sharp entry 25mm tee (figures 4.85 and 4.88).

A comparison of turbulent kinetic energy values found in a 6D 25mm loop with branch diameters of 25mm and 6.25 mm respectively is shown in figures 4.127 and 4.128. For a loop to branch ratio of 1:1 high values were noted centred high in the branch. However a considerable drop in turbulent kinetic energy was found 3D into the branch. When the branch was reduced to 6.25mm values were offset towards the downstream wall and the fall off in values within the branch was less sharp. Similar values and profiles were noted for a 50mm equal tee (figure 4.92) highlighting that loop diameter has little influence on turbulence within the branch for similar loop to branch ratios. The reduction of the branch to 6.25mm however, highlights the fact that the restricted entry damps out turbulence resulting in more uniform profiles throughout the branch (figure 4.128).

4.24 25MM LOOP WALL SHEAR STRESS

Tables 4.19 to 4.21 present wall shear stress data for a 25mm distribution loop with various loop to branch ratios. Plots of downstream and upstream wall shear stress highlight the effect of reducing branch diameter on dead-leg conditions (figures 4.129 and 4.130).

	Downstream Wall		Upstream Wall	
	Max Shear Stress	Zero Position	Max Shear Stress	Location
6D at 0.5 m/s	0.36 Pa	80mm	0.072 Pa	30 mm
6D at 1.0 m/s	0.925 Pa	85 mm	0.22 Pa	33mm
6D at 1.5 m/s	1.82 Pa	85 mm	0.425 Pa	48 mm
6D at 2.0 m/s	3.125 Pa	95mm	1.0 Pa	45 mm

*Table 4.19 : Wall shear stress values for a 25mm*25mm equal tee*

	Downstream Wall		Upstream Wall	
	Max Shear Stress	Zero Position	Max Shear Stress	Location
6D at 0.5 m/s	0.12 Pa	40 mm	0.03 Pa	37 mm
6D at 1.0 m/s	0.4 Pa	47 mm	0.13 Pa	37 mm
6D at 1.5 m/s	1.05 Pa	50 mm	0.25 Pa	40 mm
6D at 2.0 m/s	2.0 Pa	52mm	0.4 Pa	40 mm

*Table 4.20: Wall shear stress values for a 25mm*12.5mm tee*

	Downstream Wall		Upstream Wall	
	Max Shear Stress	Zero Position	Max Shear Stress	Location
6D at 0.5 m/s	0.14 Pa	25 mm	0.1 Pa	20 mm
6D at 1.0 m/s	0.3 Pa	20mm	0.25 Pa	25 mm
6D at 1.5 m/s	0.63 Pa	28 mm	0.34 Pa	25 mm
6D at 2.0 m/s	1.12 Pa	28mm	0.89 Pa	25 mm

*Table 4.21: Wall shear stress values for a 25mm*6.25mm equal tee*

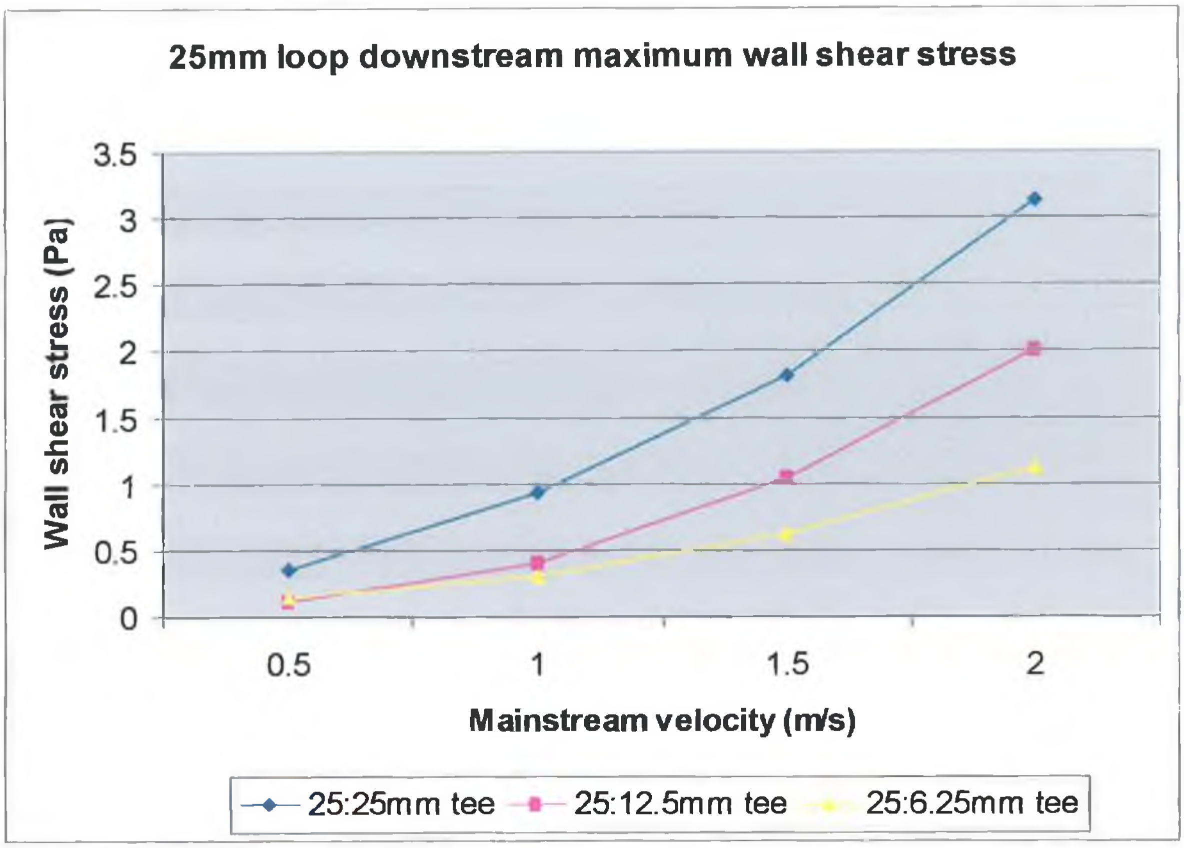

Figure 4.129: 25mm loop downstream wall shear stress

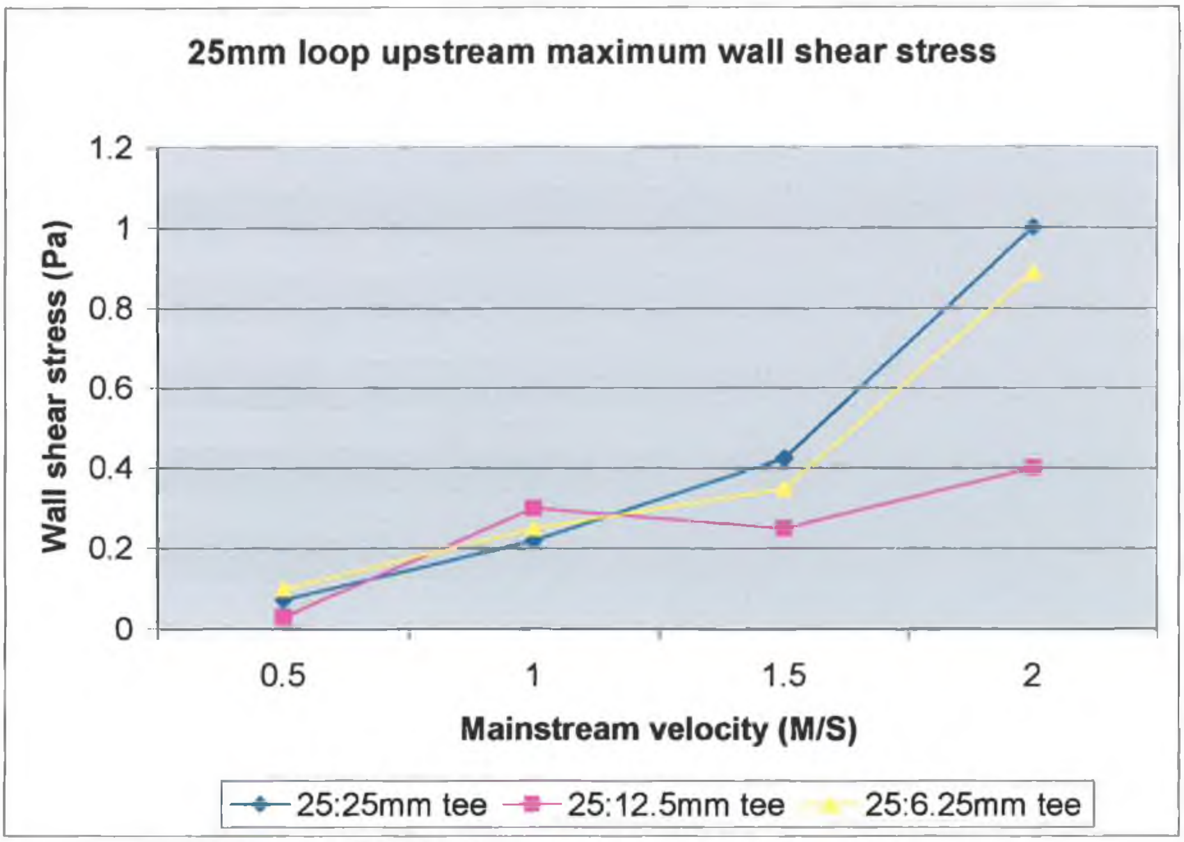

Figure 4.130: 25mm loop downstream wall shear stress

Upstream and downstream wall shear stress values were found to decrease with decreasing branch diameter (figures 4.129 and 4.130). Wall shear stress values for a 25mm equal tee were found to be higher than those of a 50mm tee. Loop to branch ratios of 1 to 0.5 resulted in similar values of wall shear for both 25mm and 50mm distribution loops. However for a 50mm loop, ratios of 1 to 0.5 and 1 to 0.25 resulted in the same values of wall shear stress but the same could not be said of a 25mm loop. Within this system a considerable drop in wall shear was noted when the branch was reduced to 6.25mm.

Upstream values also varied with loop to branch ratio. Similar to data found during a 50mm loop analysis upstream wall shear stress was found to decrease with decreasing branch diameter. However a surprisingly high value was identified for the 25mm to 6.25mm tee and this ratio also resulted in high values for a 50mm loop (figures 4.115 and 4.116). Close examination of these results identified suction on the upstream wall for these small branch diameters. This suction was generated by high-speed fluid rushing across the top of the branch drawing fluid up along the upstream wall thereby increasing wall shear stress. The confined space within the branch promoted such motion and a widening of the branch reduced this effect.

CHAPTER 5. FLOW VISUALISATION STUDIES

5.1 DYE INJECTION PLATE

To visualise and study the complicated flow patterns encountered during the CFD analysis of pharmaceutical pipe dead-legs, a flow visualization dye injection plate (figure 5.1) was designed and manufactured at Dublin City University and digital photographs taken of the flow patterns following injection of dye at various points within the dead-leg branch.

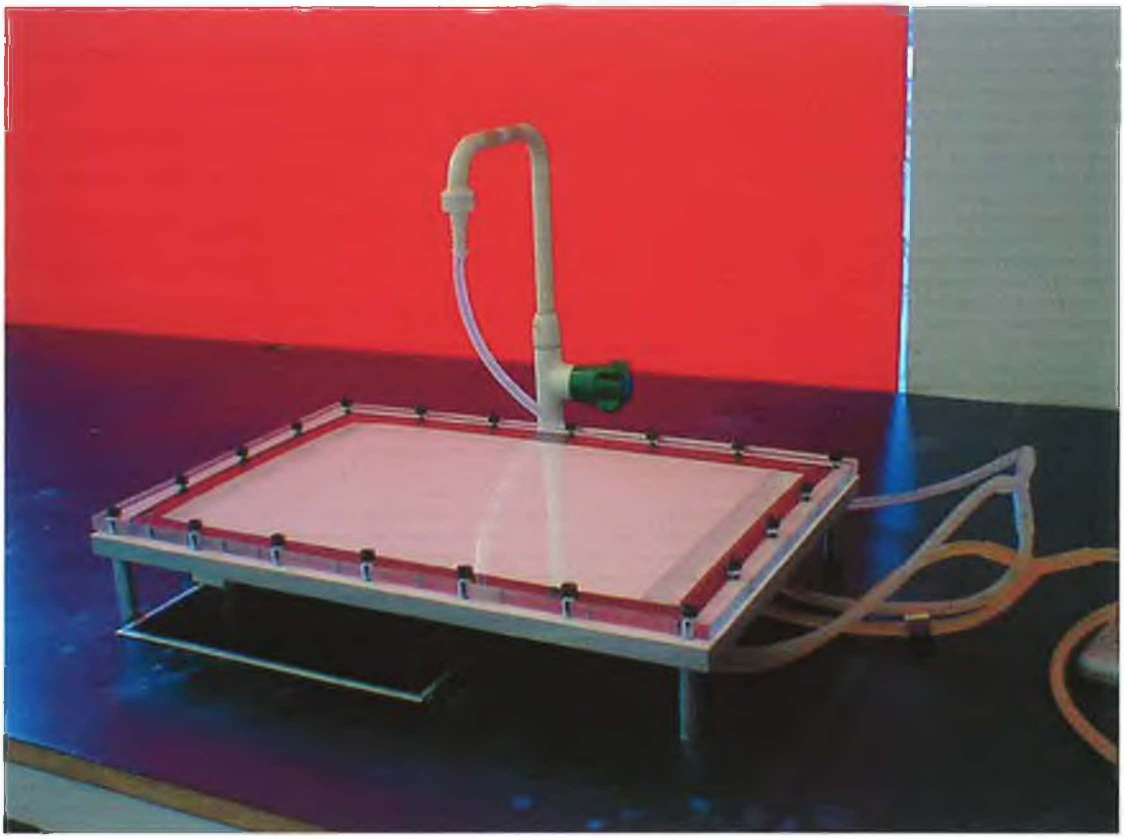

Figure 5.1: Flow Visualisation Dye Injection Plate

The rig consists of two plates, a top plate made of clear Perspex and a base plate machined from aluminum. The flow area was 35cm long and 25cm wide and the gap between the top and bottom plate was maintained at 2.5mm by means of an O-ring seal. A regulated water supply entered the rig from the left or upstream side of the base plate through two feedholes and flowed across the plate to the outlet manifold. Three discharge holes allowed the water to then flow to drain. A dye bottle was used to supply a colored dye into a series of 1mm holes through an inlet manifold located on the underside of the base plate. This arrangement allow for dye to be injected into the upstream fluid and followed as flowed from inlet to outlet (figure 5.2).

Figure 5.2: Dye injection bottle and flow plate

To investigate flow patterns in a dead-leg tee a sheet of aluminium was cut into a tee shape and placed between the top and bottom plate to form a 2D tee pattern. By modifying the aluminium shapes tees of different pipe to branch ratio could be inserted. Sharp and round entry tees could also be simulated by inserting a shape with a radius of curvature at entry to the branch. To investigate flow patterns within the dead-leg region of the branch a novel approach to dye injection had to be designed.

Although a dye injection manifold had been designed into the base plate for injection of dye into the mainstream flow a similar manifold would not work for the dead-leg region within the branch. The author decided that a manifold would quickly flood the dead-leg region with dye making it difficult to see how the patterns were developing.

It would be necessary to inject dye individually into each hole within the branch. A series of 1.5mm holes were drilled in the dead leg section of the plate to allow dye to be injected into that area. Initially the diameter of the holes was planned to be 1mm, but drilling was found to be extremely difficult at this small diameter and the drill bit broke (and to this day is still in the base plate of the rig). Therefore the size was increased to 1.5mm and the remaining holes drilled with ease (figure 5.3). A sheet of 3mm thick neoprene was stuck, using Evostick impact adhesive, to the under side of the plate covering all the previously drilled holes. Once the adhesive had set a grid was drawn over the neoprene to help to locate the previously drilled holes. The neoprene rubber sheet could then be pierced with a hypodermic needle to inject dye through the holes into the dead-leg region between the base plate and the Perspex. When the needle was retracted from the rubber the hole that has been pierced were self-sealing thus preventing air from entering the rig or water leaking from the rig.

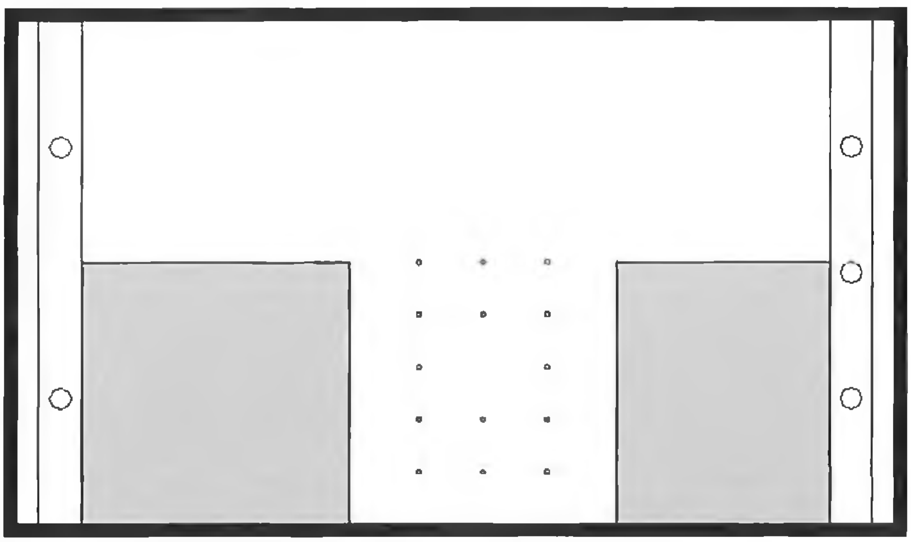

Figure 5.3. Dye injection holes in the dead-leg region.

The grid was helpful in locating the holes when the needle needed to be moved from one hole to the next but it was still difficult and time consuming locating each of the holes for individual tests. When the needle was not inserted accurately it tended to bend and eventually broke. To overcome this problem a number of needles were acquired and a needle was inserted into each hole where they remained throughout the range of tests.

5.2 ANALYSIS OF FLOW ACROSS THE DEAD-LEG INLET

In order to analyse the effect of mainstream flow across the top of the tee a short entry dead-leg was configured in the flow visualization plate. The overall dimensions are shown in figure 5.4.

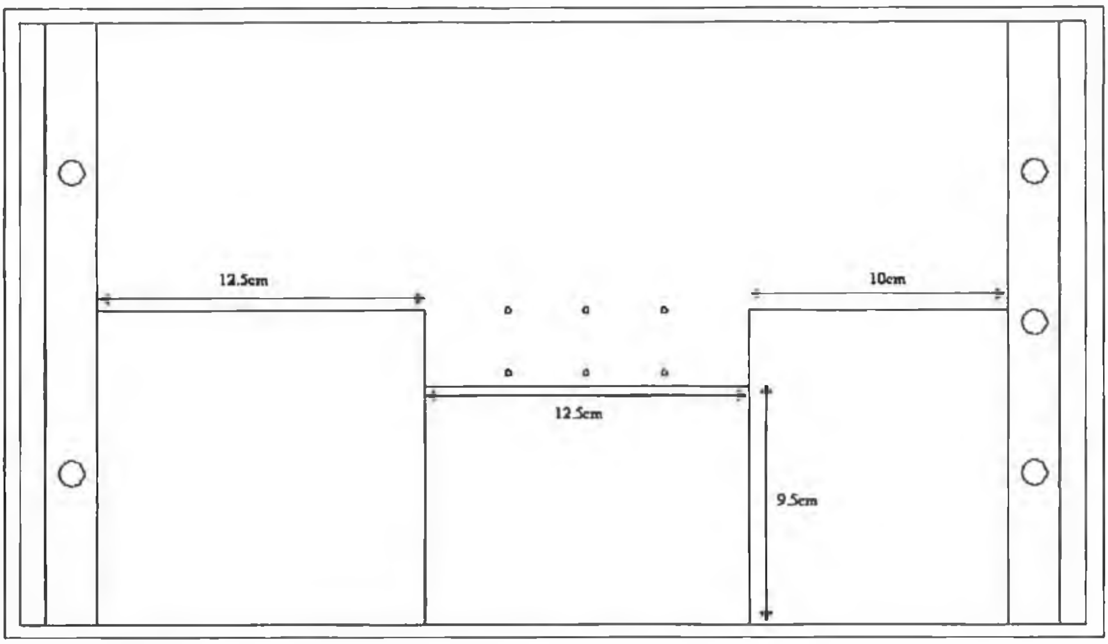

Figure 5.4: Short entry dead-leg configuration.

This particular configuration offered a clear insight into the penetration of mainstream fluid into the dead-leg. As noted previously during the CFD analysis there was little disturbance of the mainstream flow up to the entry to the branch of the tee. However beyond this point as dye was injected close to the upstream wall it was clear that the natural tendency of the mainstream fluid was to dip slightly into the dead-leg region before being forced out again by the presence of the downstream wall (figure 5.5).

Figure 5.5: Penetration of the mainstream fluid into the dead-leg region

Penetration was symmetrical about the centerline of the branch and recovery had occurred by the time the dye had reached the downstream dye hole. Beyond this point the dye line was affected by separation along the downstream wall. The fluid was forced high over the separation region created by the sharp edge of the downstream wall.

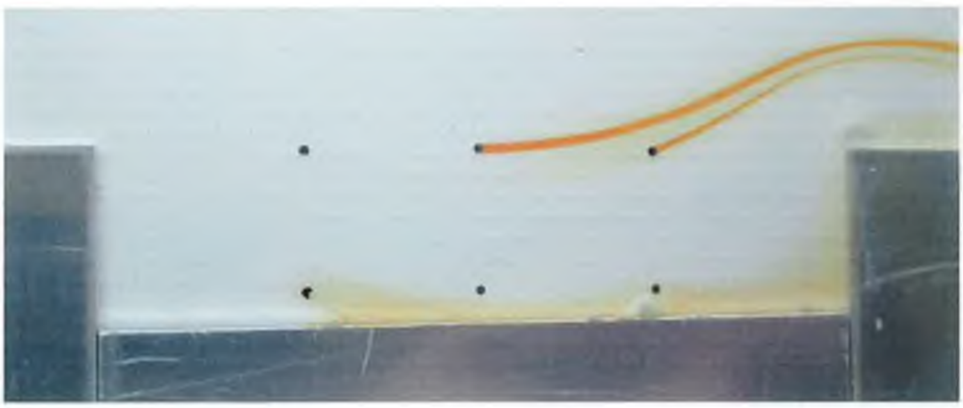

Figure 5.6: Downstream wall separation region

Injection of dye from two points at entry to the dead leg is shown in figure 5.6. Initially the dye line from the center dye injection point flowed horizontally. Mainstream fluid at entry to the tee separated along the upstream wall dragging dye into the branch as previously shown in figure 5.5. However dye injected at the center of the dead-leg was not influenced by the upstream separation. These regions were dominated by separation around the downstream wall of the branch. Both the centerline and downstream dye lines were forced high above the separation region with recovery of the flow occurring well downstream of the dead-leg branch.

Closer examination of the upstream wall reveals a separation and re-circulation area generated by the sharp entry to the dead-leg. In order to reveal this region it was necessary to move the wall of the branch closer to the dye injection holes. This was done by moving the upstream plate close to the upstream dye hole while maintaining the overall pipe to branch ratios. The result of this dye injection configuration is outlined in figures 5.7 to 5.8.

Figure 5.7. Upstream wall stagnation and re-circulation regions

It is clear form figure 5.7 that dye injected high along the upstream wall is forced well into the branch while maintaining the structure of the dye line. The penetration from this point on the rig is deeper that that identified following injection further away from the wall as shown in figure 5.5. It should be noted that these results could only be obtained by reducing the flowrate across the top of the branch. At high flowrates the branch penetration was reduced. Injection of dye close to the base of the dead-leg reveals a separation region and an area of very low velocities. Dye injection into this region was influenced by separation along the upstream wall. The dye was initially found to almost stagnate and over time to gradually creep back toward the upstream wall as well as being drawn downstream by the fast flowing fluid across the top of this region. Close examination of figure 5.7 reveals regions of re-circulation within the separation region. Eventually, when the rig was run for long enough, the dye creeps to the upper edge of the entry to the branch but does not reattach its self to the mainstream flow. This is evident from figure 5.8, which highlights separation between the dye regions.

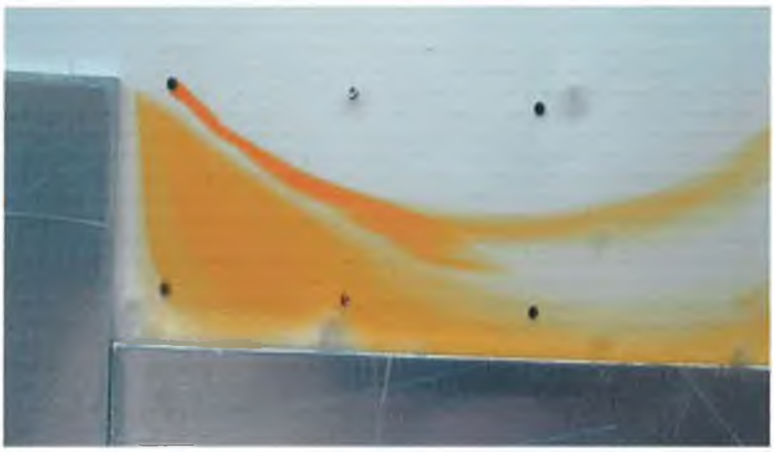

Figure 5.8: Upstream wall separation region

5.3 DEAD-LEG ANALYSIS OF A 1D EQUAL TEE CONFIGURATION

To gain an insight into the effect of dead-leg depth on flow patterns within the branch the rig was re-configured to give a 1D drop as shown in figure 5.9. This configuration allowed a number of additional holes to be injected with dye to give a better understanding of the flow trends within the branch.

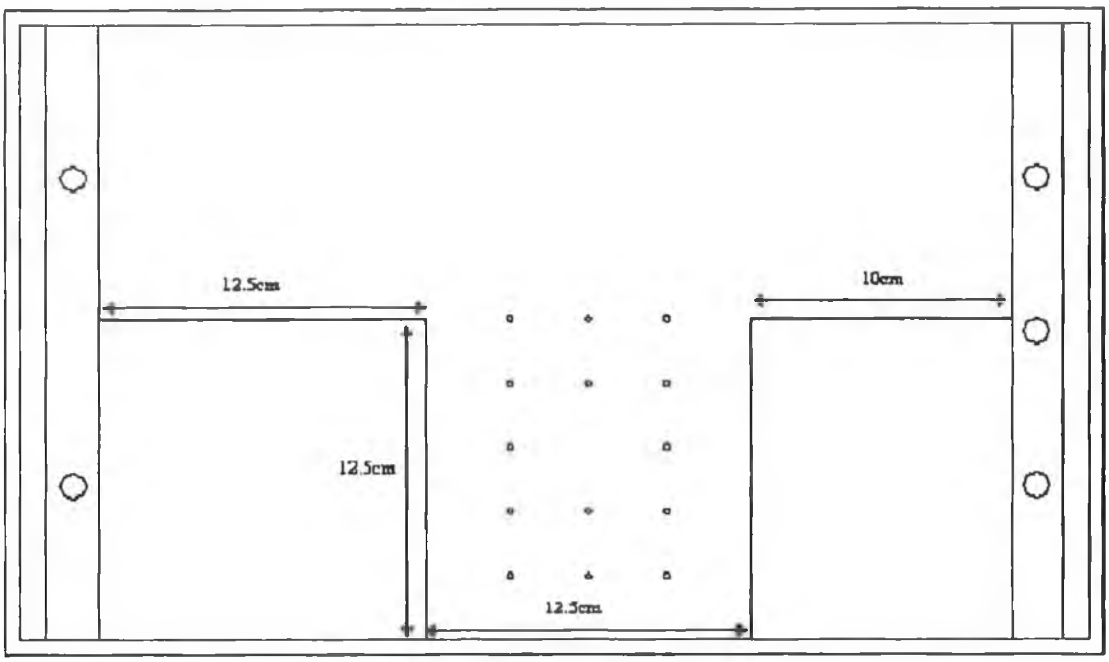

Figure 5.9: 1D dead-leg configuration with additional dye holes

Examination of the down stream wall highlighted similar trends to those already outlined for a short entry dead-leg. The separation region was still evident at exit from the branch, which once again forced the fluid high out of the dead-leg due to the sharp exit. Fluid below this point followed a similar path but at a lower profile. Close examination of figure 5.10 highlights clear evidence of separation of one of the dye streams. The lower stream while following a similar path to that of the high stream attempts to separate as the fluid begins its assent out of the branch. At this point some of the dye is restrained and begins to descend into the dead-leg. Fluid above this point travels up and out of the branch while fluid below this point will be re-circulated and forced further into the dead-leg.

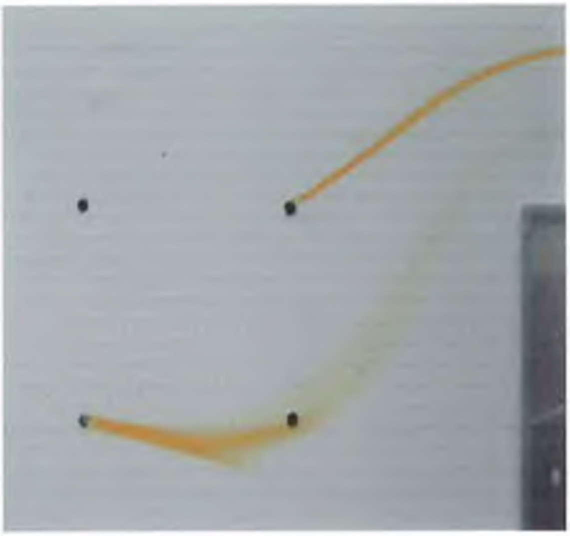

Figure 5.10: Downstream wall separation and re-circulation

Once identified these regions of separation were investigated further in an attempt to get a clearer understanding of the flow patterns within the dead-leg at low mainstream flow rates. Once again it was necessary to reconfigure the rig, as the dye hole locations (centred within the branch) did not give enough space for the patterns to fully develop. By moving the upstream wall closer to the dye holes while maintaining the overall dead-leg configuration, the patterns began to emerge (figure 5.11). This configuration meant that the downstream wall had less of an immediate effect on the developing patterns and the fluid within the branch had an opportunity to fully establish its patterns. It is evident from figure 5.11 that extending the dead-leg depth has a considerable effect on the flow regime within the branch. Dye injected high on the upstream wall was forced deep into the branch establishing patterns similar to those already identified from previous studies. Close to the downstream wall the fluid reversed its downward trend and was forced up the wall before leaving the branch and re-entering the mainstream flow. All along its path the fluid can be identified as highly strained as it did not maintain its sharp identity. The dye stream was found to be continually separating as it struggled to maintain its shape.

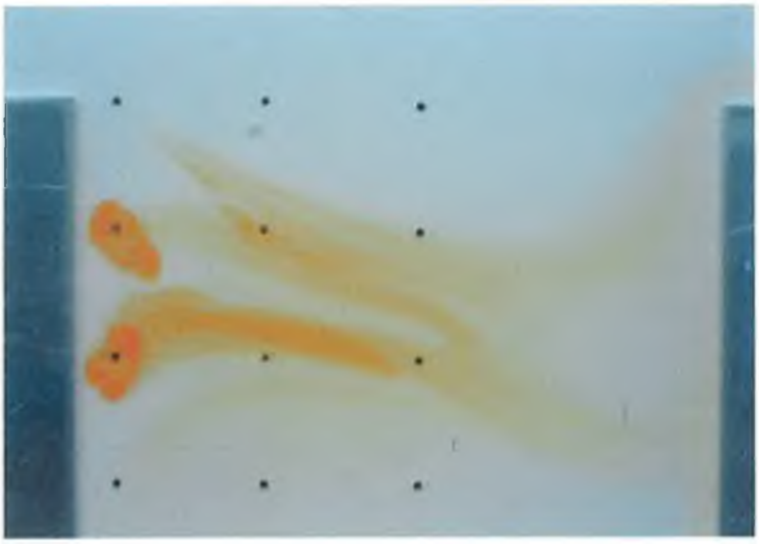

Figure 5.11: Separation regions within a 1D dead-leg

Injection of dye directly below the branch entry dye hole resulted in a stagnant zone highlighting a separation region along the upstream wall emanating from the sharp branch entry. Over time the stagnant dye drifted slightly to the right and down into the branch. This was a result of the mainstream fluid entering the branch and driving the rotating cavity identified earlier during the CFD analysis. This fact was further highlighted when dye was injected into the next hole down on the wall. This dye hole resulted in the dye slowly moving up the upstream wall before being dragged to the right by the mainstream fluid in the branch. The dye then moved steadily across the branch towards the downstream wall. The dye then move down further into the dead-leg while fluid above this line moves up and out of the branch. There is a clear divide here between two regions, the fast flowing mainstream fluid and the rotating cavity.

The cavity movement is slow allowing the dye to disperse as the slow moving fluid is pushed through the branch. This dispersion is different to the separation of the dye noted during analysis of other dye streams.

5.4. ANALYSIS OF REDUCED BRANCH DIAMETER DEAD-LEGS

The effect of mainstream to branch diameter was initially investigated based on the configuration shown in figure 5.12. This results in a 1 to 0.5 mainstream to branch ratio and a 1D dead-leg.

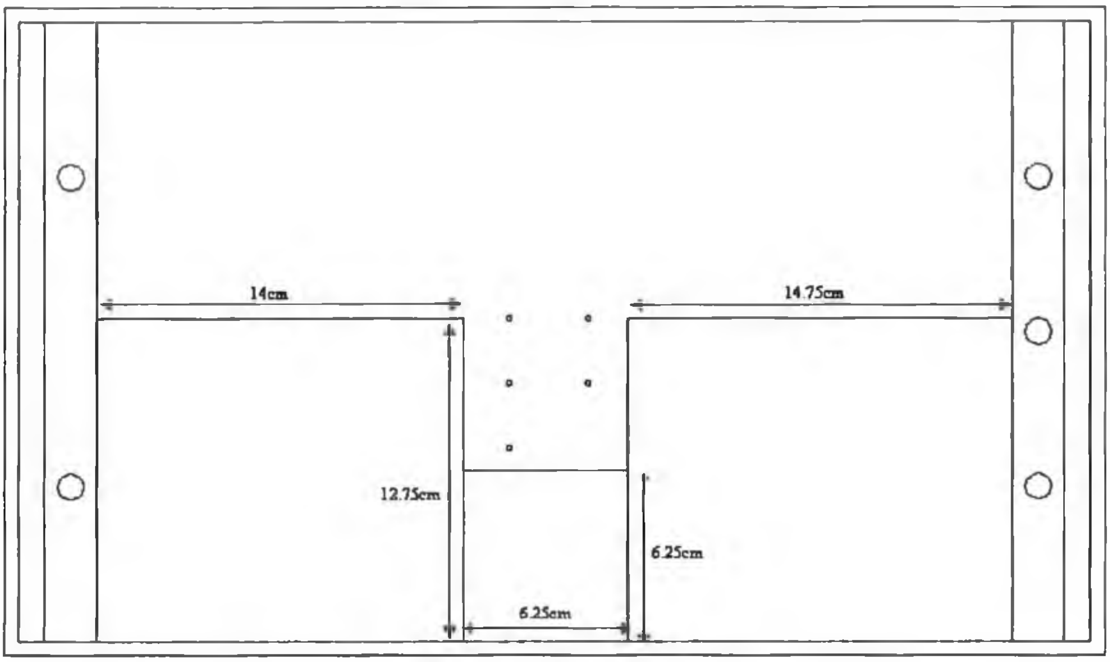

Figure 5.12: A 1 to 0.5 mainstream to branch ration with a 1D dead-leg configuration

Once again it is evident that the dead-leg results in a cavity the bulk of which acts to prevent penetration of the mainstream fluid into the branch. Some penetration is evident but the effect of the narrower branch is to reduce the penetration to a small drip across the top of the dead-leg (figure 5.13). One interesting feature of this configuration is that the upstream dye hole produces a dye stream that dips below the downstream dye stream realigning itself with this stream within the mainstream flow. Once again the separation region produced by the sharp downstream wall exit geometry forces the fluid higher into the mainstream flow than the initial injection points. As stated previously penetration, particularly from the upstream injection point, is restricted by the presence of fluid already in the branch.

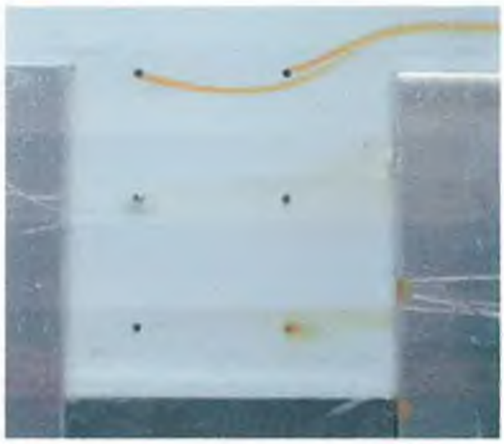

Figure 5.13: Narrow entry dead-leg flow profiles

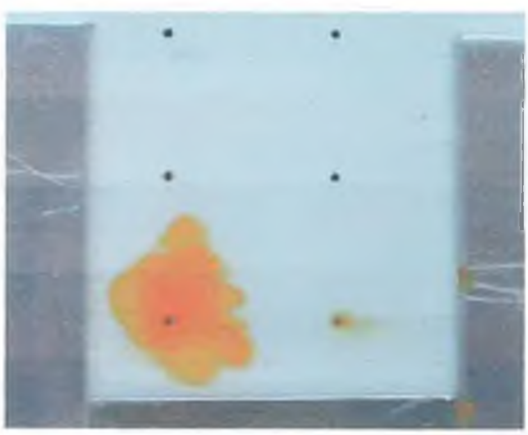

Figure 5.14: Stagnation zone in a narrow entry dead-leg

Injection of dye close to the base of a narrow entry dead-leg tee resulted in the identification of a completely stagnant zone (figure 5.14). As dye was injected at this point there was no evidence of movement in this region. The dye remained coherent with little evidence of separation, re-circulation or backflow. From the series of test carried out on this configuration motion was limited to the top ¼ of the branch.

5.5 ANALYSIS OF A 3D 50MM EQUAL DEAD-LEG TEE

The above mentioned tests were initial trials used to identify key regions within the dead-leg for various flow configurations and to demonstrate that the flow plate was capable of offering an insight into the flow patterns likely to be found as a result of setting a dead-leg configuration between the plates. To consolidate the evidence of the initial trials and in an attempt to relate it to the CFD results the flow visualization plate was re-configured into a 50mm*50mm tee with a 3D dead leg (figure 5.14).

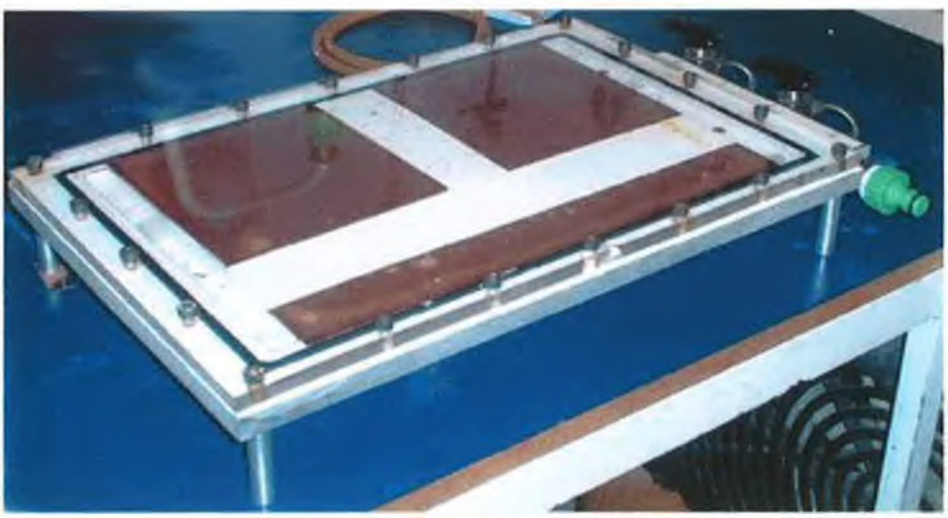

*Figure 5.14: Flow visualization plate with a 50*50 tee and a 3D dead-leg configuration*

In this layout it was possible to inject dye upstream of the branch and investigate the effect of the branch on mainstream flow. Five dye injection points were available for this analysis and the fluid flowed from upstream to downstream unhindered apart from branch effects. Within the branch a number of dye injection points were available from the top of the branch to the base and from the upstream wall of the branch to the downstream wall. The dead leg configuration was established by preventing mainstream fluid from entering the branch by sealing the base of the dead-leg using the plate seal and by placing a gasket material on top of the aluminum cut-outs.

Figure 5.15: Mainstream flow branch penetration

Figure 5.16: Separation from the upstream wall of the branch

It is clear from figure 5.15 that the branch has an effect on the mainstream flow for dead-leg configurations. The fluid flow across the top of the branch dips into the dead-leg along the upstream wall of the branch. A similar pattern was identified during the CFD analysis earlier in this thesis. Maximum penetration was found to occur between the centerline of the branch and the downstream wall. The fluid was highly strained in this region and a degree of separation of the dye line occurs as the fluid changes course from penetration to exiting the branch. Additional separation occurs within the dye line as the fluid exits the branch at the downstream wall of the tee. It is also clear that the branch influences the mainstream flow outward from the entry region. This effect, identified by the deflection of the mainstream dye lines, was found up to half way across the mainstream flow region. Figure 5.16 highlights the separation region within the branch from the upstream wall to the downstream side of the dead-leg. This effect was identified by injecting dye through the dye hole at the top of the downstream wall. The dye was found to mix with a dye line from the mainstream fluid, which separated along the upstream wall of the branch. There was little evidence of flushing of the branch in this configuration and it should be noted that the mainstream flow was less than that of figure 5.15.

Figure 5.17: Fluid movement along the downstream wall of the branch

Figure 5.18: Fluid movement along the upstream wall of the branch

Figures 5.17 and 5.18 offer an insight into flow patterns along the downstream and upstream walls of the branch. The flow patterns outline in figure 5.17 were formed following the injection of dye high up along the downstream wall of the branch. The fluid moves down into the branch flowing away from the dye injection point. However there was also upward movement within the branch and some of the dye is driven up toward the branch exit. This upward motion is limited to an area between the upstream wall and half way across the diameter of the branch. The remainder of the dye was forced further into the branch dead-leg by fluid moving down along the downstream wall. Further evidence of movement within the branch was found when dye was injected into the dye hole at the base of the upstream wall.

Figure 5.19: Long radius bend mainstream flow penetration

Figure 5.20: Long radius bend branch flow patterns

Figure 5.21: Long radius bend upstream wall flow patterns

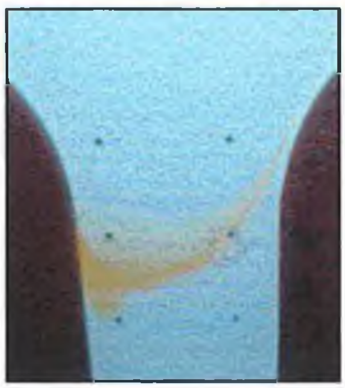

Figure 5.22: Long radius bend downstream wall flow patterns

Following injection the dry was slowly drawn up along the upstream wall indicating slow movement in this region. The dye continued to flow to the top of the branch entry region. The bulk of the dye remained around the dye injection hole indicating very little movement in this region and the presence of a stagnation region deep within the branch. The trend was for the dye to slowly creep away from the upstream wall towards the center of the branch, however this only occurred after a long time delay.

5.6 ANALYSIS OF SHARP AND ROUND ENTRY 3D 50MM EQUAL TEE DEAD-LEGS

The introduction of a long radius bend rather than a sharp entry branch was found to influence the penetration into the dead-leg. Figures 5.19 through to 5.20 offer an insight into the flow pattern found using this configuration. The mainstream flow was found to dip well into the branch to a depth of the radius of curvature of the branch. Some separation was noted from the fluid entering the branch and the fluid already within the branch. The influential effect of the mainstream flow is much greater than that found with the sharp entry tee. This is evident from figure 5.20 where dye was injected along the upstream wall of the branch. This time (at the same mainstream flow) the dye was quickly dispersed away from the dye injection point across the branch and reattached with the mainstream flow. There is also evidence of a secondary separation at this injection point were a small portion of the dye is forced further into the branch. This is shown in both figure 5.20 and 5.22. It is also clear from figure 5.21 that an injection of dye further into the branch and close to the upstream wall that there is movement present along the upstream wall of the branch. Dye is drawn upwards along the wall of the branch following the radius of curvature of the entry region. The dye is then forced sharply across the top of the branch by the mainstream fluid. This re-circulation is driven by separation within the branch dead-leg and the speed of the flow across the branch entry.

The effect of a short radius bend is outlined in figures 5.23 to 5.26. The mainstream flow was found to pass steadily across the top of the branch before impacting on the downstream wall. This impact created a stagnation point on the downstream wall around which the fluid was found to separate. Fluid above the separation point remained with the mainstream flow passing downstream of the branch. Fluid below the separation point flowed down into the branch. The fluid flowed along the downstream wall before moving back into the branch in a pattern similar to that presented figure 5.24. This pattern was found to be similar to that outlined for a sharp entry tee. Dye injected at this point moved towards the center of the branch before steadily moving up driven by the re-circulating patterns developed within the branch. There was very little difference between the long radius and short radius entry when upstream wall patterns were compared. The dye again clings to the upstream wall flowing up following the radius of the branch before being swept across the branch by the mainstream fluid (figure 5.25).

Injection deep along the downstream wall highlights a stagnation zone within the branch. Dye injected at this point stagnates around the injection point. A narrow stream is drawn away from the stagnant zone by fluid re-circulating above this region. This stream is driven across the branch to the upstream wall, clings to the wall and finally is driven across the branch, similar to the dye path outline for upstream wall patterns, by the mainstream fluid. Close examination of figure 5.26 highlights this flow pattern.

 *Figure 5.23: Short radius mainstream flow*	 *Figure 5.24: Short radius branch flow patterns*
 *Figure 5.25: Short radius upstream flow patterns*	 *Figure 5.26: Short radius downstream flow patterns*

In conclusion the dye injection plate highlighted some very interesting flow patterns for various dead-leg configurations. Complex flow conditions were found to exist for upstream and downstream walls for both sharp and round entry tees. Mainstream penetration of the branch was influenced by the speed of the mainstream fluid, branch entry cross-section and the type of branch entry (sharp or round). Stagnation zones were visible within each configuration examined highlighting the difficulty of exchanging mainstream fluid with dead-leg fluid.

5.7 HYDROGEN BUBBLE TECHNIQUE

One limitation of the dye injection plate is the range of velocities that can be studied. This is limited by the fact that the gap between the base plate and the glass top is small. The Hydrogen Bubble Technique is another flow visualization rig based on the generation of small hydrogen bubbles around a fine cathode wire that is positioned normal to the fluid flow. The bubbles are produced by electrolysis at the fine wire. By careful illumination the paths traced out by these bubbles as they are carried along, the flow patterns generated can be readily observed. The success of this technique depends on the standard of illumination and on the consistent quality of bubbles generated in terms of number and size. Owing to the small size of bubble generated (0.00125 to 0.05mm diameter), the rate of rise due to natural buoyancy is small in comparison to the average rate of flow across the rig. Streamlines, velocity profiles and fluid element distortion can easily be observed by using the appropriate cathode and by controlling the electric current.

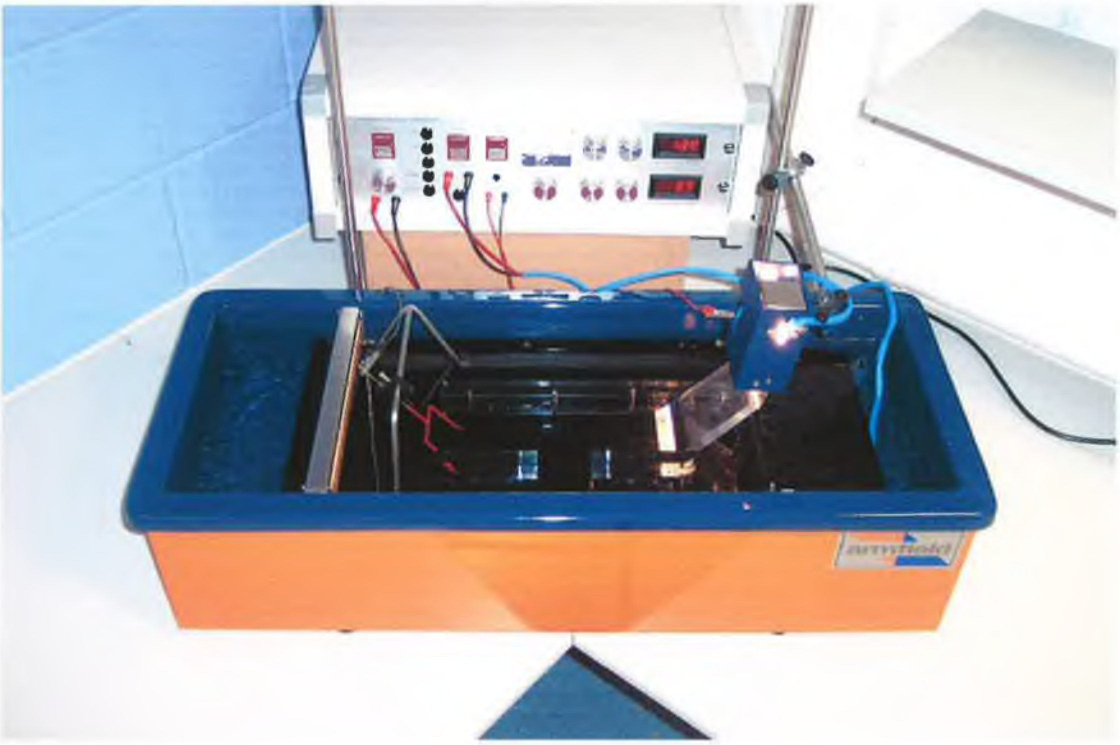

Figure 5.27: Hydrogen Bubble Flow Visualistaion Rig

The use of a pulse generator makes it possible to carry out both quantitative and qualitative analysis. The generator produces on/off pulses that are variable within the range 10-1800ms. The timing of the pulses are displayed on digital readouts. To ensure good flow visualization a large number of small equal sized bubbles are required. The most important factors that can influence the size of bubbles produced are:

A) Current supplied to the cathode

B) The nature of the Aqueous Solution

C) The size of the Cathode wire

D) The velocity of the fluid past the wire

A) Current Supply to the Cathode.

The volume of hydrogen bubbles produced at the cathode is directly proportional to the electric current supplied to the wire. The precise relationship between the applied current and the number of bubbles produced is a function of the conductivity of the fluid and the geometry of the field being studied. The conductivity can be adjusted by the addition of a suitable electrolyte. There is a complicated and incomplete understanding of the relationship between bubble size and current density, which is highly dependent on the cathode wire diameter. For the range of diameters available on the rig used for these studies the bubble size is roughly proportional to the current density. However the linearity of the relationship breaks down with increasing wire diameter and current density.

B) The Aqueous Solution.

This is probably the most important single variable in bubble formation. In general the addition of an acid to water will increase the size of bubble produced while an alkali solution will reduce the size of bubble. A neutral salt such as Sodium Bromide or Sodium Sulphate enables an increase in total current to be used thus producing a larger volume of hydrogen gas without increasing the size of individual bubbles. A major advantage of these additives is to increase the uniformity of the size of bubble produced at various points along the wire.

C) Diameter of Cathode Wire.

A general rule of thumb is the smaller the diameter of wire the better. The size used is always a compromise between the Mechanical Strength and the resulting bubble size. The maximum diameter wire used for this range of results was 0.125mm. This will produce bubbles of approximately 0.05mm diameter when a high salt concentration is used with a current density of $1.55*10^3$ amps/m^2. With current densities of $1.55*10^3$ to $3.1*10^3$ amps/m^2 the size of bubble produced by a 0.05mm diameter wire will be 0.025 to 0.037mm diameter. This is the range of bubble sizes that have been found acceptable for qualitative visualization.

D) Velocity of Flow

The size of the bubble produced at a 0.05mm diameter wire tends to be independent of the velocity of the mean flow past the wire provided the velocity is above 50mm/s. Below this speed there is a slight increase in bubble size while the maximum size is reached in stagnant water. The speed of flow past the cathode wire does effect the buoyancy of the bubbles produced. A reduction in speed increases the buoyancy effects, which can be used to highlight stagnation zones.

5.7.1 HYDROGEN BUBBLE RIG EXPERIMENTAL METHOD

The channel was filled with water and 100mls of a saturated solution of sodium sulphate, water was added until the water level was just below the top of the model under investigation. Flow guides (clear polished acrylic guides) were arranged within the rig to simulate a 2D dead leg 50*50mm tee. The flow of water along the flow visualization section was produced by means of a low voltage submersible pump located at the discharge end of the rig. The pump speed was varied to control the speed of flow across the rig from 0 to 0.65m/s and therefore across the cathode wire. A honeycomb flow straightener was positioned at the inlet of the flow visualization section and a baffle plate placed at the discharge end to smooth the flow of water across the rig.

The pulse generator was set to produce hydrogen bubbles in a series of pulses with variable on (pulse lengths) and variable off (space length) periods. This method of pulsation allows for improved visualization over continuous bubble generation while encouraging quantitative measurements to be taken. The current through the electrode wire was varied to give the optimum size, density and quantity of bubbles for each flowrate and geometry studied. Finally the light source (a 55W 12V Tungsten Halogen Bulb) was illuminated and the accompanying light guide (a clear acrylic section) positioned to give the optimum lighting of the test section. The visualization images now presented were captured using a Kodak digital camera (Easy Share DX 4330) on a high-speed sports setting.

5.8 SHARP ENTRY 50MM EQUAL TEE VISUALISATION STUDIES

Figures 5.28 and 5.29 offer an excellent insight into the flow patterns generated when fluid flowing at 0.5 m/s across the top of a sharp entry 50mm equal tee with a 2D dead-leg impacts on the downstream wall of the branch. Fluid outside of the branch flows quickly across the top of the dead-leg driven by the momentum of the mainstream flow. The flow pattern is disturbed at exit from the branch by fluid exiting from the dead-leg following separation on the downstream wall of the branch. This disruption to the mainstream fluid results in a deflection of the fluid away from the branch around the downstream wall region. The result is a separation region generated beyond the branch in the mainstream pipe. This region was noticed during CFD analysis of this configuration however the dip into the branch was not as evident as that found during the CFD simulations (figure 4.22).

Adjustment of the cathode and the lighting of the branch revealed some branch penetration and also a clearer profile of the stagnation and separation region within the branch (figure 5.30). It is clear from this image that fluid within the branch is driven further into the branch following separation along the downstream wall of the dead-leg. This fluid circulates around the slow rotating vortex previously identified by CFD simulations (figure 4.6). Following a short passage along the downstream wall the fluid is drawn back into the branch by this vortex. In order to investigate this region closer the cathode was moved adjacent to the downstream wall. In this configuration the separation region downstream of the branch was more clearly defined. This separation and re-circulation region was generated by the sharp edge of the branch and recovery only occurred well downstream of the branch. Re-circulation within the branch was found to be more complex than originally thought (figure 5.29).

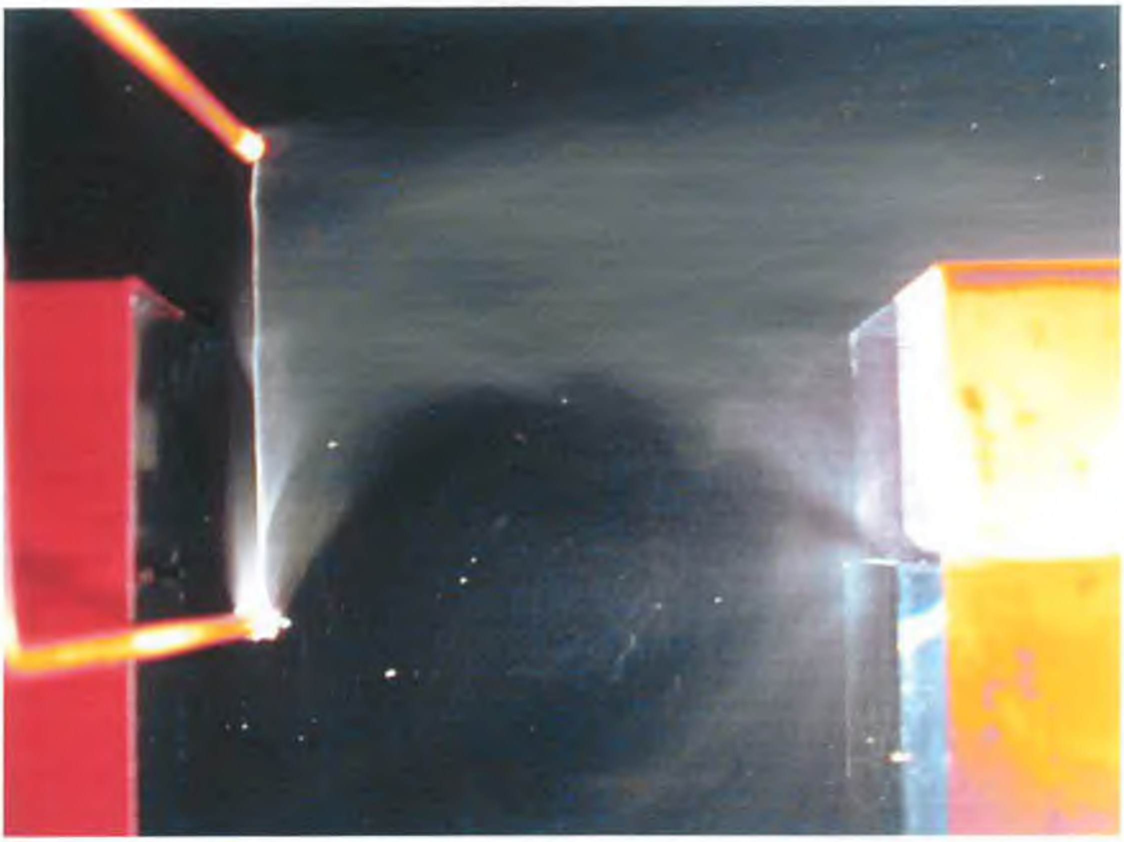

*Figure 5.28: Mainstream flow for a 50*50 sharp entry tee at 0.5 m/s*

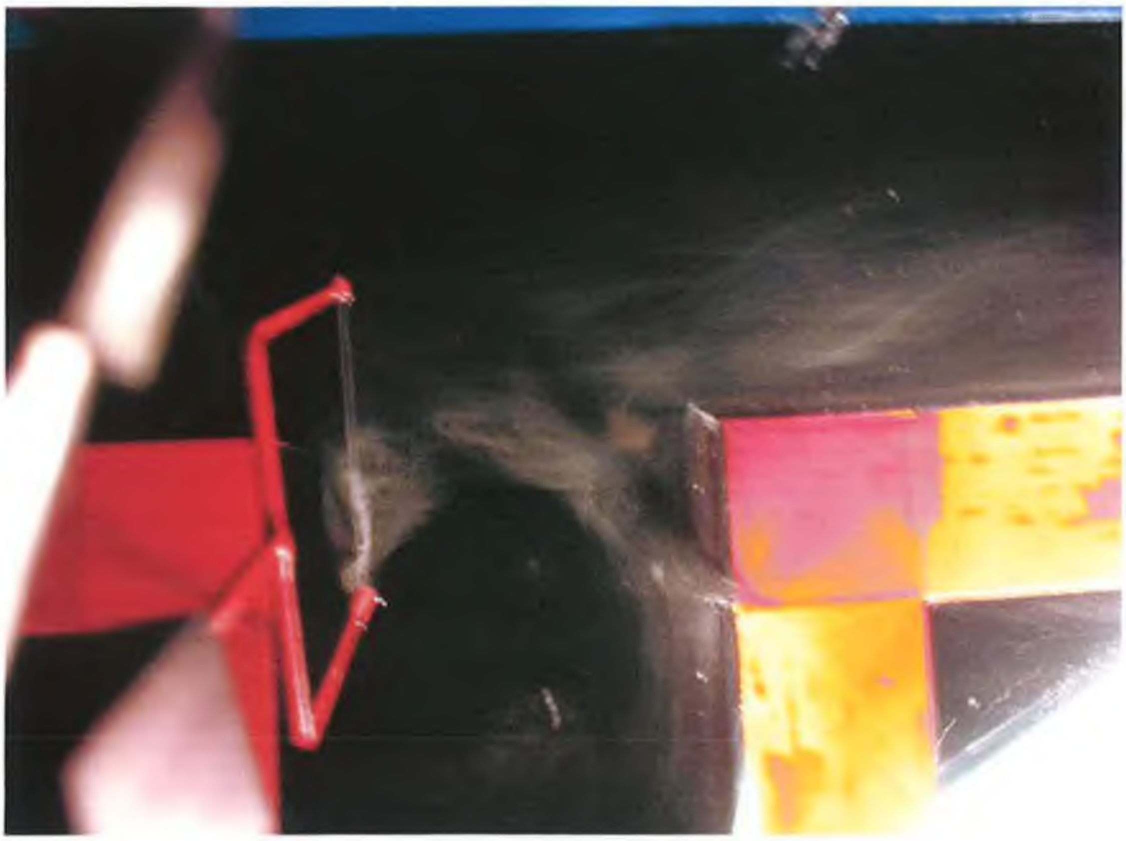

*Figure 5.29: Downstream separation for a 50*50 sharp entry tee at 0.5 m/s*

Two streams were now evident, one attached to the vortex region and one separating and flowing down into the branch. Therefore at entry to the branch three regions were defined, the mainstream separation region, the slow rotating vortex region and the downstream wall separated fluid. All three contribute to a complex flow pattern within the branch.

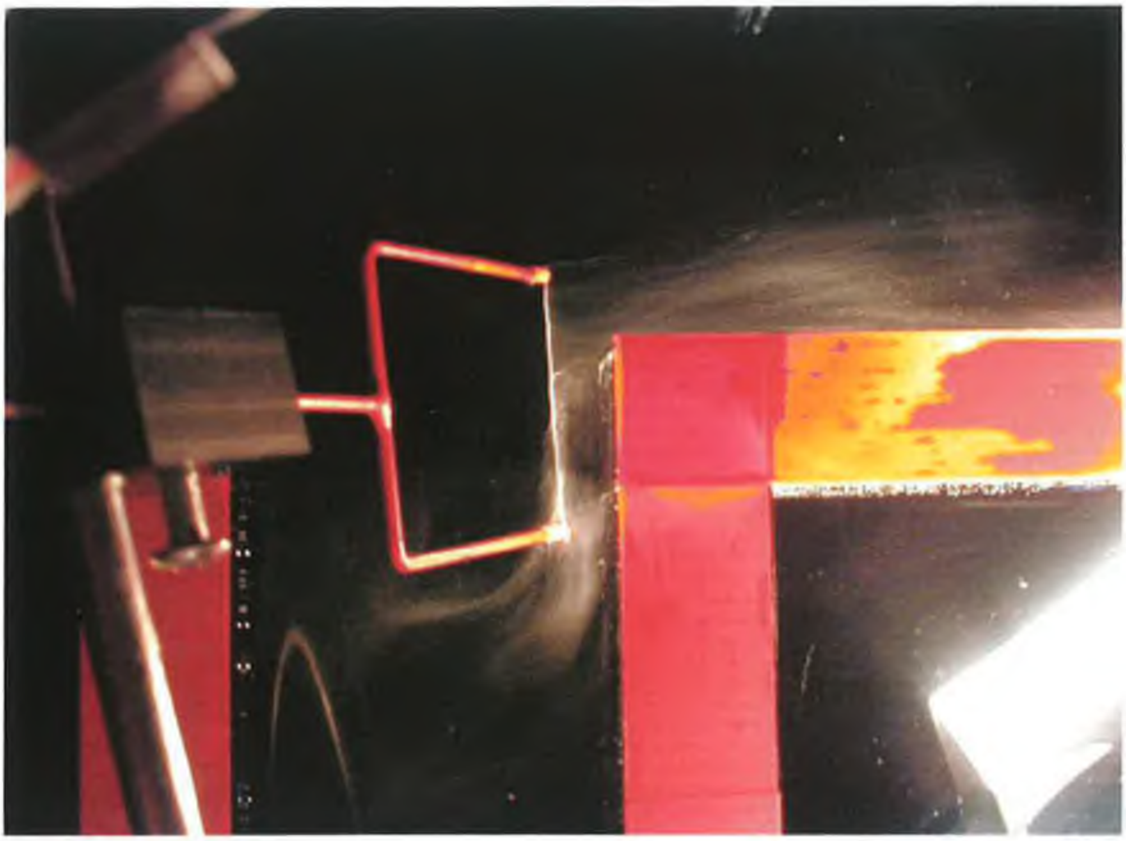

*Figure 5.30: Downstream re-circulation for a 50*50 sharp entry tee at 0.5 m/s*

To investigate the slow rotating vortex region the cathode was moved fully into the dead-leg branch adjacent to the downstream wall. Following numerous camera angles and lighting configurations the vortex suddenly emerged in all its glory (figure 5.31). At this velocity (0.5 m/s) the vortex was clearly visible. It was positioned slightly off centre of the dead-leg towards the downstream wall. The highest velocities were evident around the edge of the vortex and it appeared to be driven by the mainstream fluid flowing across the top of the branch and by fluid bouncing off the downstream wall. The vortex was compact at the top and elongated at the bottom indicating the possibility of further flow separation within the branch. Close examination of figure 5.31 highlights additional separation on the downstream wall of the dead-leg, away from the vortex region. These studies confirm the patterns identified during CFD simulations for sharp entry equal tee dead-legs (figures 4.74 and 4.78).

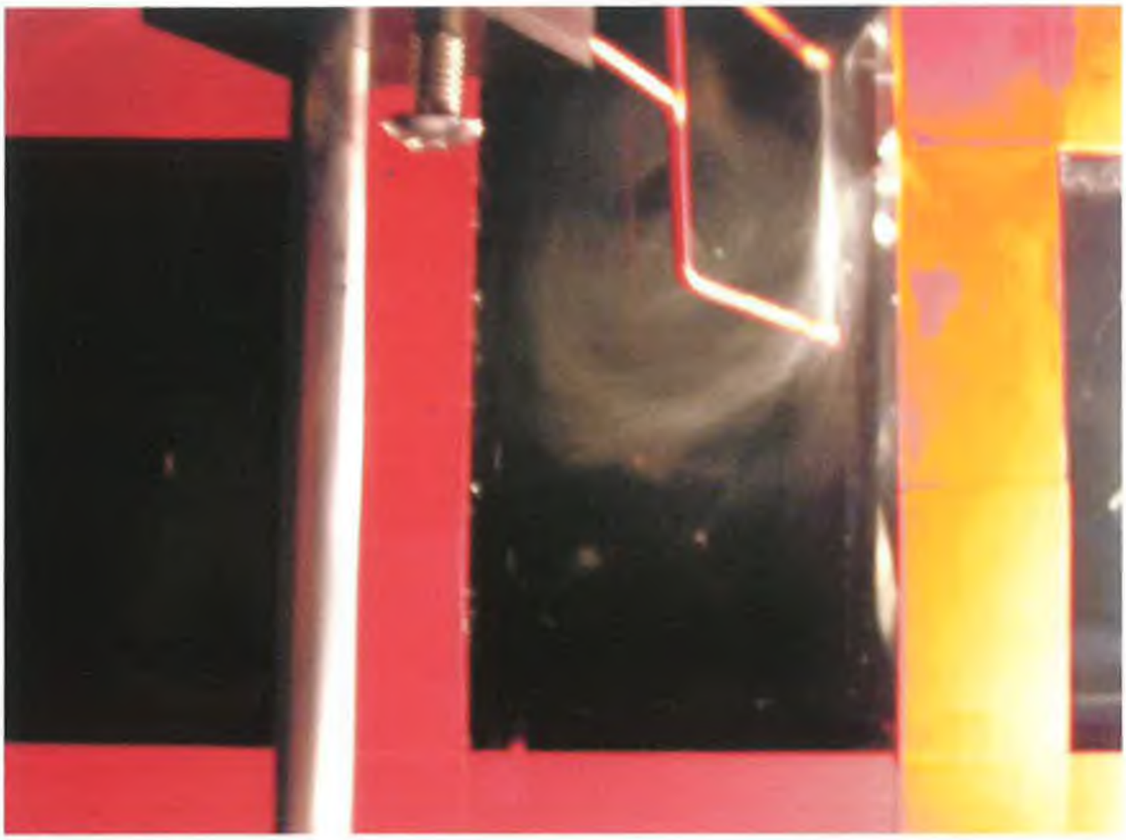

*Figure 5.31: Entry region high swirl for a 50*50 sharp entry tee at 0.5 m/s*

To investigate flow patterns deep into the branch the cathode was positioned further into the branch and half way across the dead-leg. It became evident that additional separation was taking place between the upper and lower half of the branch. Fluid moving away from the downstream wall and around the vortex region was separating between the upper and lower half of the branch (figure 5.32). Fluid above the separation point was forced up along the upstream wall of the tee while fluid below this point was forced down the upstream wall further into the corner of the branch. Examination of the upstream separation highlights the formation of the rotating vortex while the remainder of the fluid travels the entire length of the upstream wall to be driven across the top of the branch by the fast flowing mainstream fluid.

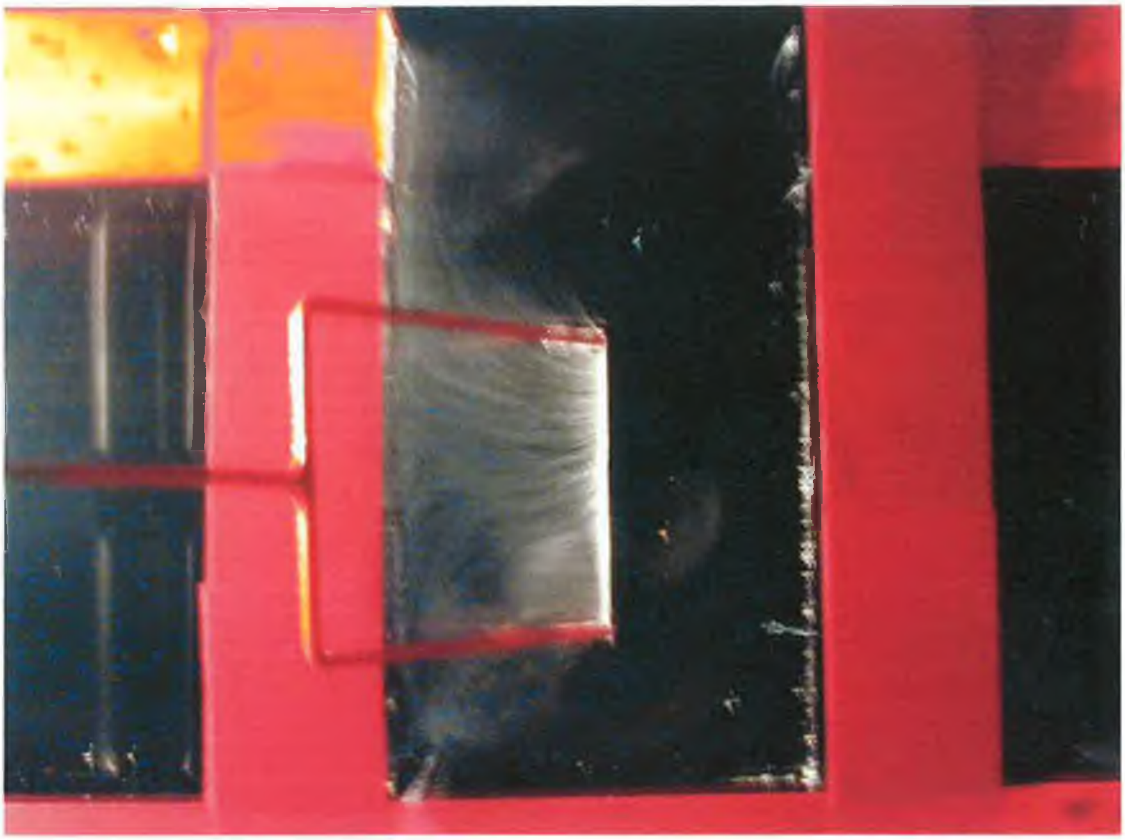

*Figure 5.32: Midstream separation for a 50*50 sharp entry tee at 0.5 m/s*

The downstream fluid, fluid below the separation point, flowed slowly into the corner of the branch generating a stagnation zone in this region. It should also be noted that the fluid in the lower half of the branch and fluid along the upstream wall of the branch flowed very slowly during the capture of these images. This is evident from figure 5.33 where the cathode is positioned across the branch. The region of fluid below the cathode is obviously flowing slower that the fluid moving along the upstream wall of the branch. This image also offers an insight into the complex nature of the patterns developed within the branch during these separations.

*Figure 5.33: Midstream flow patterns for a 50*50 sharp entry tee at 0.5 m/s*

The final set of images related to the base of the branch with the cathode positioned in the downstream corner of the branch and close to the base of the branch respectively (figure 5.34 and 5.35). It was noted that the fluid at the base of the downstream wall was stagnant. The hydrogen bubbles generated at the cathode were not carried away from the cathode by fluid flowing across the wire (figure 5.34). Instead they were found to stagnate around the cathode wire and after a period of time float, driven by buoyancy effects, vertically up away from the wire.

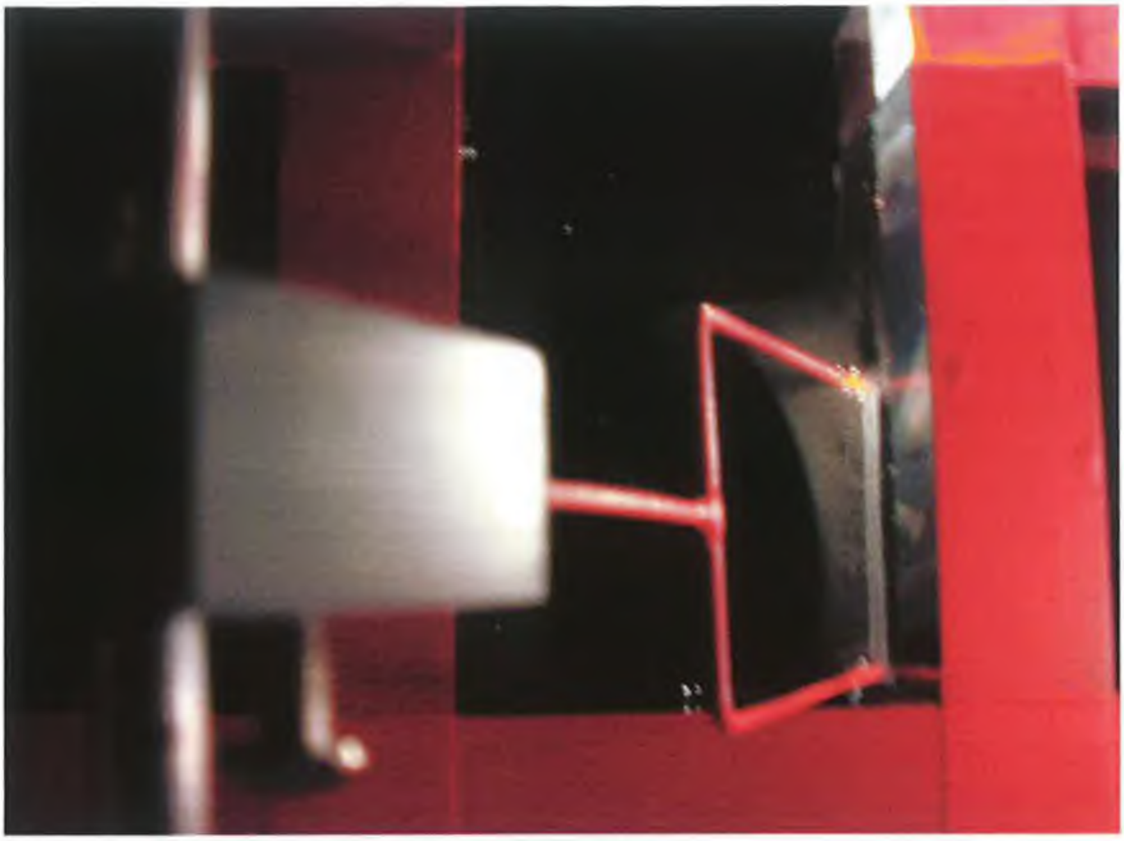

*Figure 5.34: Base patterns for a 50*50 sharp entry tee at 0.5 m/s*

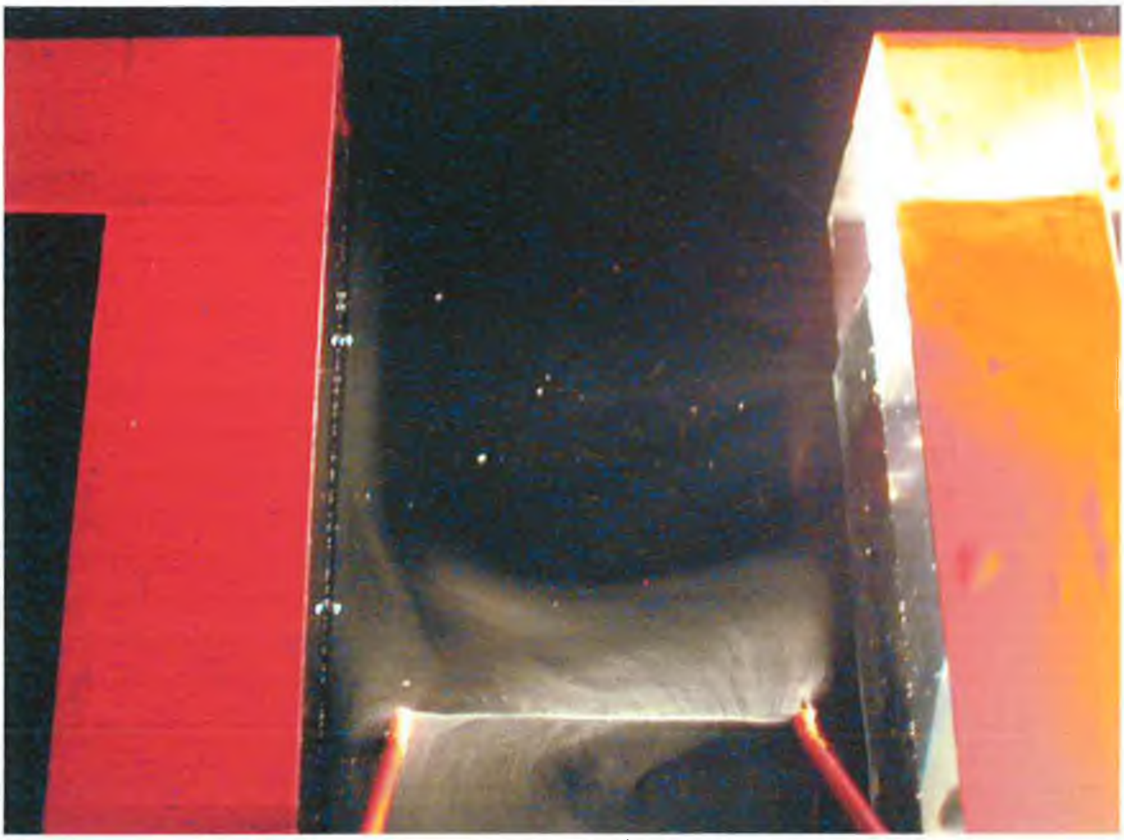

*Figure 5.35: Base separation for a 50*50 sharp entry tee at 0.5 m/s*

This is clear evidence of stagnation of the fluid in this region. Once the hydrogen bubbles reached the surface of the fluid they were slowly drawn back across the branch. This motion only occurred at the surface of the fluid and is evidence of less shear resistance at the free surface of the fluid. To further investigate this pattern the cathode was repositioned across the branch but close to the surface of the fluid. In this position a clear insight was gained into the motion at the surface of the branch (figure 5.36). Again this motion was only evident when the cathode was close to the surface. Moving the cathode further into the fluid resulted in a return to stagnant flow conditions. Bubbles simply rose vertically from the cathode wire until they reached the free surface and were then moved slowly around the branch by motion of the surface fluid. These flow patterns highlight the complex 3D nature of the flow found within the branch.

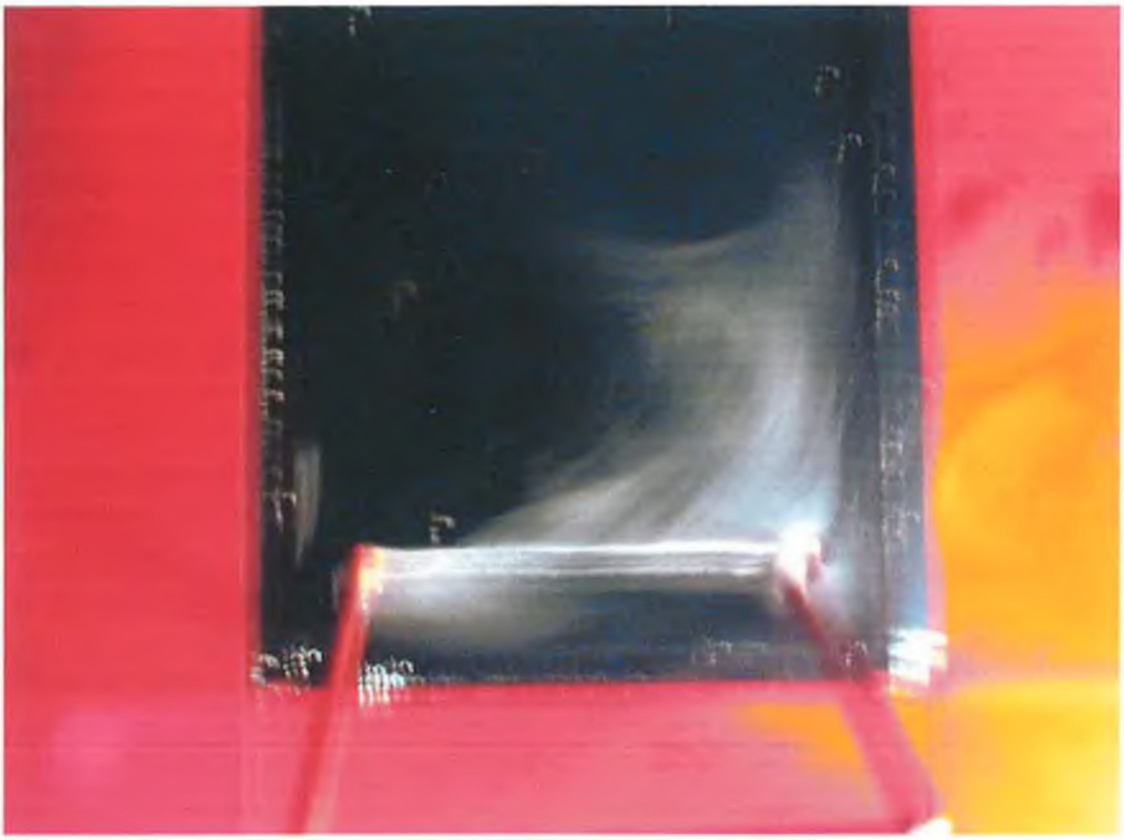

*Figure 5.36: Surface flow patterns for a 50*50 sharp entry tee at 0.5 m/s*

5.9 VIUSALISATION STUDIES FOR A ROUND ENTRY 50MM TEE

The introduction of a radius of curvature at the entry of a 50*50mm tee was examined and the key flow patterns are now presented. Figure 5.37 highlights the existence yet again of a slow rotating vortex within the entry region of the branch. The vortex is located slightly downstream of the centreline of the branch but not as far downstream as the vortex established with a sharp entry tee at the same flowrate. The separation point is on the downstream radius of curvature. Mainstream fluid is driven high at the outlet of the tee by fluid leaving the branch as a result of this separation. Figure 5.38 shows the motion of fluid following separation on the downstream wall. Some of the fluid flows back across the branch however a percentage of the fluid also continues down into the branch moving steadily away from the downstream wall similar to figure 4.35. This pattern is different from that found for a sharp entry tee where the fluid flows closer to the downstream wall. Figure 5.39 highlights flow along the upstream wall of the tee and establishes a second separation point of the upstream wall. The vortex region is also visible and was found to encourage flow along the upstream wall. Fluid flowing up this wall was prevented from leaving the branch by fluid entering the branch along the upstream radius of curvature. This collision of fluid encouraged the off-set and tilted nature of the slow rotating vortex, as established during CFD simulations of a similar configuration (figure 4.35). A further insight into these patterns is offered by figure 5.40. The cathode was positioned across the mid section of the branch and it became evident that the lower half of the branch had its own re-circulation zone moving very slowly counter to the upper region. Fluid moving away from the downstream wall can find itself either flowing up or down the upstream branch wall depending on its position relative to the separation point.

*Figure 5.37: Entry flow patterns for a round entry 50*50mm equal tee at 0.5 m/s.*

*Figure 5.38: Downstream patterns for a round entry 50*50mm equal tee at 0.5 m/s.*

*Figure 5.39 Upstream patterns for a round entry 50*50mm equal tee at 0.5 m/s.*

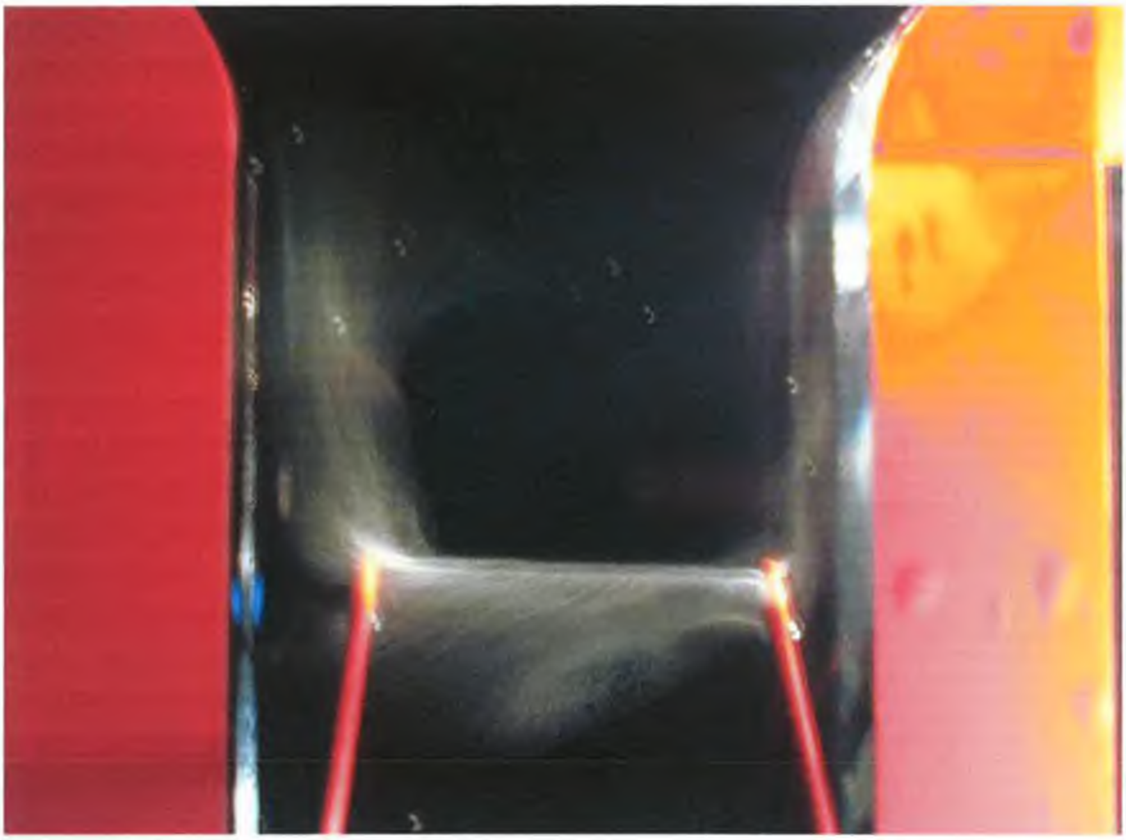

*Figure 5.40: Midstream separation for a 50*50mm equal tee at 0.5 m/s.*

The slow rotating vortex, highlighted during CFD simulations (figure 4.6), also contributes to this process driving flow that is outside the vortex further down into the branch while fluid around the vortex is forces up the upstream wall and re-circulated once again by the vortex. This secondary re-circulation within the base of the branch became clearly evident when the cathode was placed along the upstream wall towards the base of the branch. The fluid formed a figure of eight pattern with fluid flowing across the base of the branch and up the downstream wall. It should be noted that fluid trapped in this secondary pattern was flowing very slowly and that some time had passed before the pattern was fully established. The fluid in this region was effectively trapped in a slower rotating cavity with little possibility of exchange of fluid between the two regions. No bulk exchange of fluid in the base of the branch was evident from these studies (figure 5.41).

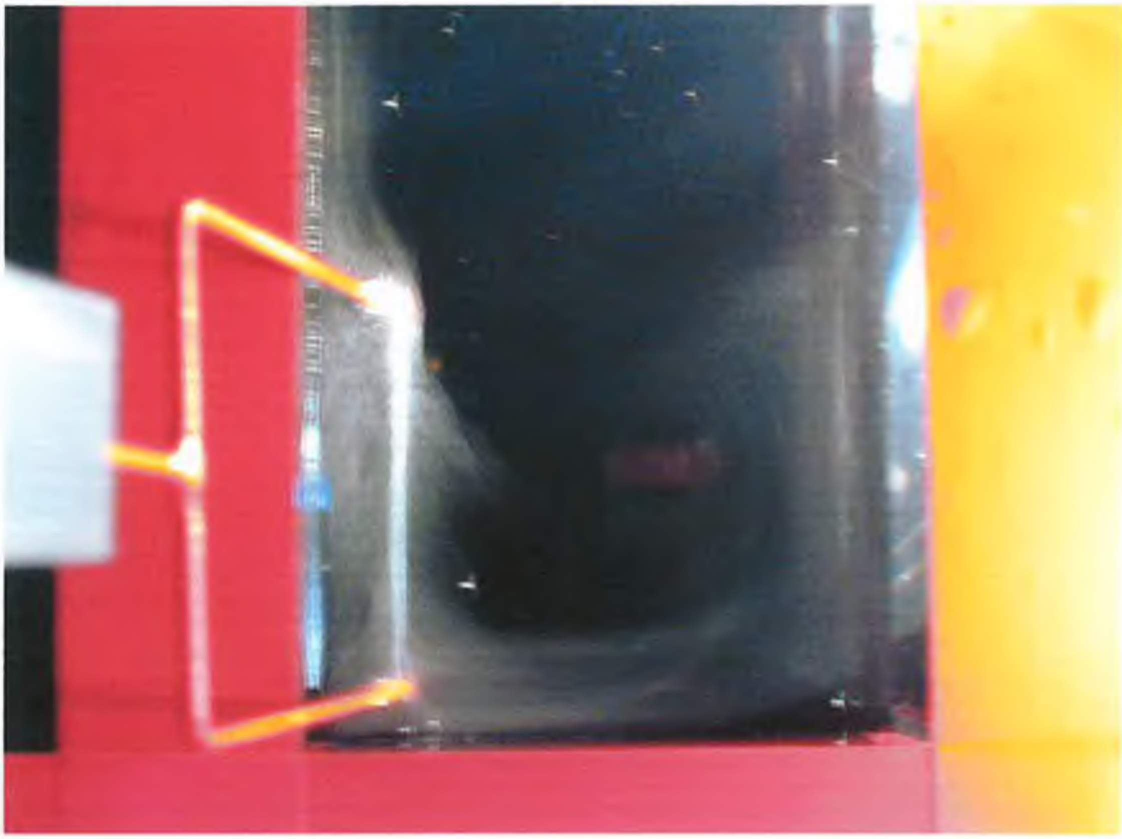

*Figure 5.41: Branch base separation for a round entry 50*50mm equal tee at 0.5 m/s.*

Positioning of the cathode across the base of the branch further highlights the flow pattern in this region (figure 5.42). Hydrogen bubbles were very slowly swept away from the wire in a curving pattern. The slow flowing nature of the motion meant that some of the bubbles dispersed vertically up to the surface of the fluid. The remainder gently flow across the base of the tee and up the downstream wall of the dead-leg.

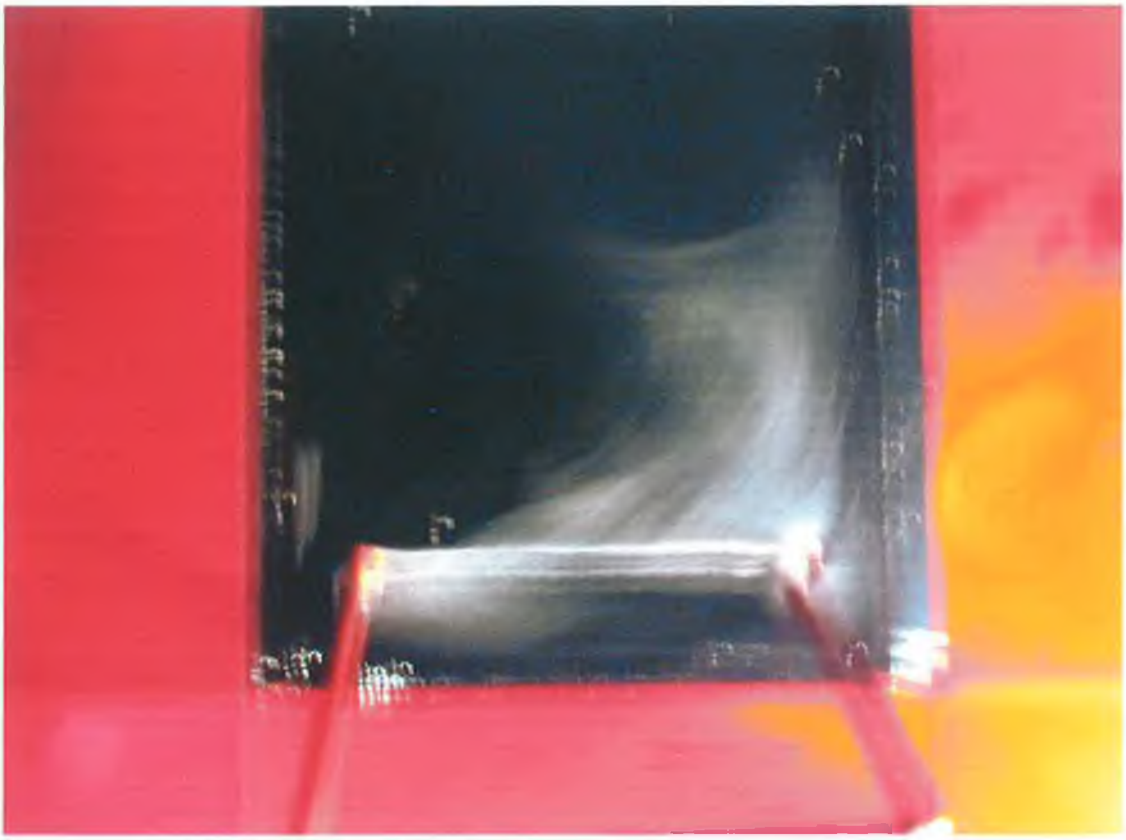

Figure 5.42: Branch base flow conditions for a sharp entry 50mm equal tee at 0.5 m/s

Eventually the fluid is forced back into the branch by the vortex fluid above it that traps the fluid within this region. There is no evidence from the data examined that substantial exchange of fluid can take place between the upper and lower regions of the dead-leg. Fluid in the lower region remains there in a slow rotation.

This slow motion is of considerable concern in relation to bio-film formation in that cells entering this lower region will remain there with the potential for attachment and growth. There is little evidence of wall shear throughout the branch. Movement of the cathode close to any wall results in vertical movement of hydrogen bubbles a pattern not conducive to high shear stress along the wall. This situation worsens the further into the branch the cathode is placed.

5.10 VISUALISATION STUDIES FOR A SHARP ENTRY 50:25MM TEE

To investigate the effect of reducing branch diameter on flow patterns within the branch the rig was reconfigured to give a 50 to 25 mm branch to mainstream ratio. The effect of this reduction is shown in figure 5.43 for a sharp entry tee. The high swirl region is still evident within the branch. However in this configuration rather than being offset towards the downstream wall it is centred in the entry region of the branch. This is a direct result of the narrower cross section entry zone. The mainstream fluid cannot penetrate the branch as easily as it could with a wider opening. Therefore it cannot push the vortex towards the downstream wall. The result is a centring of the vortex high within the branch as the mainstream fluid rushes across the top of the branch. This is exactly the same alignment that was found for a 50:25mm and also a 25:12.5 mm CFD simulation (figures 4.114 and 4.117). Separation was noted downstream of the branch as the fluid impacts the sharp edge of the tee. This separation region is not as large as that found with an equal tee configuration. Fluid entering the branch impacts the downstream wall and directly influences the formation of the vortex region. The vortex was found to be approximately 25mm in diameter. Outside of this zone separation was also noted within the branch.

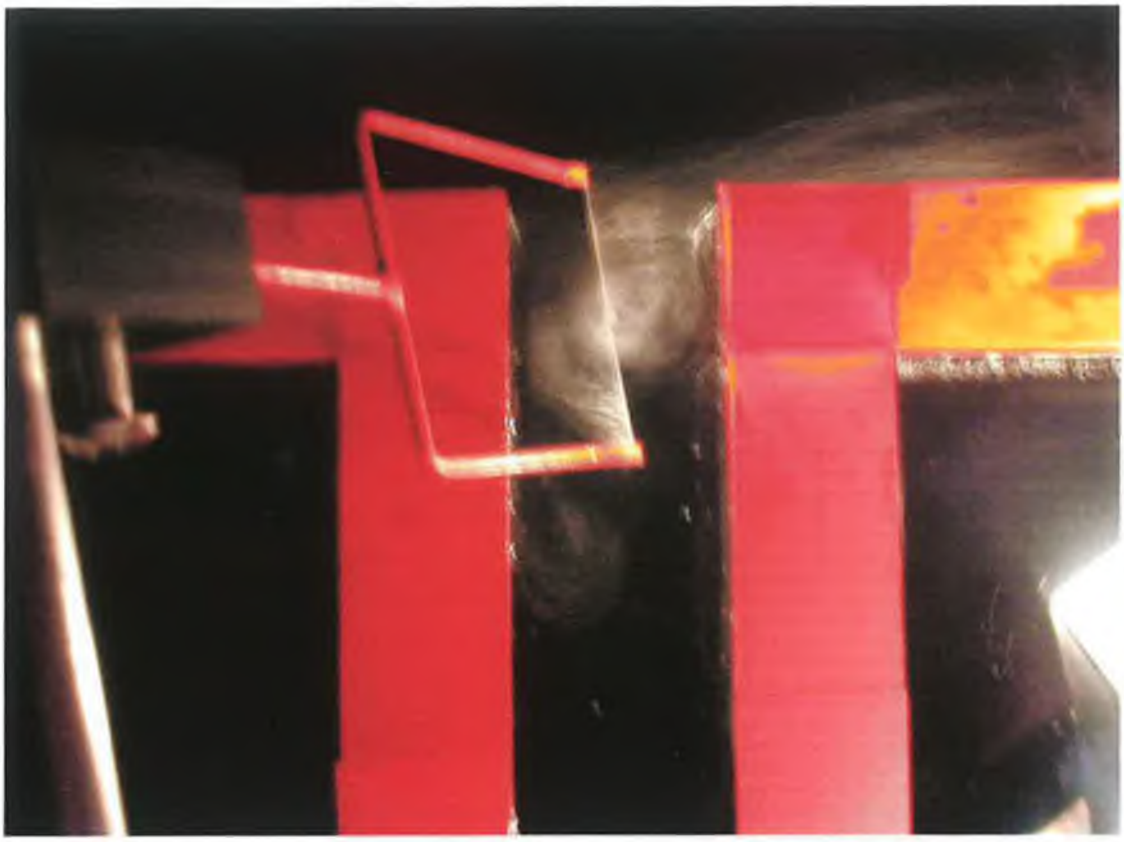

*Figure 5.43: Sharp entry 50*25 mm dead-leg tee at 0.5 m/s*

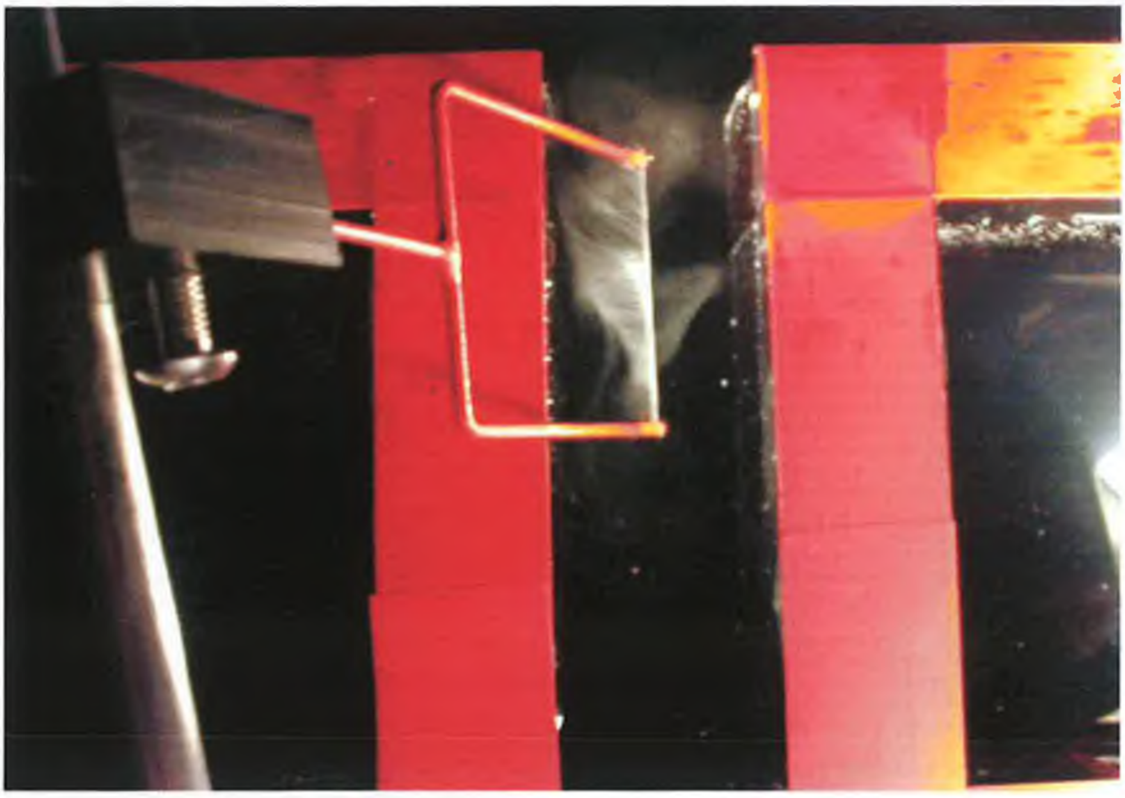

*Figure 5.44: Midstream separation in a 50*25 mm dead-leg tee at 0.5m/s*

Immediately below the vortex zone the fluid was found to separate and move in two directions. One stream followed the vortex rotation and moved towards the upstream wall. A second stream moved back across the branch towards the downstream wall. This area (figure 5.44) was significant as it marked the point at which the fluid within the branch began to stagnate. Once again this was evident from the movement of bubbles around the cathode. Within this region of the branch the hydrogen bubbles once again rose to the surface of the fluid before being dragged by surface effect towards the downstream wall.

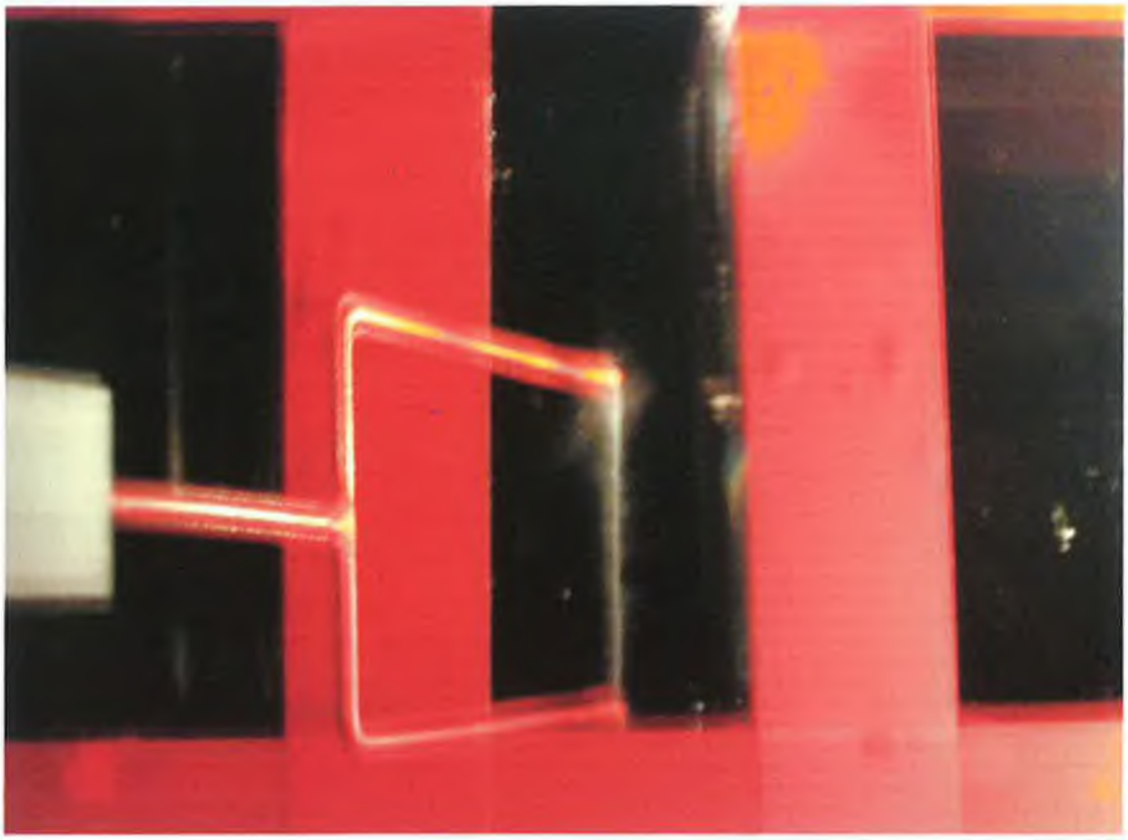

*Figure 5.45: Stagnation at the base of a 50*25 mm dead-leg tee at 0.5 m/s*

Movement towards the upstream wall was not surface bubble movement but bubbles well below the surface away from the cathode wire. Positioning of the cathode towards the base of the branch highlights a large zone of completely stagnant water (figure 5.45). In this position the hydrogen bubbles, apart from a slight surface movement at the top of the cathode, flowed vertically up from the wire. Upon reaching the surface of the fluid the bubbles simply dispersed. This indicates that there is no movement in this region of the tee, not even surface movement.

*Figure 5.46: Sharp entry re-circulation in a 50*25 mm dead-leg tee at 0.5 m/s*

Figure 5.46 highlights the effect of introducing a round entry configuration on a 50*25 mm dead-leg. Following examination of the patterns it was evident that the introduction of a radius to the branch assisted in off-setting the vortex towards the downstream wall. Mainstream fluid followed the radius of curvatures of the branch entry before being forced up and out of the branch by fluid already within the dead-leg. This motion forced the vortex further downstream within the dead-leg and also established a larger diameter swirl. Fluid above the separation point on the downstream wall was forced higher at the exit from the branch while fluid below this point contributed to the rotating motion of the vortex. The vortex also resided higher up the branch within the wider entry region. Stronger separation currents were also noted during this configuration than with a sharp entry tee of the same dimensions. Additional motion was also noted further into the branch as shown in figure 5.47. This picture captured the tail end of the vortex while highlighting slower movement and a drift of bubbles towards the surface along the downstream wall of the branch.

*Figure 5.47: Downstream flow patterns in a 50*25 mm dead-leg tee at 0.5 m/s*

Midstream and upstream wall separation is evident from figure 5.48. Fluid separating from the downstream wall is forced down into the branch by circulation around the vortex. This fluid passes across the branch to a second separation region on the upstream wall. Fluid above this point is drawn up the upstream wall by the slow rotating vortex. Fluid below is drawn down into a stagnant region where it resides for a long period of time. The only motion in this region is across the top of the stagnation zone driven by flow around the vortex.

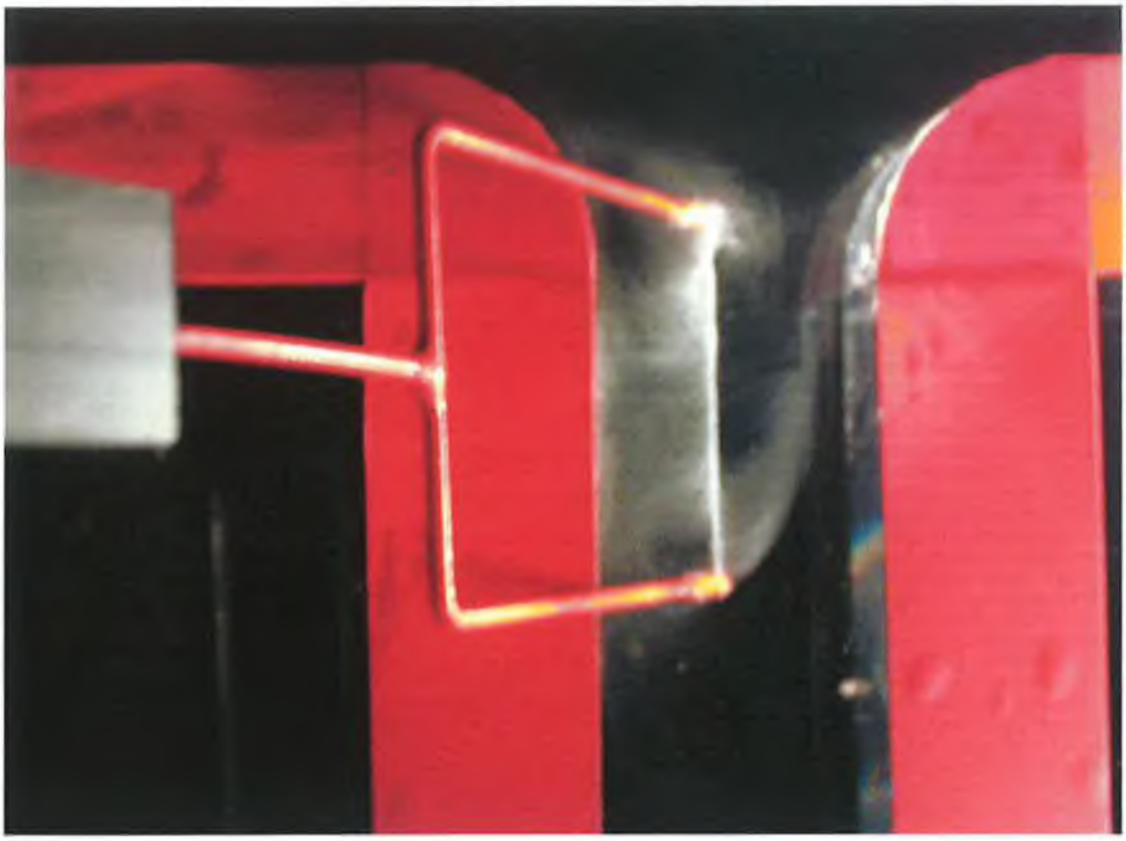

*Figure 5.48: Upstream wall separation 50*25 mm dead-leg tee at 0.5 m/s*

In conclusion the hydrogen bubble rig offered a better insight into flow patterns within a dead-leg. This particular technique also gave closer simulations of CFD results. Key highlights of these investigations include;

1) Clear evidence of a slow rotating vortex at entry to each dead-leg investigated as highlighted by previous by CFD analysis.

2) Elongation of the slow rotating vortex for wide entry tees (50:50mm dead-legs) and centring of the vortex for smaller entry tee (25:25mm dead-legs).

3) Separation zones were also evident downstream of the branch for all tees examined. The size of this zone was dependent on mainstream velocity and branch entry/exit profile (sharp or round).

4) Mid branch separation was also evident for 50:50mm dead-legs while this separation zone was found higher up the dead-leg for smaller diameter tees.

5) Slow upstream wall motion was found (driven by the slow rotating vortex) 1D into the branch for a 50mm equal tee and for a 50:25mm reduced tee. This motion was evident irrespective of sharp or round entry conditions.

6) Downstream wall conditions were influenced by entry cross-section and by both sharp and round entry conditions. Sharp entry conditions resulted in increased motion on the downstream wall of all dead-leg configurations.

7) Stagnation zones were evident in all dead-leg irrespective of all ratios examined. The smaller the branch size the larger the stagnation zones.

8) There is no evidence of bulk exchange of fluid from the mainstream flow into the dead-leg. This is in direct conflict with FDA statements and the concept of the 6D-rule.

CHAPTER 6. CONCLUSIONS AND FUTURE WORK

6.1. CONCLUSIONS FROM THIS WORK

As stated in the first sentence of this thesis 'Water is the blood of the pharmaceutical industry. Every manufacturing facility requires it and its quality is critical to virtually all pharmaceutical production processes'. Many of these facilities, following multi-million pound installations of purification equipment, regularly encounter contamination within the distribution loop. One source of this contamination is piping system dead-legs and to address this issue the regulatory bodies (FDA etc) offer the 6-D rule to piping system engineers and designers as an all encompassing quick fix. The FDA operates and encourages the use of the 6D rule in an industry confused by loop contamination following its implementation.

The aim of this thesis was to put the 6D-rule on a scientific footing and to encourage others to apply their expertise to this problem. The conclusions to be drawn from this investigation are as follows:

- Divided flow through pharmaceutical pipe tees results in the development of a stagnation point on the downstream wall of the tee and depending on the mainstream loop flowrate a separation region on the upstream wall of the tee. This separation region is of concern in the battle against bio-film formation, as a return of the system to dead-leg conditions (following the isolation of the process line) will maintain this region as a low flow region with low wall shear stress values.

- Examination of a 50mm equal tee dead-leg once again highlighted a stagnation point on the downstream wall, higher up the branch than for divided flow conditions. The dead-leg was identified as a slow rotating cavity with motion within the branch driven on by fast flowing mainstream flow across the top of the dead-leg.

- Dead-leg branch velocity profiles were found to be highest on the downstream wall of the branch, falling to almost zero at the center of the branch before increasing slightly on the upstream wall of the tee.

- A comparison of divided and dead-leg upstream and downstream wall shear stress values highlighted a considerable drop off in wall shear stress for dead-leg flow conditions. This is of considerable importance in relation to bio-film formation within the tee.

- Mainstream loop velocity was found to have little effect on a 1D dead-leg. This was also true for 2D, 4D and 6D dead-legs at velocities between 1 to 2 m/s. At 0.5m/s loop velocities, branch velocities were found to be at their lowest in all dead-legs.

- Upstream and downstream wall shear stress values were found to decrease with decreasing distribution loop velocity over the range of dead-leg configurations investigated. Both walls had maximum wall shear stress values for loop velocities of 2.0m/s and minimum values at 0.5m/s.

- Increased maximum branch velocities were noted when round entry 50mm tees were replaced with sharp entry tees. For a sharp entry 6D 50mm equal tee little benefit was found from increasing loop velocity. Branch penetration was as low as values found for an equivalent round tee.

- Sharp entry tees resulted in increased upstream and downstream wall shear stress values over round entry tees. The increase in wall shear stress was most dramatic on the downstream wall of the branch.

- For a 50mm distribution loop a reduction in branch diameter was found to increase branch penetration. The smaller the branch the higher the velocity profiles found up to 2D into a 6D dead-leg. Beyond 3D no benefit was found from increasing loop velocity or from reducing branch diameter.

- Reducing the branch diameter for a 50mm distribution loop was found to decrease downstream wall shear stress while increasing upstream wall shear stress. This was due to motion around the slow rotating cavity and the narrow entry region of the tee.

- For a 25mm distribution loop again a decrease in branch diameter was found to increased branch penetration. Maximum penetration was found at highest loop velocity up to 3-4D into the branch. As with 50mm loops equal tees were found to give the worst opportunity for branch penetration and stagnation conditions

- Reducing the branch diameter for a 25mm distribution loop was found to decrease downstream wall shear stress. Upstream wall shear stress values were lower than similar ratio 50mm loop tees. Overall the values of wall shear stress were lower than those found in a 50mm loop.

- Dye injection studies highlighted the lack of penetration of the dead-leg branch. Separation regions were evident along the upstream wall of the tee and stagnation zones present at the base of the tee.

- Complex flow conditions were evident on the upstream and downstream walls for both sharp and round entry tees. Some evidence of motion was found along the upstream wall driven by flow patterns within the branch but little exchange of fluid between the mainstream flow and the branch was found at the flowrates studied.

- Hydrogen bubble visualization offered a better insight into dead-leg flow conditions. Clear evidence of a slow rotating vortex was found at entry to the branch. This was offset towards the downstream wall for large entry tees and centered high up the branch for narrow entry tees.

- Zones were evident within the dead-leg highlighting regions of slow flowing fluid and stagnation zones. Mid branch separation was noted for 50mm equal tees and the separation was found to be located higher up the branch for smaller diameter tees

- Upstream and downstream wall motion was evident in each dead-leg studied driven by the slow rotating vortex. Reducing the branch diameter condensed this motion into a small region high up the branch of the dead-leg. Stagnation zones were present at the base of all dead-legs and these zones grew as the branch diameter was decreased. No dead-leg configuration (sharp, round, long, narrow) was completely free of stagnant water and there was little evidence of exchange of fluid from the mainstream loop into the branch.

6.2: RECOMMENDATIONS AND FUTURE WORK

This research into pharmaceutical and semi-conductor dead-legs and the 6D-rule has highlighted some key points (outline above) in relation to design, installation, commissioning and operation of high purity water systems. On the bases of the work carried out to date a number of publications have been presented and additional postgraduate projects have already begun to investigate further areas of interest. Future work in the field should include the following areas of investigation:

1. Investigation of method of increasing exchange of fluid between the dead-leg branch and the mainstream loop. This is a key objective in the reduction of dead-leg contamination.

2. Once penetration of the dead-leg has been established a flushing time model should be investigated for a range of industrial bio-bore tees. This would offer the industry a standard for cleaning in place cycles to ensure that the branch had been flushed regularly with fresh CIP solutions.

3. Investigation of heat transfer within a dead-leg is of considerable interest to both the pharmaceutical and semi-conductor industries. Some distribution loops are operated at 80C and stagnation zones highlighted in this work will prevent dead-leg tees from reaching this loop temperature. A project has begun at Dublin City University to investigate this issue (see Project 1).

4. Considerable research is ongoing into bio-film formation in the food and biotechnology industry. Biologists and chemists carry much of this work out. The establishment of a multi-disciplined team to investigate bio-film formation in dead-leg would offer a unique opportunity to get a clear insight into how these cells establish themselves within pipe tees and to investigate ways of removing them once established (see Project 3).

5. As outlined during the early stages of this thesis, distributions loop designs come in various shapes and sizes. Some have drop loops, some flexible hose connections, others have straight lengths of pipe before them, some sharp elbows. The effect of these configurations on flow patterns within the dead-leg may highlight some design areas that could be incorporated into these systems to encourage exchange of dead-leg fluid.

6. At the base of each dead-leg there is an isolating valve. The type of valve will result in a different profile at the base of the tee and will affect the flow patterns within the branch. In the high purity water

industry these valves are highly expensive and each valve claims to be better then the next in preventing loop contamination. A CFD investigation into the affect of these valves on the dead leg would be of considerable interest to engineers attempting to specify the best and most economic valve for the process.

6.3. THESIS CONTRIBUTION

FDA regulations have limited dead-leg drop in High Purity Water Systems to six pipe diameters. The evidence presented in this thesis has shown that:

1) The 6D rule is NOT industrially relevant
2) 1D and 2D dead-leg configurations should be used to avoid stagnation
3) No configuration resulted in high wall shear stress values
4) Reducing branch to loop diameter increased branch stagnation
5) There is no evidence of exchange of fluid between the loop and branch
6) Dead-legs should be measured from the base of the distribution loop
7) All configurations had some quiescent (dormant/inactive) water

I hope that this work will encourage the regulators and the industry to drop the 6D rule as a quick fix for the challenging problem of system contamination. I also hope that this work will encourage others to develop industrially relevant, scientifically based solutions to high purity water system contamination now that I have shown the irrelevance of

<u>THE 6D RULE</u>

CHAPTER 7. PUBLICATIONS AND PROJECTS

7.1: PUBLICATIONS FROM THIS WORK

Austin B and Corcoran B., 'Piping System Dead-Legs', The Irish Scientist Year Book, pg 140-141, Nov 2003, No 11.

Corcoran B., 'The 6-D rule. A CFD analysis', 2003 UK Fluent Europe User Group Meeting, 7th & 8th October, 2003

Austin B and Corcoran B., 'Hest transfer in pharmaceutical dead-legs', UK Hest transfer 2003, 8th UK National Heat Transfer Conference, Oxford, 9-10 September 2003

Corcoran B., 'CFD analysis of Pharmaceutical Pipe Dead-Legs', Irish Society for Scientific and Engineering Computing , pg25-28 , 23rd to 24th May 2003, University College Dublin

Corcoran B, Esmonde H, Hashmi S., 'Investigation of Turbulent Flow in Pharmaceutical Pipe Tee-Junctions', HEFAT2002, 8-10 April 2002, Kruger Park, South Africa.

Corcoran B., 'Pharmaceutical Pipe Dead Legs: What's that all about?'. The Irish Scientist Year Book, pg 158-159, Nov 2001, No 9.

Corcoran B., 'Investigation of Pipe Dead Legs in Pharmaceutical Pipe Tees', 4h Annual Sir Bernard Crossland Symposium, pg 148-159, Dec 6th – 7th 2000, University College Dublin

7.2: ONGOING RESEARCH PROJECTS

Project 1: High Purity Water flow in Pipes and fittings

Student: Ben Austen, Biotechnology Department, Dublin City University (Sept 2002)
(Ben.Austen@dcu.ie)

This project involves the investigation of heat transfer in Pharmaceutical and Semi-Conductor purified water systems. State-of-the-art software will be used to develop models for the investigation heat transfer in 2D, 4D and 6D 50mm equal tee bio-bore stainless fittings.

A rig has been developed to investigate heat transfer within the branch of each dead-leg tee. Preliminary results highlight the existence of stagnation zones within the branch and difficulty in transfer of heat from the distribution loop to the tee. With the distribution loop circulating water at 80C the base of a 6D dad-leg tee was only at 45C two hours into the run.

This project involves the application of the most up to date CFD (Computational Fluid Dynamics) software and has applications in the of Pharmaceutical, Chemical or Semi-Conductor and food industries where Cleaning in Place (CIP) techniques are regularly used clean piping system networks. This research project will be taken to PhD level

Project 2: Investigation of Bio-film formation in high purity water systems

Student: Amani Fathi el Sheikh, Mechanical and Manufacturing Engineering Department, Dublin City University (Sept 2002)
(Amani.elSheikh@dcu.ie)

This project involves the investigation of bio-film formation on piping system networks. A rig has been modified to incorporate glass slides and high purity water circulated across these slides for long periods of time. Following circulation the slides are removed form the rig, stained and investigated for the presence of bacteria.

Preliminary studies highlight the fact that bio-film is present in the system within 24 hours. The distribution of bio-film is not even across the slides and was found to be dependant on flowrate and location within the pipe network. An induction period was also noted during which the sides were conditioned to accept bacteria.

Further studies will apply CFD and hydrogen bubble techniques to the investigation of flow patterns around the slides. These techniques will be used to examine the variation in distribution of bacteria across the slide and highlight zones of separation and re-circulation around the slides. This project will be taken to MEng level.

Project 3: Pharmaceutical and Semi-conductor water system design and construction

Student: **Salem Elmaghrum, Mechanical and Manufacturing Engineering Department, Dublin City University (Sept 2003)**
(Salem.Elmaghrum@dcu.ie)

This project involves an investigation of design criteria and manufacturing specifications for Pharmaceutical and Semi-conductor high purify water systems. A review of current technologies will be undertaken to investigate pre-treatment equipment (filters, softners, UV systems), final treatment equipment (reverse osmosis and continuous de-ionisation) and storage/distribution networks.

Analysis will also take place of distribution loop entry configurations to piping system dead-legs. CFD models will be developed for a range of systems and investigations validated using dye injection techniques on a rig using a glass pipe tee.

This research is applicable to food, pharmaceutical or chemical industry and to engineers with a particular interest in design and manufacture of high purity water systems. Research in this project may be taken to MEng or PhD level.

Project 4: **Fouling of Double Pipe Heat Exchangers**

Student: **Antonio Llinares Fontdevilla, Mechanical and Manufacturing Engineering Department, Dublin City University (Sept 2002)**
(Antonio.Fontdevilla@dcu.ie)

Fouling (the build up of unwanted deposits on surfaces) is a major problem associated with heat transfer equipment. This project involves the investigation of fouling of tube heat exchangers using bio-materials (milk, cheese whey).

A rig has been developed to analyse deposit build up on heat exchanger tubes. The unit consists of a double pipe heat exchanger, PICO data logging system for temperature measurement and a range of instrumentation to control supply water temperature and milk temperature. Preliminary results highlight the existence of an induction period during which fouling is limited. Following this period the fouling resistance was found to rapidly increase, decreasing heat transfer within the rig.

This research is applicable to food, pharmaceutical and process industries. It is also applicable to engineers who have an interest in design of heat transfer equipment and thermodynamics.

CHAPTER 8: LIST OF REFERENCES

1) Abbott, M. B. and Basco, D. R., (1989). 'Computational Fluid Dynamics – An Introduction for Engineers', Longman Scientific and Technical, Harlow, England

2) Adin, A., Hatukai,S. (1991). 'Optmisation of Multi Layer Filter Beds', *Filteration and Separation*, Vol. 28 (1), pp. 33-36.

3) Anon, S., (1994). 'Key technologies in purifying pharmaceutical process water', *Filtration and Separation*, Vol. 31 (8), pp. 773-777.

4) Anon, S.,. (1995). 'Alternatives to distillation in the production of WFI quality water', *Filtration and Separation*, Vol. 32 (10), pp. 4-10.

5) Arnold, J.W. Bailey, G.W., (2000). 'Comparison of scanning electron and atomic force microscopy of surface finishes on stainless steel that reduce bacterial attachment' *Journal of Scanning Microscopies*, Vol. 22 (2), pp. 115-117.

6) Balazs, M.K., (1996). 'Proceedings of the 1996 Semiconductor Pure Water and Chemicals', *Proceedings of the 1996 Semiconductor Pure Water and Chemicals*, Mar 4-7, Santa Clara, CA, USA, pp. 372-380.

7) Bates, C.J. Zonuzi, F.; Faram, M.G.; O'Doherty, T., (1995). 'Experimental and numerical comparison of the flow in a 90° Tee junction', *American Society of Mechanical Engineers, Fluids Engineering Division,* Vol. 217 Separated and Complex Flows, pp. 43-50.

8) Block, J.C. Dutang, M.; Maillard, J.; Reasoner, D., (1994). 'Growth of attached bacteria in water distribution systems', *Water Supply*, Vol. 12 (1-2), pp. 5-18.

9) Bradshaw, P., Cebeci, T. and Whitelaw, J. H., (1981). 'Engineering Calculation Methods for Turbulent Flow', *Academic Press, London.*

10) Burns, M. A.; Clifford, R.; Strait, J., (1998). 'Determining the Correct Concentrations of TOC in Purified Water and WFI', *Ultrapure Water*, Vol. 15 (2), p 50.

11) Camper, A. K.; Hamilton, M.; Johnson, K. (1994). 'Bacterial Colonization of Surfaces in Flowing Systems; Methods and Analysis', *Ultrapure Water* Expo '94, Philadelphia, PA May 9 – 11.

12) Carmody, J.C.; Marthak, J.E., (1989). 'Controlling Bacterial Growth in an Ultrapure Water System', *Microcontamination*, Vol. 7 (1), pp. 28-35.

13) Cartwright, P. S., (1999). 'Water purification', *ASHRAE Journal*, Vol. 41 (5), pp. 69-74.

14) Characklis, W., (1981). 'Fouling Biofilm Development: A Process Analysis', *Biotechnology and Bioengineering*, Vol. 23, pp. 1923 – 1940.

15) Chen H. C. and Patel V. C., (1988). 'Near-Wall Turbulence Models for Complex Flows Including Separation' *AIAA Journal*, Vol. 26 (6), pp. 641-648.

16) Cleaver.J.W. and Yates. B., (1975). 'A sub-layer model for the deposition of particles from turbulent flow', *Chemical Engineering Science*, Vol. 30, pp. 983-992.

17) Cleaver.J.W. and Yates. B., (1973). 'Mechanism of detachment of colloidal particles from a flat substrate in a turbulent flow', *Journal of Colloid and interface science*. Vol. 44 (3), pp. 464-474.

18) Cloete, T.E. Westaard, D.; Van Vuuren, S.J., (2003). 'Dynamic response of biofilm to pipe surface and fluid velocity', *Water Science and Technology*, Vol. 47 (5), pp. 57-59.

19) Coleman, D.C.; Evens, R.W., (1991). 'Investigation of the Corrosion of 316L Stainless Steel Pharmaceutical Water for Injection Systems', *Pharmaceutical Engineering*, Vol. 11 (4), pp. 9-13.

20) Cooper, M.S., (1987). 'Water for Pharmaceutical and Cosmetic Manufacture', *Microbological Update*, Vol. 2 (3), pp. 55-60.

21) Corcoran B.G. and Foley G., (1996). 'Fouling of Plate Heat Exchangers by Cheese Whey Solutions', *MSc thesis*, Dublin City University, Ireland.

22) Cross, J., (1997). 'Upgrading a pharmaceutical water purification system to meet FDA requirements', *Filtration and Separation*, Vol. 34 (9), pp. 938-939.

23) Cutler, R.M.; Nykanen, J.F., (1988). 'High Purity Water Production, Storage and Distribution', *Pharmaceutical Engineering*, Vol. 8 (5), pp. 29-34.

24) Daly B. J. and. Harlow F. H., (1970) 'Transport Equations in Turbulence', *Phys. Fluids*, Vol. 13, pp. 2634-2649.

25) Dhaubhadel, M.N., (1996). 'CFD applications in the automotive industry',*Journal of Fluids Engineering*, Transactions of the ASME, Vol 118 (4), pp. 647-653.

26) Drimal, J., Janca, J., (1990) 'Biological purification of water by an ozoniser with a discharge tube electrode', *Journal of Physics*, Applied Physics, Vol. 23 (1), pp. 7-11.

27) Durst, F., Jovanovic, J and Sender, J., (1995). 'LDA measurements in the near wall region of a turbulent pipe flow,' *J.Fluid Mech*., pp. 305-335.

28) El Din, A.M.S. El-Dahshan, M.E.; El Din, A.M.T., (2003) 'Bio-film formation on stainless steels' *Desalination*, Vol. 154 (3), pp. 267-276.

29) Ferzieger J. L. and. Peric. M., (1996). 'Computational Methods for Fluid Dynamics' Springer-Verlag, Heidelberg.

30) Gagnon, S.; Rodriguez, J., (1994). 'Applying quality assurance concepts to ensure the performance of pharmaceutical high-purity water treatment systems', *Microcontamination*, Vol. 12 (1), pp. 43-49.

31) Ganzi, G.C.; Parise, P.L., (1990) 'The Production of Pharmaceutical Grade Water Using Continuous Deionisation', *Journal of Parenteral Science and Technology*, Vol. 44 (4), pp. 231-241.

32) Grant, P.W. Haveraaen, M.; Webster, M.F., (2001). 'Coordinate free programming of computational fluid dynamics problems', *Scientific Programming*, Vol. 8, (4), pp 211-230.

33) Guan, J. Ding, G., (1999). 'Purification of water for medicine and injection by reverse osmosis', *Chinese Pharmaceutical Journal*, Vol. 34 (6), pp. 391-393.

34) Guo, B. Langrish, T.A.G.; Fletcher, D.F., (2002). 'CFD simulation of precession in sudden pipe expansion flows with low inlet swirl', *Applied Mathematical Modelling*, Vol. 26 (1), pp. 1-15.

35) Hager, H., (1984) 'An approximate treatment of flow in branches and bends', *Proc. Instn. Mech. Engrs.* 198C, No. 4., pp. 63 – 69.

36) Hallam, N.B. J.R.; Forster, C.F.; Simms, J., (2001) 'The potential for biofilm growth in water distribution systems', *Water Research*, Vol. 35 (17), pp. 4063-4071.

37) Harries, R., (1991). 'Ion-exchange kinetics in ultra pure water systems', *Chemical technology and Biotechnology*, Vol. 51 (4), pp. 437-447.

38) Holden, B. Greetham, M.; Croll, B.T.; Scutt, J., (1995). 'Effect of changing inter process and final disinfection reagents on corrosion and biofilm growth in distribution pipes', *Water Science and Technology*, Vol 32 (8), pp. 213-220.

39) Horiuti, K., (1990). 'Higher order terms in the Anisotropic Representation of Reynolds Stresses', *Phys. Fluids*, Vol. 2 (10), pp.1708-1710.

40) Huchler, L. A., (2002). 'Understand your ion-exchange resin analysis', *Hydrocarbon Processing*, Vol. 81 (8), pp. 103-104.

41) Hunt, J. R., (1982). 'Particle Dynamics in Water: Implications for Predicting the fate of Discharged Particles', *Environmental Science and Technology*, Vol. 16, pp. 303 – 309.

42) Husted, G., Rutkowski, A. (1991). 'Control of Microorganisms', *Watertech '91 Proceedings*, San Jose, CA November 20-22, pp. 43-51.

43) Jones, B.W.; McManus, K.; Cross, M.; Everett, M.G.; Johnson, S., (1993). 'Parallel unstructured mesh CFD codes: A role for recursive clustering techniques in mesh decomposition', *Parallel Computational Fluid Dynamics*, pp. 207-116.

44) Jones, G.F. Galliera, J.M., (1998). 'Isothermal flow distribution in coupled manifolds: Comparison of results from CFD and an integral model', *American Society of Mechanical Engineers, Fluids Engineering Division* , Vol. 247, Fluids Engineering Division, pp. 189-195.

45) Joyce, A. Loureiro, D.; Rodriues, C.; Castro, S., (2001). 'Small reverse osmosis units using PV systems for water purification in rural places', *Desalination*, Vol. 137 (1-3), pp. 39-44.

46) Keer, D. R., 'Gathering Validation Documentation for Pharmaceutical Water Systems', *Ultrapure Water*, Vol. 12 (9), 1995, pp 24-30

47) Kim S.E. and Choudhury D., (1995). 'A Near-Wall Treatment Using Wall Functions Sensitized to Pressure Gradient', *ASME FED*, Vol. 217, Separated and Complex Flows. ASME.

48) Kim, S.-E.. Choudhury D, and. Patel B., (1997) 'Computations of Complex Turbulent Flows Using the Commercial Code FLUENT.', *Proceedings of the ICASE/LaRC/AFOSR Symposium on Modeling Complex Turbulent Flows*, Hampton, Virginia.

49) Kottler, R.E., (1990). 'Design and fabrication considerations for stainless steel fittings used for pharmaceutical fluid applications', *American Society of Mechanical Engineers, Bioengineering Division*, Vol. 16, Bioprocess Engineering Symposium, pp. 115-121.

50) Kuhlman, H.C., (1981) 'A technical Process in the Production of Water for Injection', *Journal of Parenteral Science and Technology*, Vol. 35 (2), pp. 54 –59.

51) Kumar, V. Pavithran, S., (1999). 'Turbulent flow in two-dimensional U-ducts: A computational study', *American Society of Mechanical Engineers, Pressure Vessels and Piping Division*, Vol. 396, pp. 65-78.

52) Launder B. E and Spalding. D. B., (1974) 'The Numerical Computation of Turbulent Flows', *Computer Methods in Applied Mechanics and Engineering*, Vol. 3, pp. 269-289.

53) Launder B. E. and Shima. N., (1989). 'Second-Moment Closure for the Near-Wall Sublayer: Development and Application' *AIAA Journal*, Vol. 27 (10), pp. 1319-1325.

54) Launder B. E., (1989). 'Second-Moment Closure and Its Use in Modeling Turbulent Industrial Flows'.*International Journal for Numerical Methods in Fluids*, Vol. 9, pp. 963-985.

55) Launder, B. E., Reece, G. J. and Rodi, W., (1975). 'Progress in the Development of a Reynolds Stress Turbulence Closure', *J. Fluid. Mech.*, Vol. 68, (3), pp. 537-566.

56) Launder, B.E., and Spalding, D.B., (1974) 'Numerical Computation of Turbulent Flows', *Computer Methods in Applied Mechanics and Engineering*, Vol. 3, pp. 269-289.

57) Le, H. Moen, P. and Kim, J., (1997). 'Direct numerical simulation of turbulent flow over a backward facing step'. *J. Fluid. Mech.*, Vol. 300, pp 349-374.

58) Lerman, S.I., (1988). 'The Chemical Behavior of High Purity Water', *Ultrapure Water*, Vol. 5 (9), pp. 40-44.

59) Marshall, K.C., (1992). 'Biofilms: An Overview of Bacterial Adhesion, Activity and Control at Surfaces', *American Society of Microbiology News*, Vol. 58 (4), pp. 202-207.

60) Martyak, J. E. Carmody, J. C.; Husted, G. R., (1993). 'Characterizing biofilm growth in deionized ultrapure water piping systems', *Microcontamination*, Vol. 11 (1), pp. 39-44.

61) Matthew, G.D., (1994). 'Turbulent flow in pipes: A historic speculation', *Proceedings of the Institution of Civil Engineers, Water Maritime and Energy*, Vol. 106 (4), pp. 311-316.

62) Matus, Richard J. Steinbrenner, John P.; Chawner, John R., (1999) 'Preprocessing complex geometries for computational analysis', ***American Society of Mechanical Engineers, Pressure Vessels and Piping Division***, Vol. 397 (2), pp. 135-142.

63) Mc William, A.J., (1995). 'The Design of High Purity Water Distribution Systems', *Pharmaceutical Engineering*, Vol. 15 (5), pp. 54-71.

64) McCoy , W. F., (1987). 'Chapter 9: Strategies for the Treatment of Biological Fouling', *Biological Fouling of Industrial Water Systems: A Problem Solving Approach,* Mittelman, M.W.; Geesey, G. G., Eds., Water Micro Associates, Long Beach, CA.

65) McCoy, W. F.; Costerton, J. W., (1982). 'Fouling Biofilm Development in Tubular Flow Systems', *Developments in Industrial Microbology*, Vol. 23, pp. 551 – 558.

66) McCoy, W. F.; Bryers, J. D.; Robbins, J., (1981). 'Observations of Fouling Biofilm Formation', *Canadian Journal of Microbiology*. Vol. 27, pp. 910 – 917.

67) McGarvey, F.X., (1990). 'Factors related to the Design and Operation of Mixed Bed Ion-Exchange Units', *Transcripts of the Ninth Annual Semiconductor Pure Water Conference,* Santa Clara, CA. Jan 17-18, pp. 77-89.

68) McWilliam, A.J., (1995). 'Design of High Purity Water Distribution Systems', *Pharmaceutical Engineering*, Vol. 15 (5), pp. 54 – 71.

69) Meyrick.C.E., (1989). 'Practical Design of High Purity Water Systems', *Pharm.Eng*. Vol. 9 (5), pp. 20-27.

70) Mittleman, M. W., (1985). 'Biological Fouling of Purified Water Systems, Part 1', *Microcontamination,* Vol. 3 (10), pp. 51-55.

71) Mocikat, H. Gurtler, T.; Herwig, H., (2003) 'Laser Doppler velocimetry measurements in an interior flow test facility: A database for CFD-code evaluation', *Experiments in Fluids*, Vol. 34 (3), pp. 442-448.

72) Monson,D.J., Seegmiller, H.L., Chen, Y.S., (1990) 'Comparison of experimental calculations using curvature corrected zero and two equation turbulence models for a two dimensional U-duct', *AIAA paper*

73) Mukhopadhyay, D., (1997). 'High efficiency Reverse Osmosis system', *Proceedings of the 1997 16th Annual Semiconductor Pure Water and Chemicals, SPWCC*. Part 1 (of 2), Mar 3-7, Santa Clara, CA, USA, pp. 1-20.

74) Muraca, P. W.; Yu, V.L.; Goetz, A., (1990). 'Disinfection of Water Distribution Systems: Review of Application Procedures and Methodologies', *Infection Control and Hospital Epidemiology*, Vol. 11 (2), pp. 79-88.

75) Murakami, S., (1998) 'Overview of turbulence models', *Journal of Wind Engineering and Industrial Aerodynamics*, Vol. 74, pp. 1-24.

76) Nickerson, G.T., (1990) 'A Continuous High Purity Water Improvement Program for Submicron Device Manufacturing', *Ultrapure Water*, Vol. 7 (2), pp. 71-74.

77) Nobel, P.T., (1994). 'Transport Considerations for Microbial Control in Piping', *J. Pharm Sci and Tech*. Vol. 48 (2), pp. 76 – 85.

78) Nykanen, J, F., Cutler, R, M., (1990)(a). 'Designing and operating a pharmaceutical ultrapure water system', *Microcontamination*, Vol. 8 (5), pp. 6-12.

79) Nykanen, J. F. Cutler, R. M., (1990)(b). 'Designing and operating a pharmaceutical ultrapure water system', *Microcontamination*, Vol. 8 (5), pp. 67-73.

80) Nykanen, J.; Cutler, R., (1990). 'Designing and operating a pharmaceutical ultrapure water system', *Microcontamination*, Vol. 8 (5), pp. 6-10.

81) Ogedengbe, O., (1984). 'Characterisation and Specification of Local Sands for Filters', *Filtration and Separation*, Vol. 21 (4), pp. 331-334.

82) Okouchi, S., Yamanaka, K., Ishihara, Y., Yanaka, T., Uedaira, H., (1994). 'Relationship between water qualities and treatments in the ultra pure water

production system' *Water Science and Technology*, Vol. 30 (10) pt 10, 1994, Proceedings of the 17th Biennial Conference of the International Association on Water Quality, Jul 24-30 Budapest, Hung, pp. 237-241.

83) Patel, V.C., Rodi, W. and Scheuerer, G., (1985). 'Turbulent Models for Near-Wall and Low Reynolds Number Flows', *A Review AIAA* J., Vol. 23 (9), pp. 1308-1319.

84) Patterson, M. K; Husted, G. R.; Rutkowshi, A., (1991). 'Isolation, Identification and Microscopic Properties of Biofilms in High Purity Water Distribution Systems', *Ultrapure Water*, Vol. 8 (4), pp. 18-24.

85) Percival, S.L. Knapp, J.S.; Wales, D.S.; Edyvean, R., (1998) 'Physical factors influencing bacterial fouling of type 304 and 316 stainless steels' *British Corrosion Journal*, Vol. 33 (2), pp. 121-129.

86) Pittner, G.A.; Bertler, G., (1988). 'Point of Use Contamination Control of Ultrapure Water Systems', *Ultrapure Water*, Vol. 5 (4), pp. 16 – 23.

87) Pitts, G., (1997). 'Construction issues facing ultra pure water systems', *ASCE Construction Congress Proceedings*, 1997, Managing Engineered Construction in Expanding Global Markets, Proceedings of the 1997 5th ASCE Construction Congress, Oct 4-8, Minneapolis, MN, USA, pp. 202-208.

88) Pop, M. and Sallet, W., (1983). 'Experimental Investigation of one and two phase flow through a Tee Junction', *Int Conference on the Physical Modelling of Flow*, BHRA Fluid Engineering, Paper B3, Coventry, England .

89) Reynolds. W. C., (1987). 'Fundamentals of turbulence for turbulence modeling and simulation', *Lecture Notes for Von Karman Institute Agard* Report No. 755.

90) Ridgeway, H. F.; Rigby, M. G.; Argo, D. G., (1985). 'Bacterial Adhesion and Fouling of Reverse Osmosis Membranes', *Journal of American Water Works Association*, Vol. 77, pp. 97 – 106.

91) Sanders, T.M.; Furne, T.J., (1986). 'High Purity Water Systems', *Fifth Annual Semiconductor Pure Water Conference*, , San Francisco.Jan 16-17, pp. 3-16.

92) Seiberling., (1987) 'Clean-in-Place/Sterilize-in-Place (CIP/SIP)' in W.P.Olson, M.J.Groves, Eds., *Aseptic Pharmaceutical Manufacturing*, 1st ed.: Interpharm Press: Prairie View, IL, pp. 247-314.

93) Self, T.; Olsen, P.; Banes, P., (1993). 'Investigating the roughing of stainless-steel USP water systems' *Microcontamination*, Vol. 11 (5), pp. 44-55.

94) Shih, T.-H. Liou, W. W. Shabbir, A. and Zhu, J., (1995). 'A New k- ϵ Eddy-Viscosity Model for High Reynolds Number Turbulent Flows - Model Development and Validation', *Computers Fluids*, Vol. 24 (3), pp. 227-238.

95) Sierra-Espinosa, F.Z. Bates, C.J.; O'Doherty, T., (1997). 'Reverse and fully developed flow regions in an equally divided 90 degree pipe junction', *ASME Fluids Engineering Division*, Summer meeting, June 22-26, pp. 1-8.

96) Sierra-Espinosa, F.Z. Bates, C.J.; O'Doherty, T., (2000). 'Turbulent flow in a 90° pipe junction. Part 1: Decay of fluctuations upstream the flow bifurcation', *Computers and Fluids*, Vol. 29 (2), Feb, pp. 197-213.

97) Sierra-Espinosa, F.Z. Bates, C.J.; O'Doherty, T., (2000). 'Turbulent flow in a 90° pipe junction. Part 2: Reverse flow at the branch exit', *Computers and Fluids*, Vol. 29 (2), pp. 215-233.

98) Spencer, E. A. Hector, M. V and Castro, I. P., (1995). 'Intercomparison of measurement and computation of flow through a contraction and a diffuser', *J.Flow.Meas and Inst.*, Vol. 6, (1), pp.3-14.

99) Speziale, C. G., (1991). 'Analytical Methods for the Development of Reynolds-Stress Closures in Turbulence', *Annu. Rev. Fluid Mech.*, Vol. 23, pp. 107-157.

100) Tekriwal, P., (1994). 'Heat transfer predictions in rotating radial smooth channel: comparative study of K-E models with wall function and low-re model', *American Society of Mechanical Engineers*, 94-GT-196, pp. 1-10.

101) Thakre, S.S. Joshi, J.B., (2000). 'CFD modeling of heat transfer in turbulent pipe flows', AIChE Journal, Vol. 46 (9), pp. 1798-1812.

102) Tide, C. Harkin, S. R.; Geesey, G. G.; Bremer, P. J.; Scholz, W., (1999). 'Influence of welding procedures on bacterial colonization of stainless steel weldments' *Journal of Food Engineering*, Vol. 42 (2), pp. 85-96.

103) Tomari, H., (1997). 'Slight degree of corrosion of stainless steel for semiconductor manufacturing plants', *Corrosion Engineering*, Vol. 46 (4), pp. 202-209.

104) Vanhaecke, E.; Remon, J.P.; Raes, F., (1990). 'Kinatics of Pseudomonas aeruginosa to 304 and 316-L stainless Steel: Role of Cell Surface Hydrophobicity', *Applied and Enviromental Microbology*, Vol. 56, pp. 788 – 795.

105) Wakes, S. Holdo, A., (1997). 'Wall functions used with current turbulence models', *American Society of Mechanical Engineers, Fluids Engineering Division*, Vol. 1, pp. 7-18.

106) Weiss, J. M. Maruszewski, J. P. and Smith. W. A., (1997) 'Implicit Solution of the Navier-Stokes Equations on Unstructured Meshes,' *Technical Report AIAA-97-2103*, 13th AIAA CFD Conference, Snowmass, CO.

107) Weitnauer, A.K., (1996). 'Controlling Growth in USP Purified Water', *Ultrapure Water*, Vol. 13 (3), pp. 26-30.

108) Weitnauer, A.K.; Comb, L.F., (1996). 'Two Pass Reverse Osmosis for Pharmaceutical Grade Purified Water', *Ultrapure Water*, Vol.13 (2), pp. 42-45.

109) Wilcox. D. C., (1998). 'Turbulence Modeling for CFD', *DCW Industries*, Inc., La Canada, California.

110) Yakhot V. and Orszag. S. A., (1986) 'Renormalization Group Analysis of Turbulence: I. Basic Theory,' *Journal of Scientific Computing*, Vol. 1 (1), pp. 1-51.

111) Yakhot, A Orszag, S. A.. Yakhot, V and Israeli. M., (1989). 'Renormalization Group Formulation of Large-Eddy Simulation,' *Journal of Scientific Computing*, Vol. 4, pp. 139-158.

112) Yamanaka, K., Imaoka, T., Futatsuki, T., Yamashita, Y., Aoki, H., Aoto, N., (1997). 'Excellent rinsing effect of electrolyzed ultra pure water in wet cleaning process', *Annual Semiconductor Pure Water and Chemicals Conference*, Vol. 2, 1997, Proceedings of the 1997 16th Annual Semiconductor Pure Water and Chemicals, SPWCC. Part 2 (of 2), Mar 3-7, Santa Clara, CA, USA, pp. 99-108.

113) Young, J., (1993). 'Sterilization of various diameter dead-ended tubes', *Biotechnology Bioengineering*, Vol. 42 (1), pp. 125-132.

114) Young, J., Lasher, W., Gaber, R., (1995). 'Transport processes during sterilization of vertical and 5 degree horizontal dead-legs', *Bioprocess Engineering*, Vol. 12 (6), pp. 293-304.

115) Youngberg, D.A., (1985). 'Sterilizing Storage Tanks in a Pure Water System', *Ultrapure Water*, Vol. 2 (4), pp. 45-54.

CHAPTER 9: APPENDIX

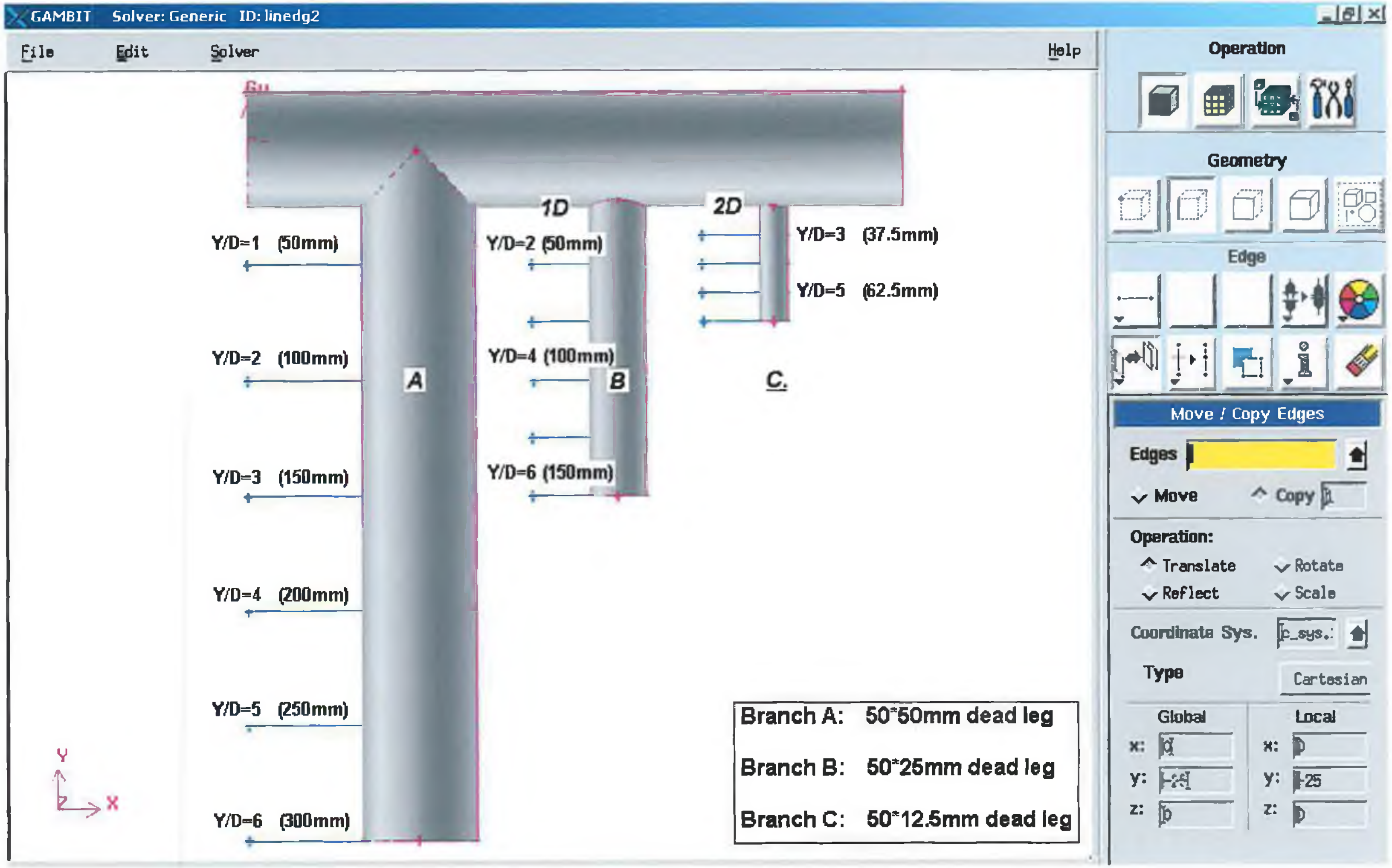

Figure 9.1: Y/D measurements for various diameter dead-leg tees

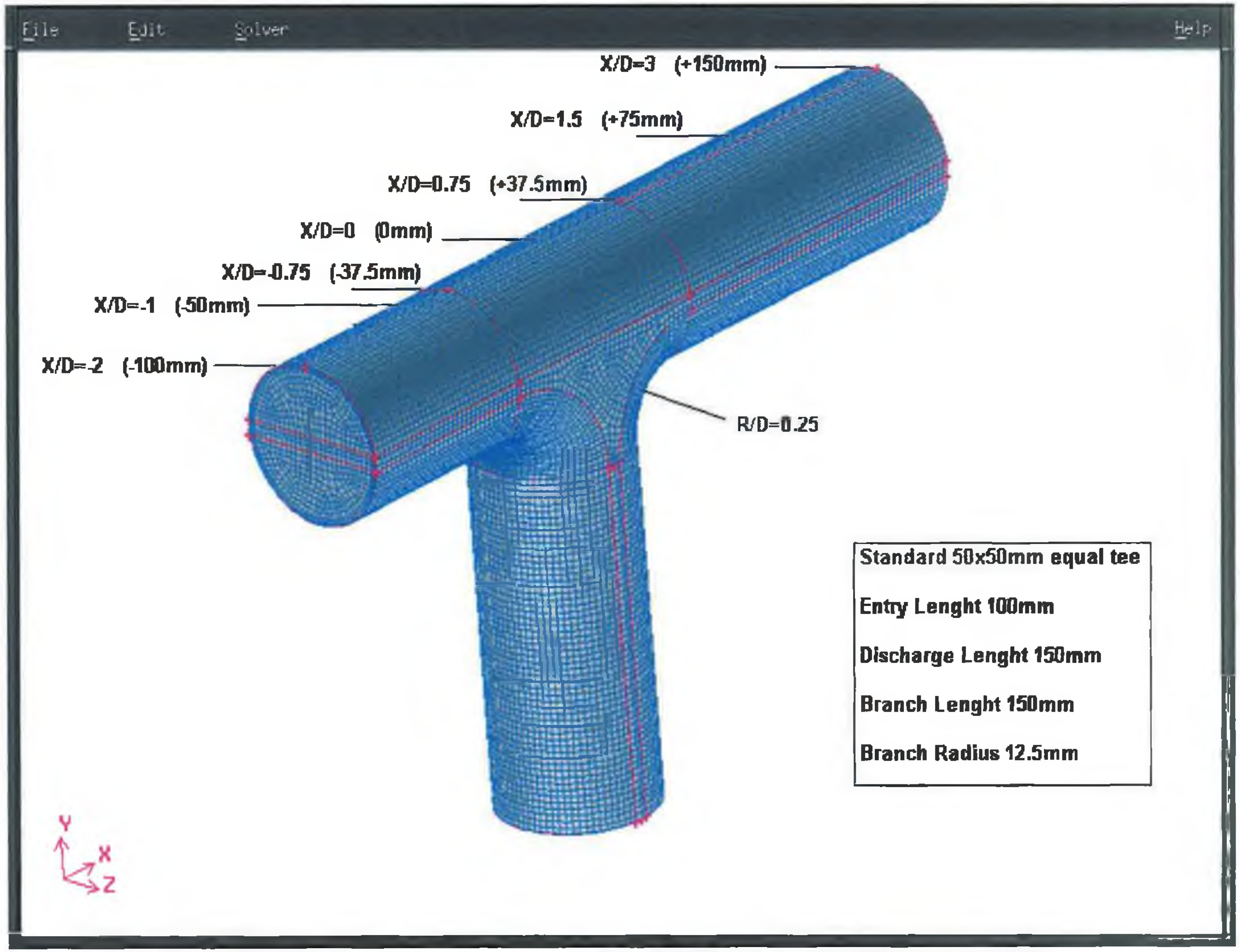

Figure 9.2: X/D measurements for a 50x50mm equal dead-leg tees